The Unified Transform Method and its semi-discrete analogue for numerically solving IBVPs

Jorge Cisneros Paz

A dissertation
submitted in partial fulfillment of the
requirements for the degree of

Doctor of Philosophy

University of Washington

2022

Reading Committee:

Bernard Deconinck, Chair

Gino Biondini

Anne Greenbaum

Randall LeVeque

Thomas Trogdon

Program Authorized to Offer Degree:
Applied Mathematics

University of Washington

Abstract

The Unified Transform Method and its semi-discrete analogue
for numerically solving IBVPs

Jorge Cisneros Paz

Chair of the Supervisory Committee:
Professor of Applied Mathematics Bernard Deconinck
Department of Applied Mathematics

Finite-difference schemes are a popular and intuitive approach to numerically solve nonlinear initial-boundary value problems (IBVPs). Often, this leads to the introduction of ghost points, where the numerical method depends on grid points outside of the working domain. The usual heuristics of doing this for second-order problems do not generalize to higher order, and incorporating boundary conditions and addressing ghost points are serious numerical issues.

Our approach proposes to tackle this problem by the implementation of split-step methods to separately solve the linear and nonlinear subproblems. In this dissertation, we discuss the Unified Transform Method (UTM), introduced by A. S. Fokas, and its semi-discrete analogue to devise finite-difference schemes for the linear problem that appropriately incorporate boundary conditions. The UTM solution representations are then treated to give analytic continuation formulas that can be applied at ghost points in the split-step method. We present our developments through examples of several linear problems and their discretizations on the half-line and finite interval, and the nonlinear Schrödinger equation on the finite interval. We discuss the continuum limit of the solutions and numerical results.

TABLE OF CONTENTS

Page

List of Figures iii

Acronyms vii

Chapter 1: Introduction 1
- 1.1 Motivation . . . 1
- 1.2 Continuous Unified Transform Method . . . 3
- 1.3 Semi-Discrete UTM . . . 5
- 1.4 Organization of the Dissertation . . . 7

Chapter 2: Half-Line Problems 8
- 2.1 Advection Equations . . . 8
- 2.2 The Heat Equation . . . 22
- 2.3 The Linear Schrödinger Equation . . . 33
- 2.4 The Convection-Diffusion Equation . . . 37
- 2.5 Small-Time Increments . . . 43

Chapter 3: Finite Interval Problems 47
- 3.1 Advection Equations . . . 47
- 3.2 The Heat Equation . . . 58
- 3.3 The Linear Schrödinger Equation . . . 76
- 3.4 Computational Comparisons . . . 83
- 3.5 Small-Time Increments . . . 84

Chapter 4: Third-Order Problems 89
- 4.1 Half-Line IBVPs . . . 89
- 4.2 Finite Interval IBVP . . . 107

Chapter 5: Analytic Continuation 123
- 5.1 Advection Equations . . . 123
- 5.2 The Heat Equation . . . 138

Chapter 6: Split-Step Finite-Difference Method 156
- 6.1 Background . . . 156
- 6.2 The Nonlinear Schrödinger Equation . . . 157

Chapter 7: Conclusion and Future Work 167

Appendix A: Starting Index on semi-discrete Transform Pair **169**

Appendix B: The "Time-Reversed" Heat Equation **172**

Bibliography **173**

LIST OF FIGURES

Figure Number — Page

1.1.1 A stencil that requires information at a ghost point. . . . 1
1.1.2 A stencil that uses an off-centered stencil near the boundary to avoid introducing the dependence of a ghost point while maintaining the same order of accuracy as the interior stencil seen in Figure 1.1.1. . . . 2
1.1.3 A stencil that assigns a value to the ghost point introduced by the interior stencil near the boundary. . . . 2

2.1.1 The shaded regions depict where $\mathrm{Re}(-W) \leq 0$ and e^{-WT} is bounded with the dispersion relation (2.1.4). . . . 10
2.1.2 (a) The semi-discrete solution (2.1.7) evaluated at various T with $h = 0.01$. (b) Error plot of the semi-discrete solution (2.1.7) relative to the exact solution as $h \to 0$ with $T = 0.5$. . . . 13
2.1.3 The shaded regions depict where $\mathrm{Re}(-W) \leq 0$ and e^{-WT} is bounded with the dispersion relation (2.1.14). . . . 15
2.1.4 (a) The semi-discrete solution (2.1.16) evaluated at various T with $h = 0.01$. (b) Error plot of the semi-discrete solution (2.1.16) relative to the exact solution as $h \to 0$ with $T = 0.5$. . . . 16
2.1.5 Several time slices for the solution to IBVP (2.1.18) with $h = 0.004$. . . . 17
2.1.6 The shaded regions depict where $\mathrm{Re}(-W) \leq 0$ and e^{-WT} is bounded with the dispersion relation (2.1.21). . . . 18
2.1.7 The blue shaded region denotes where the global relation (2.1.27) is valid with $k \to \nu_1(k)$ and the orange shaded regions depict where $\mathrm{Re}(-W) \leq 0$ and e^{-WT} is bounded with the dispersion relation (2.1.28). . . . 20
2.2.1 (a) The semi-discrete solution (2.2.9) evaluated at various T with $h = 0.01$. (b) Error plot of the semi-discrete solution (2.2.9) relative to the exact solution as $h \to 0$ with $T = 1.625$. . . . 24
2.2.2 (a) The semi-discrete solution (2.2.18) evaluated at various T with $h = 0.01$. (b) Error plot of the semi-discrete solution (2.2.18) relative to the exact solution as $h \to 0$ with $T = 0.01$. . . . 27
2.2.3 Several time slices for the solution to IBVP (2.2.20) with $h = 0.01$. . . . 28
2.2.4 The shaded region depicts where the global relation of the backward one-sided discretization of q_{xx} is valid, with $k \to \nu_1(k)$ from (2.2.24). . . . 29
2.2.5 (a) The shaded regions depict where $\mathrm{Re}(-W) \leq 0$ and e^{-WT} is bounded with the dispersion relation (2.2.28). (b) The shaded regions depict where the global relation with $k \to \nu_i(k)$ is valid from (2.2.28). . . . 30
2.2.6 (a) Contour plot of default $|\sqrt{z}|$. (b) Contour plot of redefined $|\sqrt{z}|$. . . . 32

2.3.1 (a) - (c) Real and imaginary parts and modulus squared of the semi-discrete solution profiles (2.3.9) at various T for IBVP (2.3.11) with $h = 0.01$. (d) Error plot of the semi-discrete solution (2.3.9) relative to the exact solution as $h \to 0$ with $T = 0.1$. . . 35
2.3.2 (a) - (c) Real and imaginary parts and modulus squared of the semi-discrete solution profiles (3.3.13) at various T for IBVP (2.3.17) with $h = 0.01$. (d) Error plot of the semi-discrete solution (3.3.13) relative to the exact solution as $h \to 0$ with $T = 1$. . . . 38
2.4.1 The shaded region denotes where the global relation (2.4.7) is valid with $k \to \nu_1(k)$ and the closed contour C. . . . 40
2.5.1 (a) The error (green) between the SD-UTM solution (2.1.16) and the exact solution and the error (maroon) between the exact solution and the small-time approximated SD-UTM solution (2.5.4) with $r = 2$ and $\tau = 10^{-5}$ as $h \to 0$. (b) The error between the SD-UTM solution (2.1.16) and the small-time approximated SD-UTM solution (2.5.4) (denoted as $\tilde{q}_n(\tau)$ here) for varying order r of terms kept in the approximated solution as $\tau \to 0$ with $h = 0.01$. . . . 46
3.1.1 (a) The semi-discrete solution (3.1.8) evaluated at various T with $h = 0.005$. (b) Error plot of the semi-discrete solution (3.1.8) and finite-difference schemes relative to the exact solution as $h \to 0$ with $T = 0.25$ and $\Delta t = 2.5 \times 10^{-3}$. . . . 52
3.1.2 (a) The numerical solutions to IBVP (3.1.9) at $T = 0.25$ with $h = 10^{-4}$ for all the methods and $\Delta t = 2.5 \times 10^{-3}$ for the finite-difference methods. (b) The difference between the exact solution and the numerical solutions under the same conditions as (a). . . . 53
3.1.3 (a) The shaded regions depict where $\mathrm{Re}(-W) \leq 0$ and e^{-WT} is bounded, for the dispersion relation (3.1.12). (b) The shaded regions depict where the global relation with $k \to \nu_1(k)$ is valid, *i.e.*, $\mathrm{Im}(\nu_1) \leq 0$. . . . 54
3.2.1 (a) The shaded regions depict where $\mathrm{Re}(-W) \leq 0$ and e^{-WT} is bounded, for the dispersion relation (2.2.4). The integration paths that constitute P are also shown. (b) The integration paths $\partial V^{\pm}$. . . . 59
3.2.2 (a) The integration paths $\partial \tilde{V}^{\pm}$ deformed away from the origin. (b) Deforming $\partial \tilde{V}^{+}$ to $\tilde{D}^{+}$ in the upper-half plane. Without decay from e^{-WT}, the shaded region depicts where e^{iknh} decays. . . . 61
3.2.3 The shaded regions depict where $\mathrm{Re}(-\tilde{W}) \leq 0$ and $e^{\tilde{W}T}$ is bounded, with the boundaries $\partial\tilde{\Omega}^{\pm}$ approaching $\partial\Omega^{\pm}$ asymptotically as $|k| \to \infty$. . . . 63
3.2.4 The semi-circle integration paths $\partial \tilde{V}_{\epsilon}^{\pm}$ around singularities on the real line. . . . 64
3.2.5 (a) The semi-discrete solution (3.2.14) evaluated at various t with $h = 0.01$. (b) Error plot of the semi-discrete solution (3.2.14) and finite-difference schemes relative to the exact solution as $h \to 0$ with $T = 0.01$ and $\Delta t = 6.25 \times 10^{-4}$. . . . 67
3.2.6 (a) The semi-discrete solution (3.2.26) evaluated at various T with $h = 0.01$. (b) Error plot of the semi-discrete solution (3.2.26) and finite-difference schemes relative to the exact solution as $h \to 0$ with $T = 0.005$ and $\Delta t = 6.25 \times 10^{-4}$. . . . 72
3.2.7 The shaded regions depict where $\mathrm{Re}(-W) \leq 0$ and e^{-WT} is bounded, for the dispersion relation (2.2.28). The integration paths for $\partial \tilde{V}^{\pm}$, deformed away from the singularities on the real line, are also shown. . . . 73

3.3.1 (a) The shaded regions depict where $\mathrm{Re}(-W) \leq 0$ and e^{-WT} is bounded, for the dispersion relation (2.3.5). The integration paths that constitute P are also shown. (b) The integration paths $\partial V^{\pm}$ and $P_6^{\pm}$. 77
3.3.2 The shaded regions depict where $\mathrm{Re}(-\tilde{W}) \leq 0$ and $e^{\tilde{W}T}$ is bounded. The integration paths $\partial\tilde{\Omega}^{\pm}$ are also shown. 79
3.3.3 (a) - (c) Real and imaginary parts and modulus squared of the semi-discrete solution (3.3.8) evaluated at various T for IBVP (3.3.9) with $h = 0.01$. (d) Error plot of the semi-discrete solution (3.3.8) and finite-difference schemes relative to the exact solution as $h \to 0$ with $T = 0.1$ and $\Delta t = 3.90625 \times 10^{-4}$. 86
3.3.4 (a) - (c) Real and imaginary parts and modulus squared of the semi-discrete solution (3.3.15) evaluated at various T for IBVP (3.3.9) with $h = 0.01$. (d) Error plot of the semi-discrete solution (3.3.15) and finite-difference schemes relative to the exact solution as $h \to 0$ with $T = 0.2$ and $\Delta t = 1.5625 \times 10^{-3}$. 87
3.4.1 (a) The blue curve denotes the number of spatial grid points N_x required for the SD-UTM solution to approximately reach the accuracy $E = 10^{-2}$ when solving the IBVP (3.3.9). Using this information, every finite-difference method uses the same spatial grid for each T to determine how many time-steps N_t are required to reach a similar accuracy as the SD-UTM solution. (b) The wall-clock computation time (averaged over 10 runs to rule out any effects due to background processes) required for each method to solve the IBVP (3.3.9) with the selected N_x and N_t that approximately give an accuracy E. 88
4.1.1 (a) Valid regions of the global relation (4.1.6) with $k \to \nu_j(k)$. (b) The shaded regions depict where $\mathrm{Re}(W) \leq 0$ and e^{-WT} is bounded with the dispersion relation (4.1.4). . 91
4.1.2 (a) Integration path P and (b) modified integration paths ∂V_1 and ∂V_2 for (4.1.2). . . 92
4.1.3 Deforming $\partial V_{1,2}$ to $D_{1,2}$ with $R \to \infty$. 94
4.1.4 Computation paths $\partial C_{1,2}$. 95
4.1.5 Regions where the global relation (4.1.10) is valid with $k \to \tilde{\nu}_j(k)$. 96
4.1.6 The shaded regions depict where $\mathrm{Re}(\tilde{W}) \leq 0$ and $e^{-\tilde{W}T}$ is bounded with the dispersion relation (4.1.11). 97
4.1.7 $\mathrm{Im}\,(\nu_j) \leq 0$ for symmetries (4.1.5b) and (4.1.5c) in the continuum limit (see Figures 4.1.1a and 4.1.5). 98
4.1.8 The shaded regions depict where $\mathrm{Re}(W) \leq 0$ and e^{-WT} is bounded with the dispersion relation from the forward-leaning discretization for $q_t = q_{xxx}$. 99
4.1.9 (a) Valid regions of the global relation (4.1.17) with $k \to \nu_j(k)$. (b) The shaded regions depict where $\mathrm{Re}(W) \leq 0$ and e^{-WT} is bounded with the dispersion relation (4.1.16). . 100
4.1.10 Integration path P for (4.1.14). 101
4.1.11 Integration path ∂V. 102
4.1.12 Deforming ∂V to D with $R \to \infty$. 104
4.1.13 Computation path ∂C. 106
4.2.1 (a) Integration paths $\partial V_{1,2}^{+}$ and ∂V^{-}. (b) Modified integration paths $\partial\tilde{V}_{1,2}^{+}$ and $\partial\tilde{V}^{-}$. 109
4.2.2 Numerically determined roots of $\lambda(k)$ with $h = 1/6$ (left) with zoomed in view of the poles on the positive imaginary axis (right). 110

4.2.3 Numerically determined roots of $\tilde{\lambda}(k)$ with $h = 1/6$ (left) with zoomed in view of the poles on the positive imaginary axis (right). . . . 113
4.2.4 Computation paths $\partial C^+_{1,2}$ and ∂C^-. . . . 114
4.2.5 Modified integration paths $\partial\tilde{\Omega}^+_{1,2}$ and $\partial\tilde{\Omega}^-$. . . . 115
4.2.6 Roots of $\Lambda(k)$ (black) and $\tilde{\lambda}(k)$ (green) as $h \to 0$. . . . 122

5.1.1 Extensions of half-line solution (2.1.16). . . . 128
5.1.2 Extensions of half-line solution (2.1.25) for IBVP (5.1.9) with $h = 0.04$ (left) and $h = 0.008$ (right). . . . 134
5.2.1 Extensions of half-line solution (2.2.9) for IBVP (5.2.7) with $h = 0.2$ (left) and $h = 0.05$ (right). . . . 147
5.2.2 Extensions of half-line solution (2.2.18) for IBVP (5.2.12) with $h = 0.02$ (left) and $h = 0.004$ (right). . . . 154

6.2.1 The real part of the SSFD solutions to IBVP (6.2.14) with (a) the SA formulation and (b) the AC formulation for the linear subproblem. . . . 162
6.2.2 The ∞-norm error of the AC-formulated SSFD solution to IBVP (6.2.14) with ℓ terms. 163
6.2.3 Error plot as $h \to 0$ of the SSFD solutions to IBVP (6.2.14) with (a) the SA formulation and (b) the AC formulation for the linear subproblem. We vary the number of finite-difference time steps $N_{t,FD}$ in each plot. . . . 164
6.2.4 Error plot as $\tau \to 0$ of the SSFD solutions to IBVP (6.2.14) with (a) the SA formulation and (b) the AC formulation for the linear subproblem. . . . 165
6.2.5 The real part of the SSFD solutions to IBVP (6.2.15) with (a) the SA formulation and (b) the AC formulation for the linear subproblem. . . . 165
6.2.6 The ∞-norm error of the AC-formulated SSFD solution to IBVP (6.2.15) with ℓ terms. 166
6.2.7 Error plot as $h \to 0$ of the SSFD solutions to IBVP (6.2.15) with (a) the SA formulation and (b) the AC formulation for the linear subproblem. We vary the number of finite-difference time steps $N_{t,FD}$ in each plot. . . . 166

ACRONYMS

PDE: partial differential equation

IBVP: initial-boundary value problem

UTM: Unified Transform Method

SD-UTM: semi-discrete Unified Transform Method

ODE: ordinary differential equation

FE: forward Euler time-stepping method

RK4: fourth-order Runge-Kutta time-stepping method

BE: backward Euler time-stepping method

TR: trapezoidal time-stepping method

LS: linear Schrödinger equation

KDV: Korteweg–de Vries equation

SSFD: split-step finite-difference method

NLS: nonlinear Schrödinger equation

SA: standard approach that all together avoids ghost points by applying certain spatial stencils near the boundaries

AC: approach that applies analytic continuation formulas from UTM representations wherever ghost points develop

ACKNOWLEDGMENTS

I first want to thank my supervisory PhD committee for the time and energy they have dedicated to my thesis: Bernard Deconinck, Gino Biondini, Dale Durran, Anne Greenbaum, Randy LeVeque, and Tom Trogdon. I am grateful for our conversations and feedback that have led to the final version of this work. I would like to especially thank my advisor, Bernard Deconinck, for his mentorship, guidance, and patience from the very beginning, leading a lively research group full of discussions and Belgian delicacies. I would also like to thank the Ford Foundation and UW Office of Graduate Student Equity & Excellence not only for their financial support in fellowships throughout my PhD program, but also for the general support in the minority communities across UW.

Early on during my undergraduate years at the University of Texas Rio Grande Valley, I was exposed to research in the mathematical sciences, which led me to pursue a PhD program in applied math. My journey began (and continues) with the encouragement of several mentors and research advisors: Daniel Riahi, Cristina Villalobos, Andras Balogh, and Zhijun Qiao. Outside of the university, even now, I was lucky to participate in several research programs and internships. For taking a chance on me to explore new avenues of research, thank you to Roberto Pelayo and Brian Wissman (Univ. of Hawaii at Hilo), Brian Loft (Sam Houston State Univ.), Richard Rebarber (Univ. of Nebraska-Lincoln), Susana Serna (Institute for Pure & Applied Mathematics), Johannes Brust (Argonne National Laboratory), Henry Fender (ITM TwentyFirst LLC), Dan Lu and Justin Feigelman (Genentech), Matthew Williams and Audrey Kindlon (National Science Foundation), and Christine Task (Knexus Research Corporation).

Since joining the AMATH department, many thanks go to the AMATH staff, specifically Lauren Lederer, a fellow Texan, for taking charge of any and every concern brought to her. My new and old friends, thank you for the late nights and group chats and homework sessions – it's been a pleasure surviving this PhD program with y'all.

To close, I would like to thank my family. Every step of the way since we arrived to the United States over two decades ago has been fueled by the dedication and love from my parents. Mamá y papá, gracias por todos sus esfuerzos que me lanzaron a donde estoy ahora. Todos mis triunfos y logros, incluyendo este doctorado, se los debo a los dos. To my sister, Stephanie, you have been there from the beginning, no matter what mess life throws at us, so thank you for sticking by my side, even if from a distance. Ryan Creedon, even though we are not technically brothers, you will always be a part of my family. Thank you for giving me a lifelong friendship that I can always

count on through thick and thin. Last but certainly not least, thank you, Lizeth, for joining my life during this stressful and busy PhD program. The worldwide COVID-19 pandemic brought a lot of darkness to many people, but it gave us the opportunity to move back to Texas as we welcomed our beautiful baby girl. Mi Natalia, your smile and laughter and endless “dadda”s will forever keep me going. Te amo.

DEDICATION

Para mis padres, que me han dado todo desde el principio

Chapter 1

INTRODUCTION

1.1 Motivation

Consider the numerical solution of the M^{th}-order quasilinear partial differential equation (PDE)

$$q_t = c\, q_{Mx} + F\left(q, q_x, \ldots, q_{(M-1)x}\right), \quad c \in \mathbb{C} \setminus \{0\}, \tag{1.1.1}$$

on the half-line for $x \in (0, \infty)$ or on the finite interval for $x \in (0, L)$ with $L > 0$. The problem (1.1.1) is well-posed if its solution is unique and exists globally or for a finite time t, and continuously depends on the prescribed initial condition $q(x, 0) = \phi(x)$ and the correct number of boundary conditions. We additionally impose that initial and boundary data are compatible (at least to zeroth-order) with sufficient smoothness and decay, so that $q(x, t) \to 0$ uniformly as $x \to \infty$ for half-line problems.

Arguably the most intuitive approach in solving initial-boundary value problems (IBVPs) is through the implementation of a finite-difference scheme on a discrete grid with points $x_n \equiv n\Delta x$ and $t_j \equiv j\Delta t$. Directly applying such schemes, especially those with high-order spatial stencils, introduces the dependence on grid points outside of the domain, known as *ghost points*, see Figure 1.1.1. This embeds a discrepancy into the numerical methodology, since these points originate from the choice of spatial stencil and not from the original IBVP itself. Note that with periodic boundary conditions, the issue of ghost points never arises.

One way to avoid this discrepancy for general boundary conditions is to altogether avoid ghost points by applying certain spatial stencils as we approach the boundaries [10, 63], see Figure 1.1.2. These stencils are designed, say, using the method of undetermined coefficients, to depend only on

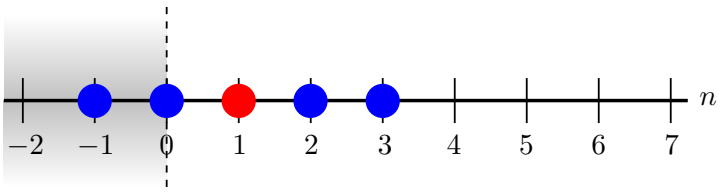

Figure 1.1.1: A stencil that requires information at a ghost point.

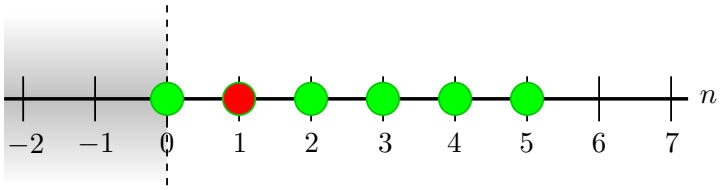

Figure 1.1.2: A stencil that uses an off-centered stencil near the boundary to avoid introducing the dependence of a ghost point while maintaining the same order of accuracy as the interior stencil seen in Figure 1.1.1.

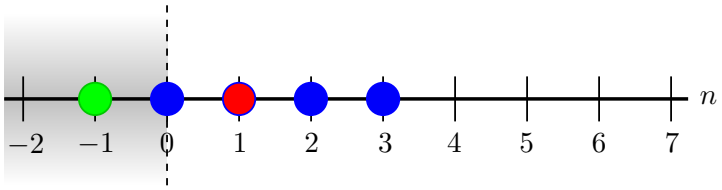

Figure 1.1.3: A stencil that assigns a value to the ghost point introduced by the interior stencil near the boundary.

grid points that lie within the domain and the boundary. The vast freedom in choosing these stencils lead to discretizations that are unstable or incompatible with the physical interpretations and modeling of the IBVP [22, 35, 60]. Although ghost points are eliminated, these stencils tend to destroy the normal structure $\left(A^TA = AA^T\right)$ of the coefficient matrix in a method-of-lines formulation, if there was one to begin with. The stability analysis is even harder now for these problems, where we may resort to studying the ϵ-pseudospectrum of the coefficient matrix [31, 43, 67].

Another way to address the discrepancy is to assign artificial conditions to the ghost points according to reflection principles, interpolations, absorbing conditions, and discretizations of the given boundary conditions [14, 35, 43, 59], see Figure 1.1.3. This option is commonly applied whenever a PDE has prescribed derivative boundary conditions, but becomes complicated when applying higher-order stencils to the PDE that lead to an underdetermined system with too many unaccounted ghost points, even if we have derivative boundary conditions to discretize. A scenario like this would require a combination of approaches, like discretizing available data and applying one-sided stencils near the boundaries to avoid introducing too many unknowns.

The choice of information at ghost points can destabilize numerical methods that are shown to be stable in the full-line or periodic problem via von Neumann analysis [22, 43]. These heuristic

methodologies do not easily transfer when treating PDEs with higher-order derivatives, and the general rules for examining stability in the presence of boundary data are not well developed [10, 14, 31, 59, 63]. Incorporating boundary conditions correctly and addressing ghost points is a non-trivial numerical issue [35, 60, 67].

Our approach to tackle this problem is set up by the ideas of operator splitting and the implementation of split-step methods. For our IBVPs of interest, we rewrite the evolution PDE (1.1.1) as

$$q_t = \mathcal{L}(q) + \mathcal{N}(q), \tag{1.1.2}$$

where $\mathcal{L}$ is a constant-coefficient linear differential operator of order M and $\mathcal{N}$ is any nonlinear operator, both operators involving spatial derivatives of $q(x,t)$. The idea behind split-step methods is to separately solve the M^{th}-order linear IBVP with

$$q_t = \mathcal{L}(q) = c\, q_{Mx}, \tag{1.1.3}$$

and combine it with the solution of the nonlinear IBVP with

$$q_t = \mathcal{N}(q) = F\left(q, q_x, \ldots, q_{(M-1)x}\right), \tag{1.1.4}$$

in an iterative way [47]. One of the greatest difficulties when applying split-step methods is the implementation of non-periodic boundary conditions [42, 44]. As with many other finite-difference approaches, the use of high-accuracy spatial discretizations of the linear $\mathcal{L}$ and nonlinear $\mathcal{N}$ operators might introduce ghost points and their artificial boundary conditions, likely affecting the overall numerical stability.

We consider the class of semi-discretized PDEs where the most nonlocal stencil is applied to the linear term $c\, q_{Mx}$. Hence, the lower-order problem (1.1.4) of (1.1.1) can be approached using established split-step techniques, while the linear problem (1.1.3) and the ghost points that arise require special attention. In this dissertation, we treat $q_t = c\, q_{Mx}$ using the Unified Transform Method on the continuous (x,t)-plane and the semi-discrete (n,t)-plane, with an eye towards split-step methods for (1.1.1).

1.2 Continuous Unified Transform Method

The Unified Transform Method (UTM) or Method of Fokas provides a powerful approach to solve evolution IBVPs, including all those with linear, constant-coefficient PDEs and some integrable nonlinear PDEs. The UTM was introduced by A. S. Fokas in 1997 for the purpose of generalizing the method of inverse scattering to IBVPs on the half-line and on a finite interval [26, 27, 28].

The UTM generates an explicit analytical solution for $q(x,t)$, with the solution written in terms of integrals along paths in the complex plane of a spectral parameter $k \in \mathbb{C}$. Through parametrization of the contours, these explicit solutions can be numerically evaluated [16, 18, 25]. The application of

the UTM is systematic, regardless of the types of boundary data, *e.g.*, nonhomogeneous Dirichlet, Neumann, Robin, etc. conditions. This is one reason the UTM is more general and effective than standard methods for evolution IBVPs [15]. Further, the method demonstrates how many and which types of boundary conditions result in a well-posed IBVP, depending on the order M of the PDE [28].

For either half-line or finite-interval IBVPs, the UTM is applied algorithmically using the following steps [17]:

1. rewrite the PDE in divergence form, depending on a spectral parameter k, to obtain the local relation and the dispersion relation $\tilde{W}(k)$,
2. integrate over the (x,T)-domain, for a finite $T>0$, to obtain the global relation,
3. invert the global relation to obtain a representation of the solution depending on known and unknown boundary data,
4. determine symmetries $\tilde{\nu}_j(k)$ of $\tilde{W}(k)$,
5. determine where in $\mathbb{C}$ the global relations evaluated at $\tilde{\nu}_j(k)$ are valid,
6. if necessary, deform integral paths involving boundary terms appropriately,
7. solve for unknown boundary data using the global relations evaluated at $\tilde{\nu}_j(k)$, and
8. check that integral terms involving $\hat{q}(\tilde{\nu}_j,T)$ vanish, resulting in a solution representation.

Although the calculations within each step are more intricate for higher-order problems and their boundary conditions, the UTM ultimately solves an IBVP by solving a set of algebraic equations involving the dispersion relation and its symmetries.

Due to its systematic implementation for linear PDEs like (1.1.3), we aim to solve the linear problems in split-step methods with the UTM, regardless of boundary conditions. Undoubtedly, the computation of these integral representations can be numerically costly [18, 25, 38, 55]. For low-order problems, the finite-interval UTM solutions can be rewritten into a series representation by deforming the integral contours down to the singularities on the real line and applying the residue theorem [17]. These series solutions are preferred over the integral representations for numerical computations, but the rewrite is not always possible, especially for higher-order problems like $q_t = \pm\, q_{xxx}$. Furthermore, the half-line UTM solutions do not have isolated singularities in their integrands, so they cannot be represented solely as series. Thus, the efficient computation of these UTM integral representations is crucial.

The cons of solving an IBVP analytically perhaps outweigh the pros from a numerical standpoint, so we propose an alternative. Rather than solving the linear split-step IBVP with (1.1.3) using the UTM for all x and T, we discretize (1.1.3) via finite difference schemes of any arbitrary accuracy and numerically solve the IBVP. Wherever ghost points develop, we employ the UTM representations for all T. As straightforward as this alternative seems, the UTM formulations cannot be trivially

extended to x outside of the original IBVP domains. It was not until recent work with Matthew Farkas that Taylor-series expansions applied to the half-line UTM representations gave rise to valid analytic extensions [24]. Expanding this methodology to the finite-interval formulations allows us to implement our approach on the ghost points when numerically solving the linear IBVP in split-step methods.

A more consistent approach to the finite difference evaluations is to apply the UTM on the semi-discrete problem instead of on the continuous one. A method-of-lines formulation allows the UTM to address ghost points directly by providing an analytical solution to the linear semi-discrete IBVP.

1.3 Semi-Discrete UTM

The UTM has received a lot of attention for continuous IBVPs, but not nearly as much for semi-discrete ones, *i.e.*, discretized in space $x_n = nh$ for $n = 0, 1, 2, \ldots$, but continuous in time t. Biondini & Hwang [5], Biondini & Wang [6], and Moon & Hwang [51] study semi-discrete problems in the context of the semi-discrete UTM (SD-UTM), but from the perspective of a purely semi-discrete problem on closed contours with discretized Lax pairs and no variable mesh spacing h. While [5] focuses primarily on the linear and nonlinear Schrödinger difference equations, the theory for semi-discrete problems is presented via examples in [6] for half-line IBVPs and in [51] for finite-interval IBVPs. Minimal discussion on the continuum limit for the SD-UTM is presented in [51].

Our goal is to further develop the SD-UTM to help solve IBVPs by addressing complications that arise with ghost points. Within the split-step method, we want to apply the SD-UTM to the linear problem, whether that includes solving the linear semi-discrete IBVP entirely or only applying the method at the ghost points generated from the choice of spatial stencil in the finite-difference scheme. As we will show, the SD-UTM formulas for the semi-discrete $q(x_n, t) \equiv q_n(t)$ are simpler than those from the continuous UTM, but further approximations are needed in order to efficiently implement them into a split-step method, see Sections 2.5 and 3.5.

In what follows for half-line problems, we consider an explicit mesh parameter $h \ll 1$. More explicitly for finite-interval problems, we define $h = L/(N+1) \ll 1$ for $n = 0, 1, \ldots, N, N+1$ with N interior-domain grid points, where $n = 0$ and $n = N+1$ correspond to $x = 0$ and $x = L$, respectively. We use the shift operator $\Delta q_n = q_{n+1} - q_n$, which effectively replaces the spatial derivative with a forward difference. For half-line IBVPs with a Dirichlet boundary condition at $x = 0$, the Fourier transform pair can be written as

$$\hat{q}(k,t) = h \sum_{n=1}^{\infty} e^{-iknh} q_n(t), \qquad \text{Im}(k) \leq 0, \tag{1.3.1a}$$

$$q_n(t) = \frac{1}{2\pi} \int_{-\pi/h}^{\pi/h} e^{iknh} \hat{q}(k,t)\, dk, \qquad k \in \mathbb{C}. \tag{1.3.1b}$$

If a Dirichlet boundary condition is not given, *i.e.*, if $q_0(t)$ is unknown, then (1.3.1a) starts at $n = 0$ (see Appendix A). For half-line IBVPs, we require $q_n \in l^1(\mathbb{N})$, the space of absolutely summable sequences, ensuring that $\hat{q}(k,t)$ is bounded for all $k \in \mathbb{C}$ with $\mathrm{Im}(k) \leq 0$. For finite interval IBVPs with Dirichlet boundary conditions on both ends, the Fourier transform pair is written as

$$\hat{q}(k,t) = h \sum_{n=1}^{N} e^{-iknh} q_n(t), \qquad k \in \mathbb{C}, \tag{1.3.2}$$

together with (1.3.1b). If a Dirichlet condition is not given at $x = 0$, then we start (1.3.2) at $n = 0$. Similarly, if there is no Dirichlet data at $x = L$, the sum ends at $N+1$. We define the time transforms of spatial *nodes* at and near the $n = 0$ boundary, including ghost points:

$$f_j(W,T) = \int_0^T e^{Wt} q_j(t)\, dt, \quad j = \ldots -1, 0, 1, \ldots, \quad k \in \mathbb{C}, \tag{1.3.3}$$

and, at and near the $n = N + 1$ boundary, including ghost points:

$$g_j(W,T) = \int_0^T e^{Wt} q_{N+1+j}(t)\, dt, \quad j = \ldots -1, 0, 1, \ldots, \quad k \in \mathbb{C}, \tag{1.3.4}$$

for an arbitrary finite $T > 0$ and semi-discrete dispersion relation $W(k)$. Note that time T is used to denote a fixed final time of interest in the time transforms (1.3.3) – (1.3.4), while $t < T$ refers to the generic time variable.

Throughout the following half-line examples, we compute the SD-UTM solutions within the window of interest $x \in (0, 1]$ if a Dirichlet boundary condition is specified or $x \in [0, 1]$ if a Neumann boundary condition is given. Similarly for finite-interval problems. The solutions are implemented in MATLAB using built-in functions, such as the vectorized `integral()`. To reduce computation time, we analytically evaluate sums, like those defining the forward discrete Fourier transform, and integrals when possible. In addition, all IBVPs have initial and boundary conditions matching at $(x,t) = (0,0)$ and, when applicable, $(x,t) = (L,0)$.

Like the continuous UTM, we develop and algorithmically apply the following steps for the SD-UTM:

1. rewrite the semidiscretized equation into divergence form to obtain the local relation and the dispersion relation $W(k)$,
2. sum over spatial indices and integrate over the temporal domain to obtain the global relation,
3. invert to obtain a representation of the solution that depends on unknown boundary data,
4. determine the symmetries $\nu_j(k)$ of $W(k)$,
5. determine where the global relations with $k \to \nu_j(k)$ are valid in $\mathbb{C}$,
6. if necessary, deform integral paths of the boundary terms appropriately,

7. *if necessary, determine additional boundary conditions from the PDE*,
8. *appropriately discretize boundary conditions*,
9. solve for unknowns using global relations with $k \to \nu_j(k)$ and time transforms of discretized boundary conditions, and
10. check integral terms involving $\hat{q}(\nu_j, T)$ vanish, resulting in the solution representation depending only on known quantities.

With the SD-UTM, we propose the notion of "natural" discretizations, which reduce the variety of stencils down to those that are compatible with the IBVP. The (not necessarily unique) natural discretization is (i) of the same order as the spatial order of the PDE, (ii) not purely one sided (except for first-order problems), and (iii) one that optimally aligns with the available boundary conditions. Once the PDE is discretized, it follows that the available discretizations for any derivative boundary conditions are dictated by the global relation and its validity under the symmetries $\nu_j(k)$, as we will see with second-order IBVPs containing Neumann data and third-order IBVPs.

1.4 Organization of the Dissertation

The majority of this dissertation presents the SD-UTM through examples of several linear semi-discretized IBVPs on the half-line and the finite interval following Steps (1) - (10) from Section 1.3. Chapter 2 focuses on first and second-order *half-line* problems, Chapter 3 on first and second-order *finite-interval* problems, and Chapter 4 on *third-order* problems on both the half line and finite interval. For each of these chapters, the first few concrete examples are followed by higher-order discretizations where ghost points play a significant role. In some cases, specifically with these higher-order discretizations, the symmetries given from the semi-discrete dispersion relation are insufficient or cannot be used to eliminate unknowns (see Sections 2.1, 2.2, 3.1, and 3.2), so discretizations of boundary conditions must be appropriately used. We also show how to rewrite the SD-UTM solution formulas as series when possible, which are more suitable for numerical computations than the integral representations.

In Chapter 5, we derive analytic continuation formulas that are valid at ghost points for several SD-UTM solutions. Lastly, Chapter 6 presents the split-step finite-difference method that uses analytic continuation formulas from the UTM to solve nonlinear problems, specifically the nonlinear Schrödinger equation on the finite interval.

Chapter 2

HALF-LINE PROBLEMS

We briefly discuss the difficulties of numerically computing the solution to half-line IBVPs via finite-difference schemes. Conventionally, we truncate the half-line problem $x \in [0, \infty)$ to a finite-interval problem $x \in [0, \tilde{L}]$, where $\tilde{L} \in \mathbb{R}$ is a large positive constant, so that the artificial numerical boundary is far from the domain of interest $x \in [0, L]$. At the artificial boundary $x = \tilde{L}$, we can apply, say, decaying boundary conditions that are compatible with the given initial condition. Now, the half-line IBVP is recast as a finite-interval problem and the usual finite-difference tactics can be applied. This approach heavily relies on $\tilde{L} \gg L$, so that contributions from the artificial boundary do not interfere with the window of interest. For dispersive problems, the effect of a tail slowly approaches zero, and $\tilde{L}$ might have to be prohibitively large, increasing the computational cost to produce an accurate solution.

An alternative is to apply "absorbing" conditions at the artificial boundary $x = \hat{L} < \tilde{L}$ that allow propagation of energy out of the domain of interest, but not into it. Such conditions can be handled by introducing sponge or dissipation layers for $L < x < \hat{L}$, in which the same equations are solved but with additional dissipation terms to absorb energy, or by devising special boundary conditions that allow energy to exit the domain with minimal reflections, like a one-way wave equation specific to the original IBVP. The first approach is more general than the second, but may still require a dense grid, while one-way wave conditions can introduce approximation errors in addition to those from the discretization errors [22, 53, 66]. For these reasons, we do not compare the half-line semi-discrete UTM solutions with traditional windowing finite-difference methods. Instead, we only compare with exact solutions. Although not shown, second-order problem solutions are derived using classical methods, written out in terms of error functions that are computed with built-in MATLAB routines.

2.1 Advection Equations

To start, we discuss advection equations in some detail, as a way to demonstrate the UTM applied to semi-discrete problems. At the same time, this will allow us to fix notation and to illustrate the types of numerical experiments we use throughout the paper.

2.1.1 *Forward Discretization of* $q_t = c\,q_x$

We start with the continuous problem on the half-line for the advection equation $q_t = c\,q_x$ with wave-speed $c > 0$:

$$\begin{cases} q_t = c\,q_x, & x > 0,\ t > 0, \\ q(x,0) = \phi(x), & x > 0. \end{cases} \tag{2.1.1}$$

For well posedness, the IBVP requires only the initial condition and no boundary data. Since information travels from right to left, it is well known that the forward discretization of $q_x(x,t)$ together with a forward discretization of $q_t(x,t)$ is a "natural" discretization, known as the upwind method. Such a method performs well for this advection equation with periodic boundary conditions or on the whole real line with $\lim_{x\to\pm\infty} q(x,t) = 0$. Let us implement this forward spacial discretization. We consider

$$\dot{q}_n(t) = c\,\frac{q_{n+1}(t) - q_n(t)}{h}, \tag{2.1.2}$$

followed by using the semi-discrete version of the UTM to *exactly* solve this system of ODEs, instead of a time-stepping method to *approximately* (because of the time discretization) solve the system. As in the continuous UTM, the local relation is determined by writing the problem into its divergence form. For this semi-discrete problem, we replace ∂_x with the shift operator ΔQ_n, and (2.1.2) is rewritten as

$$\partial_t \left(e^{-iknh} e^{Wt} q_n \right) = \frac{c}{h} \Delta \left(e^{-ik(n-1)h} e^{Wt} q_n \right), \tag{2.1.3}$$

with dispersion relation

$$W(k) = c\,\frac{1 - e^{ikh}}{h}. \tag{2.1.4}$$

The symmetries of a dispersion relation are those transformations $k \to \nu(k)$ that leave $W(k)$ invariant, *i.e.*, $W(\nu) = W(k)$. Using the substitution $z = e^{ikh}$, the fundamental theorem of algebra guarantees the existence of these symmetries. Here, (2.1.4) only has the trivial symmetry $\nu_0(k) = k$ up to periodic copies due to the complex exponential. From the local relation (2.1.3), we obtain the global relation by taking a time transform over $t \in [0,T]$ and an infinite sum from $n = 0$ (because $q_0(t)$ is not known):

$$\begin{aligned} & \sum_{n=0}^{\infty} h \int_0^T \left[\partial_t \left(e^{-iknh} e^{Wt} q_n \right) - \frac{c}{h} \Delta \left(e^{-ik(n-1)h} q_n \right) e^{Wt} \right] dt = 0 \\ \Rightarrow \quad & \sum_{n=0}^{\infty} h \left[e^{-iknh} e^{WT} q_n(T) - e^{-iknh} q_n(0) - \frac{c}{h} \Delta \left(e^{-ik(n-1)h} f_n \right) \right] = 0 \\ \Rightarrow \quad & e^{WT} \hat{q}(k,T) - \hat{q}(k,0) + c e^{ikh} f_0 = 0, \end{aligned} \tag{2.1.5}$$

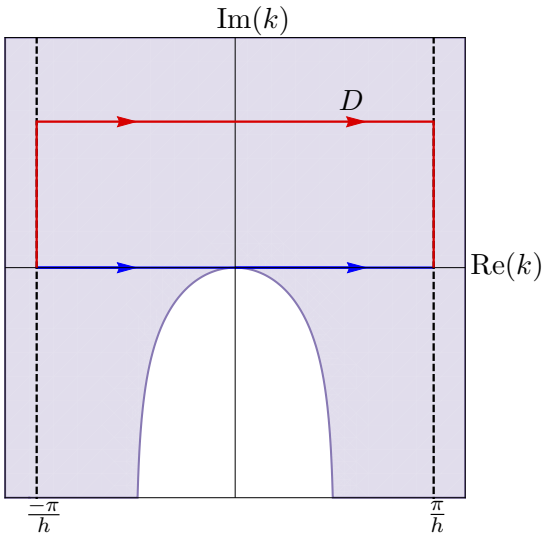

Figure 2.1.1: The shaded regions depict where $\mathrm{Re}(-W) \leq 0$ and e^{-WT} is bounded with the dispersion relation (2.1.4).

valid for $\mathrm{Im}(k) \leq 0$ due to the discrete Fourier transform terms. Solving for $\hat{q}(k,T)$ and inverting the inverse transform,

$$q_n(T) = \frac{1}{2\pi}\int_{-\pi/h}^{\pi/h} e^{iknh}e^{-WT}\hat{q}(k,0)\,dk - \frac{c}{2\pi}\int_{-\pi/h}^{\pi/h} e^{ik(n+1)h}e^{-WT}f_0\,dk. \tag{2.1.6}$$

The integrand in the first term is defined for $\mathrm{Im}(k) \leq 0$, while the integrand in the second term is defined for all $k \in \mathbb{C}$. We refer to the expression above as the "solution," since $f_0(W,T)$ in the second integral term is unknown. For all $n \in \mathbb{N}$, $e^{ik(n+1)h}$ decays in the upper half-plane and e^{-WT} is bounded in the shaded regions, including the boundary, of Figure 2.1.1. The shaded region denotes where $\mathrm{Re}(-W) \leq 0$. Figure 2.1.1 also shows the integration path for "solution" (2.1.6) from $-\pi/h$ to π/h on the real line. Note that the sign of c is essential in determining the location of the region of exponential growth of the integrand, *i.e.*, the white region in Figure 2.1.1.

We use two approaches to address the unwanted boundary integral term in "solution" (2.1.6). The first approach is more straightforward, but is not as general as the second approach. In both, we substitute the definition of $f_0(W,T)$ in order to collect the k dependence:

$$\frac{c}{2\pi}\int_{-\pi/h}^{\pi/h} e^{ik(n+1)h}e^{-WT}f_0\,dk = \frac{c}{2\pi}\int_{-\pi/h}^{\pi/h} e^{ik(n+1)h}e^{-WT}\left[\int_0^T e^{Wt}q_0(t)\,dt\right]dk = \int_0^T A(n,T-t)q_0(t)\,dt,$$

with $T - t > 0$ and

$$A(n,T) = \frac{c}{2\pi}\int_{-\pi/h}^{\pi/h} e^{ik(n+1)h}e^{-WT}\,dk.$$

(i) The first approach uses the transformation $z = e^{ikh}$:

$$A(n,T) = \frac{c}{2\pi i h} \oint_{|z|=1} z^n \exp\left[-\left(\frac{1-z}{h}\right)(T-t)\right] dz = 0,$$

by analyticity of the integrand for all n. Hence,

$$\frac{c}{2\pi} \int_{-\pi/h}^{\pi/h} e^{ik(n+1)h} e^{-WT} f_0 \, dk = 0.$$

(ii) The second approach deforms the integration path of $A(n,T)$ away from the real line. Consider $R > 0$. We define the line segment

$$D = \left\{ k \in \mathbb{C} \,\middle|\, \frac{-\pi}{h} \le \mathrm{Re}(k) \le \frac{\pi}{h} \text{ and } \mathrm{Im}(k) = R \right\}$$

with left-to-right orientation. Thus, D is a horizontal straight-line path above the real line, from $k = -\pi/h + iR$ to $k = \pi/h + iR$. Next, we introduce a closed contour that consists of four straight segments: the original real-line path, the new path D, and two vertical segments that connect the endpoints of the real-line path with those of D, as illustrated in Figure 2.1.1. The contribution to the integral from these vertical paths cancel due to periodicity. Hence,

$$A(n,T) = \frac{c}{2\pi} \int_D e^{ik(n+1)h} e^{-W(T-t)} \, dk,$$

by Cauchy's Theorem. Taking $R \to \infty$ implies taking $\mathrm{Im}(k) \to \infty$ in the integrand. Because of the exponential decay above the real line, $A(n,T) = 0$ and

$$\frac{c}{2\pi} \int_{-\pi/h}^{\pi/h} e^{ik(n+1)h} e^{-WT} f_0 \, dk = 0.$$

It follows that the solution to the half-line IBVP with the forward discretization (2.1.2) depends only on the initial condition:

$$q_n(T) = \frac{1}{2\pi} \int_{-\pi/h}^{\pi/h} e^{iknh} e^{-WT} \hat{q}(k,0) \, dk. \tag{2.1.7}$$

For reference, we solve the IBVP (2.1.1) using the continuous UTM, following the Steps (1) – (8) from Section 1.2. Briefly, we find the dispersion relation $\tilde{W}(k) = -cik$, with only the trivial symmetry $\tilde{\nu}_0(k) = k$, and the global relation

$$\hat{q}(k,0) - e^{\tilde{W}T} \hat{q}(k,T) + cF_0 = 0, \quad \mathrm{Im}(k) \le 0,$$

where

$$\hat{q}(k,t) = \int_0^\infty e^{-ikx} q(x,t) \, dx, \quad \mathrm{Im}(k) \le 0,$$

and

$$F_j(\tilde{W},T) = \int_0^T e^{\tilde{W}t}\left.\frac{\partial^j q}{dx^j}\right|_{x=0} dt, \quad k \in \mathbb{C}.$$

After inverting the transform and showing there is no dependence on $F_0(\tilde{W},T)$, the solution representation is

$$q(x,T) = \frac{1}{2\pi}\int_{-\infty}^{\infty} e^{ikx}e^{-\tilde{W}T}\hat{q}(k,0)\,dk. \tag{2.1.8}$$

Taking the limit as $h \to 0$ of (2.1.7), we recover (2.1.8) from the continuous problem, where the limits of integration approach $\pm\infty$ at rate $1/h$. Also, $\lim_{h\to 0} W(k) = -cik = \tilde{W}(k)$.

As an explicit example, we compute the numerical solution to the IBVP

$$\begin{cases} q_t = q_x, & x > 0,\ t > 0, \\ q(x,0) = \phi(x) = \frac{1}{2}\left[e^{-2x}\left(\sin(4\pi x)+1\right)\right], & x > 0. \end{cases} \tag{2.1.9}$$

The exact (continuous) solution is given by $q(x,T) = \phi(x+T)$, while the semi-discrete solution is obtained from the representation (2.1.7) with the standard forward discretization stencil. Figure 2.1.2 shows the semi-discrete solution $q_n(T)$ (left panel) and a log-log error plot (right panel) of the ∞-norm of $q_n(0.5) - q(x_n, 0.5)$, as a function of h.

From the stencil (2.1.2), we know (2.1.7) is a first-order accurate approximation to the solution $q(x,T)$ of the IBVP (2.1.1). We can reveal more information about the behavior and structure of this approximate solution by determining its modified equation [43, 71]. Suppose $q_n(t)$ exactly solves a PDE with dependent variable $p(x,t)$, such that $q_n(t) \equiv p\,(x_n,t)$. Substituting this assumption into the forward stencil (2.1.2) and Taylor-series expanding terms gives

$$\begin{aligned} \dot{q}_n(t) &= \frac{c}{h}\left[q_{n+1}(t) - q_n(t)\right] \\ \Rightarrow \quad p_t(x_n,t) &= \frac{c}{h}\left[p(x_n+h,t) - p(x_n,t)\right] \\ &= \frac{c}{h}\left[p(x_n,t) + p_x(x_n,t)h + \frac{p_{xx}(x_n,t)}{2!}h^2 + \frac{p_{xxx}(x_n,t)}{3!}h^3 + \mathcal{O}\left(h^4\right) - p(x_n,t)\right] \\ p_t &= c\,p_x + \frac{c\,p_{xx}}{2}h + \frac{c\,p_{xxx}}{6}h^2 + \mathcal{O}\left(h^3\right). \end{aligned}$$

Keeping up to the $\mathcal{O}(h)$ term, we find that (2.1.7) is a second-order accurate solution approximation to the advection-diffusion PDE

$$p_t = c\,p_x + \frac{c\,h}{2}p_{xx}, \tag{2.1.10}$$

so we expect solution profiles of (2.1.7) to travel at the correct speed c, while dissipating in time. Since $c > 0$, the diffusion coefficient $c\,h/2$ is positive. If we allow $c < 0$ or if we apply the same forward stencil to the PDE $q_t = -a\,q_x$ with $a > 0$, we obtain a similar convection-diffusion modified PDE like above, except with a negative diffusion coefficient that presents an ill-posed problem with

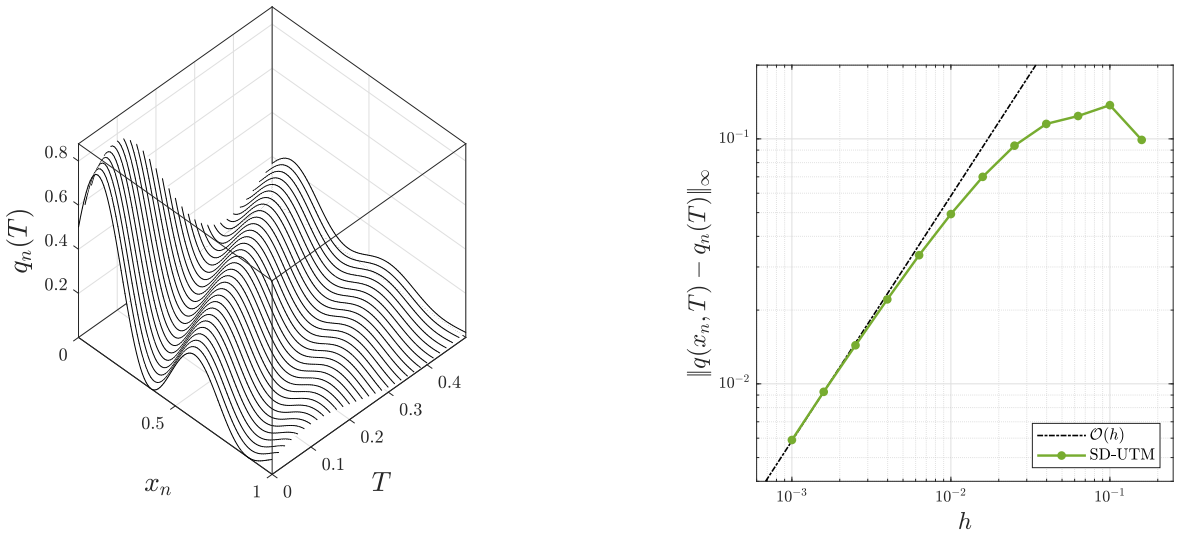

(a) (b)

Figure 2.1.2: (a) The semi-discrete solution (2.1.7) evaluated at various T with $h = 0.01$. (b) Error plot of the semi-discrete solution (2.1.7) relative to the exact solution as $h \to 0$ with $T = 0.5$.

exponentially growing solutions. The solution plot 2.1.2a displays the expected shift to the left as time progresses. For this advection equation, the solution approaches zero as $t \to \infty$, because $q(x, 0)$ decays as $x \to \infty$. Since the dissipation term is $\mathcal{O}(h)$, refining the mesh easily reduces this artificial dissipation. The error plot displays $\mathcal{O}(h)$ convergence as $h \to 0$.

Remark 2.1.1. All forward discretizations produce $f_j(W, T)$ terms with a coefficient $C_j\, e^{i\gamma_j kh}$ for some $C_j \in \mathbb{C}$ and $\gamma_j \in \mathbb{N}$. Coupled with polynomial dispersion relations $W(z)$, we can remove all integral terms containing any $f_j(W, T)$ from "solutions" using the steps above. Thus, if we solve the IBVP (2.1.1) without boundary conditions using a purely forward higher-order stencil, we find (2.1.7) as the solution, except with a different dispersion relation $W(k)$.

2.1.2 Backward Discretization of $q_t = -c\, q_x$

Next, we consider

$$\begin{cases} q_t = -c\, q_x, & x > 0,\ t > 0, \\ q(x, 0) = \phi(x), & x > 0, \\ q(0, t) = u(t), & t > 0, \end{cases} \tag{2.1.11}$$

with $c > 0$. For well posedness, the IBVP requires a Dirichlet boundary condition at $x = 0$. Since a forward discretization (2.1.2) for $q_t = c\, q_x$ was appropriate, we now apply a backward discretization to the spacial derivative q_x, resulting in

$$\dot{q}_n(t) = -c\left(\frac{q_n(t) - q_{n-1}(t)}{h}\right) = c\,\frac{q_{n-1}(t) - q_n(t)}{h}. \tag{2.1.12}$$

Following similar steps as before, the local relation is

$$\partial_t\left(e^{-iknh}e^{Wt}q_n\right) = \frac{-c}{h}\Delta\left(e^{-iknh}e^{Wt}q_{n-1}\right), \tag{2.1.13}$$

with dispersion relation

$$W(k) = c\,\frac{1 - e^{-ikh}}{h}. \tag{2.1.14}$$

As before, we only have the trivial symmetry $\nu_0(k) = k$, up to periodic copies. This time, the IBVP (2.1.11) contains a Dirichlet boundary condition, providing information at $n = 0$, so we define the forward transform as

$$\hat{q}(k,t) = h\sum_{n=1}^{\infty} e^{-iknh}q_n(t),$$

starting at $n = 1$. To obtain the global relation, we proceed as before:

$$\begin{aligned}\sum_{n=1}^{\infty} h\int_0^T \left[\partial_t\left(e^{-iknh}e^{Wt}q_n\right) + \frac{c}{h}\Delta\left(e^{-iknh}e^{Wt}q_{n-1}\right)\right]dt = 0 \\ \Rightarrow \qquad e^{WT}\hat{q}(k,T) - \hat{q}(k,0) - ce^{-ikh}f_0 = 0,\end{aligned} \tag{2.1.15}$$

valid for $\mathrm{Im}(k) \le 0$. Solving for $\hat{q}(k,T)$ and inverting, we obtain

$$q_n(T) = \frac{1}{2\pi}\int_{-\pi/h}^{\pi/h} e^{iknh}e^{-WT}\hat{q}(k,0)\,dk + \frac{c}{2\pi}\int_{-\pi/h}^{\pi/h} e^{ik(n-1)h}e^{-WT}f_0\,dk. \tag{2.1.16}$$

Since e^{-WT} grows in the upper-half plane, see Figure 2.1.3, we cannot remove the dependence on $f_0(W,T)$ and, hence, (2.1.16) is the actual solution to the backward-discretized IBVP (2.1.11) with a given Dirichlet boundary condition.

Similar to the IBVP (2.1.1), we solve (2.1.11) using the continuous UTM. We find the dispersion relation $\tilde{W}(k) = cik$, with the trivial symmetry $\tilde{\nu}_0(k) = k$, and

$$q(x,T) = \frac{1}{2\pi}\int_{-\infty}^{\infty} e^{ikx}e^{-\tilde{W}T}\hat{q}(k,0)\,dk + \frac{c}{2\pi}\int_{-\infty}^{\infty} e^{ikx}e^{-\tilde{W}T}F_0\,dk. \tag{2.1.17}$$

It is clear that (2.1.16) converges to the continuous solution (2.1.17), where

$$\lim_{h\to 0} f_j(W,T) = \lim_{h\to 0}\int_0^T e^{Wt}q(jh,t)\,dt = \int_0^T e^{\tilde{W}t}q(0,t)\,dt = F_0(\tilde{W},T),$$

for any fixed j, $\lim_{h\to 0} W(k) = \tilde{W}(k)$, and $\lim_{h\to 0} e^{ik(n-1)h} = e^{ikx}$ with $\lim_{h\to 0} nh = x$.

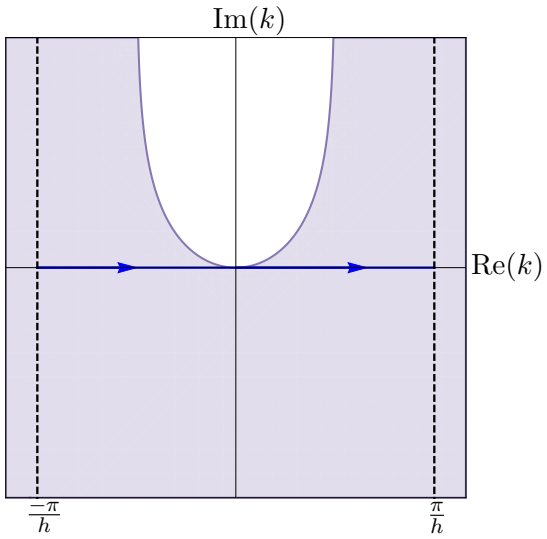

Figure 2.1.3: The shaded regions depict where $\mathrm{Re}(-W) \leq 0$ and e^{-WT} is bounded with the dispersion relation (2.1.14).

As an example, we examine the IBVP

$$\begin{cases} q_t = -q_x, & x > 0,\ t > 0, \\ q(x,0) = \phi(x) = e^{-x}\sin(4\pi x), & x > 0, \\ q(0,t) = u(t) = -\sin(4\pi t), & t > 0, \end{cases} \tag{2.1.18}$$

where the continuous solution is given by

$$q(x,t) = \begin{cases} u(t-x), & 0 < x < t, \\ \phi(x-t), & x > t. \end{cases}$$

Applying the semi-discrete solution (2.1.16) gives Figure 2.1.4, similar to Figure 2.1.2 for this IBVP, illustrating the qualitative behavior of the advection equation and the expected $\mathcal{O}(h)$ error as $h \to 0$. Since we are using a purely-one sided stencil, the standard backward stencil, we expect the solution to be better approximated near $x = 0$ and less so for larger x. From the stencil (2.1.12), we find the convection-diffusion PDE $p_t = -c\,p_x + (ch/2)p_{xx}$ as its modified PDE. Like (2.1.10), this modified equation is approximately solved by the semi-discrete solution with second-order accuracy. The presence of the dissipative term implies (2.1.16) advects the initial and boundary data at the appropriate speed, but with $\mathcal{O}(h)$ damping as time progresses. Indeed, Figure 2.1.5 displays the dissipation present in the stencil, manifested in its modified PDE, away from the boundary with a series of plots for various T and $h = 0.004$.

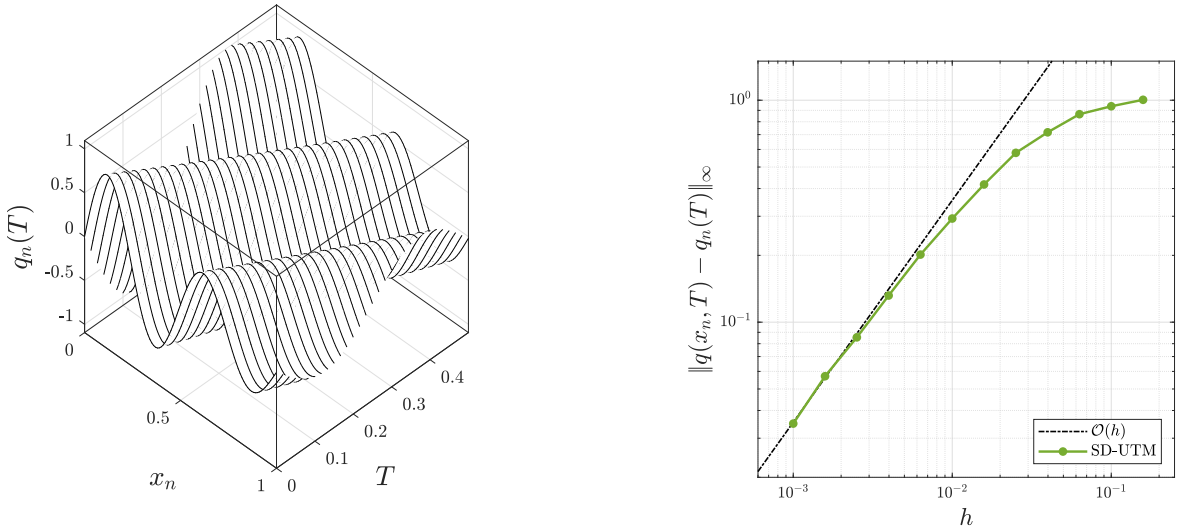

(a) (b)

Figure 2.1.4: (a) The semi-discrete solution (2.1.16) evaluated at various T with $h = 0.01$. (b) Error plot of the semi-discrete solution (2.1.16) relative to the exact solution as $h \to 0$ with $T = 0.5$.

2.1.3 Centered Discretization of $q_t = -c\, q_x$

We consider the same problem as in Section 2.1.2, but using the standard centered discretization:

$$\dot{q}_n(t) = -c \left(\frac{q_{n+1}(t) - q_{n-1}(t)}{2h} \right). \tag{2.1.19}$$

With slightly more work, the local relation is

$$\partial_t \left(e^{-iknh} e^{Wt} q_n \right) = \frac{-c}{2h} \Delta \left(e^{-iknh} e^{Wt} q_{n-1} + e^{-ik(n-1)h} e^{Wt} q_n \right), \tag{2.1.20}$$

with dispersion relation

$$W(k) = c\, \frac{e^{ikh} - e^{-ikh}}{2h} = \frac{-c \sin(kh)}{ih}. \tag{2.1.21}$$

In this case, the dispersion relation has the trivial symmetry $\nu_0 = k$ and one nontrivial symmetry

$$\nu_1(k) = -k - \frac{\pi}{h},$$

up to periodic copies. Since we have information at $q(0,t) \equiv q_0(t)$, we take an infinite sum starting at $n = 1$ and a time transform to obtain the global relation as

$$e^{WT} \hat{q}(k,T) - \hat{q}(k,0) - c \left[\frac{e^{-ikh} f_0 + f_1}{2} \right] = 0, \quad \mathrm{Im}(k) \le 0. \tag{2.1.22}$$

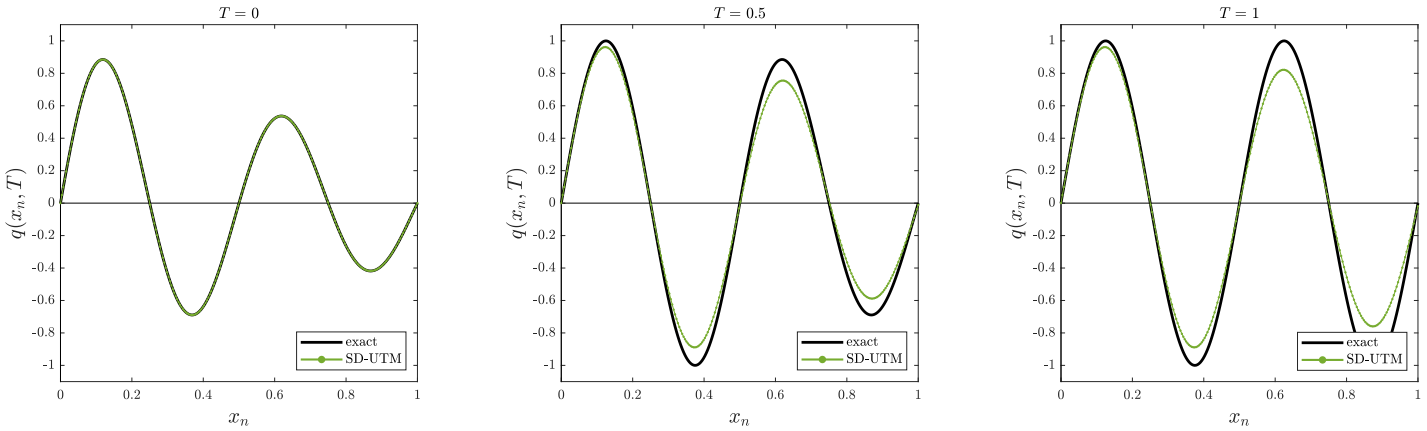

Figure 2.1.5: Several time slices for the solution to IBVP (2.1.18) with $h = 0.004$.

Taking the inverse transform, we obtain the "solution"

$$q_n(T) = \frac{1}{2\pi}\int_{-\pi/h}^{\pi/h} e^{iknh}e^{-WT}\hat{q}(k,0)\,dk + \frac{c}{2\pi}\int_{-\pi/h}^{\pi/h} e^{iknh}e^{-WT}\left[\frac{e^{-ikh}f_0 + f_1}{2}\right]dk. \tag{2.1.23}$$

"Solution" (2.1.23) contains the unknown $f_1(W,T)$, but as seen in Figure 2.1.6, we cannot deform off the real line to remove this dependence as we did with one-sided discretization stencils. Nonetheless, the global relation (2.1.22) with $k \to \nu_1(k)$ is valid for $\mathrm{Im}\,(\nu_1) \le 0$, *i.e.*, $\mathrm{Im}(k) \ge 0$, and can be used to remove the unknown without the need to deform. Replacing $k \to \nu_1$ in the global relation (2.1.22) and substituting

$$f_{-1} = -e^{-i\nu_1 h}f_0 + \frac{2}{c}\left[e^{WT}\hat{q}\,(\nu_1,T) - \hat{q}\,(\nu_1,0)\right], \quad \mathrm{Im}(k) \ge 0,$$

in the "solution" (2.1.23), we find

$$\begin{aligned} q_n(T) = {} & \frac{1}{2\pi}\int_{-\pi/h}^{\pi/h} e^{iknh}e^{-WT}\hat{q}(k,0)\,dk + \frac{1}{2\pi}\int_{-\pi/h}^{\pi/h} e^{iknh}e^{-WT}\left[c\,\cos(kh)\,f_0 - \hat{q}\,(\nu_1,0)\right]dk \\ & + \frac{1}{2\pi}\int_{-\pi/h}^{\pi/h} e^{iknh}\hat{q}\,(\nu_1,T)\,dk, \end{aligned} \tag{2.1.24}$$

after simplification.

Removing one unknown from the "solution," we have introduced another, $\hat{q}\,(\nu_1,T)$, a transform of the solution at time T. It is crucial to point out that this last integral term does not have the exponential factor e^{-WT}. We can eliminate $\hat{q}\,(\nu_1,T)$ from our "solution" as in the continuous UTM, or determine its contribution if it is nonzero. To do so, we substitute the definition of the transform into the integral term:

$$\frac{1}{2\pi}\int_{-\pi/h}^{\pi/h} e^{iknh}\hat{q}\,(\nu_1,T)\,dk = \frac{1}{2\pi}\int_{-\pi/h}^{\pi/h} e^{iknh}\left[h\sum_{m=1}^{\infty} e^{-i\nu_1 mh}q_m(T)\right]dk = \sum_{m=1}^{\infty}(-1)^m C(n+m)q_m(T),$$

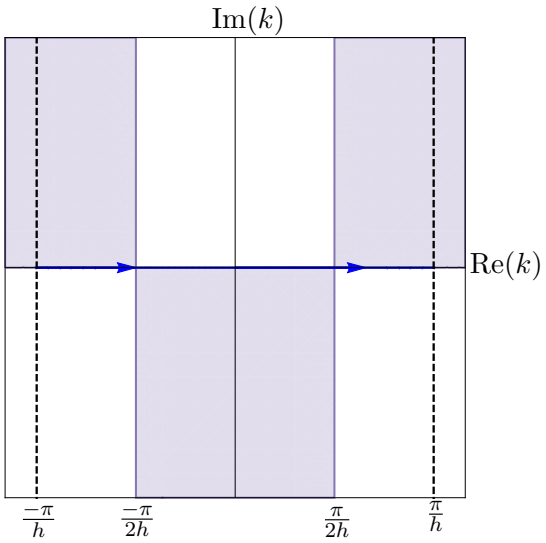

Figure 2.1.6: The shaded regions depict where $\mathrm{Re}(-W) \leq 0$ and e^{-WT} is bounded with the dispersion relation (2.1.21).

where

$$C(n) = \frac{h}{2\pi} \int_{-\pi/h}^{\pi/h} e^{iknh}\, dk.$$

Applying the first approach from Subsection 2.1.1 implies that for $n > 0$, $C(n) = 0$ via periodicity,

$$\frac{1}{2\pi} \int_{-\pi/h}^{\pi/h} e^{iknh} \hat{q}\left(\nu_1, T\right)\, dk = 0.$$

Therefore, the solution to the centered-discretized advection equation $q_t = -c\, q_x$ on the half-line with a Dirichlet boundary condition is

$$q_n(T) = \frac{1}{2\pi} \int_{-\pi/h}^{\pi/h} e^{iknh} e^{-WT} \hat{q}(k,0)\, dk + \frac{1}{2\pi} \int_{-\pi/h}^{\pi/h} e^{iknh} e^{-WT} \left[c\, \cos\left(kh\right) f_0 - \hat{q}\left(\nu_1, 0\right)\right]\, dk. \quad (2.1.25)$$

From the stencil (2.1.19), we find the modified PDE $p_t = -c\, p_x - (ch^2/6) p_{xxx}$, preserving the correct advection speed, but including a dispersive term. Hence, the solution profiles disperse as time progresses. Since the dispersion coefficient is $\mathcal{O}\left(h^2\right)$, these effects are minimal for practical $h \ll 1$.

The continuum limit of this semi-discrete solution is less straightforward than the continuum limit of the backward-discretized solution (2.1.16). The dispersion relation converges to the continuous one: $\lim_{h \to 0} W(k) = \tilde{W}(k)$. It is clear that the first integral term in the semi-discrete solution (2.1.25) converges to the first integral term in the continuous solution (2.1.17). Since

$\lim_{h\to 0}\cos(kh)=1$, the boundary component in the discrete solution also converges to its continuous counterpart.

The solution to the continuous problem requires no additional symmetries, so we expect the integral term containing $\hat{q}\,(\nu_1,0)$ to vanish. Note that

$$\hat{q}\,(\nu_1,t)=h\sum_{m=1}^{\infty}e^{-i\nu_1 mh}q_m(t)=h\sum_{m=1}^{\infty}(-1)^m e^{ikmh}q_m(t)=-h\sum_{u=1}^{\infty}e^{2ikuh}q_{2u}(t)+h\sum_{v=0}^{\infty}e^{(2v+1)ikh}q_{2v+1}(t),$$

after separating the even and odd indexed terms. Similar to $x_n=nh$, we introduce dummy variables $w_u=uh$ and $y_v=vh$, so that

$$\begin{aligned}\lim_{h\to 0}\hat{q}\,(\nu_1,t)&=-\lim_{h\to 0}h\sum_{u=1}^{\infty}e^{2ikuh}q_{2u}(t)+\lim_{h\to 0}h\sum_{v=0}^{\infty}e^{2ikvh}e^{ikh}q_{2v+1}(t)\\&=-\int_0^{\infty}e^{2ikw}q(2w,t)\,dw+\int_0^{\infty}e^{2iky}q(2y,t)\,dy=0.\end{aligned}$$

Thus,

$$\lim_{h\to 0}\frac{-1}{2\pi}\int_{-\pi/h}^{\pi/h}e^{iknh}e^{-WT}\hat{q}\,(\nu_1,0)\;dk=0,$$

and we recover the continuous solution (2.1.17).

2.1.4 Higher-Order One-Sided Discretization of $q_t=-c\,q_x$

There exist higher-order discretizations that appropriately incorporate the nontrivial symmetries to remove unknowns, where the steps in the semi-discrete UTM become more intricate and tedious, yet remain systematic. In some cases, however, the nontrivial symmetries are unusable, but a solution can still be obtained. Consider the second-order discretized advection equation

$$\dot{q}_n(t)=-c\left(\frac{q_{n-2}(t)-4q_{n-1}(t)+3q_n(t)}{2h}\right). \tag{2.1.26}$$

Following the usual steps, the global relation is

$$e^{WT}\hat{q}(k,T)-\hat{q}(k,0)-c\left(\frac{4e^{-ikh}f_0-e^{-2ikh}f_0-e^{-ikh}f_{-1}}{2}\right)=0,\quad \mathrm{Im}(k)\le 0, \tag{2.1.27}$$

with dispersion relation

$$W(k)=c\,\frac{e^{-2ikh}-4e^{-ikh}+3}{2h}, \tag{2.1.28}$$

and nontrivial symmetry

$$\nu_1(k)=\frac{i}{h}\ln\left(4-e^{-ikh}\right).$$

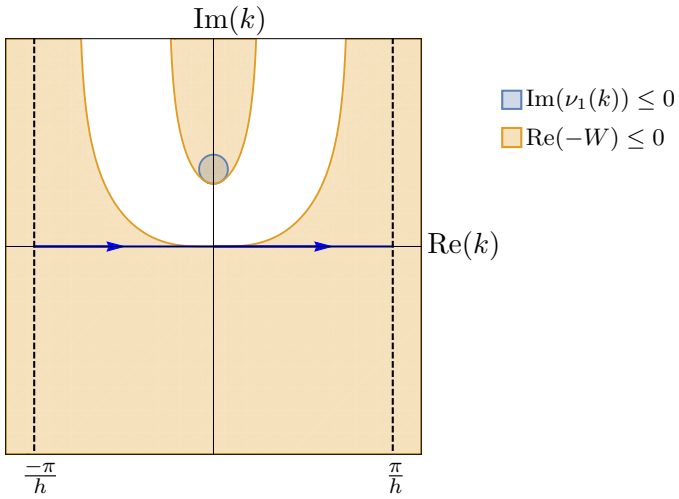

Figure 2.1.7: The blue shaded region denotes where the global relation (2.1.27) is valid with $k \to \nu_1(k)$ and the orange shaded regions depict where $\mathrm{Re}(-W) \le 0$ and e^{-WT} is bounded with the dispersion relation (2.1.28).

Solving for $\hat{q}(k,T)$ and taking the inverse transform, we obtain

$$\begin{aligned} q_n(T) = \frac{1}{2\pi}\int_{-\pi/h}^{\pi/h} e^{iknh} e^{-WT}\hat{q}(k,0)\,dk \\ + \frac{c}{2\pi}\int_{-\pi/h}^{\pi/h} e^{iknh} e^{-WT}\left(\frac{4e^{-ikh}f_0 - e^{-2ikh}f_0 - e^{-ikh}f_{-1}}{2}\right) dk. \end{aligned} \tag{2.1.29}$$

With the given Dirichlet boundary condition, we encounter the ghost point $f_{-1}(W,T)$, which is unknown. The global relation (2.1.27) is valid in the blue shaded region of Figure 2.1.7 with $k \to \nu_1(k)$, but since the path on the real line cannot be deformed to this region, the nontrivial symmetry cannot be used to eliminate the unknown $f_{-1}(W,T)$. Instead, we return to the continuous problem (2.1.11), where the PDE itself gives the Neumann boundary condition from the Dirichlet condition:

$$q_x(0,t) = \frac{-1}{c}\,q_t(0,t) = \frac{-1}{c}\,\frac{\partial}{\partial t}q(0,t) = \frac{-u'(t)}{c} = \frac{-v(t)}{c}, \quad v(t) = u'(t). \tag{2.1.30}$$

To maintain the same order of accuracy as (2.1.26), we discretize the Neumann condition using the standard centered stencil:

$$\begin{aligned} &\frac{q_1(t) - q_{-1}(t)}{2h} = \frac{-v(t)}{c} \\ \Rightarrow \qquad &\frac{f_1 - f_{-1}}{2h} = \frac{-V}{c}, \qquad V(W,T) = \int_0^T e^{Wt}v(t)\,dt. \end{aligned} \tag{2.1.31}$$

Doing so, we have introduced data $f_1(W,T)$ at another unknown point, so we require an additional equation. Again from the PDE and (2.1.30), we know the second spacial derivative at $x = 0$:

$$q_{xx}(0,t) = \left(\frac{-q_t(0,t)}{c}\right)_x = \left(\frac{-q_x(0,t)}{c}\right)_t = \left(\frac{v(t)}{c^2}\right)_t = \frac{\tilde{v}(t)}{c^2}, \quad \tilde{v}(t) = u''(t).$$

Keeping the same order of accuracy as (2.1.26) and (2.1.31), the centered approximation to $q_{xx}(0,t)$ gives

$$\begin{aligned} &\frac{q_1(t) - 2q_0(t) + q_{-1}(t)}{h^2} = \frac{\tilde{v}(t)}{c^2} \\ \Rightarrow \qquad &\frac{f_1 - 2f_0 + f_{-1}}{h^2} = \frac{\tilde{V}}{c}, \qquad \tilde{V}(W,T) = \int_0^T e^{Wt}\tilde{v}(t)\,dt. \end{aligned} \tag{2.1.32}$$

Using (2.1.31) and (2.1.32) to remove $f_{-1}(W,T)$ and $f_1(W,T)$ from (2.1.29) gives the second-order accurate solution

$$\begin{aligned} q_n(T) = &\frac{1}{2\pi}\int_{-\pi/h}^{\pi/h} e^{iknh}e^{-WT}\hat{q}(k,0)\,dk + \frac{c}{2\pi}\int_{-\pi/h}^{\pi/h} e^{iknh}e^{-WT}\left[\left(\frac{3e^{-ikh} - e^{-2ikh}}{2}\right)f_0\right]dk \\ &- \frac{1}{2\pi}\int_{-\pi/h}^{\pi/h} e^{ik(n-1)h}e^{-WT}\left(\frac{h}{2}V + \frac{h^2}{4}\tilde{V}\right)dk. \end{aligned} \tag{2.1.33}$$

As before, as $h \to 0$, the semi-discrete solution (2.1.33) converges to (2.1.17). The semi-discrete solution correctly loses dependence on the Neumann and second derivative boundary conditions in the continuum limit, with $\mathcal{O}(h)$ and $\mathcal{O}(h^2)$ leading coefficients, respectively.

Remark 2.1.2. Let us reconsider the backward discretization (2.1.12) with dispersion relation (2.1.14) and no nontrivial symmetries. With the forward transform $\hat{q}(k,t)$ starting at $n = 0$ instead of $n = 1$, we derive the global relation

$$e^{WT}\hat{q}(k,T) - \hat{q}(k,0) - cf_{-1} = 0, \quad \mathrm{Im}(k) \le 0, \tag{2.1.34}$$

with "solution"

$$q_n(T) = \frac{1}{2\pi}\int_{-\pi/h}^{\pi/h} e^{iknh}e^{-WT}\hat{q}(k,0)\,dk + \frac{c}{2\pi}\int_{-\pi/h}^{\pi/h} e^{iknh}e^{-WT}f_{-1}\,dk, \tag{2.1.35}$$

depending on $q_{-1}(t)$, which is not directly provided by the IBVP (2.1.11). As above, the advection equation itself gives the Neumann boundary condition (2.1.30) from the given Dirichlet condition and allows us to remove the dependence on $f_{-1}(W,T)$ in 2.1.35. Substituting (2.1.31), the solution is

$$\begin{aligned} q_n(T) = &\frac{1}{2\pi}\int_{-\pi/h}^{\pi/h} e^{iknh}e^{-WT}\hat{q}(k,0)\,dk + \frac{c}{2\pi}\int_{-\pi/h}^{\pi/h} e^{iknh}e^{-WT}f_0\,dk \\ &+ \frac{h}{2\pi}\int_{-\pi/h}^{\pi/h} e^{iknh}e^{-WT}V\,dk. \end{aligned} \tag{2.1.36}$$

In the continuum limit, the last integral term vanishes and we recover (2.1.17). Both (2.1.16) and (2.1.36) are solutions to the backward-discretized advection equation (2.1.12) with $q_0(t)$ data, but the transforms $\hat{q}(k,t)$ are defined differently by a shift in the starting index. Using the global relations (2.1.15) and (2.1.34), one can show that the solutions (2.1.16) and (2.1.36) are equal.

2.2 The Heat Equation

2.2.1 Centered Discretization of $q_t = q_{xx}$ with Dirichlet boundary condition

Consider the problem

$$\begin{cases} q_t = q_{xx}, & x > 0,\ t > 0, \\ q(x,0) = \phi(x), & x > 0, \\ q(0,t) = u(t), & t > 0, \end{cases} \tag{2.2.1}$$

with one Dirichlet boundary condition. We write the centered-discretized heat equation as

$$\dot{q}_n(t) = \frac{q_{n+1}(t) - 2q_n(t) + q_{n-1}(t)}{h^2}. \tag{2.2.2}$$

Carrying out similar steps as before, the local relation is

$$\partial_t \left(e^{-iknh} e^{Wt} q_n \right) = \frac{1}{h^2} \Delta \left(e^{-ik(n-1)h} e^{Wt} q_n - e^{-iknh} e^{Wt} q_{n-1} \right), \tag{2.2.3}$$

where

$$W(k) = \frac{2 - e^{ikh} - e^{-ikh}}{h^2} = \frac{2}{h^2} \left[1 - \cos(kh) \right], \tag{2.2.4}$$

with the nontrivial symmetry $\nu_1(k) = -k$ up to periodic copies. We find the global relation by summing from $n = 1$ and integrating in time:

$$e^{WT} \hat{q}(k,T) - \hat{q}(k,0) - \left[\frac{e^{-ikh} f_0 - f_1}{h} \right] = 0, \quad \mathrm{Im}(k) \le 0. \tag{2.2.5}$$

Inverting, we obtain the "solution" formula

$$q_n(T) = \frac{1}{2\pi} \int_{-\pi/h}^{\pi/h} e^{iknh} e^{-WT} \hat{q}(k,0)\, dk + \frac{1}{2\pi} \int_{-\pi/h}^{\pi/h} e^{iknh} e^{-WT} \left[\frac{e^{-ikh} f_0 - f_1}{h} \right] dk, \tag{2.2.6}$$

which depends on the unknown $f_1(W,T)$. Using $\nu_1(k)$ in the global relation (2.2.5) gives

$$f_1 = e^{ikh} f_0 - h \left[e^{WT} \hat{q}(-k,T) - \hat{q}(-k,0) \right], \quad \mathrm{Im}(k) \ge 0. \tag{2.2.7}$$

We substitute (2.2.7) into (2.2.6), so that

$$\begin{aligned} q_n(T) = {} & \frac{1}{2\pi} \int_{-\pi/h}^{\pi/h} e^{iknh} e^{-WT} \hat{q}(k,0)\, dk - \frac{1}{2\pi} \int_{-\pi/h}^{\pi/h} e^{iknh} e^{-WT} \left[\hat{q}(-k,0) + \frac{2i \sin(kh)}{h} f_0 \right] dk \\ & + \frac{1}{2\pi} \int_{-\pi/h}^{\pi/h} e^{iknh} \hat{q}(-k,T)\, dk. \end{aligned} \tag{2.2.8}$$

Removing the boundary term $f_1(W,T)$, we have introduced the transform of the solution at $t=T$ in the third integral of (2.2.8). Using the definition of the transform,

$$\frac{1}{2\pi}\int_{-\pi/h}^{\pi/h} e^{iknh}\hat{q}(-k,T)\,dk = \frac{1}{2\pi}\int_{-\pi/h}^{\pi/h} e^{iknh}\left[h\sum_{m=1}^{\infty} e^{ikmh}q_m(T)\right]dk = \sum_{m=1}^{\infty} q_m(T)\left[\frac{h}{2\pi}\int_{-\pi/h}^{\pi/h} e^{ik(n+m)h}\,dk\right].$$

For $n>0$, the integral vanishes due to periodicity, so that

$$\frac{1}{2\pi}\int_{-\pi/h}^{\pi/h} e^{iknh}\hat{q}(-k,T)\,dk = 0,$$

and the solution to (2.2.2) with the Dirichlet boundary condition is written as

$$q_n(T) = \frac{1}{2\pi}\int_{-\pi/h}^{\pi/h} e^{iknh}e^{-WT}\hat{q}(k,0)\,dk - \frac{1}{2\pi}\int_{-\pi/h}^{\pi/h} e^{iknh}e^{-WT}\left[\hat{q}(-k,0)+\frac{2i\sin(kh)f_0}{h}\right]dk. \tag{2.2.9}$$

Solving the IBVP (3.2.1) via the continuous UTM gives the dispersion relation $\tilde{W}(k)=k^2$ with nontrivial symmetry $\tilde{\nu}_1(k)=-k$ [17]. The solution is

$$q(x,T) = \frac{1}{2\pi}\int_{-\infty}^{\infty} e^{ikx}e^{-\tilde{W}T}\hat{q}(k,0)\,dk - \frac{1}{2\pi}\int_{-\infty}^{\infty} e^{ikx}e^{-\tilde{W}T}\left[\hat{q}(-k,0)+2ikF_0\right]dk. \tag{2.2.10}$$

Taking the continuum limit, (2.2.9) converges to (2.2.10), since $\lim_{h\to 0} W(k) = k^2 = \tilde{W}(k)$.

As an example, the solution to the IBVP

$$\begin{cases} q_t = q_{xx}, & x>0,\ t>0,\\ q(x,0)=\phi(x)=3xe^{-x}, & x>0,\\ q(0,t)=u(t)=\sin(4\pi t), & t>0, \end{cases} \tag{2.2.11}$$

is written in terms of error functions. Deriving the modified PDE from the centered stencil (2.2.2), we find that solution (2.2.9) is a fourth-order accurate approximation to the solution of the dissipative PDE

$$p_t = p_{xx} + \frac{h^2}{12}p_{4x}. \tag{2.2.12}$$

The presence of the higher-order dissipation term p_{4x} causes high-frequency oscillations to be damped for any $t>0$. The original heat equation is also dissipative, but solution (2.2.9) might overdamp in scenarios where the initial data contains high-frequency oscillations or the boundary condition oscillates in time with large amplitude. Although the dissipation coefficient of p_{4x} is $\mathcal{O}\left(h^2\right)$, the overdamping nature can be troublesome for a practical $h \ll 1$ as t increases, but this can be counteracted by decreasing h. With the SD-UTM solution (2.2.9), the left plot of Figure 2.2.1 shows the gradual decay away from the $x=0$ and $t=0$ boundaries as time increases and the right plot shows the expected $\mathcal{O}\left(h^2\right)$ error as $h\to 0$.

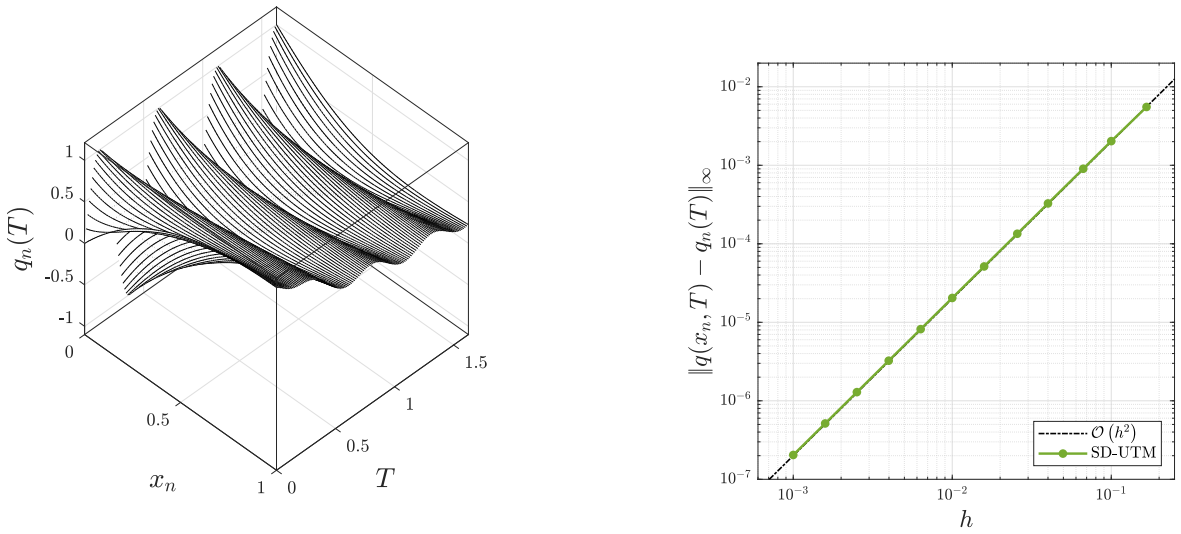

(a) (b)

Figure 2.2.1: (a) The semi-discrete solution (2.2.9) evaluated at various T with $h = 0.01$. (b) Error plot of the semi-discrete solution (2.2.9) relative to the exact solution as $h \to 0$ with $T = 1.625$.

2.2.2 Centered Discretization of $q_t = q_{xx}$ with Neumann boundary condition

We consider the continuous half-line problem:

$$\begin{cases} q_t = q_{xx}, & x > 0,\ t > 0, \\ q(x,0) = \phi(t), & x > 0, \\ q_x(0,t) = v(t), & t > 0, \end{cases} \tag{2.2.13}$$

with a Neumann boundary condition. How do we discretize this condition so that we may employ it with the centered-discretized equation (2.2.2)? This choice often leads to instabilities in finite-difference schemes, especially when dealing with higher-order problems [10, 43, 67]. We show that the SD-UTM determines which discretizations we can choose.

We proceed with the centered discretization (2.2.2) for the heat equation. This implies we retain the local relation (2.2.3) and dispersion relation (2.2.4) with nontrivial symmetry $\nu_1(k) = -k$. We cannot use the global relation (2.2.5), because we assumed Dirichlet boundary data to obtain it. Now, we do not have information at $n = 0$, so we define our forward transform to start at $n = 0$:

$$\hat{q}\,(k,t) = h \sum_{n=0}^{\infty} e^{-iknh} q_n(t),$$

directly affecting the global relation. From the local relation (2.2.3),

$$e^{WT}\hat{q}(k,T) - \hat{q}(k,0) - \left[\frac{f_{-1} - e^{ikh}f_0}{h}\right] = 0, \quad \text{Im}(k) \leq 0. \tag{2.2.14}$$

Solving for $\hat{q}(k,T)$ and inverting, we obtain

$$q_n(T) = \frac{1}{2\pi}\int_{-\pi/h}^{\pi/h} e^{iknh}e^{-WT}\hat{q}(k,0)\,dk + \frac{1}{2\pi}\int_{-\pi/h}^{\pi/h} e^{iknh}e^{-WT}\left[\frac{f_{-1} - e^{ikh}f_0}{h}\right]dk. \tag{2.2.15}$$

The global relation (2.2.14) and "solution" (2.2.15) depend on $q_0(t)$, as in the previous section, but also on $q_{-1}(t)$ instead of $q_1(t)$. For this Neumann IBVP, neither $q_{-1}(t)$ nor $q_0(t)$ are known, so both $f_{-1}(W,T)$ and $f_0(W,T)$ are unknowns. Since we only have one nontrivial symmetry to remove one unknown, we must provide another equation involving $f_{-1}(W,T)$ or $f_0(W,T)$ in such a way as to not introduce any new unknowns. If we discretize the Neumann boundary condition $q_x(0,t) = v(t)$, the only approach is to use the standard backward stencil:

$$\frac{q_0(t) - q_{-1}(t)}{h} = v(t).$$

Of course, this discretization is $\mathcal{O}(h)$, while the centered discretization (2.2.2) for q_{xx} is $\mathcal{O}(h^2)$. This suggests that the final semi-discrete solution will lose accuracy compared to the case with a Dirichlet boundary condition, but nonetheless converge to the continuous solution. Upon taking a time transform,

$$\frac{f_0(W,T) - f_{-1}(W,T)}{h} = V(W,T), \qquad V(W,T) = \int_0^T e^{Wt}v(t)\,dt. \tag{2.2.16}$$

The relation (2.2.16) becomes the second equation to remove the second unknown. Solving the system

$$\begin{cases} e^{WT}\hat{q}(-k,T) - \hat{q}(-k,0) - \left[\dfrac{f_{-1} - e^{-ikh}f_0}{h}\right] = 0, \\ \dfrac{f_0 - f_{-1}}{h} = V, \end{cases}$$

for $f_{-1}(W,T)$ and $f_0(W,T)$ results in

$$\frac{f_{-1} - e^{ikh}f_0}{h} = e^{ikh}\hat{q}(-k,0) - \left(1 + e^{ikh}\right)V - e^{WT}e^{ikh}\hat{q}(-k,T), \quad \text{Im}(k) \geq 0.$$

Since (2.2.15) has integration paths on the real line, direct substitution gives

$$\begin{aligned} q_n(T) = {} & \frac{1}{2\pi}\int_{-\pi/h}^{\pi/h} e^{iknh}e^{-WT}\hat{q}(k,0)\,dk + \frac{1}{2\pi}\int_{-\pi/h}^{\pi/h} e^{iknh}e^{-WT}\left[e^{ikh}\hat{q}(-k,0) - \left(1 + e^{ikh}\right)V\right]dk \\ & - \frac{1}{2\pi}\int_{-\pi/h}^{\pi/h} e^{ik(n+1)h}\hat{q}(-k,T)\,dk. \end{aligned} \tag{2.2.17}$$

As before, we introduced an unwanted term that depends on the transform of the solution. We show the contribution from this term is zero by substituting the definition for $\hat{q}(-k,T)$:

$$\begin{aligned}\frac{-1}{2\pi}\int_{-\pi/h}^{\pi/h} e^{ik(n+1)h}\hat{q}(-k,T)\,dk &= \frac{-1}{2\pi}\int_{-\pi/h}^{\pi/h} e^{ik(n+1)h}\left[h\sum_{m=0}^{\infty} e^{ikmh}q_m(T)\right]dk \\ &= \sum_{m=0}^{\infty}\left[\frac{-h}{2\pi}\int_{-\pi/h}^{\pi/h} e^{ik(n+1)h}e^{ikmh}\,dk\right]q_m(T) \\ &= 0,\end{aligned}$$

where the integral vanishes by periodicity. The final solution to this IBVP with a Neumann boundary condition $v(t)$, discretized as above, is

$$q_n(T) = \frac{1}{2\pi}\int_{-\pi/h}^{\pi/h} e^{iknh}e^{-WT}\hat{q}(k,0)\,dk + \frac{1}{2\pi}\int_{-\pi/h}^{\pi/h} e^{iknh}e^{-WT}\left[e^{ikh}\hat{q}(-k,0) - \left(1+e^{ikh}\right)V\right]dk. \quad (2.2.18)$$

Similarly as shown in [17], the solution representation for IBVP (3.2.16) using the continuous UTM is

$$q(x,T) = \frac{1}{2\pi}\int_{-\infty}^{\infty} e^{ikx}e^{-\tilde{W}T}\hat{q}(k,0)\,dk + \frac{1}{2\pi}\int_{-\infty}^{\infty} e^{ikx}e^{-\tilde{W}T}\left[\hat{q}(-k,0) - 2F_1\right]dk. \quad (2.2.19)$$

Referencing (2.2.18), the continuum limits of the coefficients of $\hat{q}(-k,0)$ and $V(W,T)$ converge, where

$$\lim_{h\to 0} V(W,T) = \lim_{h\to 0}\int_0^T e^{Wt}v(t)\,dt = \int_0^T e^{\tilde{W}t}v(t)\,dt = F_1(\tilde{W},T).$$

As a concrete example, we examine the solution of the IBVP

$$\begin{cases} q_t = q_{xx}, & x>0,\ t>0, \\ q(x,0) = \phi(x) = e^{-x}\cos(3\pi x), & x>0, \\ q_x(0,t) = v(t) = \frac{-1}{4\pi}\sin(4\pi t), & t>0. \end{cases} \quad (2.2.20)$$

Again, the continuous solution is given in terms of error functions, while the semi-discrete solution is given by (2.2.18). The given Neumann data is discretized using the standard first-order accurate backward stencil, which reduces the overall accuracy of the solution from $\mathcal{O}(h^2)$ to $\mathcal{O}(h)$. Since the centered stencil (2.2.2) is used, solution (2.2.18) is a fourth-order accurate approximation to the dissipative PDE (2.2.12). However, in general this is not the case, because of the discretization of the Neumann boundary condition. The modified equation for this backward discretization at $x=0$ is $q_x(0,t) = v(t) - (h/2)q_{xx}(0,t)$. Unless the next several higher-order derivatives of the solution at the boundary are zero, the standard backward discretization we employed on $v(t)$ is $\mathcal{O}(h)$, and so is solution (2.2.18). This modified PDE at the boundary implies the loss of accuracy is visible in the solution profiles of Figure 2.2.3 in the form of dissipation near the boundary. With $h = 0.01$, this drop in accuracy is illustrated in the error plot of Figure 2.2.2.

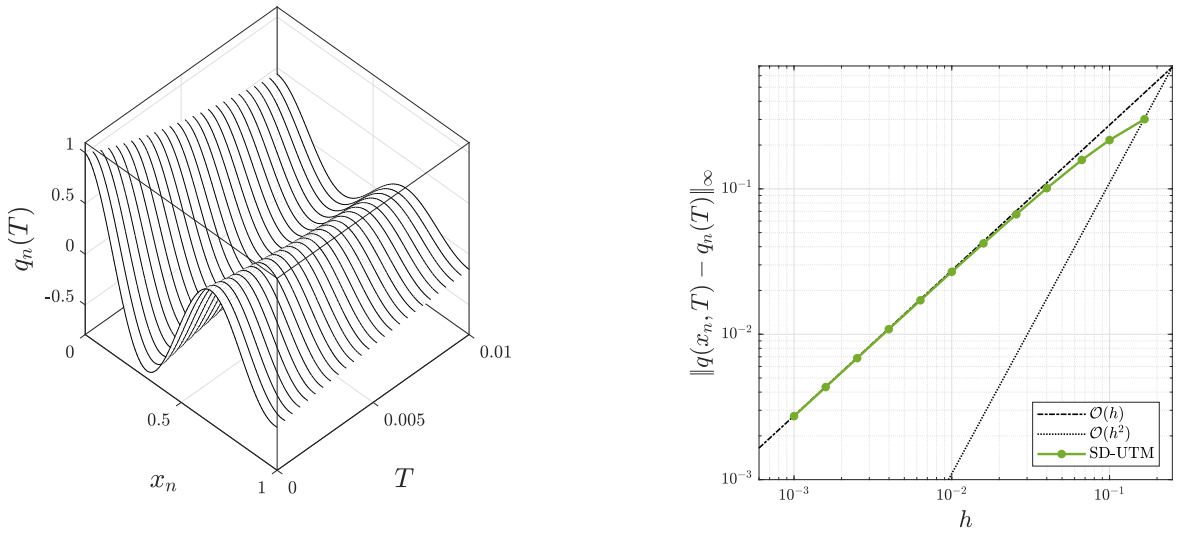

(a) (b)

Figure 2.2.2: (a) The semi-discrete solution (2.2.18) evaluated at various T with $h = 0.01$. (b) Error plot of the semi-discrete solution (2.2.18) relative to the exact solution as $h \to 0$ with $T = 0.01$.

Remark 2.2.1. We may consider different spacial discretizations of the heat equation in the IBVPs (3.2.1) or (3.2.16). For example, the standard forward one-sided discretization of the heat equation,

$$\dot{q}_n(t) = \frac{q_{n+2}(t) - 2q_{n+1}(t) + q_n(t)}{h^2}, \tag{2.2.21}$$

gives rise to the dispersion relation

$$W(k) = \frac{2e^{ikh} - e^{2ikh} - 1}{h^2}, \tag{2.2.22}$$

and

$$q_n(T) = \frac{1}{2\pi}\int_{-\pi/h}^{\pi/h} e^{iknh}e^{-WT}\hat{q}(k,0)\,dk + \frac{1}{2\pi}\int_{-\pi/h}^{\pi/h} e^{ik(n+1)h}e^{-WT}\left[\frac{\left(2-e^{ikh}\right)f_0 - f_1}{h}\right]dk, \tag{2.2.23}$$

using a forward discrete Fourier transform that starts at $n = 0$. Regardless of the starting index and available boundary conditions from the continuous problem, the second integral in the "solution" has zero contribution, *i.e.*, the solution does not depend on any boundary information at all. This can be done by deforming off the real line as in Section 2.1.1, since the dispersion relation (2.2.22) with $z = e^{ikh}$ has all nonnegative degrees and e^{-WT} is bounded in the upper half-plane. Thus, (2.2.21) gives rise to an ill-conditioned semi-discrete problem, relative to its continuous counterpart.

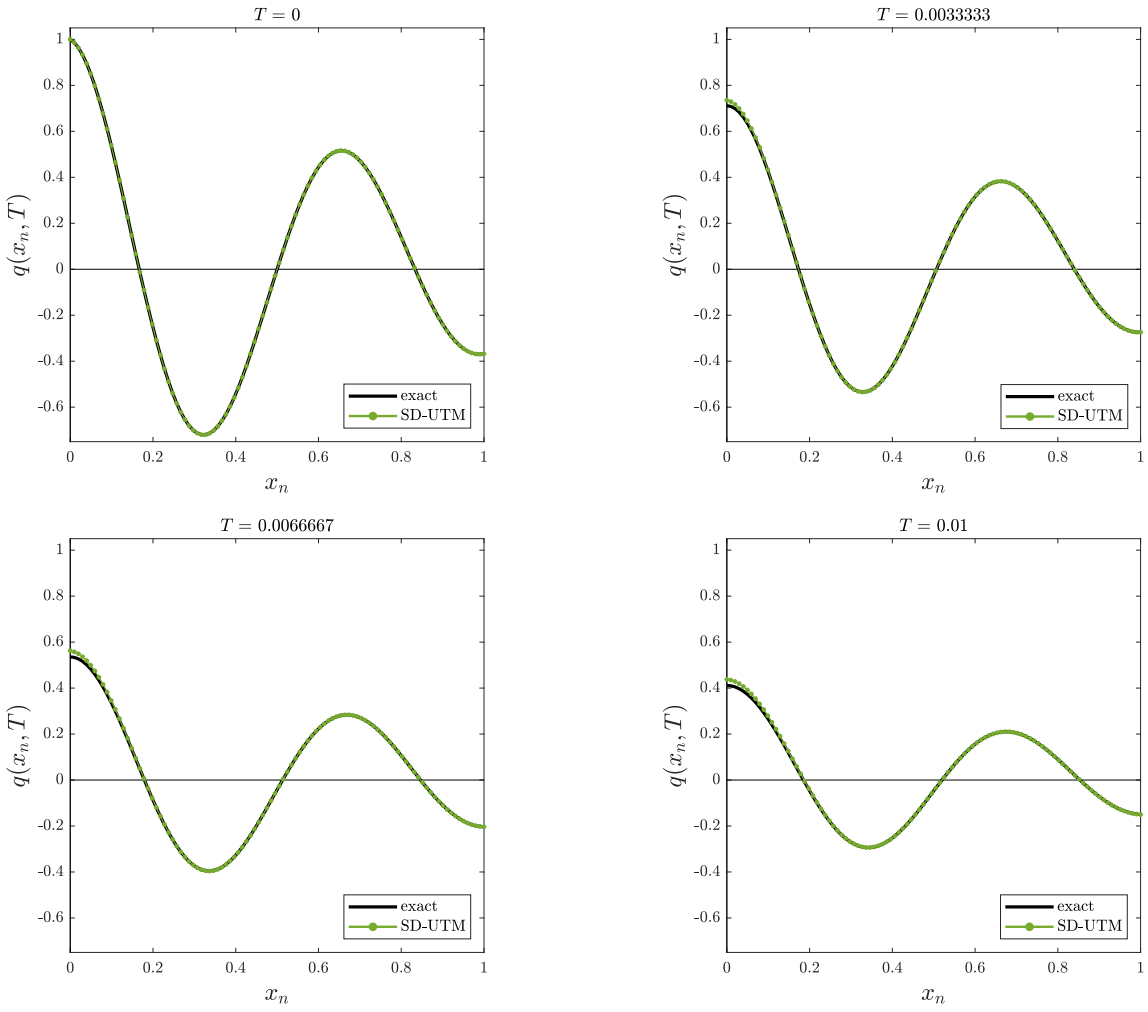

Figure 2.2.3: Several time slices for the solution to IBVP (2.2.20) with $h = 0.01$.

A similar issue arises when we consider a backward one-sided discretization for q_{xx}, except here the dispersion relation

$$W(k) = \frac{2e^{-ikh} - e^{-2ikh} - 1}{h^2}, \tag{2.2.24}$$

does not permit the removal of either unknown from

$$q_n(T) = \frac{1}{2\pi}\int_{-\pi/h}^{\pi/h} e^{iknh} e^{-WT}\hat{q}(k,0)dk + \frac{1}{2\pi}\int_{-\pi/h}^{\pi/h} e^{iknh} e^{-WT}\left[\frac{f_{-2} - \left(2 - e^{-ikh}\right) f_{-1}}{h}\right] dk. \tag{2.2.25}$$

Although the discretization is first-order accurate, it has a second-order stencil with a dispersion relation, which has a nontrivial symmetry. Even so, it is not feasible to deform to the region where the global relation with this symmetry is valid, see Figure 2.2.4. Thus, this one-sided discretization

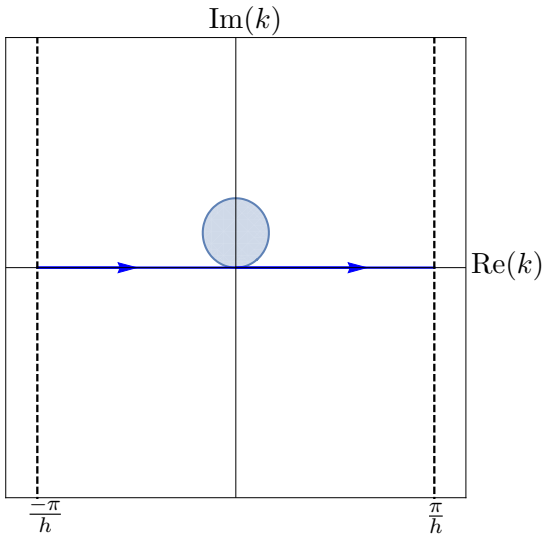

Figure 2.2.4: The shaded region depicts where the global relation of the backward one-sided discretization of q_{xx} is valid, with $k \to \nu_1(k)$ from (2.2.24).

is also problematic, requiring too much information from boundary nodes.

2.2.3 Higher-Order Discretization of $q_t = q_{xx}$ with Dirichlet boundary condition

As in Section 2.1.4, we can apply higher-order discretizations to the heat equation where the nontrivial symmetries are not enough to eliminate unknowns. Consider the heat equation in (3.2.1) with the standard centered fourth-order discretization:

$$\dot{q}_n(t) = \frac{-q_{n-2}(t) + 16q_{n-1}(t) - 30q_n(t) + 16q_{n+1}(t) - q_{n+2}(t)}{12h^2}. \tag{2.2.26}$$

After several tedious steps, the global relation is

$$e^{WT}\hat{q}(k,T) - \hat{q}(k,0) - F(k,T) = 0, \quad \text{Im}(k) \le 0, \tag{2.2.27}$$

where

$$F(k,T) = \frac{-e^{-ikh}f_{-1} + 16e^{-ikh}f_0 - e^{-2ikh}f_0 - 16f_1 + e^{ikh}f_1 + f_2}{12h},$$

with dispersion relation

$$W(k) = \frac{e^{-2ikh} - 16e^{-ikh} + 30 - 16e^{ikh} + e^{2ikh}}{12h^2}. \tag{2.2.28}$$

Solving for $\hat{q}(k,T)$ and taking the inverse transform, we obtain

$$q_n(T) = \frac{1}{2\pi}\int_{-\pi/h}^{\pi/h} e^{iknh}e^{-WT}\hat{q}(k,0)\,dk + \frac{1}{2\pi}\int_{-\pi/h}^{\pi/h} e^{iknh}e^{-WT}F(k,T)\,dk. \tag{2.2.29}$$

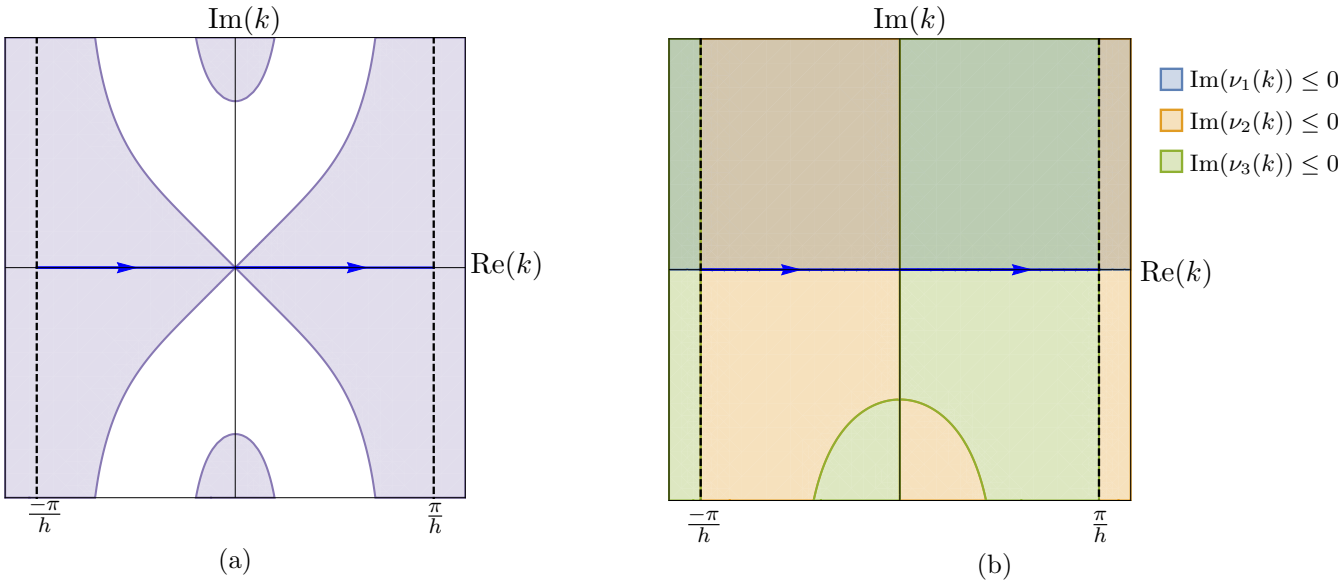

Figure 2.2.5: (a) The shaded regions depict where $\mathrm{Re}(-W) \le 0$ and e^{-WT} is bounded with the dispersion relation (2.2.28). (b) The shaded regions depict where the global relation with $k \to \nu_i(k)$ is valid from (2.2.28).

Since we are given the Dirichlet boundary condition, $f_{-1}(W,T)$, $f_1(W,T)$, and $f_2(W,T)$ are unknown and must be removed from (2.2.29). The dispersion relation gives the nontrivial symmetries

$$\begin{aligned}
\nu_1(k) &= -k, \\
\nu_2(k) &= \frac{i}{h}\ln\left(\frac{e^{-ikh}}{2}\left[16e^{ikh} - e^{2ikh} - 1 + \sqrt{\left(-16e^{ikh} + e^{2ikh} + 1\right)^2 - 4e^{2ikh}}\right]\right), \\
\nu_3(k) &= \frac{i}{h}\ln\left(\frac{e^{-ikh}}{2}\left[16e^{ikh} - e^{2ikh} - 1 - \sqrt{\left(-16e^{ikh} + e^{2ikh} + 1\right)^2 - 4e^{2ikh}}\right]\right),
\end{aligned}$$

where the branch cut for the square-root function is chosen to be on the positive real line (see Remark 2.2.2). Figure 2.2.5b depicts where in the complex k-plane the global relation (2.2.27) with $k \to \nu_i$ is valid, while Figure 2.2.5a shows the shaded regions as decay due to e^{-WT}. Both figures imply that the integration path on the real line need not be deformed to use all three nontrivial symmetries. Even so, Figure 2.2.5b tells us that both $\nu_{2,3}(k)$ may only be used to remove one unknown, since there is no region where both symmetries are simultaneously valid. Hence, the three symmetries can only remove two unknowns and we must introduce a fourth equation. With the given Dirichlet data $u(t)$, the heat equation itself gives all even-derivative boundary conditions, particularly $q_{xx}(0,t) = u'(t) = v(t)$ and $q_{4x}(0,t) = u''(t) = \tilde{v}(t)$. Discretizing the second-derivative

condition with the standard centered fourth-order stencil gives

$$\frac{-q_{-2}(t)+16q_{-1}(t)-30q_0(t)+16q_1(t)-q_2(t)}{12h^2}=v(t). \tag{2.2.30}$$

This stencil introduces the additional unknown $q_{-2}(t)$, further requiring one more equation. Generally, we can find additional equations that relate nodes to derivatives using the method of undetermined coefficients. Since we have $q_{4x}(0,t)$, we derive an equation that does not introduce any more unknowns, maintains the same order of accuracy as (2.2.26), and is linearly independent to (2.2.30):

$$\frac{q_{-2}(t)+2q_{-1}(t)-6q_0(t)+2q_1(t)+q_2(t)}{6h^2}=v(t)+\frac{h^2}{4}\tilde{v}(t). \tag{2.2.31}$$

Taking the time transforms of (2.2.30) and (2.2.31), we have the closed system of equations for all unknowns:

$$\begin{cases} 0=e^{WT}\hat{q}\left(-k,T\right)-\hat{q}\left(-k,0\right)-F\left(-k,T\right), & \mathrm{Im}(k)\geq 0,\\ 0=e^{WT}\hat{q}\left(\nu_2,T\right)-\hat{q}\left(\nu_2,0\right)-F\left(\nu_2,T\right), & \mathrm{Im}(\nu_2)\leq 0,\\ 0=e^{WT}\hat{q}\left(\nu_3,T\right)-\hat{q}\left(\nu_3,0\right)-F\left(\nu_3,T\right), & \mathrm{Im}(\nu_3)\leq 0,\\ 12h^2V=-f_{-2}+16f_{-1}-30f_0+16f_1-f_2, & k\in\mathbb{C},\\ 6h^2V+\dfrac{3h^4}{2}\tilde{V}=f_{-2}+2f_{-1}-6f_0+2f_1+f_2, & k\in\mathbb{C}, \end{cases}$$

where $V(W,T)$ is the time transform of $v(t)$ and $\tilde{V}(W,T)$ is the time transform of $\tilde{v}(t)$. Solving for the unknowns, we find

$$\begin{aligned} q_n(T)=&\frac{1}{2\pi}\int_{-\pi/h}^{\pi/h}e^{iknh}e^{-WT}\left[\hat{q}(k,0)-\hat{q}(-k,0)\right]dk+\frac{1}{2\pi}\int_{-\pi/h}^{\pi/h}e^{iknh}e^{-WT}\tilde{F}(k,T)f_0\,dk\\ &+\frac{1}{2\pi}\int_{-\pi/h}^{\pi/h}e^{iknh}e^{-WT}\left[\frac{e^{-ikh}\left(e^{2ikh}-1\right)h}{12}V+\frac{e^{-ikh}\left(e^{2ikh}-1\right)h^3}{144}\tilde{V}\right]dk, \end{aligned} \tag{2.2.32}$$

after deforming away the integral with $\hat{q}(-k,T)$, where

$$\tilde{F}(k,T)=\frac{e^{-2ikh}\left(14e^{ikh}-14e^{3ikh}+e^{4ikh}-1\right)}{12h}.$$

Note that $\tilde{F}(k,T)$ has no dependence on $\nu_{2,3}$. In the continuum limit, $\lim_{h\to 0}\tilde{F}=-2ik$ and the last integral, with derivative boundary conditions, vanishes. Particularly, expanding in Taylor series the common exponential factor between the derivative boundary conditions in (2.2.32), we have $e^{-ikh}\left(e^{2ikh}-1\right)=2ikh+\mathcal{O}(h^3)$, such that the coefficients of $V(W,T)$ and $\tilde{V}(W,T)$ vanish like $\mathcal{O}(h^2)$ and $\mathcal{O}(h^4)$, respectively, as $h\to 0$. Thus, the semi-discrete solution correctly loses dependence on the derivative boundary conditions in the continuum limit and converges to (2.2.10).

Remark 2.2.2. Since the symmetries are convolved with exponentials and square roots, the regions of validity are numerically pinned down with the help of symbolic software, like Mathematica, but

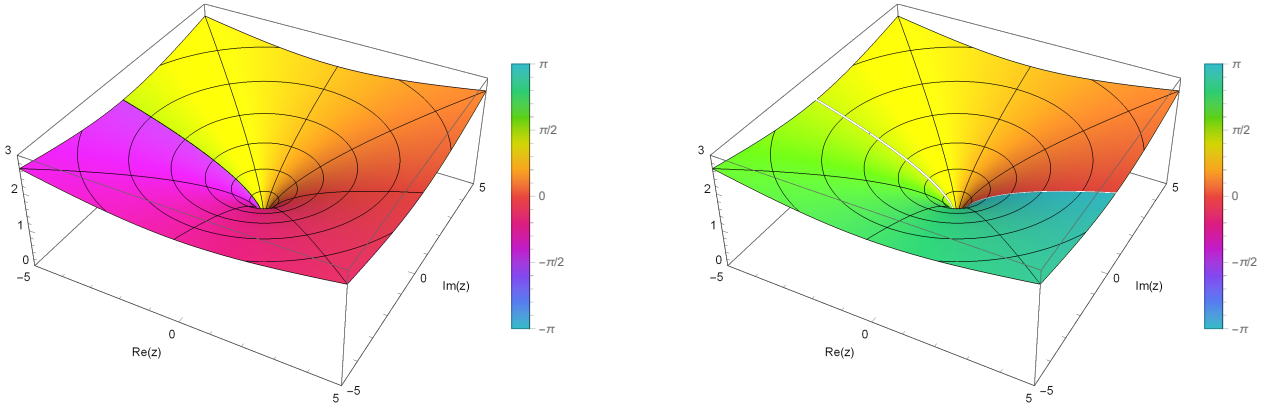

(a) (b)

Figure 2.2.6: (a) Contour plot of default $|\sqrt{z}|$. (b) Contour plot of redefined $|\sqrt{z}|$.

a few comments are in order. In general, to obtain any semi-discrete symmetry, an equation with exponentials must be solved via inverse functions, most notably the natural log function $\ln(z)$, and in this case, along with the square root function $z^{1/2}$. Both of these are multi-valued functions, so branch cuts must be chosen. Many software packages like Mathematica, Maple, and MATLAB automatically place the branch cuts for both $\ln(z)$ and $z^{1/2}$ on the negative real line, evident for the latter in Figure 2.2.6a as the discontinuity in the flow of colors by letting $z = re^{i\theta}$ with $r > 0$ and $\theta \in (-\pi, \pi]$. Following this standard convention, we find that symmetries of many higher-order dispersion relation discretizations are numerically ill-defined as $h \to 0$. Instead, the branch cut for $z^{1/2}$ must be placed on the positive real line, *i.e.,* letting $z = re^{i\theta}$ with now $\theta \in (0, 2\pi]$. We redefine

$$\left(re^{i\theta}\right)^{1/2} = \begin{cases} \sqrt{r}e^{i\theta/2}, & 0 < \theta \leq \pi, \\ -\sqrt{r}e^{i\theta/2}, & -\pi < \theta \leq 0, \end{cases}$$

where $\sqrt{\cdot}$ is the default principal-value square root. Visually, our redefined square root function is displayed in Figure 2.2.6b, where the pasting of the default $+\sqrt{z}$ and $-\sqrt{z}$ at the negative real line is noticeable as a blank section across a continuous flow of colors. The branch cut for $\ln(z)$ does not impact the continuum limit to exist numerically – at least on the upper-half k-plane for half-line problems.

Remark 2.2.3. Like in Section 2.2.2, solving the fourth-order discretization (2.2.26) with a Neumann boundary condition at $x = 0$ leads to a solution that is one less order of accuracy than that of the PDE stencil. After inverting the global relation for this IBVP, the "solution" depends on four unknowns: $f_i(W, T)$ for $i = -2, \ldots, 1$. The three nontrivial symmetries in the global relation

formulas only remove two $f_i(W,T)$ terms. In order to not introduce more unknowns, two linearly independent discretizations to eliminate the remaining two unknowns are:

$$\frac{f_1 - f_{-1}}{2h} = V + \frac{h^2}{6}\tilde{V} \quad \text{and} \quad \frac{f_{-2} - 6f_{-1} + 3f_0 + 2f_1}{6h} = V,$$

after taking time transforms of $v(t) = q_x(0,t)$ and $\tilde{v}(t) = v'(t) = q_{xxx}(0,t)$. The first stencil's accuracy is $\mathcal{O}(h^4)$, while the second's is $\mathcal{O}(h^3)$, where the $\mathcal{O}(h^3)$ terms depend on $q_{4x}(0,t)$. Replacing this last discretization with a wider, more accurate stencil introduces more unknowns that no linearly independent discretizations can eliminate. Hence, the SD-UTM solution with these discretizations is third-order accurate.

2.3 The Linear Schrödinger Equation

We consider the linear Schrödinger (LS) equation

$$iq_t + \frac{1}{2}q_{xx} = 0 \quad \text{or} \quad q_t = \frac{i}{2}q_{xx}. \tag{2.3.1}$$

In contrast to the dissipative heat equation, this problem is dispersive.

2.3.1 Centered Discretization of $q_t = \frac{i}{2}q_{xx}$ with Dirichlet boundary condition

We begin with the half-line IBVP

$$\begin{cases} q_t = \frac{i}{2}q_{xx}, & x > 0,\ t > 0, \\ q(x,0) = \phi(x), & x > 0, \\ q(0,t) = u(t), & t > 0, \end{cases} \tag{2.3.2}$$

using a centered discretization for q_{xx},

$$\dot{q}_n(t) = \frac{i}{2}\left(\frac{q_{n+1}(t) - 2q_n(t) + q_{n-1}(t)}{h^2}\right). \tag{2.3.3}$$

The local and dispersion relations are, respectively,

$$\partial_t\left(e^{-iknh}e^{Wt}q_n\right) = \frac{i}{2h^2}\Delta\left(e^{-ik(n-1)h}e^{Wt}q_n - e^{-iknh}e^{Wt}q_{n-1}\right), \tag{2.3.4}$$

$$W(k) = \frac{i}{2}\left(\frac{2 - e^{ikh} - e^{-ikh}}{h^2}\right) = \frac{i}{h^2}\left[1 - \cos(kh)\right]. \tag{2.3.5}$$

With the Dirichlet boundary condition, our transforms begin at $n = 1$ instead of at $n = 0$, resulting in the global relation

$$e^{WT}\hat{q}(k,T) - \hat{q}(k,0) - \frac{i}{2}\left[\frac{e^{-ikh}f_0 - f_1}{h}\right] = 0, \quad \text{Im}(k) \le 0. \tag{2.3.6}$$

To obtain our "solution" formula, we take the inverse transform,

$$q_n(T) = \frac{1}{2\pi}\int_{-\pi/h}^{\pi/h} e^{iknh}e^{-WT}\hat{q}(k,0)\,dk + \frac{1}{2\pi}\int_{-\pi/h}^{\pi/h} \frac{ie^{iknh}e^{-WT}}{2}\left[\frac{e^{-ikh}f_0 - f_1}{h}\right]dk. \tag{2.3.7}$$

The dispersion relation (2.3.5) admits the nontrivial symmetry $\nu_1(k) = -k$ up to periodic copies. Hence, the global relation (2.3.6) with $\nu_1(k)$ is valid in the upper-half plane, including the real line, so that there is no need to deform in order to eliminate the unknown $f_1(W,T)$ in (2.3.7). We find

$$f_1 = e^{ikh}f_0 - 2ih\left[\hat{q}(-k,0) - e^{TW}\hat{q}(-k,T)\right],$$

so that

$$\begin{aligned} q_n(T) = &\frac{1}{2\pi}\int_{-\pi/h}^{\pi/h} e^{iknh}e^{-WT}\hat{q}(k,0)\,dk + \frac{1}{2\pi}\int_{-\pi/h}^{\pi/h} e^{iknh}e^{-WT}\left[\frac{i\left(e^{-ikh}-e^{ikh}\right)}{2h}f_0 - \hat{q}(-k,0)\right]dk \\ &+ \frac{1}{2\pi}\int_{-\pi/h}^{\pi/h} e^{iknh}\hat{q}(-k,T)\,dk. \end{aligned} \tag{2.3.8}$$

As before, one shows that the last term does not contribute. Therefore, the solution to this half-line IBVP is

$$q_n(T) = \frac{1}{2\pi}\int_{-\pi/h}^{\pi/h} e^{iknh}e^{-WT}\hat{q}(k,0)\,dk - \frac{1}{2\pi}\int_{-\pi/h}^{\pi/h} e^{iknh}e^{-WT}\left[\hat{q}(-k,0) - \frac{\sin(kh)}{h}f_0\right]dk. \tag{2.3.9}$$

Since a centered stencil was used to obtain (2.3.9), the modified PDE which this semi-discrete solution better approximates solutions of is similar to (2.2.12) derived for the heat equation. Instead of being dissipative, we have the dispersive PDE $p_t = (i/2)p_{xx} + (ih^2/24)p_{4x}$. Solution (2.3.9) solves this modified PDE to fourth-order, where the dispersive behavior of the second term on the right-hand side is evident for large t and fixed h. Because this term is $\mathcal{O}\left(h^2\right)$, we can diminish the excess dispersion by decreasing h.

The continuous UTM solution [17] to (3.3.1) is

$$q(x,T) = \frac{1}{2\pi}\int_{-\infty}^{\infty} e^{ikx}e^{-\tilde{W}T}\hat{q}(k,0)\,dk - \frac{1}{2\pi}\int_{-\infty}^{\infty} e^{ikx}e^{-\tilde{W}T}\left[\hat{q}(-k,0) - kF_0\right]dk, \tag{2.3.10}$$

with dispersion relation $\tilde{W}(k) = ik^2/2$ and nontrivial symmetry $\tilde{\nu}_1 = -k$. The semi-discrete solution (2.3.9) converges to its continuous counterpart solution (2.3.10) in the continuum limit.

We examine the numerical solution to

$$\begin{cases} q_t = \frac{i}{2}q_{xx}, & x > 0,\ t > 0, \\ q(x,0) = \phi(x) = e^{-x}\cos(2\pi x), & x > 0, \\ q(0,t) = u(t) = \cos(5\pi t), & t > 0, \end{cases} \tag{2.3.11}$$

Like the heat equation, the continuous solution to this problem can be written in terms of error functions of imaginary argument. The semi-discrete solution for the second-order finite-difference approximation (2.3.3) is given by (2.3.9). Figure 2.3.1 shows the dispersive nature of the real and imaginary components of the solution, along with the square of the modulus.

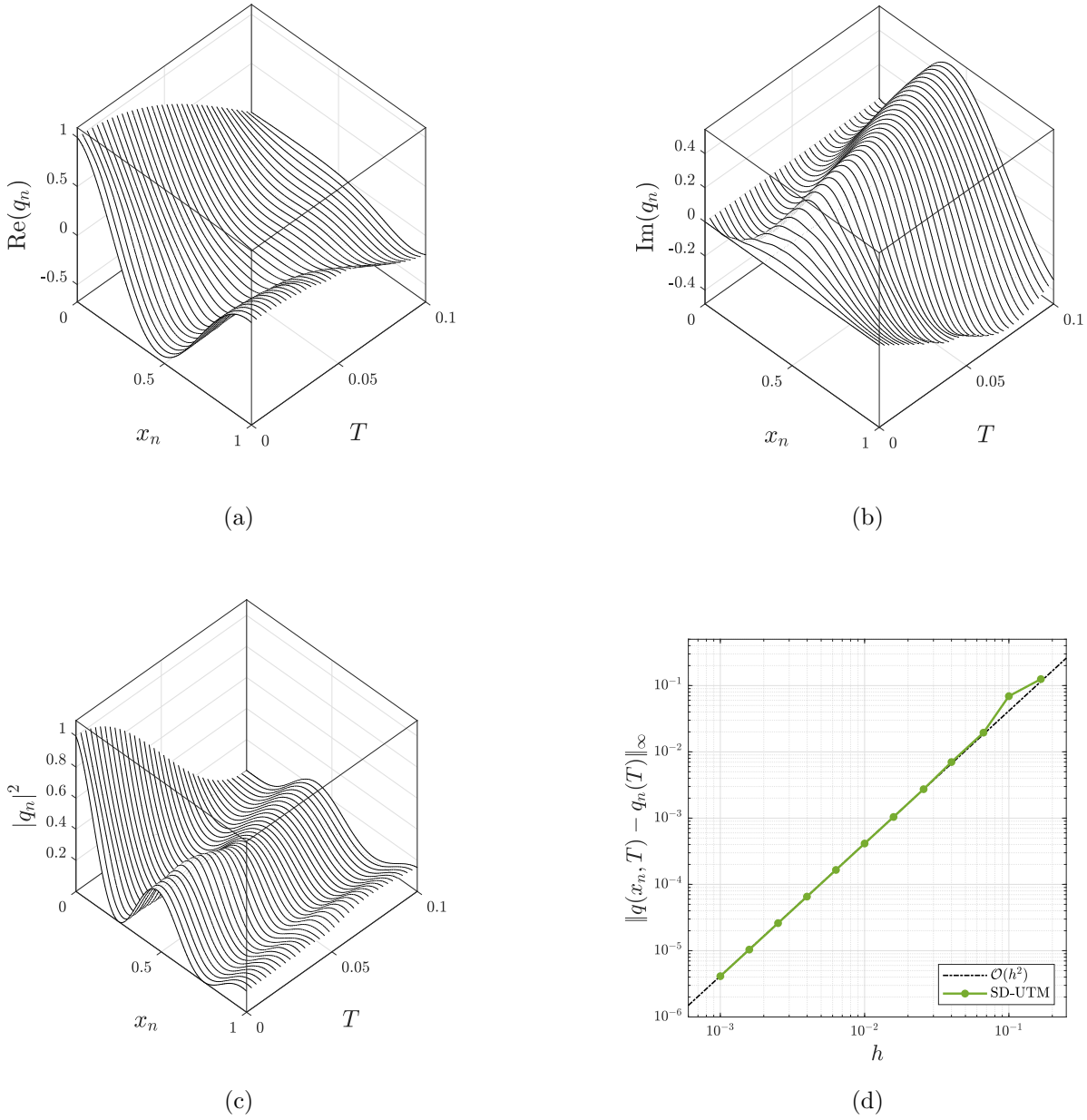

Figure 2.3.1: (a) - (c) Real and imaginary parts and modulus squared of the semi-discrete solution profiles (2.3.9) at various T for IBVP (2.3.11) with $h = 0.01$. (d) Error plot of the semi-discrete solution (2.3.9) relative to the exact solution as $h \to 0$ with $T = 0.1$.

2.3.2 *Centered Discretization of $q_t = \frac{i}{2}q_{xx}$ with Neumann boundary condition*

We consider the same centered-discretized LS equation as above with a Neumann boundary condition:

$$\begin{cases} q_t = \frac{i}{2}q_{xx}, & x > 0,\ t > 0, \\ q(x,0) = \phi(x), & x > 0, \\ q_x(0,t) = v(t), & t > 0. \end{cases} \tag{2.3.12}$$

Here, $q_0(t)$ is unknown, and we choose the discrete Fourier transform to start from $n = 0$ instead of from $n = 1$. The local and dispersion relations, (2.3.4) and (2.3.5) respectively, remain unchanged. The global relation is

$$e^{WT}\hat{q}(k,T) - \hat{q}(k,0) - \frac{i}{2}\left[\frac{f_{-1} - e^{ikh}f_0}{h}\right] = 0, \quad \mathrm{Im}(k) \le 0. \tag{2.3.13}$$

Using the inverse transform,

$$q_n(T) = \frac{1}{2\pi}\int_{-\pi/h}^{\pi/h} e^{iknh}e^{-WT}\hat{q}(k,0)\,dk + \frac{1}{2\pi}\int_{-\pi/h}^{\pi/h} \frac{ie^{iknh}e^{-WT}}{2}\left[\frac{f_{-1} - e^{ikh}f_0}{h}\right] dk. \tag{2.3.14}$$

Like the heat equation with a Neumann boundary condition at $x = 0$, we apply the standard backward discretization to $q_x(0,t)$ so as not to introduce new unknowns,

$$\frac{q_0(t) - q_{-1}(t)}{h} = v(t).$$

As discussed in Section 2.2.2, this discretization drops the accuracy to $\mathcal{O}(h)$, visible in solution profiles as dissipation near the boundary. The global relation (2.3.13) and the time transform of the discretized boundary condition give the system

$$\begin{cases} e^{WT}\hat{q}(-k,T) - \hat{q}(-k,0) - \frac{i}{2}\left[\frac{f_{-1} - e^{-ikh}f_0}{h}\right] = 0, \\ \frac{f_0 - f_{-1}}{h} = V(t), \end{cases}$$

for the two unknowns $f_{-1}(W,T)$ and $f_0(W,T)$, where

$$V(W,T) = \int_0^T e^{Wt}v(t)\,dt.$$

Solving the system and substituting into (2.3.14), we have

$$\begin{aligned} q_n(T) = {} & \frac{1}{2\pi}\int_{-\pi/h}^{\pi/h} e^{iknh}e^{-WT}\hat{q}(k,0)\,dk \\ & - \frac{1}{2\pi}\int_{-\pi/h}^{\pi/h} e^{iknh}e^{-WT}\left[\frac{i\left(e^{ikh}+1\right)}{2}V(t) - e^{ikh}\hat{q}(-k,0)\right] dk, \end{aligned} \tag{2.3.15}$$

after applying similar techniques as before to remove the integral term depending on $\hat{q}(-k,T)$. This limits to the solution [17] of the continuous problem

$$q(x,T) = \frac{1}{2\pi}\int_{-\infty}^{\infty} e^{ikx}e^{-\tilde{W}T}\hat{q}(k,0)\,dk - \frac{1}{2\pi}\int_{-\infty}^{\infty} e^{ikx}e^{-\tilde{W}T}\left[iF_1 - \hat{q}(-k,0)\right]\,dk. \tag{2.3.16}$$

Lastly, consider

$$\begin{cases} q_t = \frac{i}{2}q_{xx}, & x>0,\ t>0, \\ q(x,0) = \phi(x) = e^{-x}\sin(2\pi x), & x>0, \\ q_x(0,t) = v(t) = 2\pi\cos(\pi t), & t>0, \end{cases} \tag{2.3.17}$$

with the Neumann condition discretized using the standard backward stencil, giving rise to the $\mathcal{O}(h)$ accurate solution (3.3.13), displayed in Figure 2.3.2.

2.4 The Convection-Diffusion Equation

2.4.1 Centered Discretization of $q_t = c\,q_x + q_{xx}$ with Dirichlet boundary condition

Suppose the convection-diffusion IBVP is given with a Dirichlet boundary condition:

$$\begin{cases} q_t = c\,q_x + q_{xx}, & x>0,\ t>0, \\ q(x,0) = \phi(x), & x>0, \\ q(0,t) = u(t), & t>0, \end{cases} \tag{2.4.1}$$

and consider centered discretizations for both spacial derivatives:

$$\dot{q}_n = c\left(\frac{q_{n+1}-q_{n-1}}{2h}\right) + \frac{q_{n+1}-2q_n+q_{n-1}}{h^2}, \tag{2.4.2}$$

where $c\in\mathbb{R}$ is the advection speed. Although we saw in Section 2.1 that the natural discretizations for q_x in the advection equations were purely one-sided, this IBVP is second-order, so we proceed with a stencil that is also second-order to preserve the $\mathcal{O}\left(h^2\right)$ accuracy from the centered-discretization of q_{xx}.

The local relation is

$$\partial_t\left(e^{-iknh}e^{Wt}q_n\right) = \Delta\left(\frac{a}{h}e^{-ik(n-1)h}e^{Wt}q_n - \frac{b}{h}e^{-iknh}e^{Wt}q_{n-1}\right), \tag{2.4.3}$$

with

$$a = \frac{1}{h}+\frac{c}{2}, \qquad b = \frac{1}{h}-\frac{c}{2},$$

and

$$W(k) = \frac{2}{h^2} - \frac{ae^{ikh}+be^{-ikh}}{h}. \tag{2.4.4}$$

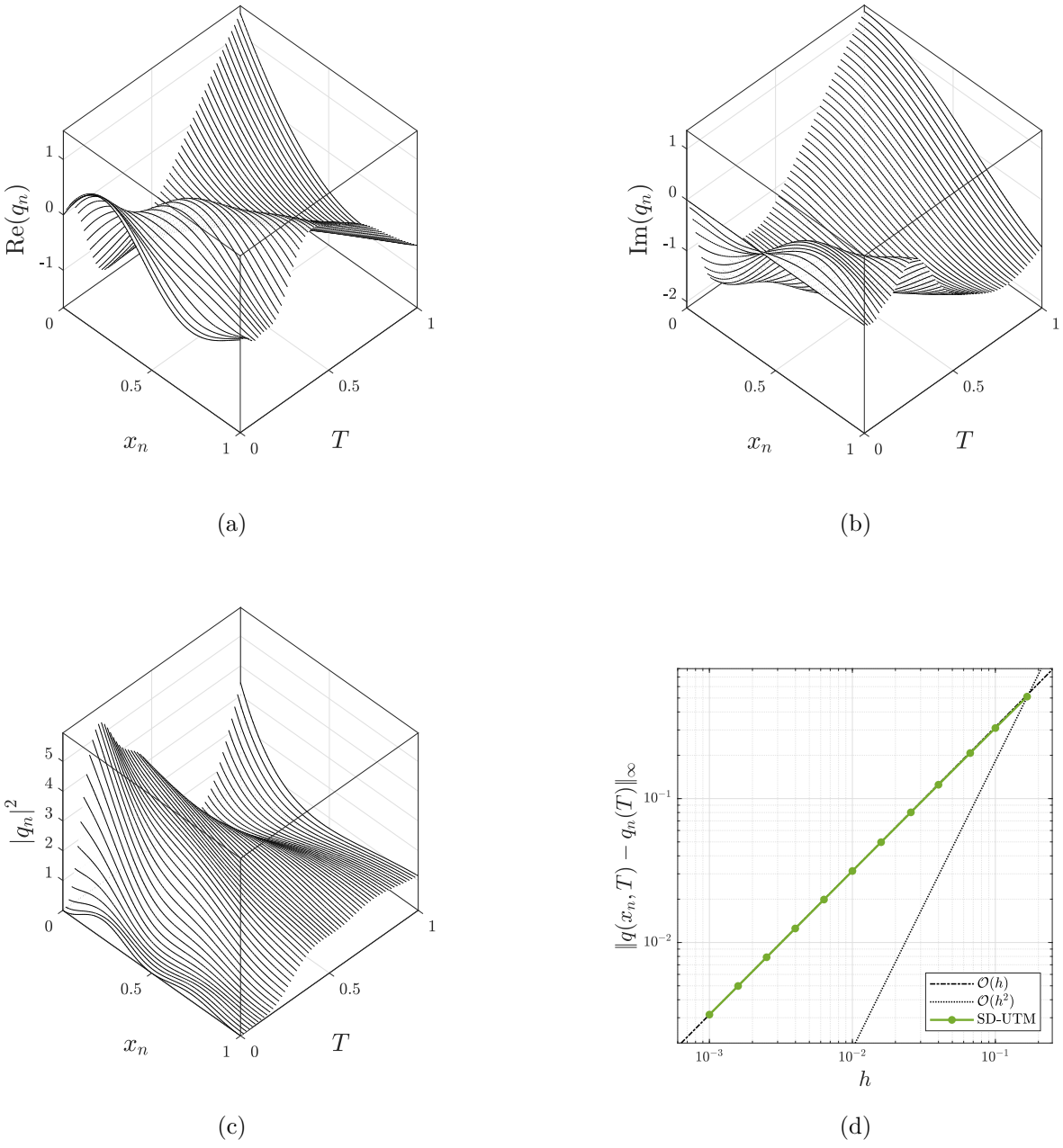

Figure 2.3.2: (a) - (c) Real and imaginary parts and modulus squared of the semi-discrete solution profiles (3.3.13) at various T for IBVP (2.3.17) with $h = 0.01$. (d) Error plot of the semi-discrete solution (3.3.13) relative to the exact solution as $h \to 0$ with $T = 1$.

The global relation is then

$$e^{WT}\hat{q}(k,T) - \hat{q}(k,0) - \left[be^{-ikh}f_0 - af_1\right] = 0, \quad \text{Im}(k) \leq 0, \tag{2.4.5}$$

so that the "solution" is

$$q_n(T) = \frac{1}{2\pi}\int_{-\pi/h}^{\pi/h} e^{iknh}e^{-WT}\hat{q}(k,0)\,dk + \frac{1}{2\pi}\int_{-\pi/h}^{\pi/h} e^{iknh}e^{-WT}\left[be^{-ikh}f_0 - af_1\right]\,dk. \tag{2.4.6}$$

Returning to (2.4.4), the symmetries are found to be $\nu_0(k) = k$ and

$$\nu_1(k) = \frac{-kh-\pi}{h} + \frac{i}{h}\ln\left(\frac{ch+2}{ch-2}\right).$$

Note that regardless of the sign of $(ch+2)/(ch-2)$,

$$\text{Im}\,(\nu_1) = -\text{Im}(k) + \frac{1}{h}\ln\left|\frac{ch+2}{ch-2}\right| \leq 0 \quad \Rightarrow \quad \text{Im}(k) \geq \frac{1}{h}\ln\left|\frac{ch+2}{ch-2}\right|$$

is the condition for the global relation (2.4.5) with $\nu_1(k)$ to be valid, namely

$$e^{WT}\hat{q}(\nu_1,T) - \hat{q}(\nu_1,0) - \left[be^{-i\nu_1 h}f_0 - af_1\right] = 0. \tag{2.4.7}$$

For convenience, we define

$$k_\nu = \frac{1}{h}\ln\left|\frac{ch+2}{ch-2}\right|$$

and the region $H = \left\{k \in \mathbb{C} \,\middle|\, \text{Im}(k) \geq k_\nu\right\}$, with

$$\partial H = \left\{k \in \mathbb{C} \,\middle|\, \frac{-\pi}{h} \leq \text{Re}(k) \leq \frac{\pi}{h} \text{ and } \text{Im}(k) = k_\nu\right\},$$

since we are only interested in the $2\pi/h$ interval centered at the origin.

We now consider three different cases for c:

(i) $c \neq \pm\frac{2}{h}$
  (a) $c > 0$
  (b) $c \leq 0$

(ii) $c = \frac{2}{h}$

(iii) $c = -\frac{2}{h}$,

where we also address $c \to \pm\infty$.

(i) (a) If $c > 0$ and ignoring $c = 2/h$ for now, we see that $k_\nu > 0$, such that (2.4.7) is not valid on our integration path along the real line. Since $W(k) \to W(z)$ would introduce an essential singularity, the transformation $z = e^{ikh}$ will not help remove a boundary term. Therefore,

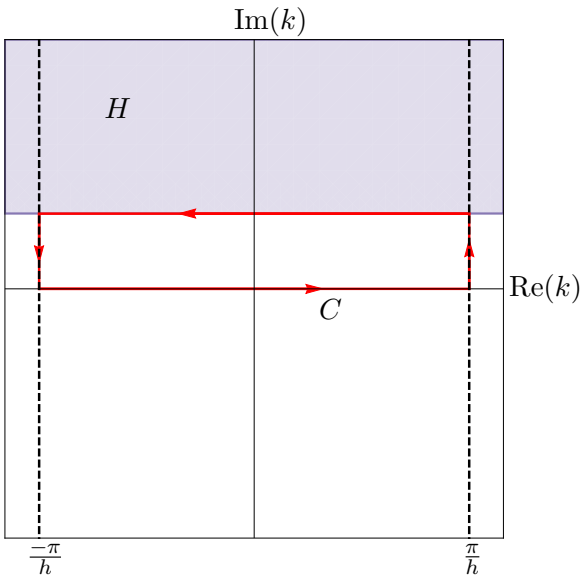

Figure 2.4.1: The shaded region denotes where the global relation (2.4.7) is valid with $k \to \nu_1(k)$ and the closed contour C.

we must deform our integration path off from the real line, so that we can use (2.4.7). Consider the counterclockwise contour C in Figure 2.4.1. The first integral in (2.4.6) is fine how it is, so we must only deform the second integral from $[-\pi/h, \pi/h]$ to ∂H like we have done before. From periodicity and Cauchy's Theorem, (2.4.6) is deformed to

$$q_n(T) = \frac{1}{2\pi}\int_{-\pi/h}^{\pi/h} e^{iknh}e^{-WT}\hat{q}(k,0)\,dk + \frac{1}{2\pi}\int_{\partial H} e^{iknh}e^{-WT}\left[be^{-ikh}f_0 - af_1\right]\,dk, \quad (2.4.8)$$

where now we can make use of (2.4.7). Solving for $f_1(W,T)$ and plugging into (2.4.8) gives

$$\begin{aligned} q_n(T) = \frac{1}{2\pi}\int_{-\pi/h}^{\pi/h} e^{iknh}e^{-WT}\hat{q}(k,0)\,dk \;+\; \frac{1}{2\pi}\int_{\partial H} e^{iknh}\hat{q}(\nu_1,T)\,dk \\ -\frac{1}{2\pi}\int_{\partial H} e^{iknh}e^{-WT}\left[\hat{q}(\nu_1,0) + a\left(e^{ikh} - e^{i\nu_1 h}\right)f_0\right]\,dk, \end{aligned} \quad (2.4.9)$$

since $b\left(e^{-ikh} - e^{-i\nu_1 h}\right) = -a\left(e^{ikh} - e^{i\nu_1 h}\right)$. For the integral term containing $\hat{q}(\nu_1, T)$, we see that

$$\frac{1}{2\pi}\int_{\partial H} e^{iknh}\hat{q}(\nu_1,T)\,dk = \frac{h}{2\pi}\sum_{m=1}^{\infty} q_m(T)\left[\int_{\partial H} e^{iknh}e^{-i\nu_1 mh}\,dk\right] = \frac{h}{2\pi}\sum_{m=1}^{\infty} q_m(T)I(n,m)$$

with

$$I(n,m) = \int_{\partial H} e^{iknh}e^{-i\nu_1 mh}\,dk.$$

Since

$$\exp\left(-i\nu_1 mh\right) = e^{i(kh+\pi)m}\left(\frac{ch+2}{ch-2}\right)^m,$$

we have

$$I(n,m) = \int_{\partial H} e^{iknh} e^{i(kh+\pi)m}\left(\frac{ch+2}{ch-2}\right)^m dk = \left(\frac{ch+2}{ch-2}\right)^m e^{i\pi m}\int_{\partial H} e^{ik(n+m)h}\, dk = 0.$$

Hence, the final solution to our convection-diffusion problem with $c > 0$ is

$$\begin{aligned} q_n(T) = &\frac{1}{2\pi}\int_{-\pi/h}^{\pi/h} e^{iknh} e^{-WT}\hat{q}(k,0)\, dk \\ &- \frac{1}{2\pi}\int_{\partial H} e^{iknh} e^{-WT}\left[\hat{q}(\nu_1,0) + a\left(e^{ikh} - e^{i\nu_1 h}\right) f_0\right] dk. \end{aligned} \tag{2.4.10}$$

Lastly, note that as $c \to \infty$ (advection becomes more dominant than diffusion),

$$k_\nu \to \frac{1}{h}\ln\left|\frac{ch}{ch}\right| = 0,$$

for a fixed h, so that

$$\partial H \to \left\{k \in \mathbb{C}\,\middle|\, \frac{-\pi}{h} \le \mathrm{Re}(k) \le \frac{\pi}{h} \text{ and } \mathrm{Im}(k) = 0\right\},$$

implying no deformation is necessary. This is similar to studying the singular perturbation problem

$$q_t = q_x + \epsilon\, q_{xx},$$

for $\epsilon \to 0$.

(b) Unlike $c > 0$, if $c \le 0$ and ignoring $c = -2/h$ for now, we see that $k_\nu \le 0$, such that (2.4.7) is valid on our integration path along the real line and there is no need to deform. Solving for $f_1(W,T)$ like above, (2.4.6) becomes (2.4.10) except back on the interval $[-\pi/h, \pi/h]$:

$$\begin{aligned} q_n(T) = &\frac{1}{2\pi}\int_{-\pi/h}^{\pi/h} e^{iknh} e^{-WT}\hat{q}(k,0)\, dk \\ &- \frac{1}{2\pi}\int_{-\pi/h}^{\pi/h} e^{iknh} e^{-WT}\left[\hat{q}(\nu_1,0) + a\left(e^{ikh} - e^{i\nu_1 h}\right) f_0\right] dk. \end{aligned} \tag{2.4.11}$$

Of course, for consistency, we could deform to ∂H like for $c > 0$. Of course, if $c = 0$, we are solving the discretized heat equation (2.2.2). As $c \to -\infty$,

$$k_\nu \to \frac{1}{h}\ln\left|\frac{ch}{ch}\right| = 0,$$

for a fixed h, so that

$$\partial H \to \left\{k \in \mathbb{C}\,\middle|\, \frac{-\pi}{h} \le \mathrm{Re}(k) \le \frac{\pi}{h} \text{ and } \mathrm{Im}(k) = 0\right\},$$

implying again no deformation is necessary.

(ii) If we set $c = 2/h$, then $a = 2/h$ and $b = 0$, so that the stencil becomes purely forward one-sided and the dispersion relation (2.4.4) now only produces the trivial symmetry. However, (2.4.6) becomes

$$q_n(T) = \frac{1}{2\pi}\int_{-\pi/h}^{\pi/h} e^{iknh}e^{-WT}\hat{q}(k,0)\,dk - \frac{a}{2\pi}\int_{-\pi/h}^{\pi/h} e^{iknh}e^{-WT}f_1\,dk, \tag{2.4.12}$$

losing dependence on $f_0(W,T)$. The problem is now ill-posed, because it does not incorporate the necessary Dirichlet boundary condition. Furthermore, we can argue away the last integral, because for this case the dispersion relation is written as a polynomial in z with all positive degrees: $W(z) = \left(2/h^2\right)(1-z)$. Deforming to an interval that goes off to $+i\infty$, the solution when $c = 2/h$ depends only on the initial condition:

$$q_n(T) = \frac{1}{2\pi}\int_{-\pi/h}^{\pi/h} e^{iknh}e^{-WT}\hat{q}(k,0)\,dk. \tag{2.4.13}$$

(iii) Lastly, if $c = -2/h$, we have $a = 0$ and $b = 2/h$, so that now the stencil becomes purely backward one-sided and the dispersion relation (2.4.4) again only produces $\nu_0(k) = k$. Therefore, the "solution" (2.4.6) is the final solution, except with $a = 0$:

$$q_n(T) = \frac{1}{2\pi}\int_{-\pi/h}^{\pi/h} e^{iknh}e^{-WT}\hat{q}(k,0)\,dk + \frac{b}{2\pi}\int_{-\pi/h}^{\pi/h} e^{ik(n-1)h}e^{-WT}f_0\,dk, \tag{2.4.14}$$

where we cannot argue away the last integral, since $W(z)$ with $z = e^{ikh}$ would introduce an essential singularity. Note that this resembles the backward discretization problem for $q_t = -\tilde{c}\,q_x$ if we let $\tilde{c} = |c| = 2/h$.

We next apply the continuous UTM to the IBVP (2.4.1). With dispersion relation $\tilde{W}(k) = k^2 - ikc$, the global relation is

$$\hat{q}(k,0) - e^{\tilde{W}T}\hat{q}(k,T) - [F_1 + (c+ik)\,F_0] = 0, \quad \mathrm{Im}(k) \le 0.$$

Inverting the transform, we obtain our first "solution:"

$$q(x,T) = \frac{1}{2\pi}\int_{-\infty}^{\infty} e^{ikx}e^{-\tilde{W}T}\hat{q}(k,0)\,dk - \frac{1}{2\pi}\int_{-\infty}^{\infty} e^{ikx}e^{-\tilde{W}T}\left[F_1 + (c+ik)\,F_0\right]\,dk. \tag{2.4.15}$$

Plugging in the nontrivial symmetry $\tilde{\nu}_1(k) = ic - k$ into the global relation,

$$\hat{q}(\tilde{\nu}_1,0) - e^{\tilde{W}T}\hat{q}(\tilde{\nu}_1,T) - [F_1 - ikF_0] = 0, \mathrm{Im}(k) \le c,$$

implies we have to lift the integration path off the real line, up to $\mathrm{Im}(k) = c$ when $c > 0$, but no deformation is necessary if $c < 0$. With the Dirichlet boundary condition, the solution for $c > 0$ is written as

$$q(x,T) = \frac{1}{2\pi}\int_{-\infty}^{\infty} e^{ikx}e^{-WT}\hat{q}(k,0)\,dk - \frac{1}{2\pi}\int_{\partial\Omega} e^{ikx}e^{-WT}\left[\hat{q}(\tilde{\nu}_1,0) + (c+2ik)\,F_0\right]\,dk, \tag{2.4.16}$$

where we introduce

$$\partial\Omega = \left\{ k \in \mathbb{C} \,\middle|\, -\infty \leq \mathrm{Re}(k) \leq \infty \text{ and } \mathrm{Im}(k) = c \right\},$$

and

$$\frac{1}{2\pi} \int_{\partial\Omega} e^{ikx} \hat{q}(\nu_1, T)\, dk = 0.$$

Similarly, if $c < 0$, the solution is (2.4.16) except back on the real line:

$$q(x,T) = \frac{1}{2\pi} \int_{-\infty}^{\infty} e^{ikx} e^{-WT} \hat{q}(k,0)\, dk - \frac{1}{2\pi} \int_{-\infty}^{\infty} e^{ikx} e^{-WT} \left[\hat{q}(\tilde{\nu}_1, 0) + (c + 2ik)\, F_0 \right] dk. \tag{2.4.17}$$

Taking the continuum limit of the dispersion relation (2.4.4) and the nontrivial symmetry $\nu_1(k)$ gives us $\lim_{h\to 0} W(k) = k^2 - ikc$ and $\lim_{h\to 0} \nu_1(k) = ic - k$, converging to their continuous counterparts. Therefore, taking the continuum limit of (2.4.10) recovers the continuous solution (2.4.16) with

$$\lim_{h\to 0} k_\nu = \lim_{h\to 0} \frac{1}{h} \ln \left| \frac{ch+2}{ch-2} \right| = c$$

for any c and hence $\lim_{h\to 0} \partial H = \partial\Omega$. Since the discrete solution (2.4.11) and continuous solution (2.4.17) with $c < 0$ are identical to the solutions with $c > 0$, it is clear that taking the continuum limit of (2.4.11) produces (2.4.17).

Remark 2.4.1. The discrete solutions (2.4.13) and (2.4.14) for $c = \pm 2/h$ exist only in the discrete realm and are ill-posed as we take $h \to 0$. Neither of the dispersion relations converge to the continuous one for these cases of c, not to mention the $1/h$ in the second term of (2.4.14).

2.5 Small-Time Increments

For nonlinear IBVPs, neither the semi-discrete nor the continuous UTM is applicable in general. Although the UTM can be used to solve IBVPs for integrable PDEs, our goal is broader: we are interested in numerically solving IBVPs for quasilinear PDEs (1.1.1), where the most nonlocal stencil is applied to the linear problem. To do so accurately, we can employ split-step methods following the ideas from operator splitting.

A split-step method requires the repeated computation of the solution to the linear problem (1.1.3) with $t \ll 1$, but the integral representations from semi-discrete UTM can be expensive to compute. In what follows, we evaluate the semi-discrete UTM solutions using a $t \ll 1$ approximation to derive an approximate semi-discrete UTM solution with predetermined accuracy in t. Here, we demonstrate this procedure for the advection equation $q_t = -c\, q_x$ on the half line with the standard backward stencil (2.1.12) applied to q_x, while more details and further investigations will be presented in a future paper. Since a split-step approach solves an updated IBVP starting from t_0, we generalize

the original IBVP (2.1.11) to

$$\begin{cases} q_t = -c\, q_x, & x > 0,\ t > t_0 \\ q\,(x, t_0) = \phi(x), & x > 0, \\ q(0, t) = u(t), & t > t_0, \end{cases} \tag{2.5.1}$$

where $\phi(x)$ is the output from the previous step.

Starting from t_0, the time transforms from the semi-discrete UTM are redefined as

$$f_j\,(W, t_0, T) = \int_{t_0}^{T} e^{Wt} q_j(t)\, dt, \quad k \in \mathbb{C},$$

which, for the IBVP (2.5.1), gives the global relation

$$\begin{aligned} & \sum_{n=1}^{\infty} h \int_{t_0}^{T} \left[\partial_t \left(e^{-iknh} e^{Wt} q_n\right) + \frac{c}{h} \Delta \left(e^{-iknh} e^{Wt} q_{n-1}\right)\right] dt = 0 \\ \Rightarrow \quad & e^{WT} \hat{q}(k, T) - e^{Wt_0} \hat{q}\,(k, t_0) - c e^{-ikh} f_0 = 0, \end{aligned} \tag{2.5.2}$$

valid for $\mathrm{Im}(k) \leq 0$. Solving for $\hat{q}(k, T)$ and inverting, we obtain

$$q_n\,(T; t_0) = \frac{1}{2\pi} \int_{-\pi/h}^{\pi/h} e^{iknh} e^{-W(T-t_0)} \hat{q}\,(k, t_0)\ dk + \frac{c}{2\pi} \int_{-\pi/h}^{\pi/h} e^{ik(n-1)h} e^{-WT} f_0\, dk. \tag{2.5.3}$$

Following similar arguments as before, (2.5.3) is the solution to the backward-discretized IBVP (2.5.1) with a given Dirichlet boundary condition at $x = 0$ and an initial condition at $t = t_0$. In what follows, we expand (2.5.3) in $\tau = T - t_0 \ll 1$, around $\tau = 0$, so as to obtain a convenient approximation to be used in a split-step method.

The first integral of (2.5.3) has time dependence only through $e^{-W\tau}$. Expanding this exponential gives a series of integrals that, in general, lead to more computations than necessary and introduce an approximation error when the series is truncated. Hence, this first integral is kept as is. The second integral of (2.5.3) has time dependence in both e^{-WT} and $f_0\,(W, t_0, T)$. We consider these together:

$$e^{-WT} f_0 = e^{-WT} \int_{t_0}^{T} e^{Wt} q_0(t)\, dt = e^{-W\tau} \int_{0}^{\tau} e^{W\tilde{t}} q_0\left(\tilde{t} + t_0\right)\ d\tilde{t}.$$

Since the limits of integration approach zero as $\tau \to 0$, we expand $e^{W\tilde{t}} q_0\left(\tilde{t} + t_0\right)$ about $\tilde{t} = 0$ up to arbitrary $\mathcal{O}\left(\tau^r\right)$ ($r = 3$ for demonstration), so that the integrals have polynomial dependence on time:

$$e^{-WT} f_0 = q_0\,(t_0)\,\tau + \frac{q_0'\,(t_0) - W q_0\,(t_0)}{2}\,\tau^2 + \frac{q_0''\,(t_0) - W q_0'\,(t_0) + W^2 q_0\,(t_0)}{6}\,\tau^3 + \mathcal{O}\left(\tau^4\right).$$

The second integral of (2.5.3) reduces to

$$\frac{c}{2\pi}\int_{-\pi/h}^{\pi/h} e^{ik(n-1)h}e^{-WT}f_0\,dk = \frac{c\,q_0\,(t_0)\,\tau}{h}\delta_{1n} + \frac{c\tau^2}{4\pi}\int_{-\pi/h}^{\pi/h} e^{ik(n-1)h}\left[q_0'\,(t_0) - Wq_0\,(t_0)\right]\,dk$$
$$+ \frac{c\tau^3}{12\pi}\int_{-\pi/h}^{\pi/h} e^{ik(n-1)h}\left[q_0''\,(t_0) - Wq_0'\,(t_0) + W^2q_0\,(t_0)\right]\,dk + \mathcal{O}\left(\tau^4\right),$$

where δ_{ij} is the Kronecker delta. Therefore, after defining $\phi(x) = q\,(x, t_0)$ and $u(t) = q(0, t)$, the solution (2.5.3) is expanded as

$$q_n(\tau) = \frac{1}{2\pi}\int_{-\pi/h}^{\pi/h} e^{iknh}e^{-W\tau}\hat{\phi}(k)\,dk \;+\; K_1(n)\tau \;+\; K_2(n)\tau^2 \;+\; K_3(n)\tau^3 \;+\; \mathcal{O}\left(\tau^4\right), \tag{2.5.4}$$

with

$$K_1(n) = \frac{c\,u\,(t_0)}{h}\delta_{1n},$$
$$K_2(n) = \frac{c}{4\pi}\int_{-\pi/h}^{\pi/h} e^{ik(n-1)h}\left[u'\,(t_0) - Wu\,(t_0)\right]\,dk,$$
$$K_3(n) = \frac{c}{12\pi}\int_{-\pi/h}^{\pi/h} e^{ik(n-1)h}\left[u''\,(t_0) - Wu'\,(t_0) + W^2u\,(t_0)\right]\,dk.$$

A similar process can be repeated for other IBVPs.

As a numerical example, consider the IBVP

$$\begin{cases} q_t = -q_x, & x > 0,\ t > t_0, \\ q\,(x, t_0) = \phi(x) = \dfrac{e^{-2x}\,(\sin\,(4\pi x) + 1)}{2}, & x > 0, \\ q(0, t) = u(t) = \dfrac{1}{2} + (1 - 2\pi)te^{-t}, & t > t_0, \end{cases} \tag{2.5.5}$$

with $t_0 = 0$. Figure 2.5.1a depicts the errors, relative to the exact solution, as $h \to 0$ for the semi-discrete UTM solution (2.1.16) and *small-time approximated* semi-discrete UTM solution (2.5.4) up to terms of order 2. Despite only including terms up to second order, the errors in the plot are indistinguishable, implying we need not include higher-order terms to obtain a suitable small-time approximate solution (2.5.4). Figure 2.5.1b depicts the errors for the small-time solution (2.5.4) as $\tau \to 0$ for a fixed h, relative to (2.1.16). This plot shows that relatively large values of τ lead to an accurate approximation to (2.1.16).

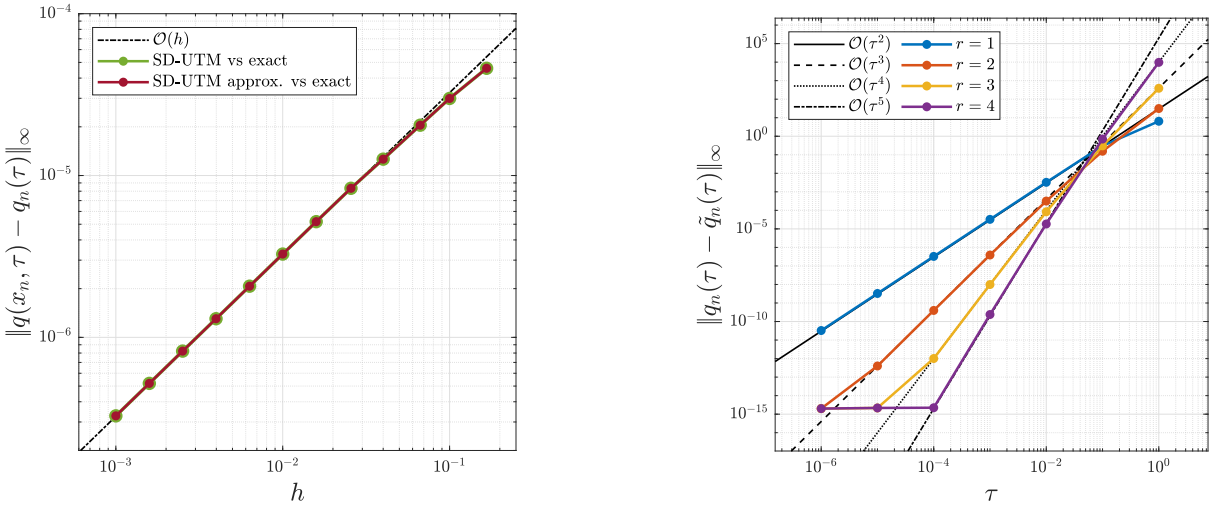

Figure 2.5.1: (a) The error (green) between the SD-UTM solution (2.1.16) and the exact solution and the error (maroon) between the exact solution and the small-time approximated SD-UTM solution (2.5.4) with $r = 2$ and $\tau = 10^{-5}$ as $h \to 0$. (b) The error between the SD-UTM solution (2.1.16) and the small-time approximated SD-UTM solution (2.5.4) (denoted as $\tilde{q}_n(\tau)$ here) for varying order r of terms kept in the approximated solution as $\tau \to 0$ with $h = 0.01$.

Chapter 3

FINITE INTERVAL PROBLEMS

Again, we begin by discussing advection equations in some detail to show how the UTM is applied to semi-discrete problems on the finite interval. The procedure is fairly similar to the previous chapter, but introducing an additional boundary at $x = L$ can lead to pole singularities within the SD-UTM integral representations. We will show how to tackle these and other features that commonly arise in finite-interval problems.

To compare with standard numerical approaches for finite-interval problems, finite-difference solutions are obtained using a method-of-lines approach with the same spatial discretization as the semi-discrete UTM approach, so that we set up the full discretization of the PDE into a large, but sparse, system of ordinary differential equations (ODEs). For example, the centered-discretized heat equation with Dirichlet boundary conditions is formulated as

$$q_t(x,t) = q_{xx}(x,t) \quad \Rightarrow \quad \dot{q}_n(t) = \frac{q_{n+1}(t) - 2q_n(t) + q_{n-1}(t)}{h^2} \quad \Rightarrow \quad \dot{Q}(t) = AQ(t) + g(t) + p(t),$$

where $Q(t) \in \mathbb{R}^N$ is a column vector composed of all $q_n(t)$, $A \in \mathbb{R}^{N\times N}$ is a sparse tridiagonal matrix, and both $g(t) \in \mathbb{R}^N$ and $p(t) \in \mathbb{R}^N$ are sparse column vectors that include boundary conditions from the left and right, respectively. The system of ODEs above is discretized in time and solved via the forward Euler (FE), Runge-Kutta fourth-order (RK4), backward Euler (BE), and trapezoidal (TR) methods. In summary, we compare the exact solution of an IBVP to these four classical numerical solutions and the SD-UTM explicit solution, which exactly solves the spatially discretized problem, *i.e.*, requires no time-stepping. These finite-difference methods are for comparisons and not the main focus, so we discuss implementation and other details only when necessary. Of course in practice, more sophisticated explicit methods would be used, but we proceed with the standard methods for demonstration purposes. The exact solutions to the example second-order IBVPs are derived using classical methods, like Fourier sine/cosine series.

3.1 Advection Equations

3.1.1 Forward Discretization of $q_t = c\,q_x$

We start with the continuous problem for the advection equation $q_t = c\,q_x$ with wave-speed $c > 0$:

$$\begin{cases} q_t = c\,q_x, & 0 < x < L,\ t > 0, \\ q(x,0) = \phi(x), & 0 < x < L, \\ q(L,t) = v^{(0)}(t), & t > 0. \end{cases} \tag{3.1.1}$$

For well posedness, the IBVP requires the initial condition and a Dirichlet boundary condition at $x = L$. Since information travels from right to left, a forward discretization of $q_x(x,t)$ is natural, and we reconsider (2.1.2):

$$\dot{q}_n(t) = c\,\frac{q_{n+1}(t) - q_n(t)}{h}.$$

Like in Section 2.1.1, (2.1.2) is rewritten as the one-parameter family of problems (2.1.3) with dispersion relation (2.1.4), which only has the trivial symmetry $\nu_0(k) = k$, up to periodic copies. From the local relation (2.1.3), we obtain the global relation by taking a time transform over $t \in [0,T]$ and a finite sum from $n = 0$ (because $q_0(t)$ is not known) to $n = N$ (because $q_{N+1}(t)$ is known):

$$\begin{aligned} &\sum_{n=0}^{N} h \int_0^T \left[\partial_t \left(e^{-iknh} e^{Wt} q_n\right) - \frac{c}{h}\Delta\left(e^{-ik(n-1)h} q_n\right) e^{Wt}\right] dt = 0 \\ \Rightarrow \qquad & e^{WT}\hat{q}(k,T) - \hat{q}(k,0) - c\left[-e^{ikh} f_0 + e^{-ik(L-h)} g_0\right] = 0, \quad k \in \mathbb{C}. \end{aligned} \tag{3.1.2}$$

Solving for $\hat{q}(k,T)$ and inverting using the inverse transform (1.3.1b),

$$q_n(T) = \frac{1}{2\pi}\int_{-\pi/h}^{\pi/h} e^{iknh} e^{-WT}\hat{q}(k,0)\,dk + \frac{c}{2\pi}\int_{-\pi/h}^{\pi/h} e^{iknh} e^{-WT}\left[-e^{ikh} f_0 + e^{-ik(L-h)} g_0\right] dk. \tag{3.1.3}$$

Since the Fourier transform $\hat{q}(k,0)$ consists of a finite sum, both integrands of (3.1.3) are defined for all $k \in \mathbb{C}$. We refer to the expression above as the "solution," since $f_0(W,T)$ in the second integral term is not known, unlike $g_0(W,T)$. For $n = 0,\dots,N$, $e^{ik(n+1)h}$ decays in the upper-half plane and e^{-WT} is bounded in the shaded regions, including on the boundary, of Figure 2.1.1.

Following the approach discussed for half-line semi-discrete problems, we show that (3.1.3) does not depend on $f_0(W,T)$, *i.e.*, no Dirichlet boundary data at $x = 0$ is required by substituting the definition of $f_0(W,T)$ and deforming to the new path D^+ (see Section 2.1.1). Because of the exponential decay above the real line,

$$\frac{c}{2\pi}\int_{-\pi/h}^{\pi/h} e^{ik(n+1)h} e^{-WT} f_0\,dk = 0.$$

It follows that the solution to the finite interval IBVP with the forward discretization (2.1.2) depends only on the initial condition and Dirichlet data at $x = L$:

$$q_n(T) = \frac{1}{2\pi}\int_{-\pi/h}^{\pi/h} e^{iknh} e^{-WT}\hat{q}(k,0)\,dk + \frac{c}{2\pi}\int_{-\pi/h}^{\pi/h} e^{ik(nh-L+h)} e^{-WT} g_0\,dk. \tag{3.1.4}$$

Note that e^{-WT} grows in the lower-half plane, and we cannot deform and remove the integral contribution from $g_0(W,T)$ for the same n. Thus, (3.1.4) is the final representation of the solution.

For reference, we solve the IBVP (3.1.1) using the continuous UTM, following Steps (1) – (8) from Section 1.2. In short, we find the dispersion relation $\tilde{W}(k) = -ick$, with only the trivial symmetry $\tilde{\nu}_0(k) = k$, and the global relation

$$\hat{q}(k,0) - e^{\tilde{W}T}\hat{q}(k,T) + c\left(-F_0 + e^{-ikL} G_0\right) = 0, \quad k \in \mathbb{C},$$

where

$$\hat{q}(k,t) = \int_0^L e^{-ikx} q(x,t)\, dx, \quad k \in \mathbb{C},$$

and the time transform at the right boundary is similarly defined as the transform on the left:

$$G_j(\tilde{W},T) = \int_0^T e^{\tilde{W}t} \left.\frac{\partial^j q}{dx^j}\right|_{x=L} dt, \quad k \in \mathbb{C}.$$

After inverting the Fourier transform and showing there is no dependence on $F_0(\tilde{W},T)$, the solution is represented as

$$q(x,T) = \frac{1}{2\pi}\int_{-\infty}^{\infty} e^{ikx} e^{-\tilde{W}T} \hat{q}(k,0)\, dk + \frac{c}{2\pi}\int_{-\infty}^{\infty} e^{ik(x-L)} e^{-\tilde{W}T} G_0\, dk. \tag{3.1.5}$$

Taking the limit as $h \to 0$ of (3.1.4), we recover (3.1.5), where the limits of integration approach $\pm\infty$ at rate $1/h$, $\lim_{h\to 0} W(k) = -cik = \tilde{W}$, and $\lim_{h\to 0} e^{ik(nh-L+h)} = e^{ik(x-L)}$ with $nh = x_n \to x$ and

$$\lim_{h\to 0} g_j(W,T) = \lim_{h\to 0}\int_0^T e^{Wt} q(L+jh,t)\, dt = \int_0^T e^{\tilde{W}t} q(L,t)\, dt = G_0(\tilde{W},T),$$

for any fixed j.

After substituting the definitions of $\hat{q}(k,0)$ and G_0 in (3.1.5), we recover the classical, traveling wave solution:

$$q(x,T) = \begin{cases} \phi(x+cT)\,, & 0 < x < L - cT, \\ v^{(0)}\left(\frac{x-L}{c} + T\right)\,, & L - cT < x < L. \end{cases} \tag{3.1.6}$$

Series Representation

To facilitate numerical computation, we simplify the solution (3.1.4) by substituting the definitions of $\hat{q}(k,0)$ and $g_0(W,T)$. For the initial-condition integral term with $\phi(x_n) \equiv \phi_n$,

$$\frac{1}{2\pi}\int_{-\pi/h}^{\pi/h} e^{iknh} e^{-WT} \hat{q}(k,0)\, dk = \sum_{m=0}^{N}\left[\frac{h}{2\pi}\int_{-\pi/h}^{\pi/h} e^{ik(n-m)h} e^{-WT}\, dk\right]\phi_m.$$

The integral can be evaluated with $z = e^{ikh}$ and $W(z) = c(1-z)/h$:

$$\frac{h}{2\pi}\int_{-\pi/h}^{\pi/h} e^{ik(n-m)h} e^{-WT}\, dk = \frac{e^{-cT/h}}{2\pi i}\oint_{|z|=1} z^{n-m-1} e^{\frac{cT}{h}z}\, dz = e^{-cT/h}\operatorname*{Res}_{z=0}\left\{z^{n-m-1} e^{\frac{cT}{h}z}\right\} = \frac{e^{-cT/h}}{(m-n)!}\left(\frac{cT}{h}\right)^{m-n}.$$

Since $m \geq n$, the initial condition integral gives

$$\frac{1}{2\pi}\int_{-\pi/h}^{\pi/h} e^{iknh} e^{-WT} \hat{q}(k,0)\, dk = \sum_{m=n}^{N}\frac{e^{-cT/h}}{(m-n)!}\left(\frac{cT}{h}\right)^{m-n}\phi_m = e^{-cT/h}\sum_{m=0}^{N-n}\left(\frac{cT}{h}\right)^{m}\frac{\phi_{n+m}}{m!}.$$

The boundary integral from (3.1.4) is treated similarly by substituting the definition for $g_0(W,T)$ in terms of $v^{(0)}(t)$:

$$\frac{c}{2\pi}\int_{-\pi/h}^{\pi/h} e^{ik(nh-L+h)}e^{-WT}g_0\,dk = c\int_0^T\left[\frac{1}{2\pi}\int_{-\pi/h}^{\pi/h} e^{ik(n-N)h}e^{-W(T-t)}\,dk\right]v^{(0)}(t)\,dt,$$

after substituting $L=(N+1)h$. Again with $z=e^{ikh}$,

$$\begin{aligned}\frac{1}{2\pi}\int_{-\pi/h}^{\pi/h} e^{ik(n-N)h}e^{-W(T-t)}\,dk &= \frac{e^{-c(T-t)/h}}{2\pi i h}\oint_{|z|=1} z^{n-N-1}e^{\frac{c(T-t)}{h}z}\,dz\\ &= \frac{e^{-c(T-t)/h}}{h}\operatorname*{Res}_{z=0}\left\{z^{n-N-1}e^{\frac{c(T-t)}{h}z}\right\}\\ &= \frac{e^{-c(T-t)/h}}{h}\left(\frac{c(T-t)}{h}\right)^{N-n}\frac{1}{(N-n)!}.\end{aligned}$$

Hence,

$$\frac{c}{2\pi}\int_{-\pi/h}^{\pi/h} e^{ik(nh-L+h)}e^{-WT}g_0\,dk = \frac{c}{h}\int_0^T e^{-c(T-t)/h}\left(\frac{c(T-t)}{h}\right)^{N-n}\frac{v^{(0)}(t)}{(N-n)!}\,dt.$$

Thus, (3.1.4) is rewritten as

$$q_n(T) = e^{-cT/h}\sum_{m=0}^{N-n}\left(\frac{cT}{h}\right)^m\frac{\phi_{n+m}}{m!} + \frac{c}{h}\int_0^T e^{-c(T-t)/h}\left(\frac{c(T-t)}{h}\right)^{N-n}\frac{v^{(0)}(t)}{(N-n)!}\,dt. \tag{3.1.7}$$

Unlike for the classical continuous solution (3.1.6), the initial and boundary conditions in the semi-discrete solution (3.1.7) are inseparable and both contribute at every mesh point. For computational purposes, the factorials become too large to store in finite precision as we refine h, and one last rewrite is in order. For the sum in (3.1.7),

$$\left(\frac{cT}{h}\right)^m\frac{1}{m!} = \exp\left[m\ln\left(\frac{cT}{h}\right) - \ln\left[\Gamma\left(m+1\right)\right]\right],$$

so that combining with $e^{-cT/h}$ gives

$$e^{-cT/h}\sum_{m=0}^{N-n}\left(\frac{cT}{h}\right)^m\frac{\phi_{n+m}}{m!} = \sum_{m=0}^{N-n}\exp\left[m\ln\left(\frac{cT}{h}\right) - \ln\left[\Gamma\left(m+1\right)\right] - \frac{cT}{h}\right]\phi_{n+m}.$$

After a similar rewrite for the integral term, (3.1.7) becomes

$$\begin{aligned}q_n(T) = &\sum_{m=0}^{N-n}\exp\left[m\ln\left(\frac{cT}{h}\right) - \ln\left[\Gamma\left(m+1\right)\right] - \frac{cT}{h}\right]\phi_{n+m}\\ &+ c\int_0^T\exp\left[(N-n)\ln\left(\frac{c(T-t)}{h}\right) - \ln\left[\Gamma\left(N-n+1\right)\right] - \frac{c(T-t)}{h} - \ln(h)\right]v^{(0)}(t)\,dt.\end{aligned} \tag{3.1.8}$$

Using MATLAB, we can make use of the built-in `integral()` and `gammaln()` functions.

From the stencil (2.1.2), we know that (3.1.4), and hence (3.1.8), is a first-order accurate approximation to the solution $q(x,T)$ of the IBVP (3.1.1). However, deriving the modified equation (2.1.10) implies that (3.1.4) is a second-order accurate solution approximation to the advection-diffusion PDE, so we expect solution profiles of (3.1.4) to travel at the correct speed c, while dissipating in time.

As an explicit example, we compute the numerical solution of

$$\begin{cases} q_t = q_x, & 0 < x < 1,\ t > 0, \\ q(x,0) = \phi(x) = \operatorname{sech}\left[200(x-0.925)\right] + \operatorname{sech}\left[40(x-0.425)\right], & 0 < x < 1, \\ q(1,t) = v^{(0)}(t) = \phi(1+t), & t > 0, \end{cases} \tag{3.1.9}$$

with $c = 1$ and $L = 1$, so that the boundary condition acts as the continuation of the initial condition from outside the interval for $t > 0$. The initial condition consists of two peaks of equal heights, except the leading peak is wider than the trailing peak. We solve (3.1.9) with the aforementioned finite-difference numerical methods and the SD-UTM solution (3.1.8) via a first-order spatial forward discretization. Figure 3.1.1 shows the semi-discrete solution $q_n(t)$ (left panel) and a log-log error plot (right panel) of the ∞-norm of $q_n(0.25) - q(x_n, 0.25)$, as a function of h, where the finite-difference schemes use a fixed time step $\Delta t = 2.5 \times 10^{-3}$. The (x_n, t)-plot in Figure 3.1.2a shows that both peaks decrease in amplitude and widen as time increases, predicted by the modified PDE (2.1.10), with the narrow peak quickly dissipating compared to the wider peak. The error plot in Figure 3.1.2b shows that SD-UTM works well compared to the traditional numerical methods. Of course, the finite difference methods will only converge when $h, \Delta t \to 0$ together, but we choose to keep Δt constant as $h \to 0$ to directly show that the SD-UTM solutions do not require any intricate stability conditions. We similarly keep Δt fixed for most numerical examples in this thesis (see Section 3.4 for the exception). The explicit methods become unstable after their CFL conditions are violated [43] and the implicit methods' errors are asymptotic to the temporal truncation errors as $h \to 0$ for a fixed time step Δt. Figure 3.1.2b demonstrates there is no CFL condition for the SD-UTM to succeed, while, for example, FE only works well for large h values where $\Delta t/h \leq 1$. The implicit methods do not have such restrictions, but have truncation error $\mathcal{O}(h) + \mathcal{O}(\Delta t^p)$, where $p = 1$ for BE and $p = 2$ for TR. For a fixed Δt, only the spatial error decreases as $h \to 0$, while $\mathcal{O}(\Delta t^p)$ remains and eventually dominates. The asymptotic limits of BE and TR in Figure 3.1.2b as $h \to 0$ reveal this temporal truncation error. Figure 3.1.2b implies that the SD-UTM solution (3.1.8) has a slow convergence rate to the continuous solution for this IBVP, likely due to the sharp peak, reaching the expected $\mathcal{O}(h)$ for $h < 10^{-5}$.

Figure 3.1.2 compares the exact solution with the numerical solution profiles for all methods, except FE and RK4 due to their instabilities, with $h = 10^{-4}$. For the SD-UTM, we simply compute the solution (3.1.8) at $T = 0.25$ once, while the finite-difference solutions time-step to $T = 0.25$

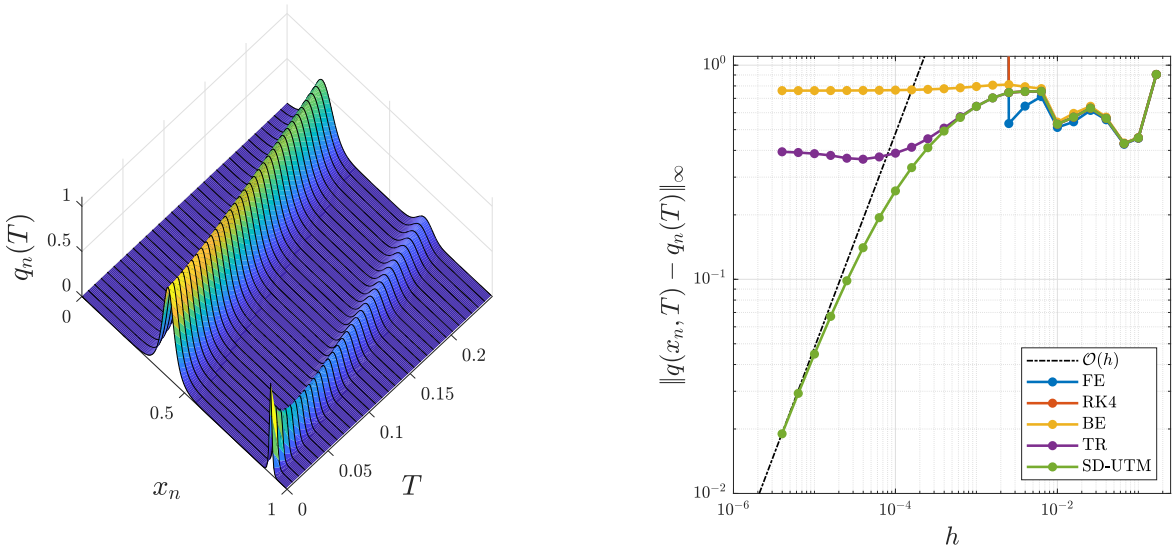

(a) (b)

Figure 3.1.1: (a) The semi-discrete solution (3.1.8) evaluated at various T with $h = 0.005$. (b) Error plot of the semi-discrete solution (3.1.8) and finite-difference schemes relative to the exact solution as $h \to 0$ with $T = 0.25$ and $\Delta t = 2.5 \times 10^{-3}$.

with step size $\Delta t = 2.5 \times 10^{-3}$. From the solution plot, it appears that every method is dissipative, including FE and RK4 (not shown), and TR is also dispersive. With the SD-UTM, both peaks drop in amplitude and diffuse, while the dispersive nature of TR is apparent near the sharper peak. Despite the lack of a dispersive tail like the other implicit method, it appears that BE is more dissipative than all the other tested methods. In summary, the SD-UTM performs better than the finite-difference methods presented. Even though dissipation is evident, dispersion is not.

3.1.2 Higher-Order One-Sided Discretization of $q_t = c\, q_x$

All forward discretizations produce $f_j(W,T)$ terms with a coefficient $C_j\, e^{i\gamma_j kh}$ for some $C_j \in \mathbb{C}$ and $\gamma_j \in \mathbb{N}$ in the global relation. Coupled with a polynomial dispersion relation $W(z)$, we can remove all integral terms containing any $f_j(W,T)$ from "solutions" using the steps above. On the opposite side of the interval, more terms with $g_j(W,T)$ are introduced, but with the help of symmetries or additional boundary conditions given by the PDE, we can remove the unknown $g_j(W,T)$ terms. The steps in the semi-discrete UTM become more intricate and tedious, yet remain systematic.

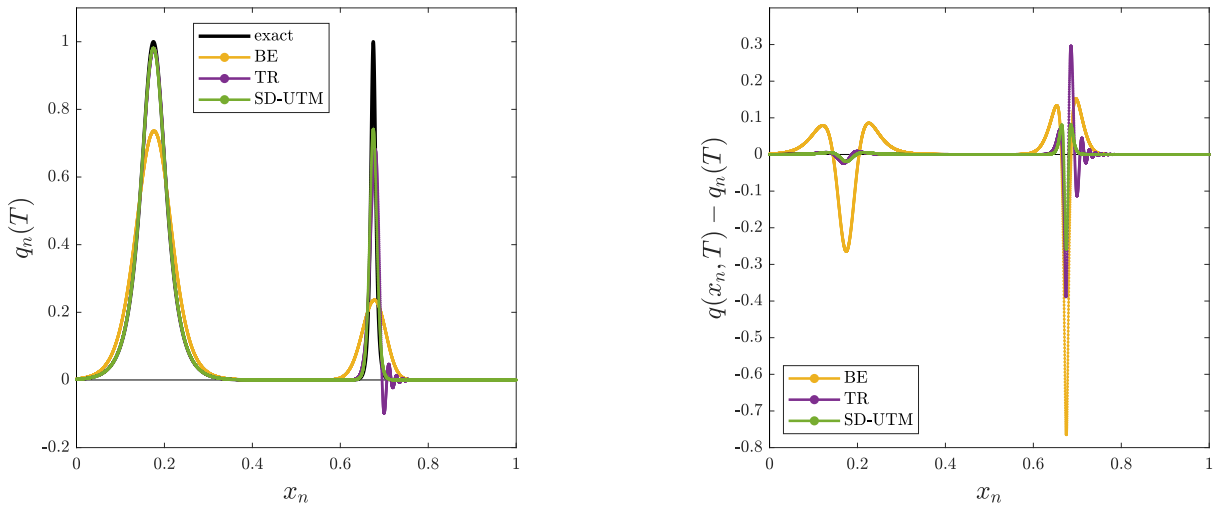

(a) (b)

Figure 3.1.2: (a) The numerical solutions to IBVP (3.1.9) at $T = 0.25$ with $h = 10^{-4}$ for all the methods and $\Delta t = 2.5 \times 10^{-3}$ for the finite-difference methods. (b) The difference between the exact solution and the numerical solutions under the same conditions as (a).

We consider a second-order stencil for a forward discretization of $q_x(x,t)$:

$$\dot{q}_n(t) = c\,\frac{-3q_n(t) + 4q_{n+1}(t) - q_{n+2}(t)}{2h}. \tag{3.1.10}$$

We find the local relation

$$\partial_t\left(e^{-iknh}e^{Wt}q_n\right) = \frac{c}{2h}\Delta\left(4e^{-ik(n-1)h}e^{Wt}q_n - e^{-ik(n-1)h}e^{Wt}q_{n+1} - e^{-ik(n-2)h}e^{Wt}q_n\right), \tag{3.1.11}$$

with dispersion relation

$$W(k) = c\,\frac{3 - 4e^{ikh} + e^{2ikh}}{2h}. \tag{3.1.12}$$

Taking a time transform and a finite sum from $n = 0$ to $n = N$, the global relation is

$$e^{WT}\hat{q}(k,T) - \hat{q}(k,0) - \frac{c}{2}\left(f(k,T) + e^{-ikL}g(k,T)\right) = 0, \quad k \in \mathbb{C}, \tag{3.1.13}$$

where

$$\begin{cases} f(k,T) = e^{2ikh}f_0 - 4e^{ikh}f_0 + e^{ikh}f_1, \\ g(k,T) = 4e^{ikh}g_0 - e^{2ikh}g_0 - e^{ikh}g_1. \end{cases}$$

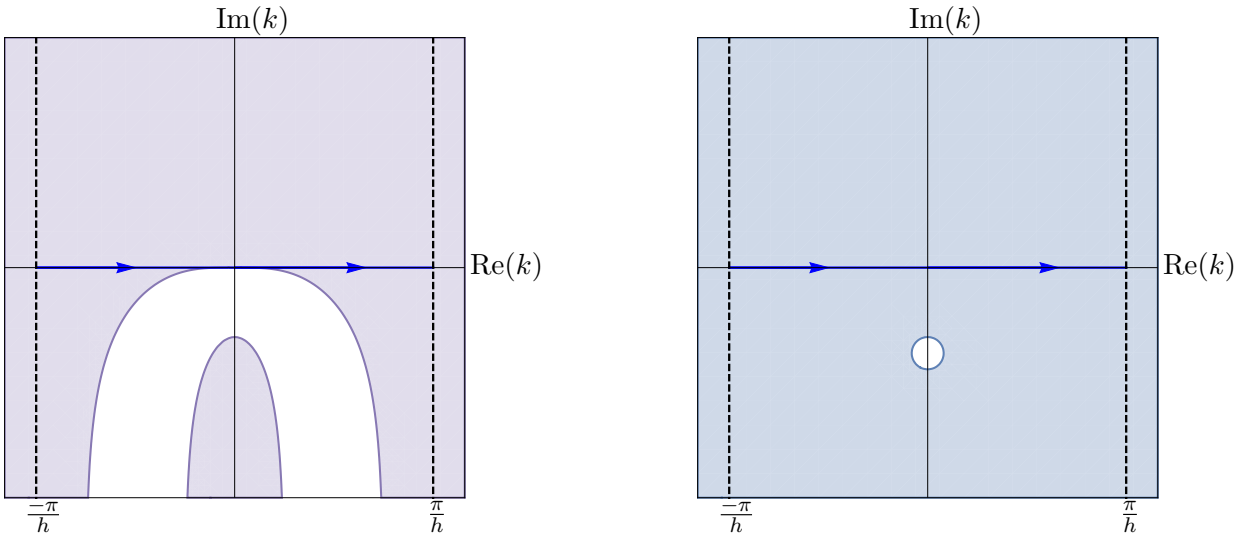

Figure 3.1.3: (a) The shaded regions depict where $\mathrm{Re}(-W) \leq 0$ and e^{-WT} is bounded, for the dispersion relation (3.1.12). (b) The shaded regions depict where the global relation with $k \to \nu_1(k)$ is valid, *i.e.*, $\mathrm{Im}(\nu_1) \leq 0$.

Solving for $\hat{q}(k,T)$ and using the inverse transform,

$$q_n(T) = \frac{1}{2\pi}\int_{-\pi/h}^{\pi/h} e^{iknh}e^{-WT}\hat{q}(k,0)\,dk + \frac{c}{2\pi}\int_{-\pi/h}^{\pi/h} e^{iknh}e^{-WT}\left[\frac{f(k,T)+e^{-ikL}g(k,T)}{2}\right]dk. \tag{3.1.14}$$

We can deform and remove $f(k,T)$ from "solution" (3.1.14), so that

$$q_n(T) = \frac{1}{2\pi}\int_{-\pi/h}^{\pi/h} e^{iknh}e^{-WT}\hat{q}(k,0)\,dk + \frac{c}{2\pi}\int_{-\pi/h}^{\pi/h} e^{ik(nh-L+h)}e^{-WT}\left[\frac{\left(4-e^{ikh}\right)g_0 - g_1}{2}\right]dk. \tag{3.1.15}$$

Figure 3.1.3a illustrates this, since e^{-WT} is bounded in the whole upper-half plane. Thus, the second integral term of (3.1.15) depends only on the transformed Dirichlet data and data at the unknown ghost point $q_{N+2}(T) = q(L+h,T)$ through $g_1(W,T)$.

The dispersion relation (3.1.12) has the nontrivial symmetry

$$\nu_1(k) = \frac{\ln\left(4-e^{ikh}\right)}{ih},$$

up to periodic copies. The global relation (3.1.13) with $k \to \nu_1(k)$ is valid for all $k \in \mathbb{C}$, except for a bounded region in the lower-half plane shown in Figure 3.1.3b. We solve this global relation for

the unknown $g_1(W,T)$ to find

$$g_1 = e^{ikh}g_0 - e^{ikh}\left(4-e^{ikh}\right)^{N+1} f_0 + \left(4-e^{ikh}\right)^{N+1} f_1 + \frac{2\left(4-e^{ikh}\right)^N}{c}\left[\hat{q}(\nu_1,0) - e^{WT}\hat{q}(\nu_1,T)\right],$$

where $e^{i\nu_1 L} = \left(4-e^{ikh}\right)^{N+1}$ with $L = (N+1)h$. Substituting into (3.1.15) does not only reintroduce dependence on $f_0(W,T)$ and $f_1(W,T)$ that can no longer be deformed away, but it also introduces a nonzero contribution from $\hat{q}(\nu_1,T)$, the transform of the solution itself.

In Section 2.1.4, we presented an alternative route to obtain a valid solution representation. Returning to the continuous problem (3.1.1), the PDE itself gives first and second-derivative boundary conditions from the Dirichlet condition:

$$q_x(L,t) = \frac{\dot{v}(t)}{c}, \quad \dot{v}(t) = \frac{d}{dt}v^{(0)}(t), \tag{3.1.16a}$$

$$q_{xx}(L,t) = \frac{\ddot{v}(t)}{c^2}, \quad \ddot{v}(t) = \frac{d^2}{dt^2}v^{(0)}(t). \tag{3.1.16b}$$

We discretize the derivative conditions using centered second-order accurate stencils and apply time transforms:

$$\frac{g_1 - g_{-1}}{2h} = \frac{\dot{V}}{c}, \qquad \dot{V}(W,T) = \int_0^T e^{Wt}\dot{v}(t)\,dt, \tag{3.1.17a}$$

$$\frac{g_1 - 2g_0 + g_{-1}}{h^2} = \frac{\ddot{V}}{c^2}, \qquad \ddot{V}(W,T) = \int_0^T e^{Wt}\ddot{v}(t)\,dt. \tag{3.1.17b}$$

Solving (3.1.17a) and (3.1.17b) for $g_1(W,T)$ and $g_{-1}(W,T)$ gives

$$\begin{aligned} q_n(T) = {} & \frac{1}{2\pi}\int_{-\pi/h}^{\pi/h} e^{iknh}e^{-WT}\hat{q}(k,0)\,dk + \frac{c}{2\pi}\int_{-\pi/h}^{\pi/h} e^{ik(nh-L+h)}e^{-WT}\left[\frac{\left(3-e^{ikh}\right)}{2}g_0\right]dk \\ & - \frac{c}{2\pi}\int_{-\pi/h}^{\pi/h} e^{ik(nh-L+h)}e^{-WT}\left[\frac{h}{2c}\dot{V} + \frac{h^2}{4c^2}\ddot{V}\right]dk. \end{aligned} \tag{3.1.18}$$

The additional steps of including (3.1.17a) and (3.1.17b) allow (3.1.18) to maintain $\mathcal{O}(h^2)$ accuracy. The modified PDE corresponding to the second-order discretization (3.1.10) is the dispersive PDE $p_t = cp_x - (ch^2/3)p_{xxx}$, and (3.1.18) is its third-order approximation (the omitted higher-order term in the modified PDE is $\mathcal{O}(h^3)$). The stencils (3.1.17a) and (3.1.17b) are both fourth-order approximations to their respective modified PDEs with nonzero $\mathcal{O}(h^2)$ coefficients. As before, the semi-discrete solution (3.1.18) converges to (3.1.5) as $h \to 0$ and correctly loses dependence on the Neumann boundary condition in the continuum limit.

Series Representation

We rewrite solution (3.1.18) by substituting the definitions of $\hat{q}(k,0)$, $g_0(W,T)$, and $\dot{V}_0(W,T)$. For the initial-condition integral term,

$$\frac{1}{2\pi}\int_{-\pi/h}^{\pi/h} e^{iknh}e^{-WT}\hat{q}(k,0)\,dk = e^{-3cT/(2h)}\sum_{m=0}^{N-n}\sum_{k=0}^{m/2}\frac{4^{m-2k}(-1)^k}{(m-2k)!\,k!}\left(\frac{cT}{2h}\right)^{m-2k}\phi_{m+n}. \tag{3.1.19}$$

For the boundary integrals from (3.1.18),

$$\frac{c}{2\pi}\int_{-\pi/h}^{\pi/h} e^{ik(nh-L+h)}e^{-WT}\left[\frac{\left(3-e^{ikh}\right)}{2}\,g_0-\frac{h}{2c}\dot{V}-\frac{h^2}{4c^2}\ddot{V}\right]dk$$
$$=3B_0\big(n,T,v^{(0)}\big)-B_1\big(n,T,v^{(0)}\big)-\frac{h}{c}B_0(n,T,\dot{v})-\frac{h^2}{2c^2}B_0(n,T,\ddot{v}),$$

with

$$B_j(n,T,v)=\frac{c}{4\pi}\int_{-\pi/h}^{\pi/h} e^{ik(nh-L+h+jh)}e^{-WT}V(W,T)\,dk$$
$$=\frac{ac}{2h}\sum_{k=0}^{(N-j-n)/2}\frac{4^{N-j-n-2k}(-1)^k}{(N-j-n-2k)!\,k!}\int_0^T e^{-3c(T-t)/(2h)}\left(\frac{c(T-t)}{2h}\right)^{N-j-n-2k}v(t)\,dt, \quad (3.1.20)$$

and

$$V(W,T)=\int_0^T e^{Wt}v(t)\,dt,$$

after substituting definitions and expanding. Combining the initial-condition term (3.1.19) and the boundary-condition term (3.1.20) allows for a different representation of (3.1.18), and we can use optimized built-in functions in MATLAB and other languages. As for (3.1.7), the initial and boundary conditions contribute at every interior mesh point.

Remark 3.1.1. The choice of equations to remove additional unknowns is not necessarily unique. The main challenge is finding equations that are linearly independent and give the desired order of accuracy. For example, instead of the centered discretization (3.1.17a) for $q_x(L,t)$, we apply the second-order forward stencil:

$$\frac{-3q_{N+1}(t)+4q_{N+2}(t)-q_{N+3}(t)}{2h}=\frac{\dot{v}(t)}{c} \qquad \Rightarrow \qquad \frac{-3g_0+4g_1-g_2}{2h}=\frac{\dot{V}}{c}. \quad (3.1.21)$$

This choice requires a second equation, different from (3.1.17b), that does not introduce any new unknowns. We discretize $q_{xx}(L,t)$ using the *first*-order forward stencil:

$$\frac{q_{N+1}(t)-2q_{N+2}(t)+q_{N+3}(t)}{h^2}=\frac{\ddot{v}(t)}{c^2} \qquad \Rightarrow \qquad \frac{g_0-2g_1+g_2}{h^2}=\frac{\ddot{V}}{c^2}. \quad (3.1.22)$$

Interestingly, both pairs of discretizations, (3.1.17a) – (3.1.17b) and (3.1.21) – (3.1.22), give the same expression for the unknown $g_1(W,T)$ and the same second-order accurate solution (3.1.18). It is noteworthy that $g_1(W,T)$ in (3.1.17a) and (3.1.21) arises as g_1/h. Similarly rewriting the $g_1(W,T)$ term in (3.1.17b) and (3.1.22), we have

$$\frac{g_1-2g_0+g_{-1}}{h}=h\frac{\ddot{V}}{c^2}+\mathcal{O}(h^3), \qquad \frac{g_0-2g_1+g_2}{h}=h\frac{\ddot{V}}{c^2}+\mathcal{O}(h^2),$$

respectively, so that $g_1(W,T)$ is solved (at least) to $\mathcal{O}(h^2)$ as in (3.1.17a) and (3.1.21). To remove $g_1(W,T)$ from (3.1.15) without introducing new unknowns, we can discretize the Neumann condition (3.1.16a) using the standard forward stencil to find

$$q_n(T) = \frac{1}{2\pi}\int_{-\pi/h}^{\pi/h} e^{iknh} e^{-WT}\hat{q}(k,0)\,dk + \frac{c}{2\pi}\int_{-\pi/h}^{\pi/h} e^{ik(nh-L+h)} e^{-WT}\left[\frac{\left(3-e^{ikh}\right)}{2}g_0 - \frac{h}{2c}\dot{V}\right] dk. \quad (3.1.23)$$

Because of the discretization of the Neumann condition, the accuracy of (3.1.23) is $\mathcal{O}(h)$ instead of the expected $\mathcal{O}(h^2)$. In fact, from this discretization, the modified PDE $p_x(L,t) = \dot{v}(t) + (h/2)p_{xx}(L,t)$ implies local dissipation near the $x = L$ boundary. Even so, solution (3.1.23) converges to (3.1.5) and loses dependence on the Neumann boundary condition as $h \to 0$. Note that an integral term with $h^2\ddot{V}/(4c^2)$ is the only difference between (3.1.18) and (3.1.23).

Remark 3.1.2. Unlike for the half-line problem, on a finite interval, the semidiscretized IBVPs for the advection equation $q_t = -c\,q_x$ $(c > 0)$ are similar to those for $q_t = +c\,q_x$, except we now apply backward stencils to $q_x(x,t)$ instead of forward ones.

Remark 3.1.3. For the half-line problem in Section 2.1.3, the centered discretization also yields a suitable SD-UTM solution that maintains $\mathcal{O}(h^2)$ accuracy through use of the nontrivial symmetry $\nu_1(k) = -k - \pi/h$ from the dispersion relation (2.1.21). In the finite interval problem, however, this is not the case. For the IBVP (2.1.11) with $c > 0$ and a centered discretization, the global relation is

$$e^{WT}\hat{q}(k,T) - \hat{q}(k,0) - c\left[\frac{e^{-ikh}f_0 + f_1 - e^{-ikL}\left(e^{-ikh}g_0 + g_1\right)}{2}\right] = 0, \quad k \in \mathbb{C}, \quad (3.1.24)$$

so that the "solution" contains three unknowns: $f_1(W,T)$ and both $g_j(W,T)$ terms. Figure 2.1.6 implies we cannot argue away dependence on all $g_j(W,T)$ terms, since we have regions of exponential growth in both the upper and lower halves of the complex k-plane. Deforming the integration paths onto the boundaries of the shaded regions in Figure 2.1.6 (see [17, 26, 27, 28] and future sections on higher-order discretizations), the global relation (3.1.24) with k and $k \to \nu_1$ provides two equations to remove one $f_j(W,T)$ and one $g_j(W,T)$ terms, say $f_1(W,T)$ and $g_1(W,T)$. We require a third equation that relates $g_0(W,T)$ to at least one of the other $f_j(W,T)$ or $g_1(W,T)$ terms. Unless we have periodic boundary conditions, there is no such relation that does not introduce more unknowns. Hence, the SD-UTM shows that a solution to the centered-discretized IBVP (2.1.11) does not exist. As in the higher-order discretization in Section 3.1.2, we could derive and discretize the Neumann and second-derivative boundary conditions, $q_x(0,t) = -\dot{u}(t)/c$ and $q_{xx}(0,t) = \ddot{u}(t)/c^2$ respectively, given by the PDE from the available Dirichlet condition $u^{(0)}(t)$, with $\dot{u}(t) = du^{(0)}(t)/dt$ and $\ddot{u}(t) = d^2u^{(0)}(t)/dt^2$. However, this approach only serves to remove $f_1(W,T)$ from the "solution," impairing the global relation equations with k and $k \to \nu_1$ to remove the remaining $g_0(W,T)$ and $g_1(W,T)$. We reach

a similar conclusion for the centered-discretized IBVP (3.1.1) with a Dirichlet condition at $x = L$. Lastly, the excess unknown terms occur near the interval's boundary where there is no prescribed condition, so this result does not change whether or not we take into consideration the known boundary points (the starting and ending index) in the Fourier transform $\hat{q}(k,t)$ definition (1.3.1a).

3.2 The Heat Equation

3.2.1 Centered Discretization of $q_t = q_{xx}$ with Dirichlet boundary conditions

Consider the problem

$$\begin{cases} q_t = q_{xx}, & 0 < x > L,\ t > 0, \\ q(x,0) = \phi(x), & 0 < x < L, \\ q(0,t) = u^{(0)}(t), & t > 0, \\ q(L,t) = v^{(0)}(t), & t > 0, \end{cases} \tag{3.2.1}$$

with Dirichlet boundary conditions on both sides of the interval. Writing the centered-discretized heat equation as in (2.2.2) again gives the local relation (2.2.3) and dispersion relation (2.2.4). The global relation is obtained by summing the local relation from $n = 1$ to $n = N$ and integrating in time:

$$e^{WT}\hat{q}(k,T) - \hat{q}(k,0) - \left[\frac{e^{-ikh}f_0 - f_1 + e^{-ikL}\left(e^{ikh}g_0 - g_{-1}\right)}{h}\right] = 0, \quad k \in \mathbb{C}. \tag{3.2.2}$$

Inverting, we obtain the "solution" formula

$$\begin{aligned} q_n(T) = {} & \frac{1}{2\pi}\int_{-\pi/h}^{\pi/h} e^{iknh}e^{-WT}\hat{q}(k,0)\,dk + \frac{1}{2\pi}\int_{-\pi/h}^{\pi/h} e^{iknh}e^{-WT}\left[\frac{e^{-ikh}f_0 - f_1}{h}\right]dk \\ & + \frac{1}{2\pi}\int_{-\pi/h}^{\pi/h} e^{ik(nh-L)}e^{-WT}\left[\frac{e^{ikh}g_0 - g_{-1}}{h}\right]dk, \end{aligned} \tag{3.2.3}$$

which depends on the unknowns $f_1(W,T)$ and $g_{-1}(W,T)$. With both trivial $\nu_0(k) = k$ and nontrivial $\nu_1(k) = -k$ symmetries, we have two equations to solve for two unknowns:

$$\begin{cases} 0 = e^{WT}\hat{q}(k,T) - \hat{q}(k,0) - \left[\dfrac{e^{-ikh}f_0 - f_1 + e^{-ikL}\left(-g_{-1} + e^{ikh}g_0\right)}{h}\right], \\ 0 = e^{WT}\hat{q}(-k,T) - \hat{q}(-k,0) - \left[\dfrac{e^{ikh}f_0 - f_1 + e^{ikL}\left(-g_{-1} + e^{-ikh}g_0\right)}{h}\right], \end{cases} \tag{3.2.4}$$

both valid for $k \in \mathbb{C}$.

To remove both unknowns with (3.2.4), we first need to deform the integration path of the second integral with the $f_j(W,T)$ terms away from the integration path of the $g_j(W,T)$ terms. Let

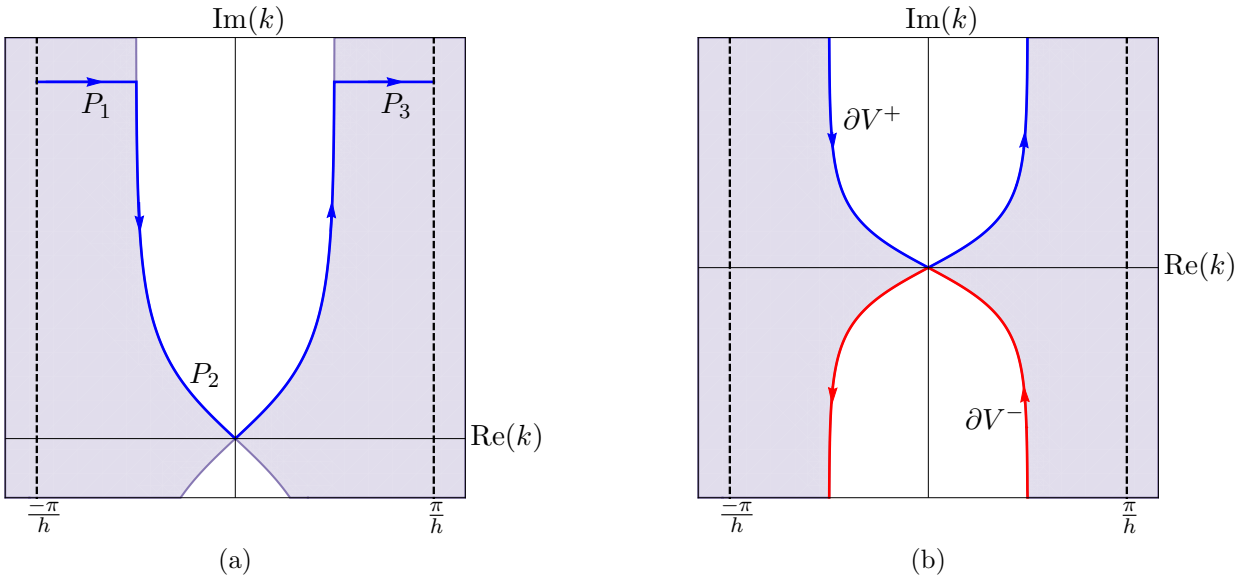

Figure 3.2.1: (a) The shaded regions depict where $\mathrm{Re}(-W) \leq 0$ and e^{-WT} is bounded, for the dispersion relation (2.2.4). The integration paths that constitute P are also shown. (b) The integration paths $\partial V^{\pm}$.

us deform the $f_j(W,T)$ terms to the upper-half plane in order to abide with well-posedness as $h \to 0$. We introduce

$$V^{\pm} = \left\{ k \in \mathbb{C}^{\pm} \,\middle|\, \mathrm{Re}(-W) \leq 0 \right\}.$$

With hindsight, we define the integration path $P = P_1 + P_2 + P_3$, shown in Figure 3.2.1a, where the two horizontal paths $P_{1,3}$ are at height $\mathrm{Im}(k) = R > 0$ above the real line and P_2 is on the boundary of V^+ up to $\mathrm{Im}(k) = R$. Using periodicity, we deform the second integral of "solution" (3.2.3) to P, so that

$$\frac{1}{2\pi}\int_{-\pi/h}^{\pi/h} e^{iknh} e^{-WT}\left(\frac{e^{-ikh}f_0 - f_1}{h}\right) dk = \frac{1}{2\pi}\int_{P} e^{iknh} e^{-WT}\left(\frac{e^{-ikh}f_0 - f_1}{h}\right) dk.$$

Since $P_{1,3}$ are in regions of exponential decay, we let $R \to \infty$, so that the integrals on $P_{1,3}$ vanish, the endpoints of P_2 are extended to $+i\infty$ approaching the vertical asymptotes $\mathrm{Re}(k) = \pm\pi/(2h)$, and $\lim_{R\to\infty} P_2 = \partial V^+$ (the entire boundary of V^+ in the upper-half plane). Figure 3.2.1b shows $\partial V^{\pm}$, where ∂V^- is obtained in a similar fashion for the third integral of "solution" (3.2.3) containing the

$g_j(W,T)$ terms. Hence,

$$\begin{aligned} q_n(T) = \frac{1}{2\pi}\int_{-\pi/h}^{\pi/h} e^{iknh}e^{-WT}\hat{q}(k,0)\,dk + \frac{1}{2\pi}\int_{\partial V^+} e^{iknh}e^{-WT}\left(\frac{e^{-ikh}f_0 - f_1}{h}\right)dk \\ - \frac{1}{2\pi}\int_{\partial V^-} e^{ik(nh-L)}e^{-WT}\left(\frac{e^{ikh}g_0 - g_{-1}}{h}\right)dk. \end{aligned} \tag{3.2.5}$$

Note the path directions, which have introduced a minus sign on the third integral. Now that the $f_j(W,T)$ and $g_j(W,T)$ terms are on different integration paths, we solve the two global relation equations (3.2.4) for $f_1(W,T)$ and $g_{-1}(W,T)$, obtaining

$$\begin{cases} \dfrac{e^{-ikh}f_0 - f_1}{h} = \dfrac{h\left[\hat{q}(-k,0) - e^{2ikL}\hat{q}(k,0) + e^{2ikL}e^{WT}\hat{q}(k,T) - e^{WT}\hat{q}(-k,T)\right] + 2i\sin(kh)\left(f_0 - e^{ikL}g_0\right)}{h\left(e^{2ikL}-1\right)}, \\ \dfrac{e^{-ikL}\left(-g_{-1} + e^{ikh}g_0\right)}{h} = \dfrac{h\left[\hat{q}(k,0) - \hat{q}(-k,0) + e^{WT}\hat{q}(-k,T) - e^{WT}\hat{q}(k,T)\right] - 2i\sin(kh)\left(f_0 - e^{ikL}g_0\right)}{h\left(e^{2ikL}-1\right)}. \end{cases} \tag{3.2.6}$$

Both left-hand sides are analytic in k, thus the roots of the denominator, $k_\ell = \pi\ell/L$, $\ell \in \mathbb{Z}$, are removable singularities, including at the ends of the interval $[-\pi/h, \pi/h]$ and at the origin $k_0 = 0$. Since we are only interested in this interval, we can restrict ℓ to $-(N+1) \le \ell \le N+1$, using $L = (N+1)h$. For any finite h, the number of singularities is finite and increasing as $h \to 0$. Our integration paths are off the real line except at the origin. To avoid passing through the removable singularity k_0, it is convenient to deform $\partial V^\pm$ to $\partial\tilde{V}^\pm$, which is entirely off the real line as depicted in Figure 3.2.2a. Of course, $\partial\tilde{V}^\pm$ now crosses into the unshaded regions where e^{-WT} grows, but this growth is bounded on this segment. On $\partial\tilde{V}^\pm$, "solution" (3.2.5) becomes

$$\begin{aligned} q_n(T) = \frac{1}{2\pi}\int_{-\pi/h}^{\pi/h} e^{iknh}e^{-WT}\hat{q}(k,0)\,dk + \frac{1}{2\pi}\int_{\partial\tilde{V}^+} e^{iknh}e^{-WT}\left(\frac{e^{-ikh}f_0 - f_1}{h}\right)dk \\ - \frac{1}{2\pi}\int_{\partial\tilde{V}^-} e^{ik(nh-L)}e^{-WT}\left(\frac{e^{ikh}g_0 - g_{-1}}{h}\right)dk. \end{aligned} \tag{3.2.7}$$

Using (3.2.6),

$$\begin{aligned} q_n(T) = \frac{1}{2\pi}\int_{-\pi/h}^{\pi/h} e^{iknh}e^{-WT}\hat{q}(k,0)\,dk \\ + \frac{1}{2\pi}\int_{\partial\tilde{V}^+} e^{iknh}e^{-WT}\left[\frac{\hat{q}(-k,0) - e^{2ikL}\hat{q}(k,0)}{e^{2ikL}-1} + \frac{2i\sin(kh)\left(f_0 - e^{ikL}g_0\right)}{h\left(e^{2ikL}-1\right)}\right]dk \\ - \frac{1}{2\pi}\int_{\partial\tilde{V}^-} e^{iknh}e^{-WT}\left[\frac{\hat{q}(k,0) - \hat{q}(-k,0)}{e^{2ikL}-1} - \frac{2i\sin(kh)\left(f_0 - e^{ikL}g_0\right)}{h\left(e^{2ikL}-1\right)}\right]dk \;+\; S(n), \end{aligned} \tag{3.2.8}$$

where

$$S(n) = \frac{1}{2\pi}\int_{\partial\tilde{V}^+} e^{iknh}\left[\frac{e^{2ikL}\hat{q}(k,T) - \hat{q}(-k,T)}{e^{2ikL}-1}\right]dk - \frac{1}{2\pi}\int_{\partial\tilde{V}^-} e^{iknh}\left[\frac{\hat{q}(-k,T) - \hat{q}(k,T)}{e^{2ikL}-1}\right]dk.$$

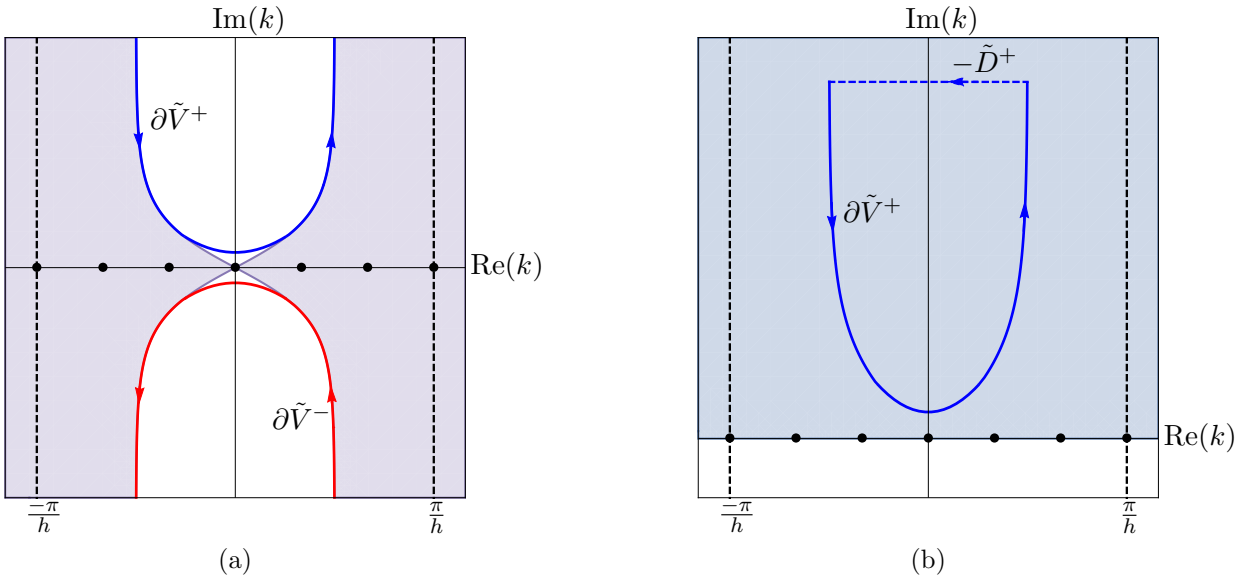

Figure 3.2.2: (a) The integration paths $\partial\tilde{V}^{\pm}$ deformed away from the origin. (b) Deforming $\partial\tilde{V}^+$ to $\tilde{D}^+$ in the upper-half plane. Without decay from e^{-WT}, the shaded region depicts where e^{iknh} decays.

We wish to determine the contributions from $S(n)$. Since the exponential e^{-WT} is not present, our aim is to close the contours using a path at infinity. First, we truncate the infinite paths $\partial\tilde{V}^{\pm}$ and close the curves by introducing

$$\tilde{D}^{\pm} = \left\{ k \in \mathbb{C} \,\middle|\, \frac{-\pi}{2h} \leq \mathrm{Re}(k) \leq \frac{\pi}{2h} \text{ and } \mathrm{Im}(k) = \pm R \right\},$$

with $R > 0$, so that $\tilde{D}^{\pm}$ is a horizontal interval above/below $\partial\tilde{V}^{\pm}$ in the complex k-plane, as shown in Figure 3.2.2b for $\tilde{D}^+$, and $\lim_{R\to\infty} \tilde{D}^{\pm} = \pm\partial\tilde{V}^{\pm}$.

Now,

$$S(n) = \lim_{R\to\infty} \left(\frac{1}{2\pi} \int_{\tilde{D}^+} e^{iknh} \left[\frac{e^{2ikL}\hat{q}(k,T) - \hat{q}(-k,T)}{e^{2ikL}-1} \right] dk + \frac{1}{2\pi} \int_{\tilde{D}^-} e^{iknh} \left[\frac{\hat{q}(-k,T) - \hat{q}(k,T)}{e^{2ikL}-1} \right] dk \right).$$

Notice the sign change for $\tilde{D}^-$. For the first integral on $\tilde{D}^+$, $\hat{q}(k,T)$ grows exponentially as $R \to \infty$. However, we rewrite the first term as

$$\begin{aligned} \frac{1}{2\pi} \int_{\tilde{D}^+} \frac{e^{ik(nh+2L)}}{e^{2ikL}-1} \hat{q}(k,T)\, dk &= \frac{1}{2\pi} \int_{\tilde{D}^+} \frac{e^{ik(nh+2L)}}{e^{2ikL}-1} \left[h \sum_{m=1}^{N} e^{-ikmh} q_m(T) \right] dk \\ &= \frac{h}{2\pi} \sum_{m=1}^{N} q_m(T) \left[\int_{\tilde{D}^+} \frac{e^{ik(n-m+2N+2)h}}{e^{2ikL}-1}\, dk \right], \end{aligned}$$

after using $L = (N+1)h$. For all n and m, $n - m + 2N + 2 > 0$. Letting $R \to \infty$ on $\tilde{D}^+$ implies $e^{ik(n-m+2N+2)h} \to 0$ and $e^{2ikL} \to 0$. In this limit, the integrand approaches zero and we recover the original integration paths, so that

$$\frac{1}{2\pi}\int_{\partial\tilde{V}^+} \frac{e^{ik(nh+2L)}}{e^{2ikL}-1}\hat{q}(k,T)\,dk = 0,$$

for all n. The second term with $\hat{q}(-k,T)$ on $\tilde{D}^+$ similarly goes to zero as $R \to \infty$. The third term is rewritten as

$$\frac{1}{2\pi}\int_{\tilde{D}^-} \frac{e^{iknh}}{e^{2ikL}-1}\hat{q}(-k,T)\,dk = \frac{h}{2\pi}\sum_{m=1}^{N} q_m(T)\left[\int_{\tilde{D}^-} \frac{e^{ik(n+m)h}}{e^{2ikL}-1}\,dk\right].$$

On $\tilde{D}^-$, $e^{ik(n+m)h}$ and e^{2ikL} grow as $R \to \infty$ for all n and m, but

$$\frac{e^{ik(n+m)h}}{e^{2ikL}-1} \sim \frac{e^{ik(n+m)h}}{e^{2ikL}} = e^{ik(n+m-2N-2)h}.$$

Since $n < N+1$ and $m < N+1$, $n+m-2N-2 < 0$, and the integrand approaches zero, as $R \to \infty$. Thus,

$$\frac{1}{2\pi}\int_{\partial\tilde{V}^-} \frac{e^{iknh}}{e^{2ikL}-1}\hat{q}(-k,T)\,dk = 0,$$

for all n. Similarly, the fourth term is zero. Hence, $S(n) = 0$ and the final representation for the solution to the finite-interval problem for the heat equation (2.2.2) with Dirichlet boundary conditions is

$$\begin{aligned} q_n(T) = {} & \frac{1}{2\pi}\int_{-\pi/h}^{\pi/h} e^{iknh}e^{-WT}\hat{q}(k,0)\,dk \\ & + \frac{1}{2\pi}\int_{\partial\tilde{V}^+} e^{iknh}e^{-WT}\left[\frac{\hat{q}(-k,0) - e^{2ikL}\hat{q}(k,0)}{e^{2ikL}-1} + \frac{2i\sin(kh)\left(f_0 - e^{ikL}g_0\right)}{h\left(e^{2ikL}-1\right)}\right]dk \\ & - \frac{1}{2\pi}\int_{\partial\tilde{V}^-} e^{iknh}e^{-WT}\left[\frac{\hat{q}(k,0) - \hat{q}(-k,0)}{e^{2ikL}-1} - \frac{2i\sin(kh)\left(f_0 - e^{ikL}g_0\right)}{h\left(e^{2ikL}-1\right)}\right]dk. \end{aligned} \tag{3.2.9}$$

For the IBVP (3.2.1), using the continuous UTM [17], we find the dispersion relation $\tilde{W}(k) = k^2$ and define

$$\Omega^{\pm} = \left\{k \in \mathbb{C}^{\pm} \,\middle|\, \mathrm{Re}(-k^2) \le 0\right\},$$

to use the integration paths $\partial\tilde{\Omega}^{\pm}$ as illustrated in Figure 3.2.3. As in the semi-discrete case, there is a (removable) singularity at the origin, so $\partial\Omega^{\pm}$ is deformed to $\partial\tilde{\Omega}^{\pm}$. The solution is

$$\begin{aligned} q(x,T) = {} & \frac{1}{2\pi}\int_{-\infty}^{\infty} e^{ikx}e^{-\tilde{W}T}\hat{q}(k,0)\,dk \\ & + \frac{1}{2\pi}\int_{\partial\tilde{\Omega}^+} e^{ikx}e^{-\tilde{W}T}\left[\frac{\hat{q}(-k,0) - e^{2ikL}\hat{q}(k,0) + 2ik\left(F_0 - e^{ikL}G_0\right)}{e^{2ikL}-1}\right]dk \\ & - \frac{1}{2\pi}\int_{\partial\tilde{\Omega}^-} e^{ikx}e^{-\tilde{W}T}\left[\frac{\hat{q}(k,0) - \hat{q}(-k,0) - 2ik\left(F_0 - e^{ikL}G_0\right)}{e^{2ikL}-1}\right]dk. \end{aligned} \tag{3.2.10}$$

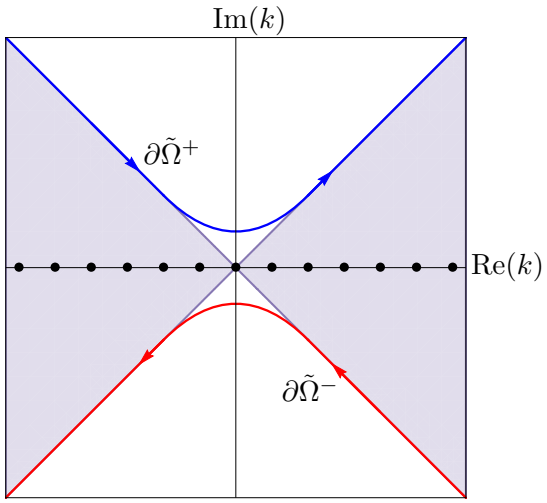

Figure 3.2.3: The shaded regions depict where $\mathrm{Re}(-\tilde{W}) \leq 0$ and $e^{\tilde{W}T}$ is bounded, with the boundaries $\partial\tilde{\Omega}^{\pm}$ approaching $\partial\Omega^{\pm}$ asymptotically as $|k| \to \infty$.

Taking the continuum limit, it is clear that $\lim_{h\to 0} W(k) = \tilde{W}(k)$ and thus $\lim_{h\to 0} \partial\tilde{V}^{\pm} = \partial\tilde{\Omega}^{\pm}$, as well. In addition, the coefficient of the boundary terms from either $\partial\tilde{V}^{\pm}$ integral converge to $2ik/(e^{2ikL} - 1)$ with $\lim_{h\to 0} \left(f_0 - e^{ikL} g_0\right) = F_0 - e^{ikL} G_0$, so that the SD-UTM solution (3.2.9) converges to the continuous UTM solution (3.2.10).

Unlike for the heat equation on the half-line and the previous advection IBVPs, the integration paths of the last two integral terms in (3.2.9) are off the real line, avoiding the integrands' simple poles. To numerically evaluate the integrals, we design any contour path that is within the shaded regions of Figure 3.2.2a and off the real line, with endpoints that have real part $\pm\pi/h$. For computational purposes, having paths off of the boundaries $\partial\tilde{V}^{\pm}$ is preferred in order to have some exponential decay. Since we are taking $h \ll 1$ in practical settings, we must orient our contours so that in the continuum limit, the semi-discrete solution converges to the continuous one. There are several approaches to tackle this task for the UTM integrals of continuous IBVPs [18, 25, 27, 38, 55] that can be adapted for SD-UTM integrals.

Series Representation

To bypass complex integration paths, we derive a series representation equivalent to (3.2.9), as before. For any n, we deform the first integral term to $\partial\tilde{V}^{+}$, since $\hat{q}(k, 0)$ is valid for all $k \in \mathbb{C}$ and the bounds on the integral with respect to k are finite. Combining with the other initial condition

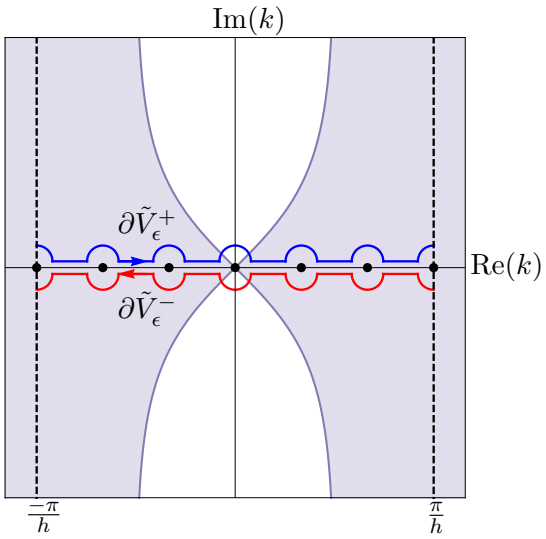

Figure 3.2.4: The semi-circle integration paths $\partial\tilde{V}_\epsilon^\pm$ around singularities on the real line.

terms on $\partial\tilde{V}^+$, solution (3.2.9) becomes

$$q_n(T) = \frac{-1}{2\pi}\left(\int_{\partial\tilde{V}^+} + \int_{\partial\tilde{V}^-}\right) A(n,T,k)\,dk + \frac{i}{\pi h}\left(\int_{\partial\tilde{V}^+} + \int_{\partial\tilde{V}^-}\right) B(n,T,k)\,dk, \tag{3.2.11}$$

with

$$A(n,T,k) = e^{iknh}e^{-WT}\left[\frac{\hat{q}(k,0)-\hat{q}(-k,0)}{e^{2ikL}-1}\right] \quad \text{and} \quad B(n,T,k) = e^{iknh}e^{-WT}\left[\frac{\sin(kh)\left(f_0 - e^{ikL}g_0\right)}{e^{2ikL}-1}\right].$$

Next, we deform the paths back to the real line, excluding the $2(N+1)+1$ singularities on $[-\pi/h, \pi/h]$ using half-circles with radius ϵ smaller than half the distance between singularities, see Figure 3.2.4. The horizontal line segments for both $\partial\tilde{V}_\epsilon^\pm$ are on the real line, but are drawn above and below for illustrative purposes. We obtain

$$q_n(T) = \frac{-1}{2\pi}\left(\int_{\partial\tilde{V}_\epsilon^+} + \int_{\partial\tilde{V}_\epsilon^-}\right) A(n,T,k)\,dk + \frac{i}{\pi h}\left(\int_{\partial\tilde{V}_\epsilon^+} + \int_{\partial\tilde{V}_\epsilon^-}\right) B(n,T,k)\,dk. \tag{3.2.12}$$

Taking the limit of (3.2.12) as $\epsilon \to 0$, the integrals give rise to residue contributions and principal value integrals. For instance, the first term above becomes

$$\begin{aligned}\frac{-1}{2\pi}\int_{\partial\tilde{V}_\epsilon^+} A(n,T,k)\,dk = \frac{i}{4}\left[\operatorname*{Res}_{k=-\pi/h} A(n,T,k) + \operatorname*{Res}_{k=\pi/h} A(n,T,k)\right] + \frac{i}{2}\sum_{\ell=-N}^{N}\operatorname*{Res}_{k=k_\ell} A(n,T,k) \\ - \frac{1}{2\pi}\fint_{-\pi/h}^{\pi/h} A(n,T,k)\,dk.\end{aligned}$$

We have two contributions of the quarter-circle contours from the singularities on the edges of the integration path plus contributions from the half-circle contours from the inner singularities. Similarly, for the second term in (3.2.12),

$$\frac{-1}{2\pi}\int_{\partial\tilde{V}_\epsilon^-} A(n,T,k)\,dk = \frac{i}{4}\left[\operatorname*{Res}_{k=-\pi/h} A(n,T,k) + \operatorname*{Res}_{k=\pi/h} A(n,T,k)\right] + \frac{i}{2}\sum_{\ell=-N}^{N}\operatorname*{Res}_{k=k_\ell} A(n,T,k) + \frac{1}{2\pi}\fint_{-\pi/h}^{\pi/h} A(n,T,k)\,dk.$$

Combining the two rewrites above cancels the integrals, so that

$$\frac{-1}{2\pi}\left(\int_{\partial\tilde{V}_\epsilon^+} + \int_{\partial\tilde{V}_\epsilon^-}\right) A(n,T,k)\,dk = i\left[\frac{1}{2}\operatorname*{Res}_{k=-\pi/h} A(n,T,k) + \sum_{\ell=-N}^{N}\operatorname*{Res}_{k=k_\ell} A(n,T,k) + \frac{1}{2}\operatorname*{Res}_{k=\pi/h} A(n,T,k)\right].$$

Similarly, the $B(n,T,k)$ integrals in (3.2.12) are rewritten using residue contributions, so that substituting into (3.2.12) gives an expression with residue contributions only:

$$\begin{aligned} q_n(T) = {} & i\left[\frac{1}{2}\operatorname*{Res}_{k=-\pi/h} A(n,T,k) + \sum_{\ell=-N}^{N}\operatorname*{Res}_{k=k_\ell} A(n,T,k) + \frac{1}{2}\operatorname*{Res}_{k=\pi/h} A(n,T,k)\right] \\ & + \frac{1}{h}\left[\operatorname*{Res}_{k=-\pi/h} B(n,T,k) + 2\sum_{\ell=-N}^{N}\operatorname*{Res}_{k=k_\ell} B(n,T,k) + \operatorname*{Res}_{k=\pi/h} B(n,T,k)\right]. \end{aligned} \tag{3.2.13}$$

Next, we determine these residues, starting with the $A(n,T,k)$ residues for $\ell = -N-1,\ldots,N+1$, where the lone residues at $k = \pm\pi/h$ or $\ell = \pm(N+1)$ follow trivially. Since we only have simple poles at $k = k_\ell$,

$$\operatorname*{Res}_{k=k_\ell} A(n,T,k) = e^{ik_\ell nh}e^{-W(k_\ell)T}\left[\frac{\hat{q}\,(k_\ell,0) - \hat{q}\,(-k_\ell,0)}{2iL}\right].$$

Using the definitions of $\hat{q}(\pm k,0)$,

$$\hat{q}\,(k_\ell,0) - \hat{q}\,(-k_\ell,0) = -2ih\sum_{m=1}^{N}\sin\left(\frac{\pi\ell mh}{L}\right)\phi_m = -iLb_\ell, \qquad b_\ell = \frac{2h}{L}\sum_{m=1}^{N}\sin\left(\frac{\pi\ell mh}{L}\right)\phi_m.$$

Note that $b_0 = b_{\pm(N+1)} = 0$, $b_{-\ell} = -b_\ell$, $k_{-\ell} = -k_\ell$, and $W(k_\ell) = W(-k_\ell)$. Using these observations,

$$\sum_{\ell=-N}^{N}\operatorname*{Res}_{k=k_\ell} A(n,T,k) = \frac{-1}{2}\sum_{\ell=-N}^{N} e^{ik_\ell nh}e^{-W(k_\ell)T}b_\ell = -i\sum_{\ell=1}^{N} e^{-W(k_\ell)T}\sin\left(\frac{\pi\ell nh}{L}\right)b_\ell.$$

Similarly,

$$\operatorname*{Res}_{k=k_\ell} B(n,T,k) = e^{ik_\ell nh}e^{-W_\ell T}\sin\left(\frac{\pi\ell h}{L}\right)\frac{H(W_\ell,T)}{2iL},$$

where we have introduced $W_\ell \equiv W(k_\ell)$ for brevity, with

$$H(W_\ell, T) = f_0(W_\ell, T) + (-1)^{\ell+1} g_0(W_\ell, T).$$

As with the residues of $A(n, T, k)$, one can show there are no contributions from the poles at the endpoints and at the origin. After rearranging,

$$\sum_{\ell=-N}^{N} \operatorname*{Res}_{k=k_\ell} B(n, T, k) = \frac{1}{L} \sum_{\ell=1}^{N} e^{-W_\ell T} \sin\left(\frac{\pi \ell h}{L}\right) \sin\left(\frac{\pi \ell n h}{L}\right) H(W_\ell, T).$$

Returning to (3.2.13), we recover the classical series solution:

$$q_n(T) = \sum_{\ell=1}^{N} e^{-W_\ell T} \sin\left(\frac{\pi \ell n h}{L}\right) \left[b_\ell + \frac{2}{Lh} \sin\left(\frac{\pi \ell h}{L}\right) H(W_\ell, T) \right]. \tag{3.2.14}$$

From a numerical point of view, this solution representation is favored over the integral representation (3.2.9).

As an example, the exact solution to the IBVP

$$\begin{cases} q_t = q_{xx}, & 0 < x < 1,\ t > 0, \\ q(x, 0) = \phi(x) = 2x + \sin(5\pi x), & 0 < x < 1, \\ q(0, t) = u^{(0)}(t) = 0, & t > 0, \\ q(1, t) = v^{(0)}(t) = 2, & t > 0, \end{cases} \tag{3.2.15}$$

is $q(x, t) = 2x + \sin(5\pi x) e^{-25\pi^2 t}$. We have chosen time-independent boundary conditions for simplicity only. We solve the IBVP (3.2.15) with the centered finite-difference methods and the series SD-UTM solution (3.2.14). Deriving the modified PDE from the centered stencil (2.2.2), we find that (3.2.9), and hence (3.2.14), is a fourth-order accurate approximation to the solution of the dissipative PDE (2.2.12). With the SD-UTM solution (3.2.9), the left plot of Figure 3.2.5 shows the exponential decay as time increases and the right plot shows the expected $\mathcal{O}(h^2)$ error as $h \to 0$. The SD-UTM solution outperforms the traditional numerical methods in the continuum limit, where the explicit methods become unstable and the implicit methods are asymptotic to their respective temporal truncation error as $h \to 0$. The finite-difference solutions have stability conditions that must be satisfied, but Figure 3.2.5b shows that there is no such restriction for the SD-UTM to succeed. The dips in this error plot are due to mesh points being placed near stationary points in the solution. With these boundary conditions, we know that $\lim_{t\to\infty} q(x, t) = 2x$. Hence, mesh points on the initial condition that are near $q = 2x$ tend to stay there as t increases.

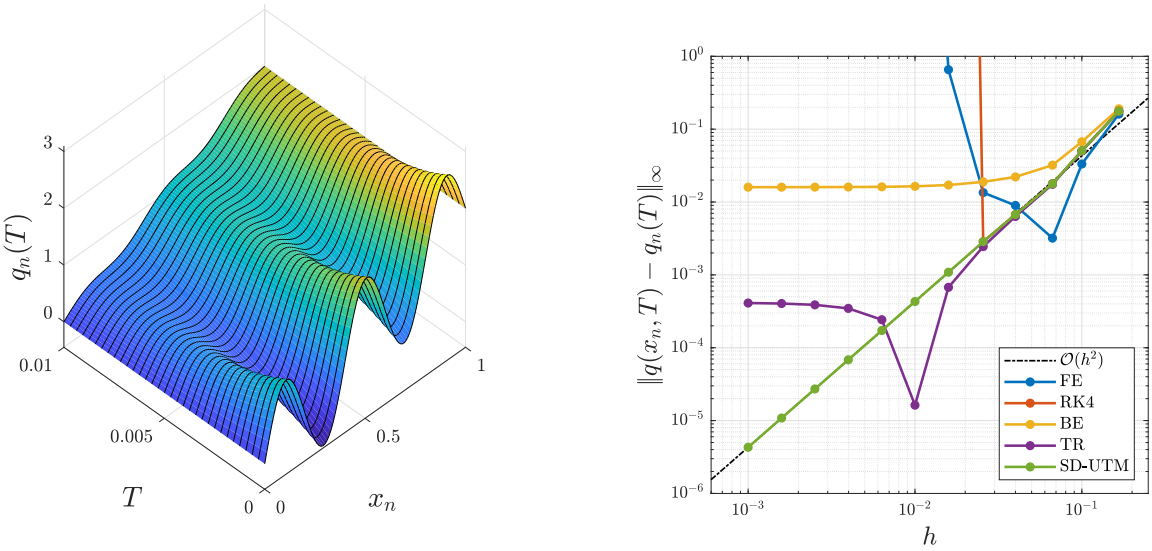

(a) (b)

Figure 3.2.5: (a) The semi-discrete solution (3.2.14) evaluated at various t with $h = 0.01$. (b) Error plot of the semi-discrete solution (3.2.14) and finite-difference schemes relative to the exact solution as $h \to 0$ with $T = 0.01$ and $\Delta t = 6.25 \times 10^{-4}$.

3.2.2 Centered Discretization of $q_t = q_{xx}$ with Neumann boundary conditions

We consider the same centered-discretized heat equation (2.2.2), now with Neumann boundary conditions at both ends of the interval:

$$\begin{cases} q_t = q_{xx}, & 0 < x < L,\ t > 0, \\ q(x,0) = \phi(t), & 0 < x < L, \\ q_x(0,t) = u^{(1)}(t), & t > 0, \\ q_x(L,t) = v^{(1)}(t), & t > 0. \end{cases} \tag{3.2.16}$$

We can discretize the Neumann data with many different stencils, but we show that the SD-UTM restricts which of these are available to be paired with (2.2.2).

With the centered discretization (2.2.2), we retain the local relation (2.2.3) and dispersion relation (2.2.4) with nontrivial symmetry $\nu_1(k) = -k$. We cannot use the global relation (3.2.2), because we assumed Dirichlet boundary data to obtain it. Without information at $n = 0$ or $n = N + 1$, we

define the forward transform to start and end at these points like in Section 2.2.2:

$$\hat{q}\,(k,t) = h\sum_{n=0}^{N+1} e^{-iknh} q_n(t),$$

directly affecting the global relation. From the local relation (2.2.3),

$$e^{WT}\hat{q}(k,T) - \hat{q}(k,0) - \left[\frac{f_{-1} - e^{ikh}f_0 + e^{-ikL}\left(g_1 - e^{-ikh}g_0\right)}{h}\right] = 0, \quad k \in \mathbb{C}. \tag{3.2.17}$$

Solving for $\hat{q}(k,T)$ and inverting, we obtain

$$\begin{aligned} q_n(T) = {} & \frac{1}{2\pi}\int_{-\pi/h}^{\pi/h} e^{iknh}e^{-WT}\hat{q}(k,0)\,dk \\ & + \frac{1}{2\pi}\int_{-\pi/h}^{\pi/h} e^{iknh}e^{-WT}\left[\frac{f_{-1} - e^{ikh}f_0 + e^{-ikL}\left(g_1 - e^{-ikh}g_0\right)}{h}\right] dk, \end{aligned} \tag{3.2.18}$$

with unknowns $f_{-1}(W,T)$, $f_0(W,T)$, $g_0(W,T)$, and $g_1(W,T)$. In order to use the global relation (3.2.17) with k and $k \to -k$, we separate and deform the integration paths of the $f_j(W,T)$ terms from the $g_j(W,T)$ terms. As in (3.2.7) with Dirichlet boundary conditions, we deform the boundary terms in "solution" (3.2.18) off the real line to $\partial\tilde{V}^{\pm}$:

$$\begin{aligned} q_n(T) = {} & \frac{1}{2\pi}\int_{-\pi/h}^{\pi/h} e^{iknh}e^{-WT}\hat{q}(k,0)\,dk + \frac{1}{2\pi}\int_{\partial\tilde{V}^+} e^{iknh}e^{-WT}\left[\frac{f_{-1} - e^{ikh}f_0}{h}\right] dk \\ & - \frac{1}{2\pi}\int_{\partial\tilde{V}^-} e^{ik(nh-L)}e^{-WT}\left[\frac{g_1 - e^{-ikh}g_0}{h}\right] dk. \end{aligned} \tag{3.2.19}$$

Through the time transforms, the global relation (3.2.17) contains boundary nodal information $n = -1, 0$ at the interval's left boundary and $n = N+1, N+2$ at the right, leading us to backward-discretize $q_x\,(0,t)$ and forward-discretize $q_x\,(L,t)$ with $\mathcal{O}(h)$ stencils to obtain

$$\frac{q_0(t) - q_{-1}(t)}{h} = u^{(1)}(t) \qquad \text{and} \qquad \frac{q_{N+2}(t) - q_{N+1}(t)}{h} = v^{(1)}(t). \tag{3.2.20}$$

Second-order discretizations, both in stencil width and accuracy, introduce additional unknowns, despite having information of all odd derivatives at either boundary. Without even derivatives, one can show these discretizations are linearly dependent through the method of undetermined coefficients and the Casoratian [75], the discrete analogue of the Wronskian. Taking the time integrals of the $\mathcal{O}(h)$ discretizations above, we have four equations to remove four unknowns $f_{-1}(W,T)$, $f_0(W,T)$,

$g_0(W,T)$, and $g_1(W,T)$:

$$\begin{cases} e^{WT}\hat{q}(k,T) - \hat{q}(k,0) - \left[\dfrac{f_{-1} - e^{ikh}f_0 + e^{-ikL}\left(g_1 - e^{-ikh}g_0\right)}{h}\right] = 0, \\ e^{WT}\hat{q}(-k,T) - \hat{q}(-k,0) - \left[\dfrac{f_{-1} - e^{-ikh}f_0 + e^{ikL}\left(g_1 - e^{ikh}g_0\right)}{h}\right] = 0, \\ \dfrac{f_0 - f_{-1}}{h} = U^{(1)}, \\ \dfrac{g_1 - g_0}{h} = V^{(1)}, \end{cases} \tag{3.2.21}$$

with

$$U^{(1)}(W,T) = \int_0^T e^{Wt}u^{(1)}(t)\,dt, \qquad \text{and} \qquad V^{(1)}(W,T) = \int_0^T e^{Wt}v^{(1)}(t)\,dt.$$

Solving (3.2.21),

$$\begin{cases} \dfrac{f_{-1} - e^{ikh}f_0}{h} = \dfrac{1}{e^{2ik(L+h)} - 1}\Big[e^{2ik(L+h)}e^{WT}\hat{q}(k,T) - e^{2ik(L+h)}\hat{q}(k,0) + e^{ikh}e^{WT}\hat{q}(-k,T) \\ \qquad\qquad -e^{ikh}\hat{q}(-k,0) + \left(1 + e^{ikh}\right)U^{(1)} - \left(e^{ik(L+h)} + e^{ik(L+2h)}\right)V^{(1)}\Big], \\ \dfrac{e^{-ikL}\left(g_1 - e^{-ikh}g_0\right)}{h} = \dfrac{1}{e^{2ik(L+h)} - 1}\Big[- e^{ikh}e^{WT}\hat{q}(-k,T) + e^{ikh}\hat{q}(-k,0) - e^{WT}\hat{q}(k,T) + \hat{q}(k,0) \\ \qquad\qquad - \left(1 + e^{ikh}\right)U^{(1)} + \left(e^{ik(L+h)} + e^{ik(L+2h)}\right)V^{(1)}\Big], \end{cases} \tag{3.2.22}$$

with (removable) singularities at $k_\ell = \pi\ell/(L+h)$ for $-(N+2) \le \ell \le N+2$. Since the boundary integrals of (3.2.19) are off the real line, substituting (3.2.22) into (3.2.19) gives

$$\begin{aligned} q_n(T) = &\frac{1}{2\pi}\int_{-\pi/h}^{\pi/h} e^{iknh}e^{-WT}\hat{q}(k,0)\,dk \\ &- \frac{1}{2\pi}\int_{\partial\tilde{V}^+} e^{iknh}e^{-WT}\left[\frac{e^{2ik(L+h)}\hat{q}(k,0) + e^{ikh}\hat{q}(-k,0)}{e^{2ik(L+h)} - 1} - \frac{\left(1 + e^{ikh}\right)\left(U^{(1)} - e^{ik(L+h)}V^{(1)}\right)}{e^{2ik(L+h)} - 1}\right]dk \\ &- \frac{1}{2\pi}\int_{\partial\tilde{V}^-} e^{iknh}e^{-WT}\left[\frac{e^{ikh}\hat{q}(-k,0) + \hat{q}(k,0)}{e^{2ik(L+h)} - 1} - \frac{\left(1 + e^{ikh}\right)\left(U^{(1)} - e^{ik(L+h)}V^{(1)}\right)}{e^{2ik(L+h)} - 1}\right]dk. \end{aligned} \tag{3.2.23}$$

after checking that the integrals with $\hat{q}(k,T)$ and $\hat{q}(-k,T)$ vanish by deforming the paths to $\tilde{D}^\pm$ and taking $R \to \infty$.

The solution representation for IBVP (3.2.16) using the continuous UTM [17] is

$$\begin{aligned} q(x,T) = &\frac{1}{2\pi}\int_{-\pi/h}^{\pi/h} e^{ikx}e^{-\tilde{W}T}\hat{q}(k,0)\,dk \\ &- \frac{1}{2\pi}\int_{\partial\tilde{\Omega}^+} e^{ikx}e^{-\tilde{W}T}\left[\frac{e^{2ikL}\hat{q}(k,0)+\hat{q}(-k,0)}{e^{2ikL}-1} - \frac{2\left(F_1 - e^{ikL}G_1\right)}{e^{2ikL}-1}\right]dk \\ &- \frac{1}{2\pi}\int_{\partial\tilde{\Omega}^-} e^{ikx}e^{-\tilde{W}T}\left[\frac{\hat{q}(-k,0)+\hat{q}(k,0)}{e^{2ikL}-1} - \frac{2\left(F_1 - e^{ikL}G_1\right)}{e^{2ikL}-1}\right]dk, \end{aligned} \tag{3.2.24}$$

where $\tilde{\Omega}^{\pm}$ is illustrated in Figure 3.2.3. Referencing (3.2.23), the continuum limits of the coefficients of $\hat{q}(\pm k,0)$, $U^{(1)}$, and $V^{(1)}$ converge to their continuous counterparts, where

$$\begin{aligned} \lim_{h\to 0} U^{(1)} &= \lim_{h\to 0}\int_0^T e^{Wt}u^{(1)}(t)\,dt = \int_0^T e^{\tilde{W}t}u^{(1)}(t)\,dt = F_1, \\ \lim_{h\to 0} V^{(1)} &= \lim_{h\to 0}\int_0^T e^{Wt}v^{(1)}(t)\,dt = \int_0^T e^{\tilde{W}t}v^{(1)}(t)\,dt = G_1. \end{aligned}$$

Series Representation

Following similar steps to those in Section 3.2.1, we deform $\partial\tilde{V}^{\pm}$ to $\partial\tilde{V}_{\epsilon}^{\pm}$, so that the integral representation of (3.2.24) is rewritten in terms of residue contributions:

$$q_n(T) = i\left(\sum_{\ell=-N-1}^{N+1}\operatorname*{Res}_{k=k_\ell} A(n,T,k) - \sum_{\ell=-N-1}^{N+1}\operatorname*{Res}_{k=k_\ell} B(n,T,k)\right), \tag{3.2.25}$$

with

$$A(n,T,k) = e^{iknh}e^{-WT}\left[\frac{e^{ikh}\hat{q}(-k,0)+\hat{q}(k,0)}{e^{2ik(L+h)}-1}\right],$$

and

$$B(n,T,k) = e^{iknh}e^{-WT}\left[\frac{\left(1+e^{ikh}\right)\left(U^{(1)} - e^{ik(L+h)}V^{(1)}\right)}{e^{2ik(L+h)}-1}\right].$$

There are no contributions from the residues at the endpoints $k_{\pm(N+2)} = \pm\pi/h$ as in Section 3.2.1, but we find a nonzero contribution at $k_0 = 0$. Specifically,

$$\begin{cases} \displaystyle\sum_{\ell=-N-1}^{N+1}\operatorname*{Res}_{k=k_\ell}\{A(n,T,k)\} = \frac{L}{i\,(L+h)}\left[\frac{b_0}{2} + \sum_{\ell=1}^{N+1} e^{-W_\ell T}b_\ell\cos\left(\frac{\pi\ell\left(n+\frac{1}{2}\right)h}{L+h}\right)\right], \\ \displaystyle\sum_{\ell=-N-1}^{N+1}\operatorname*{Res}_{k=k_\ell}\{B(n,T,k)\} = \frac{2}{i(L+h)}\left[\frac{H(W_0)}{2} + \sum_{\ell=1}^{N+1} e^{-W_\ell T}\cos\left(\frac{\pi\ell h}{2\,(L+h)}\right)\cos\left(\frac{\pi\ell\left(n+\frac{1}{2}\right)h}{L+h}\right)H(W_\ell)\right], \end{cases}$$

where $W_\ell \equiv W\left(k_\ell\right)$,

$$b_\ell = \frac{2h}{L}\sum_{m=0}^{N+1}\cos\left(\frac{\pi\ell\left(m+\frac{1}{2}\right)h}{L+h}\right)\phi_m, \qquad H(W_\ell,T) = U^{(1)}(W_\ell,T) + (-1)^{\ell+1}V^{(1)}(W_\ell,T).$$

Returning to (3.2.25), we find

$$q_n(T) = \frac{L}{L+h}\sum_{\ell=1}^{N+1} e^{-W_\ell T}\cos\left(\frac{\pi\ell\left(n+\frac{1}{2}\right)h}{L+h}\right)\left[b_\ell - \frac{2}{L}\cos\left(\frac{\pi\ell h}{2\left(L+h\right)}\right)H(W_\ell)\right] + \frac{Lb_0}{2(L+h)} - \frac{H(W_0)}{L+h}. \tag{3.2.26}$$

Using the series representation (3.2.26) and the finite-difference schemes, we examine the solution of the IBVP

$$\begin{cases} q_t = q_{xx}, & 0 < x < 1,\ t > 0, \\ q(x,0) = \phi(x) = 12x - 10x^2 + \dfrac{1}{2}\sin(20\pi x^3), & 0 < x < 1, \\ q_x(0,t) = u^{(0)}(t) = 12, & t > 0, \\ q_x(1,t) = v^{(0)}(t) = 30\pi - 8, & t > 0. \end{cases} \tag{3.2.27}$$

The exact solution to (3.2.27) is given by

$$q(x,t) = (15\pi - 10)\,x^2 + 12x + (30\pi - 20)\,t + a_0 + \sum_{n=1}^{\infty} a_n e^{-(n\pi)^2 t}\cos\left(n\pi x\right),$$

with

$$a_0 = \int_0^1 \left[\frac{\sin(20\pi x^3)}{2} - 15\pi x^2\right] dx, \qquad \text{and} \qquad a_n = 2\int_0^1 \left[\frac{\sin(20\pi x^3)}{2} - 15\pi x^2\right]\cos\left(n\pi x\right)\, dx.$$

The given Neumann data is discretized using the first-order accurate stencils (3.2.20), which reduce the overall accuracy of the solution from the expected $\mathcal{O}(h^2)$ to $\mathcal{O}(h)$. With the centered stencil (2.2.2), solutions (3.2.23) and (3.2.26) are fourth-order accurate approximations to the dissipative PDE (2.2.12). However, the modified equations from the Neumann boundary conditions are

$$q_x(0,t) = u^{(1)}(t) - \left(\frac{h}{2}\right)q_{xx}(0,t), \qquad \text{and} \qquad q_x(L,t) = v^{(1)}(t) + \left(\frac{h}{2}\right)q_{xx}(L,t),$$

implying the loss of accuracy is through the form of dissipation near the boundaries. Even so, the solution profiles from Figure 3.2.6a depict the general diffusive behavior of the heat equation, quickly damping the high-frequency oscillations. Evaluating a_0 and a_n numerically, we obtain the error plot in Figure 3.2.6b. For consistency, the finite-difference schemes there also incorporate the Neumann boundary conditions using the first-order stencils (3.2.20).

3.2.3 Higher-Order Discretization of $q_t = q_{xx}$ with Dirichlet boundary conditions

As in Section 3.1.2, we can apply higher-order centered discretizations to the heat equation. As before, we need extra equations in addition to the global relation formulas with $k \to \nu_j(k)$

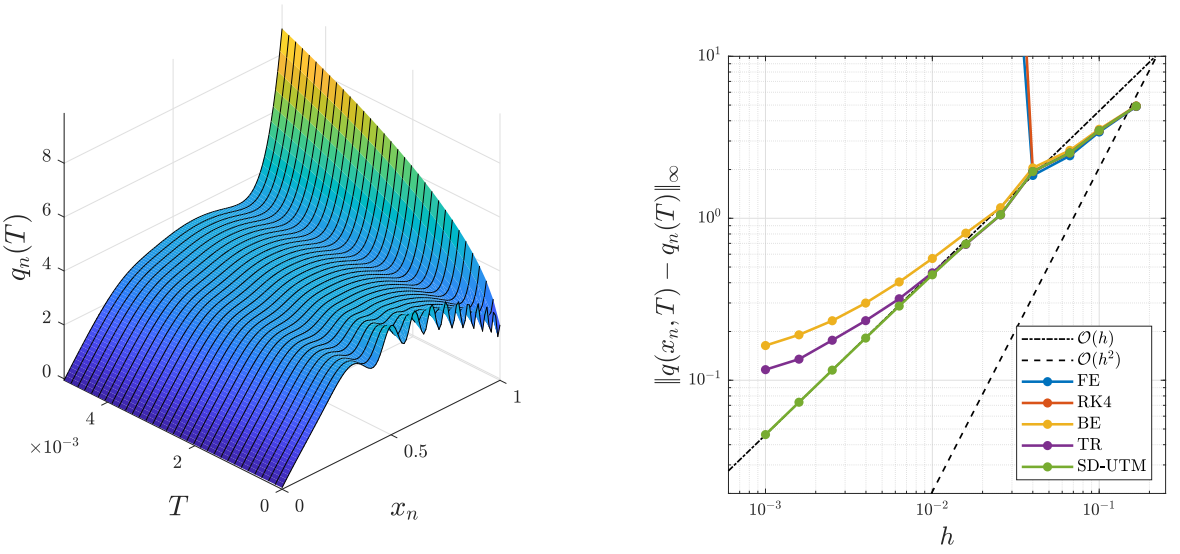

(a) (b)

Figure 3.2.6: (a) The semi-discrete solution (3.2.26) evaluated at various T with $h = 0.01$. (b) Error plot of the semi-discrete solution (3.2.26) and finite-difference schemes relative to the exact solution as $h \to 0$ with $T = 0.005$ and $\Delta t = 6.25 \times 10^{-4}$.

to eliminate unknowns. As an example, consider the Dirichlet problem (3.2.1) with the standard centered fourth-order discretization (2.2.26). After some tedious steps, the global relation is

$$e^{WT}\hat{q}(k,T) - \hat{q}(k,0) - \left[\frac{f(k,T) + e^{-ikL}g(k,T)}{12h}\right] = 0, \quad k \in \mathbb{C}, \tag{3.2.28}$$

where

$$\begin{cases} f(k,T) = -e^{-ikh}f_{-1} + 16e^{-ikh}f_0 - e^{-2ikh}f_0 + e^{ikh}f_1 - 16f_1 + f_2, \\ g(k,T) = e^{-ikh}g_{-1} + 16e^{ikh}g_0 - e^{2ikh}g_0 - e^{ikh}g_1 + g_{-2} - 16g_{-1}, \end{cases}$$

with dispersion relation (2.2.28). Solving for $\hat{q}(k,T)$ and taking the inverse transform, we obtain

$$q_n(T) = \frac{1}{2\pi}\int_{-\pi/h}^{\pi/h} e^{iknh}e^{-WT}\hat{q}(k,0)\,dk + \frac{1}{2\pi}\int_{-\pi/h}^{\pi/h} e^{iknh}e^{-WT}\left[\frac{f(k,T) + e^{-ikL}g(k,T)}{12h}\right]dk, \tag{3.2.29}$$

which depends on the six unknowns $f_{-1}(W,T)$, $f_1(W,T)$, $f_2(W,T)$, $g_{-2}(W,T)$, $g_{-1}(W,T)$, and $g_1(W,T)$. The dispersion relation has the trivial symmetry $\nu_0(k) = k$ and three nontrivial symme-

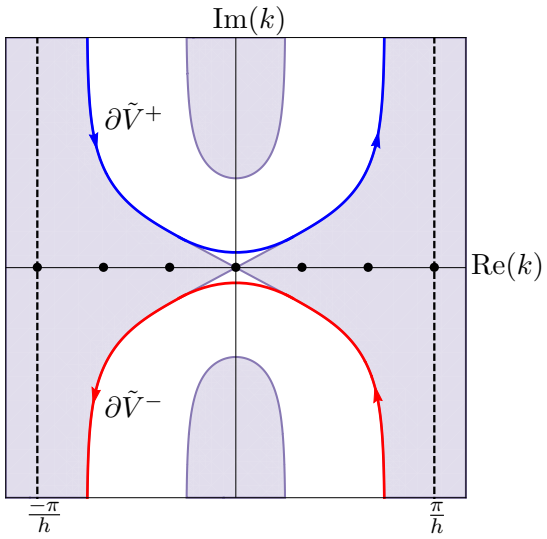

Figure 3.2.7: The shaded regions depict where $\mathrm{Re}(-W) \leq 0$ and e^{-WT} is bounded, for the dispersion relation (2.2.28). The integration paths for $\partial\tilde{V}^{\pm}$, deformed away from the singularities on the real line, are also shown.

tries:

$$\begin{aligned}
\nu_1(k) &= -k, \\
\nu_2(k) &= \frac{i}{h}\ln\left(\frac{e^{-ikh}}{2}\left[16e^{ikh} - e^{2ikh} - 1 + \sqrt{(-16e^{ikh} + e^{2ikh} + 1)^2 - 4e^{2ikh}}\right]\right), \\
\nu_3(k) &= \frac{i}{h}\ln\left(\frac{e^{-ikh}}{2}\left[16e^{ikh} - e^{2ikh} - 1 - \sqrt{(-16e^{ikh} + e^{2ikh} + 1)^2 - 4e^{2ikh}}\right]\right),
\end{aligned}$$

where the branch cut for the square-root function is chosen to be on the positive real line. We separate $f(k,T)$ from $g(k,T)$ in the last integral of (3.2.29) and, anticipating singularities, deform that integration path to $\partial\tilde{V}^{\pm}$, as shown in Figure 3.2.7:

$$\begin{aligned}
q_n(T) = \frac{1}{2\pi}\int_{-\pi/h}^{\pi/h} e^{iknh}e^{-WT}\hat{q}(k,0)\,dk + \frac{1}{2\pi}\int_{\partial\tilde{V}^+} e^{iknh}e^{-WT}\left[\frac{f(k,T)}{12h}\right]dk \\
- \frac{1}{2\pi}\int_{\partial\tilde{V}^-} e^{ik(nh-L)}e^{-WT}\left[\frac{g(k,T)}{12h}\right]dk.
\end{aligned} \tag{3.2.30}$$

In contrast to the half-line problem [11], the global relations with $k \to \nu_{2,3}(k)$ are valid for all $k \in \mathbb{C}$. Using all symmetries, including $\nu_0(k)$, the global relations give four equations to remove four unknowns, specifically two $f_j(W,T)$ and two $g_j(W,T)$ contributions. To remove the remaining pair of $f_j(W,T)$ and $g_j(W,T)$ terms, we must introduce (at least) one more equation for each unknown.

Using the given Dirichlet data, the heat equation itself gives all even-derivative boundary conditions, particularly $q_{xx}(0,t) = \dot{u}(t)$ and $q_{4x}(0,t) = \ddot{u}(t)$ on the left, and $q_{xx}(L,t) = \dot{v}(t)$ and $q_{4x}(L,t) = \ddot{v}(t)$ on the right, where $\dot{u} = du^{(0)}(t)/dt$, $\ddot{u} = d^2u^{(0)}(t)/dt^2$, $\dot{v} = dv^{(0)}(t)/dt$, and $\ddot{v} = d^2v^{(0)}(t)/dt^2$. Discretizing the second-derivative conditions with the standard centered fourth-order stencils gives

$$\frac{-q_{-2}(t) + 16q_{-1}(t) - 30q_0(t) + 16q_1(t) - q_2(t)}{12h^2} = \dot{u}(t), \tag{3.2.31}$$

$$\frac{-q_{N-1}(t) + 16q_N(t) - 30q_{N+1}(t) + 16q_{N+2}(t) - q_{N+3}(t)}{12h^2} = \dot{v}(t). \tag{3.2.32}$$

These stencils introduce an additional unknown, each requiring two more equations. We can find additional equations that relate nodal points with derivatives using the method of undetermined coefficients. Since we know $q_{4x}(0,t)$ and $q_{4x}(L,t)$, we derive the last pair of equations that does not introduce any more unknowns, maintains the same order of accuracy as (2.2.26), and is linearly independent of (3.2.31) – (3.2.32):

$$\frac{q_{-2}(t) + 2q_{-1}(t) - 6q_0(t) + 2q_1(t) + q_2(t)}{6h^2} = \dot{u}(t) + \frac{h^2}{4}\ddot{u}(t), \tag{3.2.33}$$

$$\frac{q_{N-1}(t) + 2q_N(t) - 6q_{N+1}(t) + 2q_{N+2}(t) + q_{N+3}(t)}{6h^2} = \dot{v}(t) + \frac{h^2}{4}\ddot{v}(t). \tag{3.2.34}$$

Taking the time transforms of (3.2.31) – (3.2.34), we have a closed system of eight equations for all unknowns:

$$\begin{cases} 0 = e^{WT}\hat{q}(k,T) - \hat{q}(k,0) - \left[\dfrac{f(k,T) + e^{-ikL}g(k,T)}{12h}\right], & \dfrac{-f_{-2} + 16f_{-1} - 30f_0 + 16f_1 - f_2}{12h^2} = \dot{U}, \\ 0 = e^{WT}\hat{q}(-k,T) - \hat{q}(-k,0) - \left[\dfrac{f(-k,T) + e^{ikL}g(-k,T)}{12h}\right], & \dfrac{-g_{-2} + 16g_{-1} - 30g_0 + 16g_1 - g_2}{12h^2} = \dot{V}, \\ 0 = e^{WT}\hat{q}(\nu_2,T) - \hat{q}(\nu_2,0) - \left[\dfrac{f(\nu_2,T) + e^{-i\nu_2 L}g(\nu_2,T)}{12h}\right], & \dfrac{f_{-2} + 2f_{-1} - 6f_0 + 2f_1 + f_2}{6h^2} = \dot{U} + \dfrac{h^2}{4}\ddot{U}, \\ 0 = e^{WT}\hat{q}(\nu_3,T) - \hat{q}(\nu_3,0) - \left[\dfrac{f(\nu_3,T) + e^{-i\nu_3 L}g(\nu_3,T)}{12h}\right], & \dfrac{g_{-2} + 2g_{-1} - 6g_0 + 2g_1 + g_2}{6h^2} = \dot{V} + \dfrac{h^2}{4}\ddot{V}, \end{cases}$$

where $\dot{U}(W,T)$ is the time transform of $\dot{u}(t)$, $\ddot{U}(W,T)$ is the time transform of $\ddot{u}(t)$, etc. Solving the

system, we substitute our findings into (3.2.30):

$$
\begin{aligned}
q_n(T) = &\frac{1}{2\pi}\int_{-\pi/h}^{\pi/h} e^{iknh}e^{-WT}\hat{q}(k,0)\,dk \\
&+ \frac{1}{2\pi}\int_{\partial\tilde{V}^+} e^{iknh}e^{-WT}\left[\frac{\hat{q}(-k,0)-e^{2ikL}\hat{q}(k,0)}{e^{2ikL}-1}\right]dk + \frac{1}{2\pi}\int_{\partial\tilde{V}^-} e^{iknh}e^{-WT}\left[\frac{\hat{q}(-k,0)-\hat{q}(k,0)}{e^{2ikL}-1}\right]dk \\
&+ \frac{1}{2\pi}\left(\int_{\partial\tilde{V}^+}+\int_{\partial\tilde{V}^-}\right)e^{iknh}e^{-WT}\left[\frac{\left(e^{-2ikh}-14e^{-ikh}+14e^{ikh}-e^{2ikh}\right)\left(f_0-e^{ikL}g_0\right)}{12h\left(e^{2ikL}-1\right)}\right]dk \quad (3.2.35) \\
&- \frac{1}{2\pi}\left(\int_{\partial\tilde{V}^+}+\int_{\partial\tilde{V}^-}\right)e^{iknh}e^{-WT}\left[\frac{e^{-ikh}\left(e^{2ikh}-1\right)}{12\left(e^{2ikL}-1\right)}\left(h\,\dot{U}+\frac{h^3}{12}\,\ddot{U}\right)\right]dk \\
&+ \frac{1}{2\pi}\left(\int_{\partial\tilde{V}^+}+\int_{\partial\tilde{V}^-}\right)e^{ik(nh+L)}e^{-WT}\left[\frac{e^{-ikh}\left(e^{2ikh}-1\right)}{12\left(e^{2ikL}-1\right)}\left(h\,\dot{V}+\frac{h^3}{12}\,\ddot{V}\right)\right]dk,
\end{aligned}
$$

after showing integral terms with $\hat{q}(\pm k,T)$ vanish. Note that (3.2.35) has no dependence on $\nu_{2,3}(k)$ and the integration paths $\partial\tilde{V}^{\pm}$ are above/below the singularities given by $k_\ell = \pi\ell/h$, exactly as for the heat equation discretized to second order (2.2.2). To the best of our knowledge, (3.2.35) is the first explicit solution expression to this fourth-order discretized IBVP.

In the continuum limit,

$$
\lim_{h\to 0}\frac{e^{-2ikh}-14e^{-ikh}+14e^{ikh}-e^{2ikh}}{12h} = 2ik.
$$

Expanding the common factor between the derivative boundary conditions in (3.2.35),

$$
\frac{e^{-ikh}\left(e^{2ikh}-1\right)}{12\left(e^{2ikL}-1\right)} = \frac{ik}{6\left(e^{2ikL}-1\right)}\,h + \mathcal{O}(h^3),
$$

so that the coefficients of $\dot{U}$ and $\dot{V}$ are $\mathcal{O}(h^2)$, while the coefficients for $\ddot{U}$ and $\ddot{V}$ are $\mathcal{O}(h^4)$. Hence, the SD-UTM solution loses dependence on the second and fourth-derivative boundary conditions in the continuum limit and the semi-discrete solution (3.2.35) converges to (3.2.10). Although the expressions are tedious to derive, a series representation can be written down as before.

Remark 3.2.1. To avoid the need for the additional equations (3.2.33) – (3.2.34), we can discretize the second-derivative boundary conditions with $\mathcal{O}(h^2)$ centered stencils:

$$
\frac{q_{-1}(t)-2q_0(t)+q_1(t)}{h^2} = \dot{u}(t), \qquad \frac{q_N(t)-2q_{N+1}(t)+q_{N+2}(t)}{h^2} = \dot{v}(t).
$$

Together with the four global relation formulas, we solve for the original six unknowns in (3.2.30), which gives rise to a second-order accurate SD-UTM solution. As a consequence, there is a drop in accuracy from the intended $\mathcal{O}(h^4)$. This solution is exactly (3.2.35), but without the inclusion of $h^3\ddot{U}/12$ and $h^3\ddot{V}/12$.

Remark 3.2.2. As in Section 3.2.2, solving the fourth-order discretization (2.2.26) with Neumann boundary conditions leads to a solution that is one order of accuracy less than that of the PDE stencil. After inverting the global relation for this IBVP, the "solution" depends on eight unknowns: $f_i(W,T)$ for $i = -2,\dots,1$ and $g_j(W,T)$ for $j = -1,\dots,2$. The four symmetries result in four global relation formulas to remove two $f_i(W,T)$ and two $g_j(W,T)$ terms after deforming off the real line to $\partial\tilde{V}^{\pm}$, as illustrated in Figure 3.2.7. In order to not introduce more unknowns, four linearly independent discretizations to eliminate the remaining four unknowns are:

$$\frac{f_1 - f_{-1}}{2h} = U^{(1)} + \frac{h^2}{6}\dot{U}, \qquad \frac{g_1 - g_{-1}}{2h} = V^{(1)} + \frac{h^2}{6}\dot{V},$$

and

$$\frac{f_{-2} - 6f_{-1} + 3f_0 + 2f_1}{6h} = U^{(1)}, \qquad \frac{g_{-2} - 6g_{-1} + 3g_0 + 2g_1}{6h} = V^{(1)},$$

after taking time transforms. Here,

$$\dot{U}(W,T) = \int_0^T e^{Wt}\dot{u}(t)\,dt, \qquad \dot{V}(W,T) = \int_0^T e^{Wt}\dot{v}(t)\,dt,$$

where $\dot{u}(t) = du^{(1)}(t)/dt$ and $\dot{v}(t) = dv^{(1)}(t)/dt$. The first pair of discretizations is $\mathcal{O}(h^4)$, but the second is $\mathcal{O}(h^3)$, where the $\mathcal{O}(h^3)$ terms depend on $q_{4x}(0,t)$ and $q_{4x}(L,t)$, respectively. Replacing this last pair of discretizations with a wider, more accurate stencil introduces more unknowns that no linearly independent discretizations can eliminate. Hence, the SD-UTM solution with these discretizations is third-order accurate.

3.3 The Linear Schrödinger Equation

3.3.1 Centered Discretization of $q_t = (i/2)q_{xx}$ with Dirichlet boundary conditions

The finite-interval IBVP with Dirichlet boundary conditions at both ends is

$$\begin{cases} q_t = \frac{i}{2}q_{xx}, & 0 < x < L,\ t > 0, \\ q(x,0) = \phi(x), & 0 < x < L, \\ q(0,t) = u^{(0)}(t), & t > 0, \\ q(L,t) = v^{(0)}(t), & t > 0. \end{cases} \tag{3.3.1}$$

Using the second-order centered discretization (2.3.3), the local and dispersion relations are (2.3.4) and (2.3.5), respectively. Starting the forward transform at $n = 1$ and ending at $n = N$ gives the global relation

$$e^{WT}\hat{q}(k,T) - \hat{q}(k,0) - \frac{i}{2}\left[\frac{e^{-ikh}f_0 - f_1 + e^{-ikL}\left(e^{ikh}g_0 - g_{-1}\right)}{h}\right] = 0, \quad k \in \mathbb{C}. \tag{3.3.2}$$

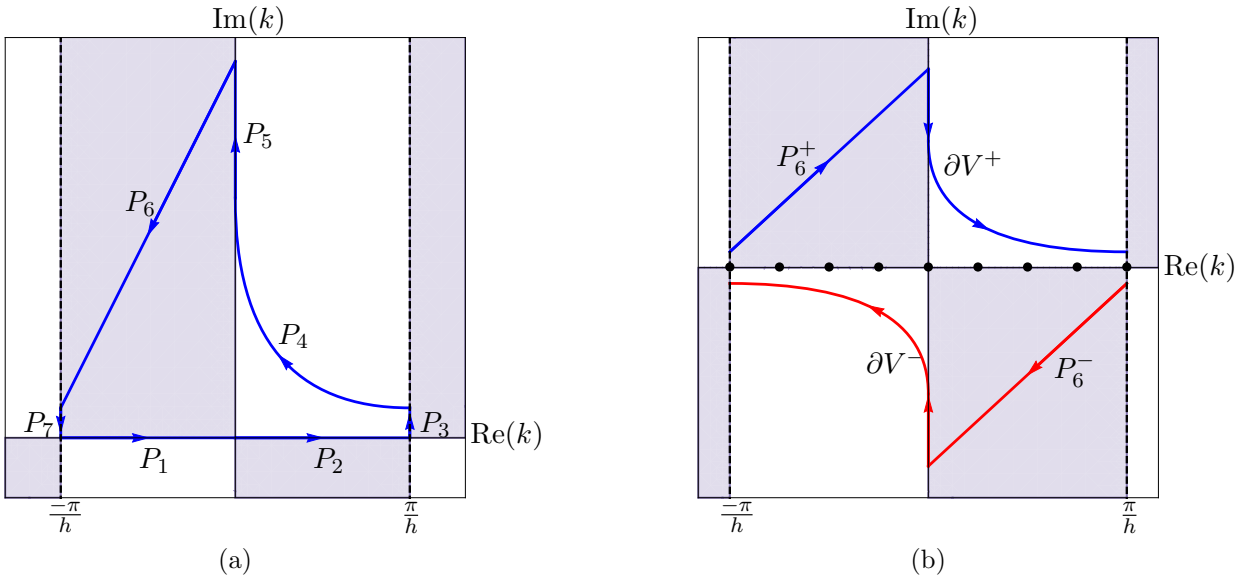

Figure 3.3.1: (a) The shaded regions depict where $\mathrm{Re}(-W) \leq 0$ and e^{-WT} is bounded, for the dispersion relation (2.3.5). The integration paths that constitute P are also shown. (b) The integration paths $\partial V^{\pm}$ and $P_6^{\pm}$.

We obtain our "solution" formula by solving for $\hat{q}(k,T)$ and taking the inverse transform:

$$\begin{aligned} q_n(T) = \frac{1}{2\pi}\int_{-\pi/h}^{\pi/h} e^{iknh}e^{-WT}\hat{q}(k,0)\,dk + \frac{1}{2\pi}\int_{-\pi/h}^{\pi/h} \frac{ie^{iknh}e^{-WT}}{2}\left[\frac{e^{-ikh}f_0 - f_1}{h}\right] dk \\ + \frac{1}{2\pi}\int_{-\pi/h}^{\pi/h} \frac{ie^{ik(nh-L)}e^{-WT}}{2}\left[\frac{e^{ikh}g_0 - g_{-1}}{h}\right] dk. \end{aligned} \tag{3.3.3}$$

The dispersion relation (2.3.5) has the symmetries $\nu_0(k) = k$ and $\nu_1(k) = -k$ up to periodic copies, which can be used to remove the unknowns $f_1(W,T)$ and $g_{-1}(W,T)$ from (3.3.3). First, we separate the integral with the $f_j(W,T)$ terms from the integral with $g_j(W,T)$, and deform both integration paths off the real line (where we have singularities after solving for the unknowns). For the integral with the left boundary terms, consider the integration contour $P = P_1 + \ldots + P_7$, depicted in Figure 3.3.1a. Note that not all paths are straight lines. We define the integration

paths' start and end points as

$$\begin{aligned} P_1 &: \text{ from } -\frac{\pi}{h} \text{ to } 0, & P_5 &: \text{ from } ic \text{ to } \frac{\pi}{h}i, \\ P_2 &: \text{ from } 0 \text{ to } \frac{\pi}{h}, & P_6 &: \text{ from } \frac{\pi}{h}i \text{ to } -\frac{\pi}{h}+i\delta, \\ P_3 &: \text{ from } \frac{\pi}{h} \text{ to } \frac{\pi}{h}+i\delta, & P_7 &: \text{ from } -\frac{\pi}{h}+i\delta \text{ to } -\frac{\pi}{h}, \\ P_4 &: \text{ from } \frac{\pi}{h}+i\delta \text{ to } ic, \end{aligned}$$

where $\delta, c \in \mathbb{R}^+$ are nonzero constants. The point that connects P_4 to P_5 can be conveniently chosen, fixed or varying with respect to h, but the choice must keep the area underneath P_4 small, since this path is in the region of exponential growth. It is vital, however, for the curve P_4 to asymptotically approach the real line from above as $h \to 0$, so $\delta \ll 1$ but never zero for a finite h. The path P_6 is chosen as a straight line also for convenience, but any curved path suffices. From periodicity, $P_3 = -P_7$, so that

$$\begin{aligned} \frac{1}{2\pi}\int_{-\pi/h}^{\pi/h} \frac{ie^{iknh}e^{-WT}}{2}\left(\frac{e^{-ikh}f_0 - f_1}{h}\right) dk &= \frac{1}{2\pi}\left(\int_{-P_4}+\int_{-P_5}+\int_{-P_6}\right)\frac{ie^{iknh}e^{-WT}}{2}\left(\frac{e^{-ikh}f_0 - f_1}{h}\right) dk \\ &= \frac{1}{2\pi}\int_{\partial\tilde{V}^+}\frac{ie^{iknh}e^{-WT}}{2}\left(\frac{e^{-ikh}f_0 - f_1}{h}\right) dk, \end{aligned}$$

after defining $\partial V^+ = -P_4 - P_5$ and $\partial\tilde{V}^+ = \partial V^+ + P_6^+$ with $P_6^+ = -P_6$. Following similar arguments to deform the integral containing the right boundary information, (3.3.3) becomes

$$\begin{aligned} q_n(T) = \frac{1}{2\pi}\int_{-\pi/h}^{\pi/h} e^{iknh}e^{-WT}\hat{q}(k,0)\,dk + \frac{1}{2\pi}\int_{\partial\tilde{V}^+}\frac{ie^{iknh}e^{-WT}}{2}\left(\frac{e^{-ikh}f_0 - f_1}{h}\right) dk \\ - \frac{1}{2\pi}\int_{\partial\tilde{V}^-}\frac{ie^{ik(nh-L)}e^{-WT}}{2}\left(\frac{e^{ikh}g_0 - g_{-1}}{h}\right) dk, \end{aligned} \tag{3.3.4}$$

where $\partial\tilde{V}^- = \partial V^- + P_6^-$, as shown in Figure 3.3.1b. Now off the real line, solving the system

$$\begin{cases} e^{WT}\hat{q}(k,T) - \hat{q}(k,0) - \dfrac{i}{2}\left[\dfrac{e^{-ikh}f_0 - f_1 + e^{-ikL}\left(e^{ikh}g_0 - g_{-1}\right)}{h}\right] = 0, \\ e^{WT}\hat{q}(-k,T) - \hat{q}(-k,0) - \dfrac{i}{2}\left[\dfrac{e^{ikh}f_0 - f_1 + e^{ikL}\left(e^{-ikh}g_0 - g_{-1}\right)}{h}\right] = 0, \end{cases}$$

for $f_1(W,T)$ and $g_{-1}(W,T)$ gives

$$\begin{aligned} q_n(T) = \frac{1}{2\pi}\int_{-\pi/h}^{\pi/h} e^{iknh}e^{-WT}\hat{q}(k,0)\,dk \\ - \frac{1}{2\pi}\int_{\partial\tilde{V}^+} e^{iknh}e^{-WT}\left[\frac{e^{2ikL}\hat{q}(k,0) - \hat{q}(-k,0)}{e^{2ikL}-1} + \frac{\sin(kh)\left(f_0 - e^{ikL}g_0\right)}{h\left(e^{2ikL}-1\right)}\right] dk \\ - \frac{1}{2\pi}\int_{\partial\tilde{V}^-} e^{iknh}e^{-WT}\left[\frac{\hat{q}(k,0) - \hat{q}(-k,0)}{e^{2ikL}-1} + \frac{\sin(kh)\left(f_0 - e^{ikL}g_0\right)}{h\left(e^{2ikL}-1\right)}\right] dk, \end{aligned} \tag{3.3.5}$$

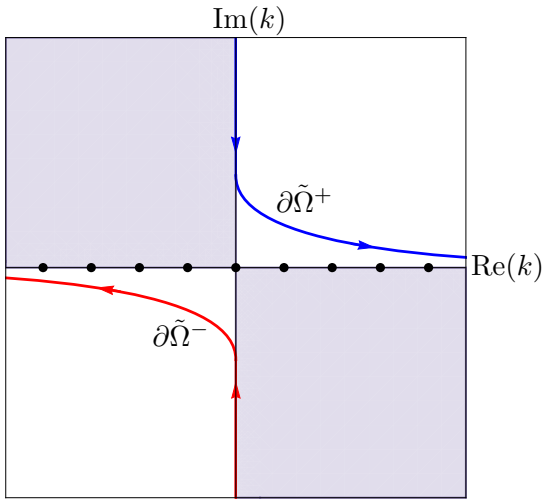

Figure 3.3.2: The shaded regions depict where $\mathrm{Re}(-\tilde{W}) \leq 0$ and $e^{\tilde{W}T}$ is bounded. The integration paths $\partial\tilde{\Omega}^{\pm}$ are also shown.

after removing the integral terms with $\hat{q}(\pm k, T)$. The simple poles at $k_\ell = \pi\ell/L$, the same as in (3.2.9) to the second-order discretized heat equation, do not interfere with the integration paths $\partial\tilde{V}^{\pm}$. When numerically evaluating the integrals above, the paths P_4 in $\partial\tilde{V}^{\pm}$ are parameterized as exponentially-decaying curves toward the real line as $\mathrm{Re}(k) \to \infty$.

With the integration paths $\tilde{\Omega}^{\pm}$ illustrated in Figure 3.3.2 and the dispersion relation $\tilde{W}(k) = ik^2/2$, the continuous UTM solution [17] to (3.3.1) is

$$\begin{aligned} q(x,T) = \frac{1}{2\pi}\int_{-\infty}^{\infty} e^{ikx}e^{-\tilde{W}T}\hat{q}(k,0)\,dk \\ - \frac{1}{2\pi}\int_{\partial\tilde{\Omega}^+} e^{ikx}e^{-\tilde{W}T}\left[\frac{e^{2ikL}\hat{q}(k,0) - \hat{q}(-k,0) + k\left(F_0 - e^{ikL}G_0\right)}{e^{2ikL}-1}\right]dk \\ - \frac{1}{2\pi}\int_{\partial\tilde{\Omega}^-} e^{ikx}e^{-\tilde{W}T}\left[\frac{\hat{q}(k,0) - \hat{q}(-k,0) + k\left(F_0 - e^{ikL}G_0\right)}{e^{2ikL}-1}\right]dk. \end{aligned} \tag{3.3.6}$$

Taking the continuum limit, we find $\lim_{h\to 0} W(k) = \tilde{W}(k)$ and $\lim_{h\to 0}\partial V^{\pm} = \tilde{\Omega}^{\pm}$, where $\partial\tilde{V}^{\pm} = \partial V^{\pm} + P_6^{\pm}$. For P_6^+ in the upper-half plane, we have

$$\begin{aligned} \lim_{h\to 0}\frac{1}{2\pi}\int_{-\frac{\pi}{h}+i\delta}^{\frac{\pi}{h}i} e^{iknh}e^{-WT}\left[\frac{e^{2ikL}\hat{q}(k,0) - \hat{q}(-k,0)}{e^{2ikL}-1} + \frac{\sin(kh)\left(f_0 - e^{ikL}g_0\right)}{h\left(e^{2ikL}-1\right)}\right]dk \\ = \frac{1}{2\pi}\int_{-\infty+i\delta}^{i\infty} e^{ikx}e^{-\tilde{W}T}\left[\frac{e^{2ikL}\hat{q}(k,0) - \hat{q}(-k,0) + k\left(F_0 - e^{ikL}G_0\right)}{e^{2ikL}-1}\right]dk. \end{aligned} \tag{3.3.7}$$

With $R \gg 1$,

$$\frac{1}{2\pi}\int_{-R+i\delta}^{iR} e^{ikx}e^{-\tilde{W}T}\left[\frac{e^{2ikL}\hat{q}(k,0)-\hat{q}(-k,0)}{e^{2ikL}-1}\right]dk$$
$$=\frac{1}{2\pi}\int_0^L\left[\int_{-R+i\delta}^{iR} e^{ikx}e^{-\tilde{W}T}\left(\frac{e^{2ikL}e^{-iky}-e^{iky}}{e^{2ikL}-1}\right)dk\right]q(y,0)\,dy.$$

Because the integration path is in the shaded region of Figure 3.3.2, taking $R\to\infty$ implies the integrand

$$e^{ikx}e^{-\tilde{W}T}\left[\frac{e^{ik(2L-y)}-e^{iky}}{e^{2ikL}-1}\right]\to 0,$$

since every exponent is positive and decays in the integration region. Similarly for (3.3.7). Hence,

$$\frac{1}{2\pi}\int_{-\infty+i\delta}^{i\infty} e^{ikx}e^{-\tilde{W}T}\left[\frac{e^{2ikL}\hat{q}(k,0)-\hat{q}(-k,0)+k\left(F_0-e^{ikL}G_0\right)}{e^{2ikL}-1}\right]dk=0,$$

and in the continuum limit,

$$\lim_{h\to 0}\frac{1}{2\pi}\int_{P_6^+} e^{iknh}e^{-WT}\left[\frac{\hat{q}(-k,0)-e^{2ikL}\hat{q}(k,0)}{e^{2ikL}-1}+\frac{\sin(kh)\left(e^{ikL}g_0-f_0\right)}{h\left(e^{2ikL}-1\right)}\right]dk=0.$$

We reach a similar conclusion for the P_6^- integral. Therefore, the SD-UTM solution (3.3.5) converges to its continuous counterpart (3.3.6).

Series Representation

Although this is a dispersive problem, the series representation of (3.3.5) is obtained following almost exactly the same steps as those in Section 3.2.1 for the heat equation with Dirichlet boundary conditions. Deforming the integration paths $\partial\tilde{V}^{\pm}$ to the singularities on the real line and determining the residue contributions gives

$$q_n(T)=\sum_{\ell=1}^{N} e^{-W_\ell T}\sin\left(\frac{\pi\ell nh}{L}\right)\left[b_\ell+\frac{i}{Lh}\sin\left(\frac{\pi\ell h}{L}\right)H(W_\ell,T)\right], \tag{3.3.8}$$

where $W(k_\ell)\equiv W_\ell$ and

$$b_\ell=\frac{2h}{L}\sum_{m=0}^{N+1}\sin\left(\frac{\pi\ell mh}{L}\right)\phi_m,\qquad H(W_\ell,T)=f_0(W_\ell,T)+(-1)^{\ell+1}g_0(W_\ell,T).$$

Using (3.3.8), we examine the numerical solution to

$$\begin{cases} q_t=\frac{i}{2}q_{xx}, & 0<x<1,\ t>0,\\ q(x,0)=\phi(x)=2(6+5i)x-10(1+i)x^2+\frac{1}{2}\sin\left(4\pi x^3\right), & 0<x<1,\\ q(0,t)=u^{(0)}(t)=0, & t>0,\\ q(1,t)=v^{(0)}(t)=2, & t>0. \end{cases} \tag{3.3.9}$$

For this IBVP, the continuous solution is traditionally determined using Fourier series. The modified PDE is $p_t = (i/2)p_{xx} + (ih^2/24)p_{4x}$, which is dispersive. Figure 3.3.3 shows the dispersive nature of the real and imaginary components of the SD-UTM solution, along with the square of the modulus. Once more, the SD-UTM outperforms the standard finite-difference methods, where BE's dissipative behavior practically dampens all oscillations. From the error plot in Figure 3.3.3d, TR attempts to capture these oscillations, but not as accurately as the SD-UTM.

3.3.2 Centered Discretization of $q_t = (i/2)q_{xx}$ with Neumann boundary conditions

Lastly, we consider the second-order discretization (2.3.3), but with Neumann boundary conditions at both ends of the interval:

$$\begin{cases} q_t = \frac{i}{2}q_{xx}, & 0 < x < L,\ t > 0, \\ q(x,0) = \phi(x), & 0 < x < L, \\ q_x(0,t) = u^{(1)}(t), & t > 0, \\ q_x(L,t) = v^{(1)}(t), & t > 0. \end{cases} \tag{3.3.10}$$

The local and dispersion relations, (2.3.4) and (2.3.5) respectively, transfer over from the previous section and half-line problems. Now without Dirichlet data, $q_0(t)$ and $q_{N+1}(t)$ are unknown, and the global relation is

$$e^{WT}\hat{q}(k,T) - \hat{q}(k,0) - \frac{i}{2}\left[\frac{f_{-1} - e^{ikh}f_0 + e^{-ikL}\left(g_1 - e^{-ikh}g_0\right)}{h}\right] = 0, \quad k \in \mathbb{C}. \tag{3.3.11}$$

Solving for $\hat{q}(k,T)$ and using the inverse transform, we obtain

$$\begin{aligned} q_n(T) = {} & \frac{1}{2\pi}\int_{-\pi/h}^{\pi/h} e^{iknh}e^{-WT}\hat{q}(k,0)\,dk + \frac{1}{2\pi}\int_{-\pi/h}^{\pi/h} \frac{ie^{iknh}e^{-WT}}{2}\left[\frac{f_{-1} - e^{ikh}f_0}{h}\right]dk \\ & + \frac{1}{2\pi}\int_{-\pi/h}^{\pi/h} \frac{ie^{ik(nh-L)}e^{-WT}}{2}\left[\frac{g_1 - e^{-ikh}g_0}{h}\right]dk. \end{aligned} \tag{3.3.12}$$

The global relations (3.3.11) with k and $k \to -k$ remove two of the four unknowns. To not introduce new unknowns, we apply the first-order backward discretization to $q_x(0,t)$ and the first-order forward discretization to $q_x(L,t)$. Upon taking time transforms, we solve the system

$$\begin{cases} e^{WT}\hat{q}(k,T) - \hat{q}(k,0) - \frac{i}{2}\left[\frac{f_{-1} - e^{ikh}f_0 + e^{-ikL}\left(g_1 - e^{-ikh}g_0\right)}{h}\right] = 0, \\ e^{WT}\hat{q}(-k,T) - \hat{q}(-k,0) - \frac{i}{2}\left[\frac{f_{-1} - e^{-ikh}f_0 + e^{ikL}\left(g_1 - e^{ikh}g_0\right)}{h}\right] = 0, \\ \frac{f_0 - f_{-1}}{h} = U^{(1)}, \\ \frac{g_1 - g_0}{h} = V^{(1)}, \end{cases}$$

to remove all four unknowns from "solution" (3.3.12), where

$$U^{(1)}(W,T) = \int_0^T e^{Wt}u^{(1)}(t)\,dt, \qquad \text{and} \qquad V^{(1)}(W,T) = \int_0^T e^{Wt}v^{(1)}(t)\,dt.$$

Doing so and substituting into (3.3.12) after deforming to $\partial\tilde{V}^{\pm}$, depicted in Figure 3.3.1b, gives the first-order accurate solution

$$\begin{aligned} q_n(T) = &\frac{1}{2\pi}\int_{-\pi/h}^{\pi/h} e^{iknh}e^{-WT}\hat{q}(k,0)\,dk \\ &- \frac{1}{2\pi}\int_{\partial\tilde{V}^+} e^{iknh}e^{-WT}\left[\frac{e^{2ik(L+h)}\hat{q}(k,0)+e^{ikh}\hat{q}(-k,0)}{e^{2ik(L+h)}-1} - \frac{i\left(1+e^{ikh}\right)\left(U^{(1)}-e^{ik(L+h)}V^{(1)}\right)}{2\left(e^{2ik(L+h)}-1\right)}\right]dk \\ &- \frac{1}{2\pi}\int_{\partial\tilde{V}^-} e^{iknh}e^{-WT}\left[\frac{\hat{q}(k,0)+e^{ikh}\hat{q}(-k,0)}{e^{2ik(L+h)}-1} - \frac{i\left(1+e^{ikh}\right)\left(U^{(1)}-e^{ik(L+h)}V^{(1)}\right)}{2\left(e^{2ik(L+h)}-1\right)}\right]dk, \end{aligned} \tag{3.3.13}$$

after applying similar techniques as before to remove the integral terms depending on $\hat{q}(\pm k,T)$. In the continuum limit, (3.3.13) converges to the continuous UTM solution [17]:

$$\begin{aligned} q(x,T) = &\frac{1}{2\pi}\int_{-\pi/h}^{\pi/h} e^{ikx}e^{-\tilde{W}T}\hat{q}(k,0)\,dk \\ &- \frac{1}{2\pi}\int_{\partial\tilde{\Omega}^+} e^{ikx}e^{-\tilde{W}T}\left[\frac{e^{2ikL}\hat{q}(k,0)+\hat{q}(-k,0)-i\left(F_1-e^{ikL}G_1\right)}{e^{2ikL}-1}\right]dk \\ &- \frac{1}{2\pi}\int_{\partial\tilde{\Omega}^-} e^{ikx}e^{-\tilde{W}T}\left[\frac{\hat{q}(-k,0)+\hat{q}(k,0)-i\left(F_1-e^{ikL}G_1\right)}{e^{2ikL}-1}\right]dk, \end{aligned} \tag{3.3.14}$$

where $\lim_{h\to 0} U^{(1)} = F_1$ and $\lim_{h\to 0} V^{(1)} = G_1$.

Series Representation

Proceeding as in the previous sections, the series representation for (3.3.13) is

$$\begin{aligned} q_n(T) = &\frac{L}{L+h}\sum_{\ell=1}^{N+1} e^{-W_\ell T}\cos\left(\frac{\pi\ell\left(n+\frac{1}{2}\right)h}{L+h}\right)\left[b_\ell - \frac{i}{L}\cos\left[\frac{\pi\ell h}{2\left(L+h\right)}\right]H(W_\ell,T)\right] \\ &+ \frac{Lb_0 - iH(W_0,T)}{2(L+h)}. \end{aligned} \tag{3.3.15}$$

where

$$b_\ell = \frac{2h}{L}\sum_{m=0}^{N+1}\cos\left(\frac{\pi\ell\left(m+\frac{1}{2}\right)h}{L+h}\right)\phi_m, \qquad H(W_\ell,T) = U^{(1)}(W_\ell,T) + (-1)^{\ell+1}V^{(1)}(W_\ell,T).$$

For a numerical example, consider the IBVP (3.3.9), but with Neumann boundary conditions:

$$\begin{cases} q_t = \frac{i}{2} q_{xx}, & 0 < x < 1,\ t > 0, \\ q(x,0) = \phi(x) = 12x - 10x^2 + \frac{1}{2}\sin\left(4\pi x^3\right), & 0 < x < 1, \\ q_x(0,t) = u^{(1)}(t) = 12, & t > 0, \\ q_x(1,t) = v^{(1)}(t) = 6\pi - 8, & t > 0. \end{cases} \tag{3.3.16}$$

The dispersive nature of the LS equation is captured by the SD-UTM solution (3.3.15) in the three (x_n, t)-plots of Figure 3.3.4, while its first-order accuracy is presented in Figure 3.3.4d.

3.4 Computational Comparisons

For each of the previous numerical examples, we compared the performance of the SD-UTM solutions to standard finite-difference schemes as $h \to 0$ for a fixed time step. In this section, we compare all numerical methods in terms of wall-clock time needed to achieve a target accuracy. We use the IBVP (3.3.9) as an example, which poses the challenge of accurately capturing dispersive behavior as T increases. Note that the initial and boundary conditions here are not first-order compatible, *i.e.*, $\phi''(0) \neq 0 \neq \phi''(1)$.

For all methods, we impose a mild target accuracy $\|q(x_n, T) - q_n(T)\|_\infty \approx E$ with $E = 10^{-2}$ for $10^{-2} \leq T \leq 10^1$. First, we determine the number of spatial grid points N_x needed for the SD-UTM solution to reach the target accuracy. Using this spatial grid, we determine the number of time steps N_t needed for each finite-difference solution to reach a similar accuracy. We use the SD-UTM series representation (3.3.8) with $f_0(W_\ell, T) = 0$ and $g_0(W_\ell, T) = 2\big(1 - e^{-W_\ell T}\big)/W_\ell$, while the finite difference solutions are set up in a standard method-of-lines approach with sparse tridiagonal linear systems that are efficiently solved. For every T, Figure 3.4.1 presents N_x and N_t together (left panel) and the methods' wall-clock computation times T_C (right panel) when solving the IBVP to the target accuracy E. The simulations were conducted in MATLAB R2021b on an Intel Core i7-8705G processor with 12GB of RAM.

Starting from $T = 10^{-2}$, we stop computing the finite-difference solutions if $T_C > 10^3$ seconds for the most recent T. This threshold roughly translates to 91 million time steps for FE, 4 million time steps for RK4, 11 million time steps for BE, and 2 million time steps for TR, which we deem impractical, and terminate the computations to avoid excessive wall-clock times in trying to reach the final $T = 10$. All methods achieved an accuracy of $E \pm 10^{-4}$ for all successful T. Although the SD-UTM solution itself does not rely on a time-stepping procedure, we must refine the spatial mesh as T increases to remove higher-order dispersive effects (see Section 3.3.1 for the modified PDE). Note that at the finest mesh of 3810 grid points, the computation time is still less than 1 second. In addition, the finite-difference time steps shown in Figure 3.4.1a are abnormal under

practical circumstances. We could re-run these simulations allowing an upper-bound target accuracy of $E + 10^{-3}$ or even $E + 10^{-2}$ to reduce the number of time steps.

3.5 Small-Time Increments

For half-line problems in Section 2.5, we showed how to derive small-time approximate solutions with predetermined accuracy for SD-UTM integral representations. A similar approach is applied for finite-interval SD-UTM integral representations. For the forward-discretized advection equation (2.1.2), we show how to briefly derive these approximate solutions.

To include an arbitrary initial time t_0, we generalize the original IBVP (2.1.1) to

$$\begin{cases} q_t = c\, q_x, & 0 < x < L,\ t > t_0, \\ q(x, t_0) = \phi(x), & 0 < x < L, \\ q(L, t) = v^{(0)}(t), & t > t_0, \end{cases} \tag{3.5.1}$$

where $\phi(x)$ is the output from the previous split-step. Following the procedure in Section 3.1.1, the solution to (3.5.1) is

$$q_n(\tau) = \frac{1}{2\pi} \int_{-\pi/h}^{\pi/h} e^{iknh} e^{-W\tau} \hat{q}(k, t_0)\, dk + \frac{c}{2\pi} \int_{-\pi/h}^{\pi/h} e^{ik(nh-L+h)} e^{-WT} g_0\, dk, \tag{3.5.2}$$

where

$$g_j\,(W, \tau) = \int_0^{\tau} e^{W(t+t_0)} q_{N+1+j}(t + t_0)\, dt, \quad k \in \mathbb{C},$$

after making the substitution $\tau = T - t_0 \ll 1$. We expand (3.5.2) around $\tau = 0$ to obtain a convenient approximation for a split-step method. We do not expand the initial-condition integral term, since the only time dependence is through $e^{-W\tau}$. For this term, we simply follow the steps in Section 3.1.1 to rewrite the integral as a series. The boundary-condition term of (3.5.2) has a more intricate dependence on time. Rewriting this integral into a series and then expanding the time-dependent terms leads to representations unique to the IBVP that generally cannot be addressed (see Remark 3.5.1). First, we expand the integrand and then rewrite each of the resulting expansion terms as finite series. Doing so up to third-order terms, we have

$$q_n(\tau) = e^{-c\tau/h} \sum_{m=0}^{N-n} \left(\frac{c\tau}{h}\right)^m \frac{\phi_{n+m}}{m!} + K_1(n)\tau + K_2(n)\tau^2 + K_3(n)\tau^3 + \mathcal{O}(\tau^4), \tag{3.5.3}$$

where $L = (N+1)h$ and

$$K_1(n) = \frac{c}{2\pi}\int_{-\pi/h}^{\pi/h} e^{ik(n-N)h} v^{(0)}(t_0)\,dk = \frac{cv^{(0)}(t_0)}{h}\delta_{Nn},$$
$$K_2(n) = \frac{c}{4\pi}\int_{-\pi/h}^{\pi/h} e^{ik(n-N)h}\left[\dot{v}^{(0)}(t_0) - Wv^{(0)}(t_0)\right]\,dk,$$
$$K_3(n) = \frac{c}{12\pi}\int_{-\pi/h}^{\pi/h} e^{ik(n-N)h}\left[\ddot{v}^{(0)}(t_0) - W\dot{v}^{(0)}(t_0) + W^2v^{(0)}(t_0)\right]\,dk.$$

The only dependence on k within the integrands of $K_\ell(n)$ for $\ell = 1, 2, \ldots$, are through $e^{ik(n-N)h}$ and powers of $W(k,\tau)$, and we want to rewrite

$$I_m(n) = \int_{-\pi/h}^{\pi/h} e^{ik(n-N)h} W^m\,dk, \quad m = 0, 1, \ldots,$$

as a series in terms of

$$K_\ell(n) = \frac{c}{2\pi\cdot\ell!}\sum_{j=0}^{\ell-1} I_{\ell-1-j}(n)\left.\frac{d^jv^{(0)}(t)}{dt^j}\right|_{t=t_0}.$$

With $z = e^{ikh}$, the dispersion relation for this IBVP gives

$$I_m(n) = \frac{1}{ih}\left(\frac{c}{h}\right)^m \oint_{|z|=1} \frac{(1-z)^m}{z^{N-n+1}}\,dz = \frac{2\pi(-1)^{N-n}}{h(N-n)!}\left(\frac{c}{h}\right)^m \frac{m!}{(m-N+n)!}.$$

Note that $I_m(n)$ is nonzero only for $m+n \geq N$. Substituting into $K_\ell(n)$ yields the small-time approximation (3.5.3), free of integral computations, where

$$K_\ell(n) = \frac{(-1)^{N-n}}{(N-n)!\,\ell!}\sum_{j=0}^{\ell-1}\frac{(-1)^j(\ell-1-j)!}{(\ell-1-j-N+n)!}\left(\frac{c}{h}\right)^{\ell-j}\left.\frac{d^jv^{(0)}(t)}{dt^j}\right|_{t=t_0}.$$

A similar process can be repeated for other IBVPs.

Remark 3.5.1. Although the process of rewriting an SD-UTM integral representation into a series is straightforward, the resulting formulas are specific to the IBVPs and their dispersion relations. To obtain these small-time approximation solutions in general, we must start from the integral representations – not the series.

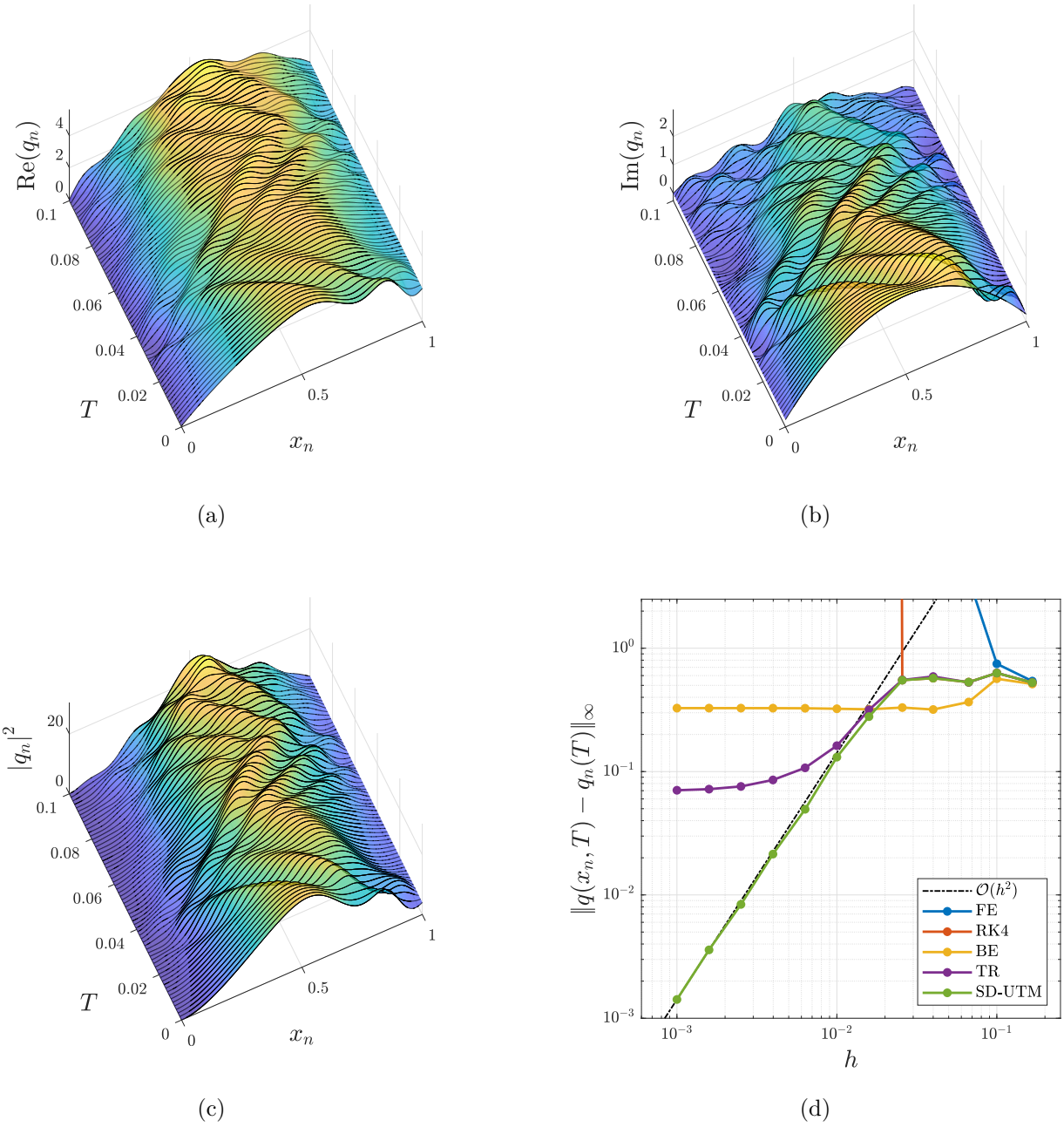

Figure 3.3.3: (a) - (c) Real and imaginary parts and modulus squared of the semi-discrete solution (3.3.8) evaluated at various T for IBVP (3.3.9) with $h = 0.01$. (d) Error plot of the semi-discrete solution (3.3.8) and finite-difference schemes relative to the exact solution as $h \to 0$ with $T = 0.1$ and $\Delta t = 3.90625 \times 10^{-4}$.

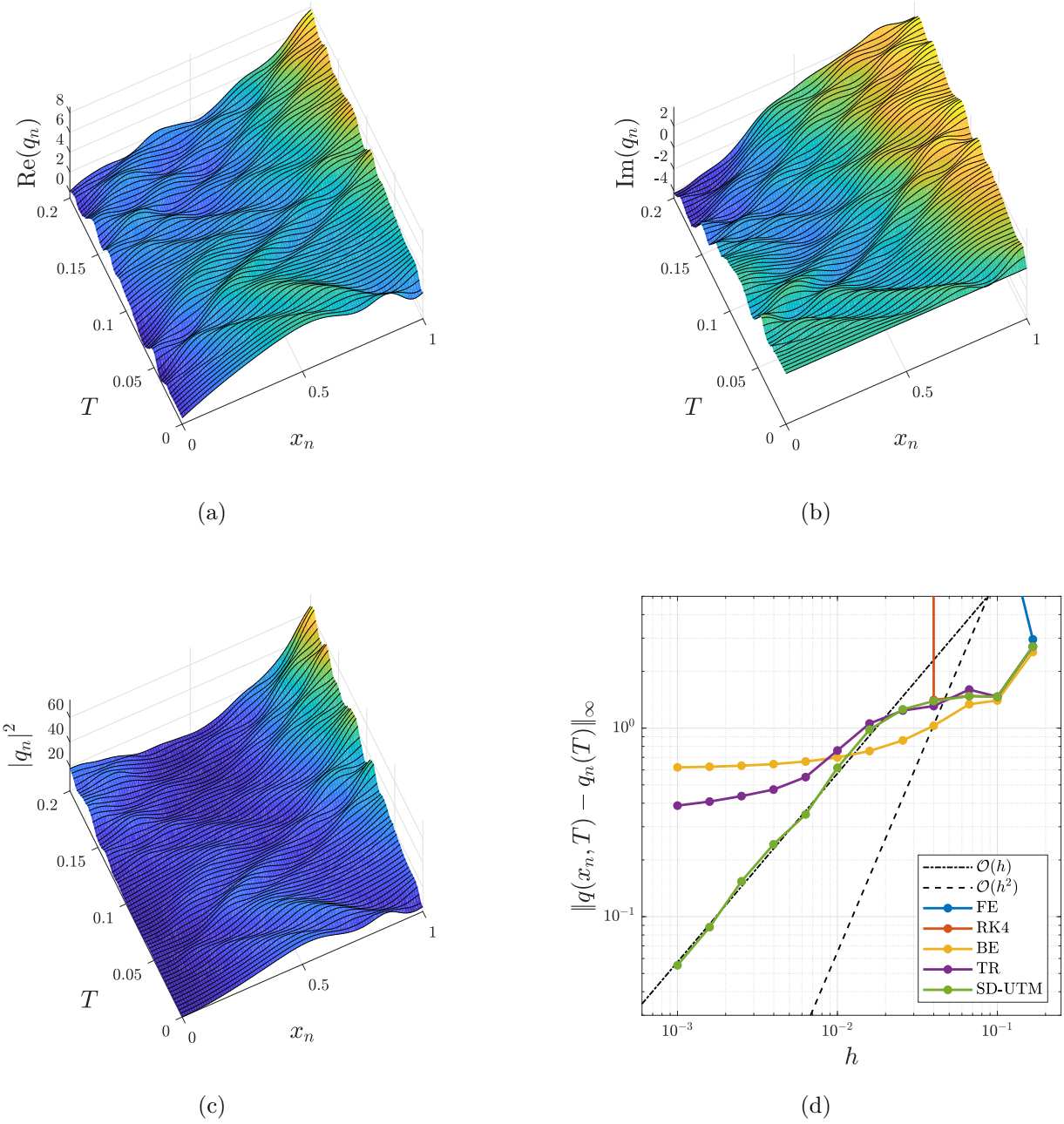

Figure 3.3.4: (a) - (c) Real and imaginary parts and modulus squared of the semi-discrete solution (3.3.15) evaluated at various T for IBVP (3.3.9) with $h = 0.01$. (d) Error plot of the semi-discrete solution (3.3.15) and finite-difference schemes relative to the exact solution as $h \to 0$ with $T = 0.2$ and $\Delta t = 1.5625 \times 10^{-3}$.

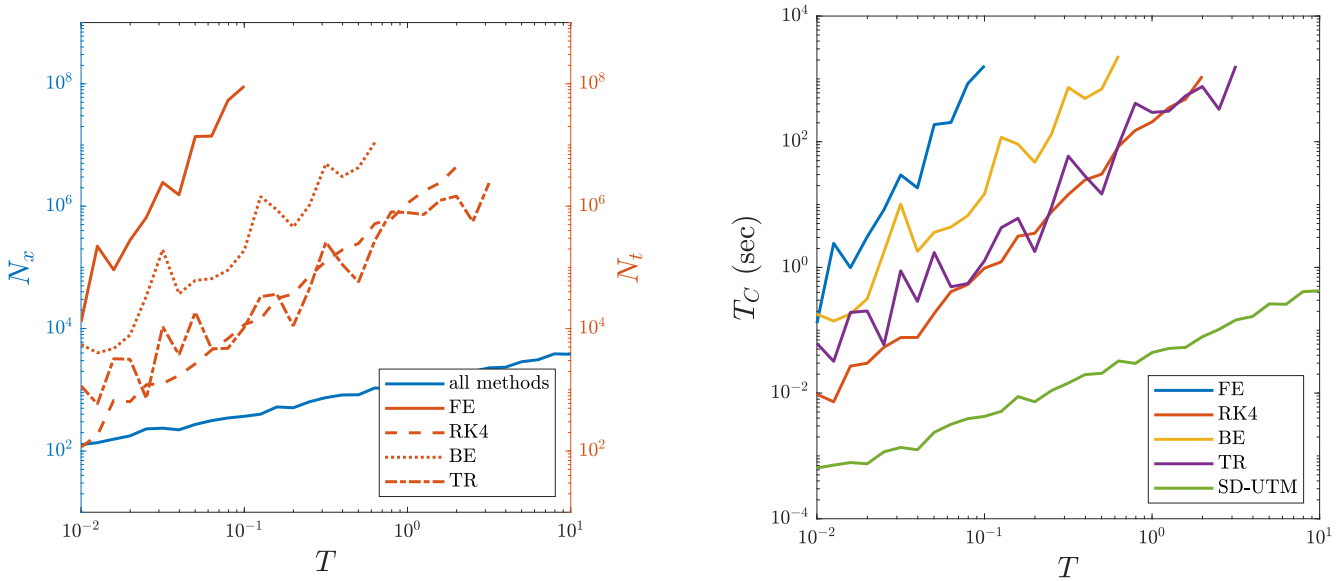

(a) (b)

Figure 3.4.1: (a) The blue curve denotes the number of spatial grid points N_x required for the SD-UTM solution to approximately reach the accuracy $E = 10^{-2}$ when solving the IBVP (3.3.9). Using this information, every finite-difference method uses the same spatial grid for each T to determine how many time-steps N_t are required to reach a similar accuracy as the SD-UTM solution. (b) The wall-clock computation time (averaged over 10 runs to rule out any effects due to background processes) required for each method to solve the IBVP (3.3.9) with the selected N_x and N_t that approximately give an accuracy E.

Chapter 4

THIRD-ORDER PROBLEMS

The Korteweg–de Vries (KdV) equation is commonly given as

$$q_t + 6qq_x + q_{xxx} = 0,$$

such that linearizing around the trivial solution, we obtain the linear KdV equation: $q_t + q_{xxx} = 0$. For the following sections, we will be discretizing

$$q_t = \pm q_{xxx} \tag{4.0.1}$$

in various stencils, depending on the sign of the right-hand side. For the "positive" linear KdV equation $q_t = q_{xxx}$, the half-line problem requires two boundary conditions at $x = 0$, while the "negative" equation $q_t = -q_{xxx}$ requires only one.

This type of third-order problem was first solved using the UTM and its systematic implementation [17], so we next show how the SD-UTM performs for this class of third-order problems on both the half-line and finite interval.

4.1 Half-Line IBVPs

4.1.1 Off-Centered Backward Discretization of $q_t = q_{xxx}$

Consider the half-line IBVP for the "positive" linear KdV equation:

$$\begin{cases} q_t = q_{xxx}, & x > 0,\ t > 0, \\ q(x,0) = \phi(t), & x > 0, \\ q(0,t) = u^{(0)}(t), & t > 0, \\ q_x(0,t) = u^{(1)}(t), & t > 0, \end{cases} \tag{4.1.1}$$

and a first-order accurate, off-centered discretization that leans backward:

$$\dot{q}_n = \frac{1}{h^3}\left(-q_{n-2} + 3q_{n-1} - 3q_n + q_{n+1}\right). \tag{4.1.2}$$

The local relation is found to be

$$\begin{aligned} \partial_t \left(e^{-iknh} e^{Wt} q_n\right) = \frac{1}{h^3}\Delta\Big(& e^{-iknh} e^{Wt} q_{n-2} - 3e^{-iknh} e^{Wt} q_{n-1} + e^{-ik(n-1)h} e^{Wt} q_n \\ & + e^{-ik(n+1)h} e^{Wt} q_{n-1}\Big) \end{aligned} \tag{4.1.3}$$

with dispersion relation

$$W(k) = \frac{1}{h^3}\left(3 - 3e^{-ikh} - e^{ikh} + e^{-2ikh}\right), \tag{4.1.4}$$

and its symmetries

$$\nu_0(k) = k, \tag{4.1.5a}$$

$$\nu_1(k) = \frac{i}{h}\ln\left[\frac{e^{-ikh}\left(3e^{ikh} - 1 + \left[\left(1 - 3e^{ikh}\right)^2 - 4e^{3ikh}\right]^{1/2}\right)}{2}\right], \tag{4.1.5b}$$

$$\nu_2(k) = \frac{i}{h}\ln\left[\frac{e^{-ikh}\left(3e^{ikh} - 1 - \left[\left(1 - 3e^{ikh}\right)^2 - 4e^{3ikh}\right]^{1/2}\right)}{2}\right]. \tag{4.1.5c}$$

Since the half-line problem (4.1.1) has a Dirichlet boundary condition $u^{(0)}(t)$, we know the information at $q(0,t) \equiv q_0(t)$ for all t. From (4.1.3), we determine the global relation by using a summation starting from $n = 1$:

$$\Rightarrow \quad e^{WT}\hat{q}(k,T) - \hat{q}(k,0) - \frac{1}{h^2}\left[-e^{-ikh}f_{-1} + e^{-ikh}\left(3 - e^{-ikh}\right)f_0 - f_1\right] = 0, \quad \mathrm{Im}(k) \le 0. \tag{4.1.6}$$

It follows that the "solution" is written as

$$\begin{aligned} q_n(T) = {} & \frac{1}{2\pi}\int_{-\pi/h}^{\pi/h} e^{iknh}e^{-WT}\hat{q}(k,0)\,dk \\ & + \frac{1}{2\pi}\int_{-\pi/h}^{\pi/h} e^{iknh}e^{-WT}\left[\frac{-e^{-ikh}f_{-1} + e^{-ikh}\left(3 - e^{-ikh}\right)f_0 - f_1}{h^2}\right]dk. \end{aligned} \tag{4.1.7}$$

Based on the $f_j(W,T)$ functions above, we can apply the standard backward, center, or forward discretizations for the Neumann boundary condition $q_x(0,t) = u^{(1)}(t)$ so as to not introduce any further unknown $f_j(W,T)$. Since the main stencil (4.1.2) leans backward, we choose the standard first-order backward discretization:

$$\frac{q_0(t) - q_{-1}(t)}{h} = u^{(1)}(t) \quad \Rightarrow \quad \frac{f_0(W,T) - f_{-1}(W,T)}{h} = U^{(1)}(W,T),$$

after taking time transforms, where

$$U^{(1)}(W,T) = \int_0^T e^{Wt}u^{(1)}(t)\,dt.$$

Now, only $f_1(W,T)$ remains unknown, which can be removed with the given nontrivial symmetries (4.1.5b) - (4.1.5c). First let us determine where the global relation (4.1.6) with the substituted symmetries is valid in the complex k-plane. By defining the branch cut for $z^{1/2}$ on the positive real line (see Remark 2.2.2), Figure 4.1.1a depicts shaded regions where the global relation (4.1.6)

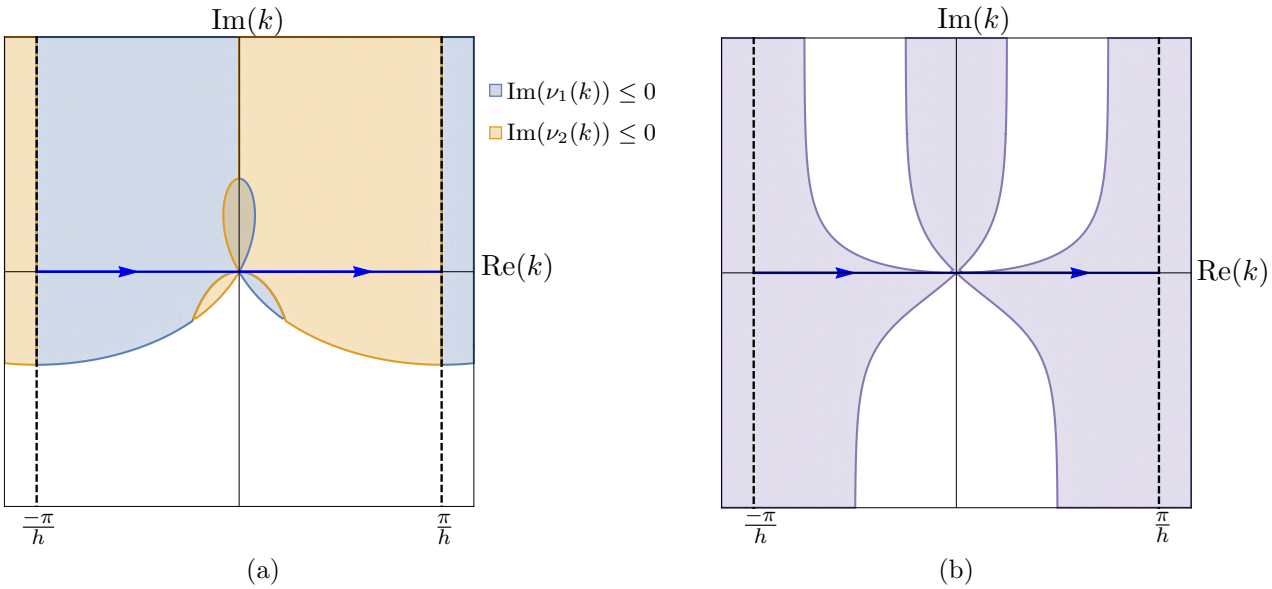

Figure 4.1.1: (a) Valid regions of the global relation (4.1.6) with $k \to \nu_j(k)$. (b) The shaded regions depict where $\mathrm{Re}(W) \leq 0$ and e^{-WT} is bounded with the dispersion relation (4.1.4).

is valid with each of the nontrivial symmetries. Figure 4.1.1a implies that the global relation with either symmetry is not valid across the entire half-plane, such that both symmetries must be used simultaneously to remove one unknown. We see that the global relation with $\nu_1(k)$ is valid for all $\mathrm{Im}(k) \geq 0$ with $-\pi/h \leq \mathrm{Re}(k) \leq 0$ and the global relation with $\nu_2(k)$ is valid for all $\mathrm{Im}(k) \geq 0$ with $0 \leq \mathrm{Re}(k) \leq \pi/h$. Hence, we must split up the integration path of the second term in (4.1.7). With some hindsight, we want these new paths to align with the exponential decay of e^{-WT}, depicted as the shaded regions in Figure 4.1.1b.

We introduce contour paths in Figure 4.1.2a as $P = (P_1 + P_2) + (P_3 + P_4 + P_5) + (P_6 + P_7)$, where $P_{3,4,5}$ outline the middle wedge and the straight-line paths $P_{1,4,7}$ are all at a fixed height $R > 0$ above the real line. By Cauchy's Theorem, it is clear that

$$\frac{1}{2\pi} \int_{\partial P_{3,4,5}} e^{iknh} e^{-WT} \left[\frac{-e^{-ikh} f_{-1} + e^{-ikh} \left(3 - e^{-ikh}\right) f_0 - f_1}{h^2} \right] dk = 0,$$

so that (4.1.7) becomes

$$\begin{aligned} q_n(T) = \frac{1}{2\pi} \int_{-\pi/h}^{\pi/h} e^{iknh} e^{-WT} \hat{q}(k,0)\, dk \\ + \frac{1}{2\pi} \int_{P} e^{iknh} e^{-WT} \left[\frac{-e^{-ikh} f_{-1} + e^{-ikh} \left(3 - e^{-ikh}\right) f_0 - f_1}{h^2} \right] dk, \end{aligned}$$

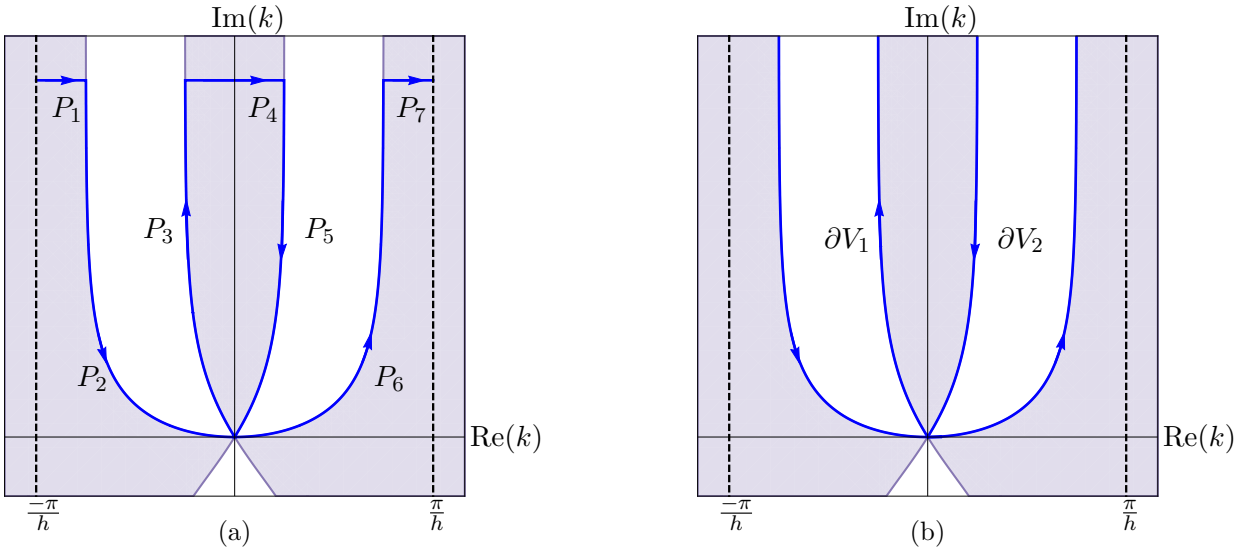

Figure 4.1.2: (a) Integration path P and (b) modified integration paths ∂V_1 and ∂V_2 for (4.1.2).

after deforming the path on the negative real line $k \in [-\pi/h, 0]$ to $P_1 + P_2$ and the other path on the positive real line $k \in [0, \pi/h]$ to $P_6 + P_7$. The vertical integration paths on the boundary of the domain cancel each other by periodicity, but only at the boundary where $\mathrm{Re}\,(\nu_1) = -\mathrm{Re}\,(\nu_2)$ and $\mathrm{Im}\,(\nu_1) = \mathrm{Im}\,(\nu_2)$. Since paths $P_{1,4,7}$ are in regions of exponential decay, we deform them to $i\infty$, such that $R \to \infty$, effectively extending the adjacent vertical paths off to $i\infty$ as well. We now define the integration paths $\partial V_1 = \lim_{R\to\infty}(P_2 + P_3)$ and $\partial V_2 = \lim_{R\to\infty}(P_5 + P_6)$, as depicted in Figure 4.1.2b, where $V = \left\{ k \in \mathbb{C}^+ \,\middle|\, \mathrm{Re}(-W) \le 0 \right\}$ and $\partial V = \partial V_1 \cup \partial V_2$. Thus,

$$\begin{aligned} q_n(T) = \frac{1}{2\pi}\int_{-\pi/h}^{\pi/h} e^{iknh} e^{-WT}\hat{q}(k,0)\,dk \\ + \frac{1}{2\pi}\int_{\partial V_1} e^{iknh} e^{-WT}\left[\frac{-e^{-ikh}f_{-1} + e^{-ikh}\left(3 - e^{-ikh}\right)f_0 - f_1}{h^2}\right] dk \\ + \frac{1}{2\pi}\int_{\partial V_2} e^{iknh} e^{-WT}\left[\frac{-e^{-ikh}f_{-1} + e^{-ikh}\left(3 - e^{-ikh}\right)f_0 - f_1}{h^2}\right] dk. \end{aligned} \tag{4.1.8}$$

Note that the integral path ∂V_1 in (4.1.8) lies in the second quadrant of the complex k plane, while ∂V_2 lies in the first quadrant. Deforming the path allows us to eliminate the unknown $f_1(W,T)$ by use of both nontrivial symmetries. Employing $\nu_1(k)$ into the global relation (4.1.6), we find

$$f_1 = h^2 e^{-2i\nu_1 h}\left[e^{2i\nu_1 h}\hat{q}\,(\nu_1,0) - e^{2i\nu_1 h}e^{WT}\hat{q}\,(\nu_1,T) + \frac{2e^{i\nu_1 h}-1}{h^2}f_0 + \frac{e^{i\nu_1 h}}{h}U^{(1)}\right],$$

valid in the blue region of Figure 4.1.1a. Employing $\nu_2(k)$, we correspondingly find

$$f_1 = h^2 e^{-2i\nu_2 h}\left[e^{2i\nu_2 h}\hat{q}\left(\nu_2,0\right) - e^{2i\nu_2 h}e^{WT}\hat{q}\left(\nu_2,T\right) + \frac{2e^{i\nu_2 h}-1}{h^2}f_0 + \frac{e^{i\nu_2 h}}{h}U^{(1)}\right],$$

now valid in the orange region of Figure 4.1.1a. Respectively substituting into (4.1.8),

$$\begin{aligned} q_n(T) = {} & \frac{1}{2\pi}\int_{-\pi/h}^{\pi/h} e^{iknh}e^{-WT}\hat{q}(k,0)\,dk \\ & + \frac{1}{2\pi}\int_{\partial V_1} e^{iknh}e^{-WT}\left[\frac{2e^{-ikh}-e^{-2ikh}-2e^{-i\nu_1 h}+e^{-2i\nu_1 h}}{h^2}f_0 + \frac{e^{-ikh}-e^{-i\nu_1 h}}{h}U^{(1)} - \hat{q}\left(\nu_1,0\right)\right]dk \\ & + \frac{1}{2\pi}\int_{\partial V_2} e^{iknh}e^{-WT}\left[\frac{2e^{-ikh}-e^{-2ikh}-2e^{-i\nu_2 h}+e^{-2i\nu_2 h}}{h^2}f_0 + \frac{e^{-ikh}-e^{-i\nu_2 h}}{h}U^{(1)} - \hat{q}\left(\nu_2,0\right)\right]dk \\ & + S(n), \end{aligned}$$

with

$$S(n) = \frac{1}{2\pi}\int_{\partial V_1} e^{iknh}\hat{q}\left(\nu_1,T\right)\,dk + \frac{1}{2\pi}\int_{\partial V_2} e^{iknh}\hat{q}\left(\nu_2,T\right)\,dk.$$

Lastly, we want to show that $S(n)$ vanishes for all n and T. We deform $\partial V_{1,2}$ to $D_{1,2}$, respectively, where

$$D_1 = \left\{k\in\mathbb{C}\,\middle|\,\frac{-3\pi}{4h}\le \mathrm{Re}(k)\le\frac{-\pi}{4h}\ \text{ and }\ \mathrm{Im}(k)=R\right\},$$

and

$$D_2 = \left\{k\in\mathbb{C}\,\middle|\,\frac{\pi}{4h}\le \mathrm{Re}(k)\le\frac{3\pi}{4h}\ \text{ and }\ \mathrm{Im}(k)=R\right\},$$

with positive $R\to\infty$ as denoted in Figure 4.1.3, where we recall the definition of cumulative path P from Figure 4.1.2a. Note that the orientation of paths $D_{1,2}$ are reversed with a minus sign and the integrands on paths $\partial V_{1,2}$ are identical up to which symmetry is being used. Hence, the vertical integration paths cancel each other, so that

$$S(n) = \frac{1}{2\pi}\int_{D_1} e^{iknh}\hat{q}\left(\nu_1,T\right)\,dk + \frac{1}{2\pi}\int_{D_2} e^{iknh}\hat{q}\left(\nu_2,T\right)\,dk,$$

with $R\to\infty$. From the global relation (4.1.2) and Figure 4.1.3, we know that as $R\to\infty$, $\hat{q}\left(\nu_1,T\right)$ will exponentially decay for $k\in D_1$ and $\hat{q}\left(\nu_2,T\right)$ will exponentially decay for $k\in D_2$. Therefore, $S(n)=0$ and the final solution to this IBVP is

$$\begin{aligned} q_n(T) = {} & \frac{1}{2\pi}\int_{-\pi/h}^{\pi/h} e^{iknh}e^{-WT}\hat{q}(k,0)\,dk \\ & + \frac{1}{2\pi}\int_{\partial V_1} e^{iknh}e^{-WT}\left[\frac{2e^{-ikh}-e^{-2ikh}-2e^{-i\nu_1 h}+e^{-2i\nu_1 h}}{h^2}f_0 + \frac{e^{-ikh}-e^{-i\nu_1 h}}{h}U^{(1)} - \hat{q}\left(\nu_1,0\right)\right]dk \\ & + \frac{1}{2\pi}\int_{\partial V_2} e^{iknh}e^{-WT}\left[\frac{2e^{-ikh}-e^{-2ikh}-2e^{-i\nu_2 h}+e^{-2i\nu_2 h}}{h^2}f_0 + \frac{e^{-ikh}-e^{-i\nu_2 h}}{h}U^{(1)} - \hat{q}\left(\nu_2,0\right)\right]dk. \end{aligned} \tag{4.1.9}$$

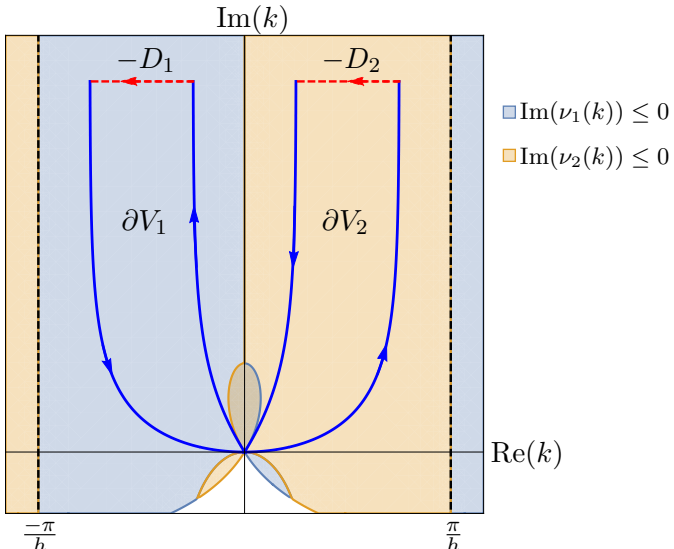

Figure 4.1.3: Deforming $\partial V_{1,2}$ to $D_{1,2}$ with $R \to \infty$.

With anticipation, we constructed $\partial V_{1,2}$ so that in the continuum limit, these integration paths approach those from the continuous problem [17, 28]. The integration paths from the continuous problem must contain paths on the real line, which then requires the integration of highly-oscillatory integrals, since these real-line paths involve no decay from either e^{ikx} nor e^{-WT}. This differs from the semi-discrete problem, where in Figures 4.1.1 – 4.1.2, we deformed all integration paths off the real line, which became $P_{1,2}$ and $P_{6,7}$ for the negative line and positive line paths, respectively. Unlike the continuous problem, we have decay on the real line due to e^{-WT}. For numerical purposes, it is beneficial to leave the real-line paths on the real line, especially since the boundary between the unshaded and shaded region becomes vertical and extends to $+i\infty$, effectively trading a finite integration path for an infinite one.

Figure 4.1.4 depicts possible computation paths $\partial C_{1,2}$ for the integration paths $\partial V_{1,2}$, where the dots are the waypoints implemented into MATLAB's `integral()` function when numerically evaluating the solution above. Note that the top wedge paths are off the boundary of decay/growth due to e^{-WT}, placed closer to the positive imaginary axis. In addition, the paths no longer pass directly through the origin, now slightly curved above it. This modification is legitimate analytically, but if the curve is placed far into the unshaded regions of exponential growth, the integrand may grow uncontrollably and not converge when implemented numerically. The general structures of $\partial C_{1,2}$ persist as $h \to 0$.

Applying the continuous UTM to (4.1.1) gives the global relation

$$\hat{q}(k,0) - e^{\tilde{W}T}\hat{q}(k,T) - \left(-k^2F_0 + ikF_1 + F_2\right) = 0, \quad \mathrm{Im}(k) \leq 0, \tag{4.1.10}$$

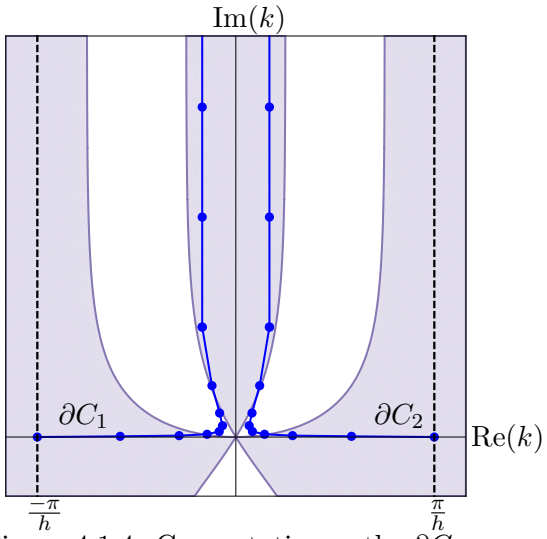

Figure 4.1.4: Computation paths $\partial C_{1,2}$.

and dispersion relation

$$\tilde{W}(k) = ik^3, \tag{4.1.11}$$

with symmetries $\tilde{\nu}_0(k) = k$, $\tilde{\nu}_1(k) = \alpha k$, and $\tilde{\nu}_2(k) = \alpha^2 k$. Figure 4.1.5 depicts the regions where the global relation (4.1.10) with the two nontrivial symmetries is valid. Introducing

$$\Omega = \left\{ k \in \mathbb{C} \,\middle|\, \mathrm{Re}\left(-\tilde{W}\right) > 0 \right\},$$

we define the path $\partial\Omega = \partial\Omega_1 + \partial\Omega_2$ as depicted in Figure 4.1.6. Like in the semi-discrete case, Figure 4.1.5 implies we can employ only $\tilde{\nu}_1(k)$ on $\partial\Omega_1$ and only $\tilde{\nu}_2(k)$ on $\partial\Omega_2$ to remove the same, single unknown $F_2(W,T)$ function. Then, the solution to the linear "positive" KdV half-line problem (4.1.1) is

$$\begin{aligned} q(x,T) = \frac{1}{2\pi}\int_{-\infty}^{\infty} e^{ikx} e^{-\tilde{W}T} \hat{q}(k,0)\, dk \\ - \frac{1}{2\pi}\int_{\partial\Omega_1} e^{ikx} e^{-\tilde{W}T} \left[k^2\left(\alpha^2-1\right)F_0 - ik(\alpha-1)F_1 + \hat{q}(\alpha k,0)\right] dk \\ - \frac{1}{2\pi}\int_{\partial\Omega_2} e^{ikx} e^{-\tilde{W}T} \left[k^2\left(\alpha-1\right)F_0 - ik(\alpha^2-1)F_1 + \hat{q}(\alpha^2 k,0)\right] dk. \end{aligned} \tag{4.1.12}$$

When numerically evaluating the solution above, the paths of $\partial\Omega_{1,2}$ that are on the real line will be the most troublesome to deal with, since the integrand contains no decay from e^{ikx} nor $e^{-\tilde{W}T}$. The top wedge paths, however, can be further deformed toward the imaginary line to exploit the decay from both exponential terms.

We want to show that the semi-discrete solution (4.1.9) converges to the continuous solution (4.1.12) as $h \to 0$. It is straightforward to show that $\lim_{h\to 0} W(k) = ik^3$. For the nontrivial

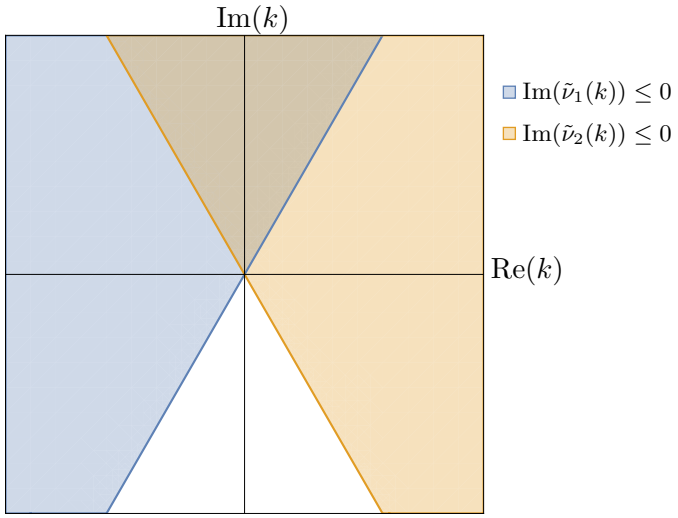

Figure 4.1.5: Regions where the global relation (4.1.10) is valid with $k \to \tilde{\nu}_j(k)$.

symmetries, we take Taylor series expansions about $h = 0$, so that

$$\nu_1(k) = \frac{1}{2} i \left(i + \sqrt{3}\right) k + \frac{k^2}{2\sqrt{3}} h + \mathcal{O}\left(h^2\right), \qquad \nu_2(k) = \frac{1}{2} i \left(i - \sqrt{3}\right) k - \frac{k^2}{2\sqrt{3}} h + \mathcal{O}\left(h^2\right),$$

where $k \in \mathbb{C}$ with $\text{Im}(k) \geq 0$ implies $z^{1/2} = \sqrt{z}$. Thus, taking the continuum limit,

$$\lim_{h \to 0} \nu_j(k) = \alpha^j k,$$

which further implies that

$$\lim_{h \to 0} \hat{q}\left(\nu_j, 0\right) = \hat{q}\left(\alpha^j k, 0\right).$$

Graphically, these limits appear in Figure 4.1.7, depicting $\text{Im}\left(\nu_j\right) \leq 0$ for comparison with Figure 4.1.5.

Similarly, the coefficient for $f_0(W,T)$ on the integration path ∂V_1 gives

$$\frac{2e^{-ikh} - e^{-2ikh} - 2e^{-i\nu_1 h} + e^{-2i\nu_1 h}}{h^2} = \frac{1}{2} k^2 \left(3 + i\sqrt{3}\right) - \frac{k^3\left(\sqrt{3} - 3i\right)}{6} h + \mathcal{O}\left(h^2\right).$$

Hence,

$$\lim_{h \to 0} \frac{2e^{-ikh} - e^{-2ikh} - 2e^{-i\nu_1 h} + e^{-2i\nu_1 h}}{h^2} = -\left(\alpha^2 - 1\right),$$

the coefficient of $F_0(W,T)$ on $\partial\Omega_1$, where $-\left(\alpha^2 - 1\right) = \left(3 + i\sqrt{3}\right)/2$ and $\lim_{h \to 0} f_0(W,T) = F_0(W,T)$. In the same fashion, we can show that the coefficient for $U^{(1)}(W,T)$ on ∂V_1 converges to the coefficient of $F_1(W,T)$ on $\partial\Omega_1$. We follow similar steps to show that the second integral of (4.1.9) converges to the second integral of (4.1.12).

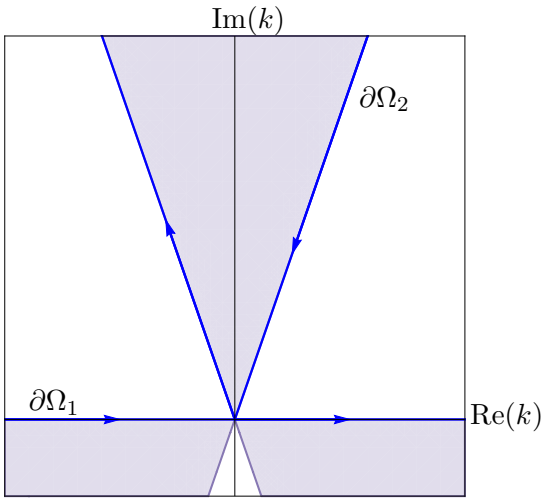

Figure 4.1.6: The shaded regions depict where $\mathrm{Re}(\tilde{W}) \leq 0$ and $e^{-\tilde{W}T}$ is bounded with the dispersion relation (4.1.11).

Remark 4.1.1. Note that if $k \in \mathbb{C}$ with $\mathrm{Im}(k) \leq 0$, then our branch cut implies

$$\lim_{h\to 0} \nu_1(k) = \lim_{h\to 0} \left[\frac{1}{2} i \left(i - \sqrt{3}\right) k - \frac{k^2}{2\sqrt{3}} h + \mathcal{O}\left(h^2\right)\right] = \alpha^2 k,$$
$$\lim_{h\to 0} \nu_2(k) = \lim_{h\to 0} \left[\frac{1}{2} i \left(i + \sqrt{3}\right) k + \frac{k^2}{2\sqrt{3}} h + \mathcal{O}\left(h^2\right)\right] = \alpha k.$$

This is also seen in Figure 4.1.7. However, for the half-line problem and eventually the finite-interval problem, this discrepancy is not an issue.

Remark 4.1.2. What if we had chosen a discretization other than the backward-leaning stencil (4.1.2)? Another option that would give us the same number of total symmetries is the off-centered discretization that leans forward:

$$\dot{q}_n = \frac{1}{h^3}\left(-q_{n-1} + 3q_n - 3q_{n+1} + q_{n+2}\right),$$

the same one we will use for the "negative" linear KdV equation $q_t = -q_{xxx}$ (see Section 4.1.2). Briefly, the dispersion relation is $W(k) = \left(e^{-ikh} - 3 + 3e^{ikh} - e^{2ikh}\right)/h^3$, where Figure 4.1.8 depicts the shaded regions of decay due to e^{-WT}. Note that the real line is unshaded and a path here cannot be deformed without containing a path in a region of exponential growth, *i.e.,* whatever solution we obtain will contain integrands that grow uncontrollably for large $k \in \mathbb{R}$ and any given h – just like the time-reversed heat equation (see Appendix B), even though $\lim_{h\to 0} W(k) = ik^3$. Therefore, we will refer to the leaning-backward discretization (4.1.2) as the *natural* discretization for this IBVP.

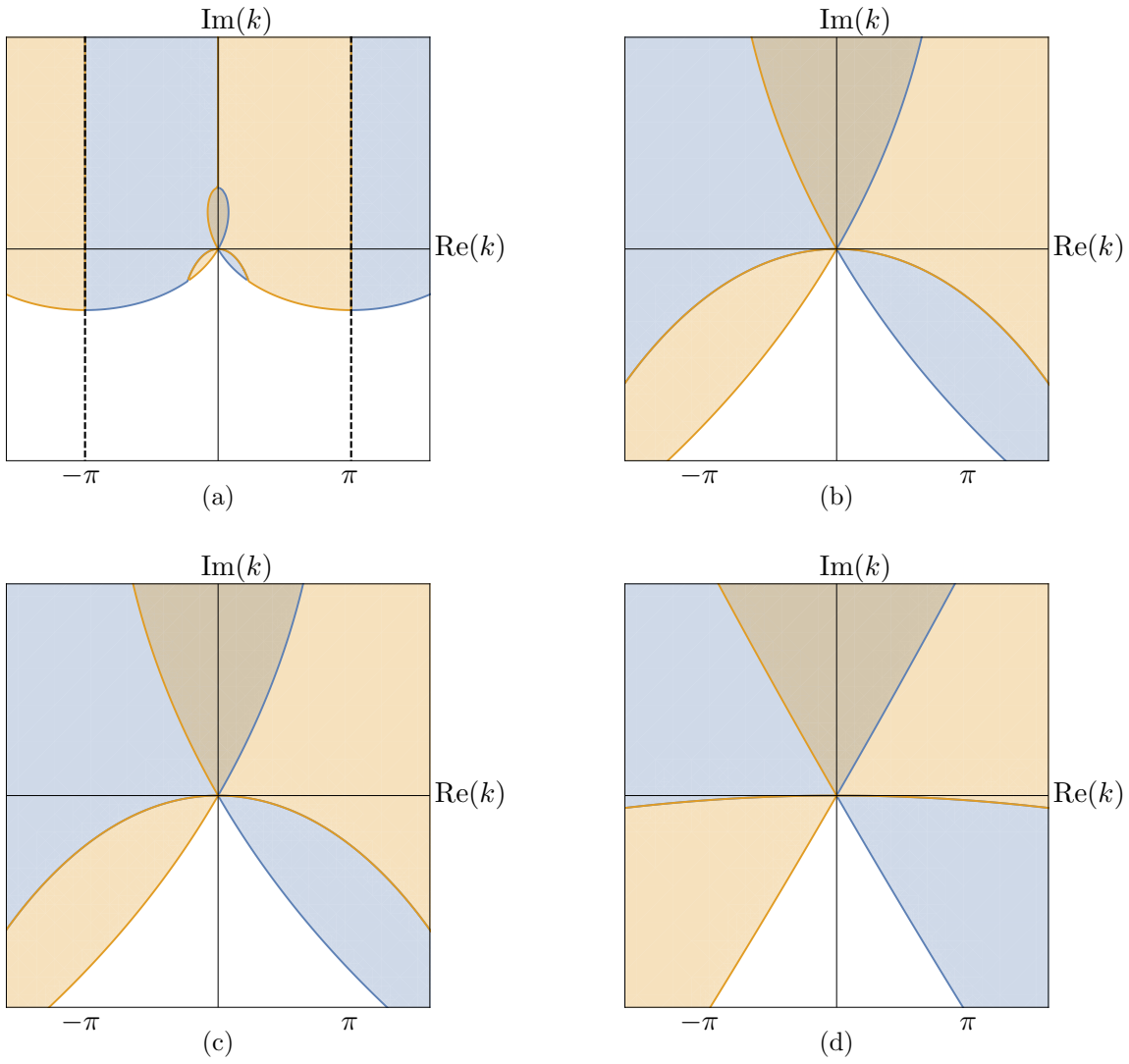

Figure 4.1.7: $\mathrm{Im}\,(\nu_j) \leq 0$ for symmetries (4.1.5b) and (4.1.5c) in the continuum limit (see Figures 4.1.1a and 4.1.5).

4.1.2 Off-Centered Forward Discretization of $q_t = -q_{xxx}$

We next study the "negative" linear KdV equation on the half-line:

$$\begin{cases} q_t = -q_{xxx}, & x > 0,\ t > 0, \\ q(x,0) = \phi(t), & x > 0, \\ q(0,t) = u^{(0)}(t), & t > 0. \end{cases} \tag{4.1.13}$$

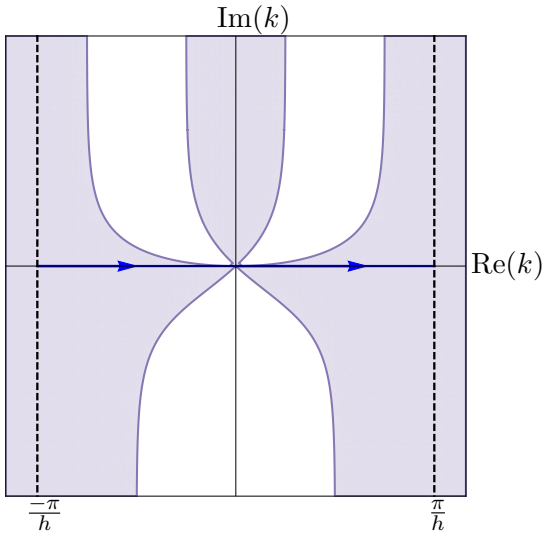

Figure 4.1.8: The shaded regions depict where $\mathrm{Re}(W) \leq 0$ and e^{-WT} is bounded with the dispersion relation from the forward-leaning discretization for $q_t = q_{xxx}$.

Applying a first-order accurate, off-centered discretization to $q_t = -q_{xxx}$ that leans forward gives

$$\dot{q}_n = \frac{-1}{h^3}\left(-q_{n-1} + 3q_n - 3q_{n+1} + q_{n+2}\right). \tag{4.1.14}$$

The local relation is found to be

$$\begin{aligned}\partial_t\left(e^{-iknh}e^{Wt}q_n\right) = \frac{-1}{h^3}\Delta\Big(&e^{-iknh}e^{Wt}q_{n-1} - 3e^{-ik(n-1)h}e^{Wt}q_n + e^{-ik(n-1)h}e^{Wt}q_{n+1} \\ &+ e^{-ik(n-2)h}e^{Wt}q_n\Big),\end{aligned} \tag{4.1.15}$$

with dispersion relation

$$W(k) = \frac{-1}{h^3}\left(-3 + e^{-ikh} + 3e^{ikh} - e^{2ikh}\right). \tag{4.1.16}$$

From (4.1.15), we determine the global relation as

$$e^{WT}\hat{q}(k,T) - \hat{q}(k,0) + \frac{1}{h^2}\left[-e^{-ikh}f_0 + \left(3 - e^{ikh}\right)f_1 - f_2\right] = 0, \quad \mathrm{Im}(k) \leq 0, \tag{4.1.17}$$

Note that the sum began at $n = 1$ instead of $n = 0$, because we have the known Dirichlet boundary condition at $x = 0$, *i.e.,* at $n = 0$. It follows that

$$\begin{aligned}q_n(T) = &\frac{1}{2\pi}\int_{-\pi/h}^{\pi/h} e^{iknh}e^{-WT}\hat{q}(k,0)\,dk \\ &- \frac{1}{2\pi}\int_{-\pi/h}^{\pi/h} e^{iknh}e^{-WT}\left[\frac{-e^{-ikh}f_0 + \left(3 - e^{ikh}\right)f_1 - f_2}{h^2}\right]dk.\end{aligned} \tag{4.1.18}$$

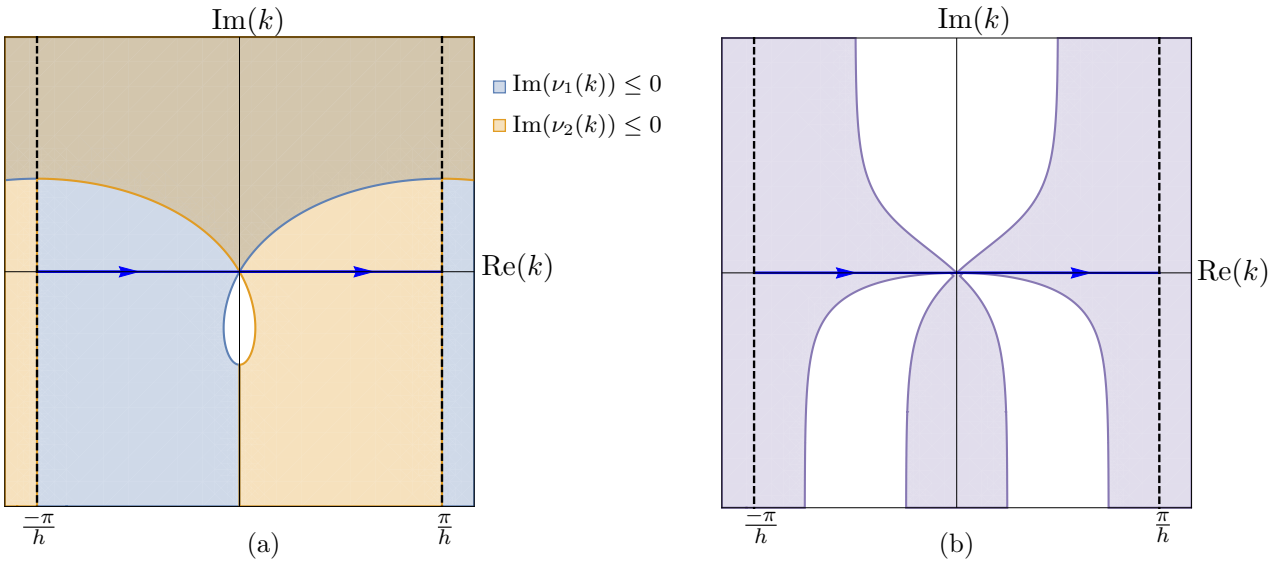

Figure 4.1.9: (a) Valid regions of the global relation (4.1.17) with $k \to \nu_j(k)$. (b) The shaded regions depict where $\mathrm{Re}(W) \leq 0$ and e^{-WT} is bounded with the dispersion relation (4.1.16).

Since we only have the Dirichlet boundary condition $u^{(0)}(t)$, we need to eliminate dependence from $f_1(W,T)$ and $f_2(W,T)$. To determine the symmetries, we solve $W(\nu) = W(k)$ for $\nu(k)$ and find

$$\nu_0(k) = k, \tag{4.1.19a}$$

$$\nu_1(k) = \frac{i}{h} \ln \left[\frac{3e^{ikh} - e^{2ikh} - \left(e^{ikh} - 1\right)\left(e^{2ikh} - 4e^{ikh}\right)^{1/2}}{2} \right], \tag{4.1.19b}$$

$$\nu_2(k) = \frac{i}{h} \ln \left[\frac{3e^{ikh} - e^{2ikh} + \left(e^{ikh} - 1\right)\left(e^{2ikh} - 4e^{ikh}\right)^{1/2}}{2} \right]. \tag{4.1.19c}$$

Like with the symmetries of the discretization (4.1.2) for $q_t = +q_{xxx}$, we relocate the branch cut of $z^{1/2}$ onto the positive real line. We introduce Figure 4.1.9a, depicting shaded regions where $\mathrm{Im}\,(\nu_j) \leq 0$ holds for $j = 1, 2$. In order to remove two unknowns, we require the use of both symmetries, such that the second integral term of (4.1.18) must be deformed off the real line. With some hindsight when taking the continuum limit, we want these new paths to align with the exponential decay of e^{-WT}, depicted as the shaded regions in Figure 4.1.9b. Similar to the stencil (4.1.2) for the "positive" linear KdV IBVP (4.1.1), we define integration paths $P = P_1 + P_2 + P_3$, shown in Figure 4.1.10, where the horizontal paths $P_{1,3}$ are at some fixed height $R > 0$ above the real line. Through periodicity, we deform the second integral of (4.1.18) to P, so that

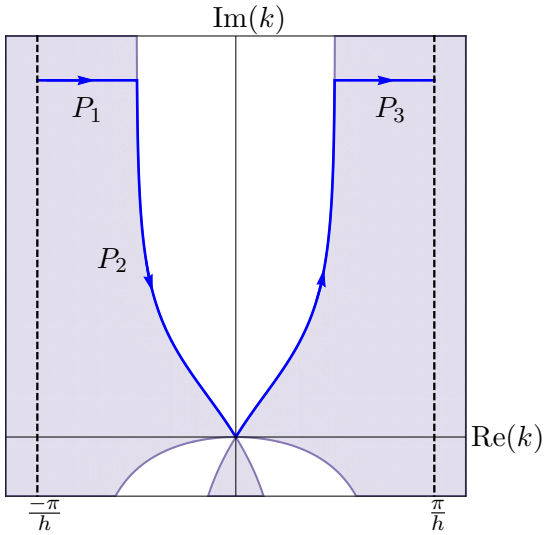

Figure 4.1.10: Integration path P for (4.1.14).

$$\begin{aligned} q_n(T) = &\frac{1}{2\pi}\int_{-\pi/h}^{\pi/h} e^{iknh}e^{-WT}\hat{q}(k,0)\,dk \\ &- \frac{1}{2\pi}\int_{P} e^{iknh}e^{-WT}\left[\frac{-e^{-ikh}f_0 + \left(3-e^{ikh}\right)f_1 - f_2}{h^2}\right]dk. \end{aligned} \tag{4.1.20}$$

Since $P_{1,3}$ are in regions of exponential decay, we can take $R \to \infty$, so that $P_{1,3}$ vanish and the endpoints of P_2 are extended to $+i\infty$, with $\partial V = \lim_{R\to\infty} P_2$, as outlined in Figure 4.1.11, where $V = \left\{k \in \mathbb{C}^+ \,\middle|\, \mathrm{Re}(-W) \le 0\right\}$. Hence, "solution" (4.1.20) becomes

$$\begin{aligned} q_n(T) = &\frac{1}{2\pi}\int_{-\pi/h}^{\pi/h} e^{iknh}e^{-WT}\hat{q}(k,0)\,dk \\ &- \frac{1}{2\pi}\int_{\partial V} e^{iknh}e^{-WT}\left[\frac{-e^{-ikh}f_0 + \left(3-e^{ikh}\right)f_1 - f_2}{h^2}\right]dk. \end{aligned} \tag{4.1.21}$$

Of course, taking $R \to \infty$ effectively traded three finite paths $P_{1,2,3}$ for one infinite path ∂V.

With both symmetries valid on the integration path ∂V, we use the global relation (4.1.17) with $k \to \nu_1(k)$ and $k \to \nu_2(k)$:

$$\begin{cases} e^{WT}\hat{q}\left(\nu_1,T\right) - \hat{q}\left(\nu_1,0\right) + \dfrac{1}{h^2}\left[-e^{-i\nu_1 h}f_0 + \left(3-e^{i\nu_1 h}\right)f_1 - f_2\right] = 0, \\ e^{WT}\hat{q}\left(\nu_2,T\right) - \hat{q}\left(\nu_2,0\right) + \dfrac{1}{h^2}\left[-e^{-i\nu_2 h}f_0 + \left(3-e^{i\nu_2 h}\right)f_1 - f_2\right] = 0, \end{cases} \tag{4.1.22}$$

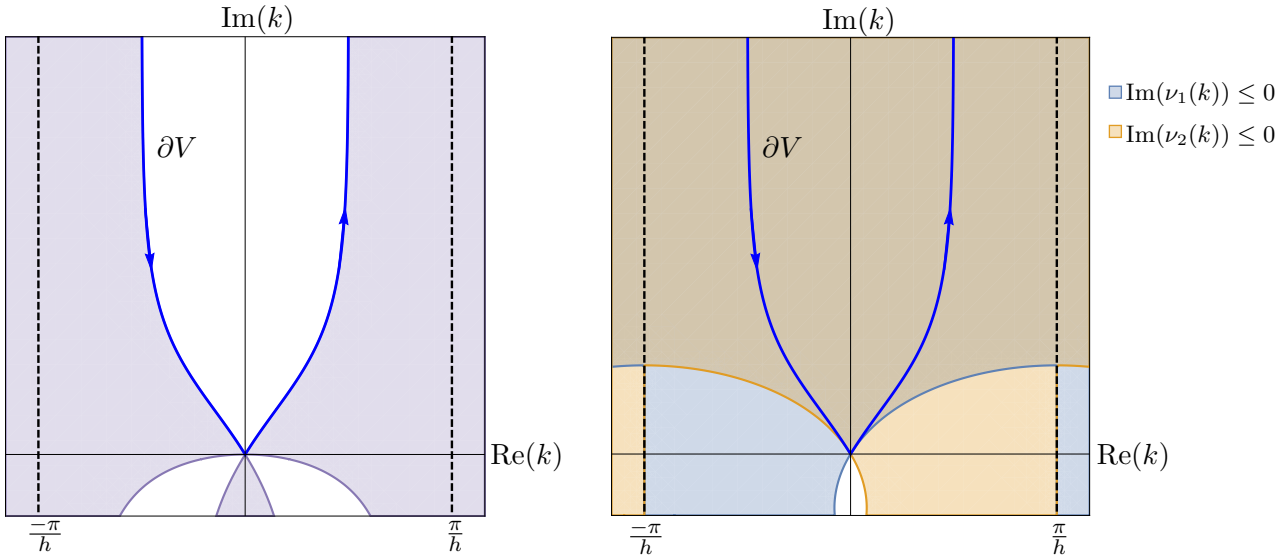

Figure 4.1.11: Integration path ∂V.

to solve for the two unknowns $f_{-1}(W,T)$ and $f_1(W,T)$. After some algebra, (4.1.21) becomes

$$\begin{aligned} q_n(T) = {} & \frac{1}{2\pi}\int_{-\pi/h}^{\pi/h} e^{iknh}e^{-WT}\hat{q}(k,0)\,dk \\ & - \frac{1}{2\pi}\int_{\partial V} e^{iknh}e^{-WT}\left[\frac{\left(e^{ikh}-e^{i\nu_2 h}\right)\hat{q}(\nu_1,0)+\left(e^{i\nu_1 h}-e^{ikh}\right)\hat{q}(\nu_2,0)}{e^{i\nu_1 h}-e^{i\nu_2 h}}\right]dk \\ & + \frac{1}{2\pi}\int_{\partial V} e^{iknh}e^{-WT}\left[\frac{e^{-ikh-i(\nu_1+\nu_2)h}\left(e^{ikh}-e^{i\nu_1 h}\right)\left(e^{ikh}-e^{i\nu_2 h}\right)}{h^2}f_0\right]dk \;-\; S(n), \end{aligned} \tag{4.1.23}$$

with

$$S(n) = \frac{1}{2\pi}\int_{\partial V} e^{iknh}\left[\frac{\left(e^{i\nu_2 h}-e^{ikh}\right)\hat{q}(\nu_1,T)+\left(e^{ikh}-e^{i\nu_1 h}\right)\hat{q}(\nu_2,T)}{e^{i\nu_1 h}-e^{i\nu_2 h}}\right]dk,$$

or substituting in $\nu_1(k)$ and $\nu_2(k)$,

$$\begin{aligned} q_n(T) = {} & \frac{1}{2\pi}\int_{-\pi/h}^{\pi/h} e^{iknh}e^{-WT}\hat{q}(k,0)\,dk \\ & - \frac{1}{2\pi}\int_{\partial V} e^{iknh}e^{-WT}\left[\frac{\left(\sqrt{e^{ikh}-4}+3e^{ikh/2}\right)\hat{q}(\nu_1,0)+\left(\sqrt{e^{ikh}-4}-3e^{ikh/2}\right)\hat{q}(\nu_2,0)}{2\sqrt{e^{ikh}-4}}\right]dk \\ & + \frac{1}{2\pi}\int_{\partial V} e^{iknh}e^{-WT}\left[\frac{e^{-ikh}-3e^{ikh}+2e^{2ikh}}{h^2}f_0\right]dk \;+\; S(n), \end{aligned} \tag{4.1.24}$$

with

$$S(n) = \frac{1}{2\pi}\int_{\partial V} e^{iknh}\left[\frac{\left(3e^{ikh/2}+\sqrt{e^{ikh}-4}\right)\hat{q}(\nu_1,T)-\left(3e^{ikh/2}-\sqrt{e^{ikh}-4}\right)\hat{q}(\nu_2,T)}{2\sqrt{e^{ikh}-4}}\right]dk.$$

Note that we have already made the correct branch cut choice in "solution" (4.1.24).

From (4.1.23), it would appear that the second integral and $S(n)$ terms have poles at

$$k_\alpha^{(1)} = \frac{-4\pi\alpha}{h}, \qquad k_\beta^{(2)} = \frac{-4\pi\beta - i\ln(4)}{h}, \qquad k_\gamma^{(3)} = \frac{-4\pi\gamma - 2\pi}{h}, \qquad k_\delta^{(4)} = \frac{-4\pi\delta - 2\pi - i\ln(4)}{h}$$

for $\alpha, \beta, \gamma, \delta \in \mathbb{Z}$. In fact, all of these singularities are removable. We could show this by taking limits of the integrands in question, but due to their intricacies, it is beneficial to instead determine their Taylor-series expansions about these singularities after making substitutions of $\hat{q}\left(\nu_1, 0\right)$, $\hat{q}\left(\nu_2, 0\right)$, $\hat{q}\left(\nu_1, T\right)$, and $\hat{q}\left(\nu_2, T\right)$. Since we only care about the plane $(\mathrm{Re}(k), \mathrm{Im}(k)) = [-\pi/h, \pi/h] \times (-\infty, \infty)$, the singularities of interest are $k_0^{(1)} = 0$ and $k_0^{(2)} = -i\ln(4)/h$. After substituting definitions of $\hat{q}\left(\nu_j, 0\right)$, the integrand in the second integral term expanded about $k = k_0^{(1)}$ becomes

$$\frac{\left(e^{ikh} - e^{i\nu_2 h}\right) e^{-i\nu_1 mh} + \left(e^{i\nu_1 h} - e^{ikh}\right) e^{-i\nu_2 mh}}{e^{i\nu_1 h} - e^{i\nu_2 h}} = 1 - ikmh + \mathcal{O}\left(k^2\right).$$

It is clear that the limit exists for this integrand as $k \to k_0^{(1)}$, such that $k_0^{(1)}$ is a removable singularity. Similarly for $k_0^{(2)}$, the same integrand expands to

$$\begin{aligned}
&\frac{\left(e^{ikh} - e^{i\nu_2 h}\right) e^{-i\nu_1 mh} + \left(e^{i\nu_1 h} - e^{ikh}\right) e^{-i\nu_2 mh}}{e^{i\nu_1 h} - e^{i\nu_2 h}} \\
&\quad = (-2)^m(1+9m) \;+\; ih(-1)^m 2^{m-1} m\left[9m(3m+2)+7\right]\left(k + \frac{i\ln(4)}{h}\right) + \mathcal{O}\left[\left(k + \frac{i\ln(4)}{h}\right)^2\right].
\end{aligned}$$

Taking the limit as $k \to k_0^{(2)}$, we see that $k_0^{(2)}$ is also a removable singularity. Likewise, one can show that the singularities are removable for the $S(n)$ integrands.

From (4.1.24), it would also appear that the second integral and $S(n)$ terms have poles at

$$k_b = \frac{2\pi b - i\ln(4)}{h}$$

for $b \in \mathbb{Z}$ or setting $b = 0$, at

$$k_0 = \frac{-i\ln(4)}{h} = k_0^{(2)}.$$

Following the same procedure as above, the integrand in the second integral term expanded about $k = k_0$ has the same expansion from (4.1.23) about $k = k_0^{(2)}$:

$$\begin{aligned}
&\frac{\left(\sqrt{e^{ikh} - 4} + 3e^{ikh/2}\right)\hat{q}(\nu_1, 0) + \left(\sqrt{e^{ikh} - 4} - 3e^{ikh/2}\right)\hat{q}(\nu_2, 0)}{2\sqrt{e^{ikh} - 4}} \\
&\quad = (-2)^m(1+9m) \;+\; ih(-1)^m 2^{m-1} m\left[9m(3m+2)+7\right]\left(k + \frac{i\ln(4)}{h}\right) + \mathcal{O}\left[\left(k + \frac{i\ln(4)}{h}\right)^2\right].
\end{aligned}$$

Thus, both (4.1.23) and (4.1.24) have removable singularities in their integrands. For simplicity, we proceed solely with (4.1.24), although the next steps could be repeated with (4.1.23).

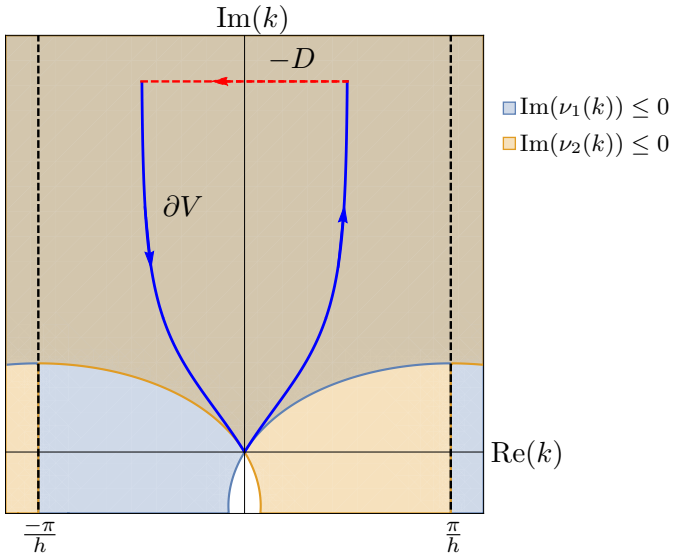

Figure 4.1.12: Deforming ∂V to D with $R \to \infty$.

To determine the contribution from $S(n)$, we again substitute the definition of the transforms for $\hat{q}(\nu_1, T)$ and $\hat{q}(\nu_2, T)$, so that we have

$$S(n) = \frac{h}{2\pi} \sum_{m=1}^{\infty} q_m(T) I(n, m),$$

with

$$I(n,m) = \int_{\partial V} e^{iknh} \left[\frac{\left(3e^{ikh/2} + \sqrt{e^{ikh} - 4}\right) e^{-i\nu_1 mh} - \left(3e^{ikh/2} - \sqrt{e^{ikh} - 4}\right) e^{-i\nu_2 mh}}{2\sqrt{e^{ikh} - 4}} \right] dk.$$

To remove the unwanted integral terms, we deform ∂V to D, where

$$D = \left\{ k \in \mathbb{C} \,\middle|\, \frac{-\pi}{2h} \leq \mathrm{Re}(k) \leq \frac{\pi}{2h} \text{ and } \mathrm{Im}(k) = R \right\},$$

with positive $R \to \infty$ as denoted in Figure 4.1.12. The orientation of path D is reversed with a minus sign. Of course, the global relations (4.1.22) are still valid on D. Hence, due to analyticity and with $R \to \infty$, we can write

$$I(n,m) = \int_{D} e^{iknh} \left[\frac{\left(3e^{ikh/2} + \sqrt{e^{ikh} - 4}\right) e^{-i\nu_1 mh} - \left(3e^{ikh/2} - \sqrt{e^{ikh} - 4}\right) e^{-i\nu_2 mh}}{2\sqrt{e^{ikh} - 4}} \right] dk.$$

For all nonzero n and m, we take $R \to \infty$, so that

$$I(n,m) = \int_D \frac{e^{iknh}}{2^m} \left[\frac{\left(3e^{ikh/2} + \sqrt{e^{ikh}-4}\right)\left[3e^{ikh} - e^{2ikh} - e^{\frac{ikh}{2}}\left(e^{ikh}-1\right)\sqrt{e^{ikh}-4}\right]^m}{2\sqrt{e^{ikh}-4}} \right.$$
$$\left. - \frac{\left(3e^{ikh/2} - \sqrt{e^{ikh}-4}\right)\left[3e^{ikh} - e^{2ikh} + e^{\frac{ikh}{2}}\left(e^{ikh}-1\right)\sqrt{e^{ikh}-4}\right]^m}{2\sqrt{e^{ikh}-4}} \right] dk$$
$$\sim \int_D \frac{e^{iknh}}{2^m} \left[\frac{\left(3e^{ikh/2} + 2i\right)\left[3e^{ikh} - e^{2ikh} + 2ie^{\frac{ikh}{2}}\right]^m}{4i} - \frac{\left(3e^{ikh/2} - 2i\right)\left[3e^{ikh} - e^{2ikh} - 2ie^{\frac{ikh}{2}}\right]^m}{4i} \right] dk$$
$$\sim 0,$$

since all the exponentials decay. Therefore, $S(n) = 0$ for all $n = 1, 2, 3, \ldots$ and (4.1.24) becomes

$$\begin{aligned} q_n(T) = & \frac{1}{2\pi}\int_{-\pi/h}^{\pi/h} e^{iknh}e^{-WT}\hat{q}(k,0)\,dk \\ & - \frac{1}{2\pi}\int_{\partial V} e^{iknh}e^{-WT}\left[\frac{\left(\sqrt{e^{ikh}-4} + 3e^{ikh/2}\right)\hat{q}(\nu_1,0) + \left(\sqrt{e^{ikh}-4} - 3e^{ikh/2}\right)\hat{q}(\nu_2,0)}{2\sqrt{e^{ikh}-4}}\right] dk \\ & + \frac{1}{2\pi}\int_{\partial V} e^{iknh}e^{-WT}\left[\frac{e^{-ikh} - 3e^{ikh} + 2e^{2ikh}}{h^2} f_0\right] dk. \end{aligned} \tag{4.1.25}$$

Note that numerically evaluating these integrals might be troublesome as $h \to 0$, because as shown in the left plot of Figure 4.1.11, ∂V is along the region satisfying $\mathrm{Re}(-W) = 0$, such that there is no exponential decay due to e^{-WT}. Integrating along this path, for large $|k|$, could be problematic as any machine error introduced could place the integration path into the unshaded regions of exponential growth, allowing the integrand to grow uncontrollably in magnitude. Thus, we must modify the analytical integration path ∂V to a computation path ∂C, depicted in Figure 4.1.13. These paths are numerically better suited when evaluating the second integral term of (4.1.25), where ∂C continues to be within both regions of validity for the global relations with $\nu_1(k)$ and $\nu_2(k)$. Note that the visible points in Figure 4.1.13 are the complex waypoints implemented into MATLAB's `integral()` function. The general structure of ∂C persists as $h \to 0$.

Applying the continuous UTM to IBVP (4.1.13) gives the dispersion relation $\tilde{W}(k) = -ik^3$ and solution

$$\begin{aligned} q(x,T) = & \frac{1}{2\pi}\int_{-\infty}^{\infty} e^{ikx}e^{-\tilde{W}T}\hat{q}(k,0)\,dk \\ & - \frac{1}{2\pi}\int_{\partial\Omega} e^{ikx}e^{-\tilde{W}T}\left[3k^2F_0 - \alpha\hat{q}(\alpha k,0) - \alpha^2\hat{q}(\alpha^2 k,0)\right] dk, \end{aligned} \tag{4.1.26}$$

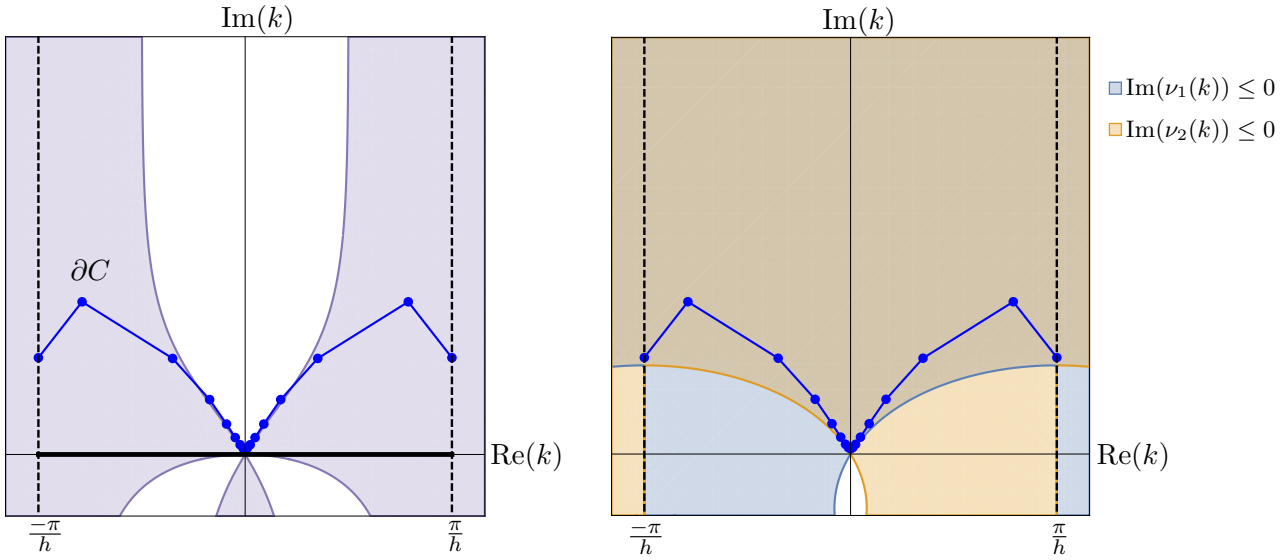

Figure 4.1.13: Computation path ∂C.

where $\Omega = \left\{ k \in \mathbb{C} \,\middle|\, \mathrm{Re}\left(-\tilde{W}\right) > 0 \right\}$.

We now show that the continuum limit of the SD-UTM solution (4.1.25) converges to (4.1.26). Following similar steps from the previous section, we Taylor expand the nontrivial symmetries with the appropriate choice of branch cut for $z^{1/2}$ on the positive real line and take the continuum limit:

$$\nu_1(k) = \frac{i}{2}\left(i+\sqrt{3}\right)k - \frac{k^2}{2\sqrt{3}}h + \mathcal{O}\left(h^2\right), \qquad \nu_2(k) = \frac{i}{2}\left(i-\sqrt{3}\right)k + \frac{k^2}{2\sqrt{3}}h + \mathcal{O}\left(h^2\right),$$

so that $\lim_{h\to 0}\nu_j(k) = \alpha^j k$, which further implies $\lim_{h\to 0}\hat{q}(\nu_j,0) = \hat{q}(\alpha^j k,0)$. From the second integral of the semi-discrete solution, we have

$$\begin{aligned}\lim_{h\to 0}\frac{\left(\sqrt{e^{ikh}-4}+3e^{ikh/2}\right)\hat{q}(\nu_1,0)+\left(\sqrt{e^{ikh}-4}-3e^{ikh/2}\right)\hat{q}(\nu_2,0)}{2\sqrt{e^{ikh}-4}} &= -\frac{i}{2}\left(i+\sqrt{3}\right)\hat{q}\left(\alpha k,0\right) - \frac{i}{2}\left(i-\sqrt{3}\right)\hat{q}\left(\alpha^2 k,0\right)\\ &= -\alpha\hat{q}\left(\alpha k,0\right) - \alpha^2\hat{q}\left(\alpha^2 k,0\right),\end{aligned}$$

and from the third integral,

$$\lim_{h\to 0}\frac{e^{-ikh}-3e^{ikh}+2e^{2ikh}}{h^2} = -3k^2.$$

Therefore, we recover exactly the continuous solution (4.1.26) with $\lim_{h\to 0} f_0 = F_0$.

4.2 Finite Interval IBVP

4.2.1 Off-Centered Backward Discretization of $q_t = q_{xxx}$

We return to the first-order accurate, off-centered discretization (4.1.2) from Section 4.1.1, except now for the finite interval problem

$$\begin{cases} q_t = q_{xxx}, & 0 < x < L,\ t > 0, \\ q(x,0) = \phi(x), & 0 < x < L, \\ q(0,t) = u^{(0)}(t), & t > 0, \\ q_x(0,t) = u^{(1)}(t), & t > 0, \\ q(L,t) = v^{(0)}(t), & t > 0. \end{cases} \tag{4.2.1}$$

The local relation (4.1.3) and dispersion relation (4.1.4) give rise to the global relation

$$e^{WT}\hat{q}(k,T) - \hat{q}(k,0) - \frac{1}{h^2}\left(f + e^{-ikL}g\right) = 0, \quad k \in \mathbb{C}, \tag{4.2.2}$$

where

$$\begin{cases} f(k,T) = -e^{-ikh}f_{-1} + e^{-ikh}\left(3 - e^{-ikh}\right)f_0 - f_1, \\ g(k,T) = g_{-2} + \left(e^{-ikh} - 3\right)g_{-1} + e^{ikh}g_0, \end{cases}$$

so that

$$q_n(T) = \frac{1}{2\pi}\int_{-\pi/h}^{\pi/h} e^{iknh}e^{-WT}\hat{q}(k,0)\,dk + \frac{1}{2\pi}\int_{-\pi/h}^{\pi/h} e^{iknh}e^{-WT}\left(\frac{f + e^{-ikL}g}{h^2}\right)dk. \tag{4.2.3}$$

Based on the $f_j(W,T)$ above, we can use standard backward, center, or forward discretizations for $q_x(0,t) = u^{(1)}(t)$ as to not introduce any further unknown $f_j(W,T)$ functions. We choose the third option for now, such that

$$\frac{q_1(t) - q_0(t)}{h} = u^{(1)}(t) \quad \Rightarrow \quad \frac{f_1 - f_0}{h} = U^{(1)},$$

after taking time transforms, where

$$U^{(1)}(W,T) = \int_0^T e^{Wt}u^{(1)}(t)\,dt.$$

Thus, we have the four equations

$$\begin{cases} 0 = e^{WT}\hat{q}\left(\nu_0,T\right) - \hat{q}\left(\nu_0,0\right) - \dfrac{1}{h^2}\left[f + e^{-i\nu_0 L}g\right], \\ 0 = e^{WT}\hat{q}\left(\nu_1,T\right) - \hat{q}\left(\nu_1,0\right) - \dfrac{1}{h^2}\left[f + e^{-i\nu_1 L}g\right], \\ 0 = e^{WT}\hat{q}\left(\nu_2,T\right) - \hat{q}\left(\nu_2,0\right) - \dfrac{1}{h^2}\left[f + e^{-i\nu_2 L}g\right], \\ \dfrac{f_1 - f_0}{h} = U^{(1)}, \end{cases}$$

to remove the four unknowns $f_{-1}(W,T)$, $f_1(W,T)$, $g_{-2}(W,T)$, and $g_{-1}(W,T)$, where $f_0(W,T)$ and $g_0(W,T)$ are known from the Dirichlet boundary conditions $u^{(0)}(t)$ and $v^{(0)}(t)$. In order to substitute our findings from simultaneously solving the equations above, we must first deform $f(W,T)$ from $g(W,T)$ within (4.2.3). For the sake of taking the continuum limit later, let us deform $g(W,T)$ off the real line. Figure 4.1.1b depicts where e^{-WT} decays as shaded regions.

Let us focus first on the $f(W,T)$ terms. Like in the half-line case, we introduce contour paths in Figure 4.1.2a as $P = (P_1 + P_2) + (P_3 + P_4 + P_5) + (P_6 + P_7)$, where $P_{3,4,5}$ outline the middle wedge and the straight-line paths $P_{1,4,7}$ are all at a fixed height $R > 0$ above the real line. By Cauchy's integral theorem, it is clear that

$$\frac{1}{2\pi}\int_{\partial P_{3,4,5}} e^{iknh}e^{-WT}\left(\frac{f}{h^2}\right)\,dk = 0,$$

so that

$$\frac{1}{2\pi}\int_{-\pi/h}^{\pi/h} e^{iknh}e^{-WT}\left(\frac{f}{h^2}\right)\,dk = \frac{1}{2\pi}\int_{P} e^{iknh}e^{-WT}\left(\frac{f}{h^2}\right)\,dk,$$

after deforming the path on the negative-real line $k \in [-\pi/h, 0]$ to $P_1 + P_2$ and the other path on the positive-real line $k \in [0, \pi/h]$ to $P_6 + P_7$. The vertical integration paths on the boundary of the domain cancel each other by periodicity, but only there at the boundary where $\mathrm{Re}\,(\nu_1) = -\mathrm{Re}\,(\nu_2)$ and $\mathrm{Im}\,(\nu_1) = \mathrm{Im}\,(\nu_2)$. In addition, since paths $P_{1,4,7}$ are in regions of exponential decay, we deform them to $i\infty$, such that $R \to \infty$, effectively extending the adjacent vertical paths off to $i\infty$ as well, so that now we define the integration paths

$$\partial V_1^+ = \lim_{R\to\infty}(P_2 + P_3) \qquad \text{and} \qquad \partial V_2^+ = \lim_{R\to\infty}(P_5 + P_6)\,.$$

We similarly deform $g(W,T)$:

$$\frac{1}{2\pi}\int_{-\pi/h}^{\pi/h} e^{ik(nh-L)}e^{-WT}\left(\frac{g}{h^2}\right)\,dk = \frac{-1}{2\pi}\int_{\partial V^-} e^{ik(nh-L)}e^{-WT}\left(\frac{g}{h^2}\right)\,dk,$$

below the real line. See Figure 4.2.1a. Hence, we deform (4.2.3):

$$\begin{aligned} q_n(T) = {} & \frac{1}{2\pi}\int_{-\pi/h}^{\pi/h} e^{iknh}e^{-WT}\hat{q}(k,0)\,dk + \frac{1}{2\pi}\left(\int_{\partial V_1^+} + \int_{\partial V_2^+}\right) e^{iknh}e^{-WT}\left(\frac{f}{h^2}\right)\,dk \\ & - \frac{1}{2\pi}\int_{\partial V^-} e^{ik(nh-L)}e^{-WT}\left(\frac{g}{h^2}\right)\,dk. \end{aligned} \tag{4.2.4}$$

With some hindsight, we further deform the paths off the origin, as depicted in Figure 4.2.1b, so that now

$$\begin{aligned} q_n(T) = {} & \frac{1}{2\pi}\int_{-\pi/h}^{\pi/h} e^{iknh}e^{-WT}\hat{q}(k,0)\,dk + \frac{1}{2\pi}\left(\int_{\partial \tilde{V}_1^+} + \int_{\partial \tilde{V}_2^+}\right) e^{iknh}e^{-WT}\left(\frac{f}{h^2}\right)\,dk \\ & - \frac{1}{2\pi}\int_{\partial \tilde{V}^-} e^{ik(nh-L)}e^{-WT}\left(\frac{g}{h^2}\right)\,dk. \end{aligned} \tag{4.2.5}$$

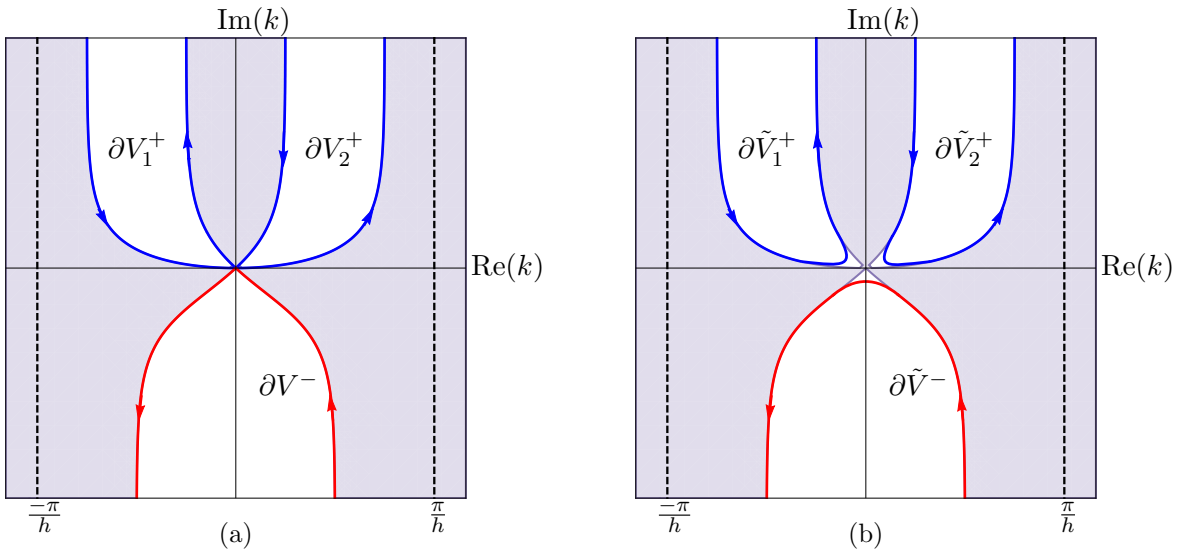

Figure 4.2.1: (a) Integration paths $\partial V_{1,2}^+$ and ∂V^-. (b) Modified integration paths $\partial \tilde{V}_{1,2}^+$ and $\partial \tilde{V}^-$.

With (4.2.5) off the origin, let us return to solving the four equations for the four unknowns $f_{-1}(W,T)$, $f_1(W,T)$, $g_{-2}(W,T)$, and $g_{-1}(W,T)$. Substituting, we find

$$\begin{aligned}\frac{f}{h^2} = \frac{1}{\lambda(k)}\Big\{ & e^{ikL}\left(e^{i\nu_2 h}-e^{i\nu_1 h}\right)\hat{q}(k,0) + e^{i\nu_1(h+L)-ikh}\left(e^{ikh}-e^{i\nu_2 h}\right)\hat{q}\left(\nu_1,0\right) \\ & + e^{i\nu_2(h+L)-ikh}\left(e^{i\nu_1 h}-e^{ikh}\right)\hat{q}\left(\nu_2,0\right) - \eta_1(k)f_0 + \eta_2(k)U^{(1)} + \eta_3(k)g_0\Big\} \\ + \frac{e^{WT}}{\lambda(k)}\Big\{ & e^{ikL}\left(e^{i\nu_1 h}-e^{i\nu_2 h}\right)\hat{q}(k,T) + e^{i\nu_1(h+L)-ikh}\left(e^{i\nu_2 h}-e^{ikh}\right)\hat{q}\left(\nu_1,T\right) \\ & + e^{i\nu_2(h+L)-ikh}\left(e^{ikh}-e^{i\nu_1 h}\right)\hat{q}\left(\nu_2,T\right)\Big\},\end{aligned}$$

and

$$\begin{aligned}\frac{e^{-ikL}g}{h^2} = \frac{1}{\lambda(k)}\Big\{ & \left[e^{i\nu_2 L}\left(e^{i\nu_1 h}-e^{ikh}\right)+e^{i\nu_1 L}\left(e^{ikh}-e^{i\nu_2 h}\right)\right]\hat{q}(k,0) - e^{i\nu_1(h+L)-ikh}\left(e^{ikh}-e^{i\nu_2 h}\right)\hat{q}\left(\nu_1,0\right) \\ & - e^{i\nu_2(h+L)-ikh}\left(e^{i\nu_1 h}-e^{ikh}\right)\hat{q}\left(\nu_2,0\right) + \eta_1(k)f_0 - \eta_2(k)U^{(1)} - \eta_3(k)g_0\Big\} \\ + \frac{e^{WT}}{\lambda(k)}\Big\{ & \left[e^{i\nu_2 L}\left(e^{ikh}-e^{i\nu_1 h}\right)+e^{i\nu_1 L}\left(e^{i\nu_2 h}-e^{ikh}\right)\right]\hat{q}(k,T) - e^{i\nu_1(h+L)-ikh}\left(e^{i\nu_2 h}-e^{ikh}\right)\hat{q}\left(\nu_1,T\right) \\ & - e^{i\nu_2(h+L)-ikh}\left(e^{ikh}-e^{i\nu_1 h}\right)\hat{q}\left(\nu_2,T\right)\Big\},\end{aligned}$$

where

$$\lambda(k) = e^{i\nu_1 h+ikL} - e^{ikh+i\nu_1 L} - e^{i\nu_2 h+ikL} + e^{ikh+i\nu_2 L} + e^{i\nu_2 h+i\nu_1 L} - e^{i\nu_1 h+i\nu_2 L},$$

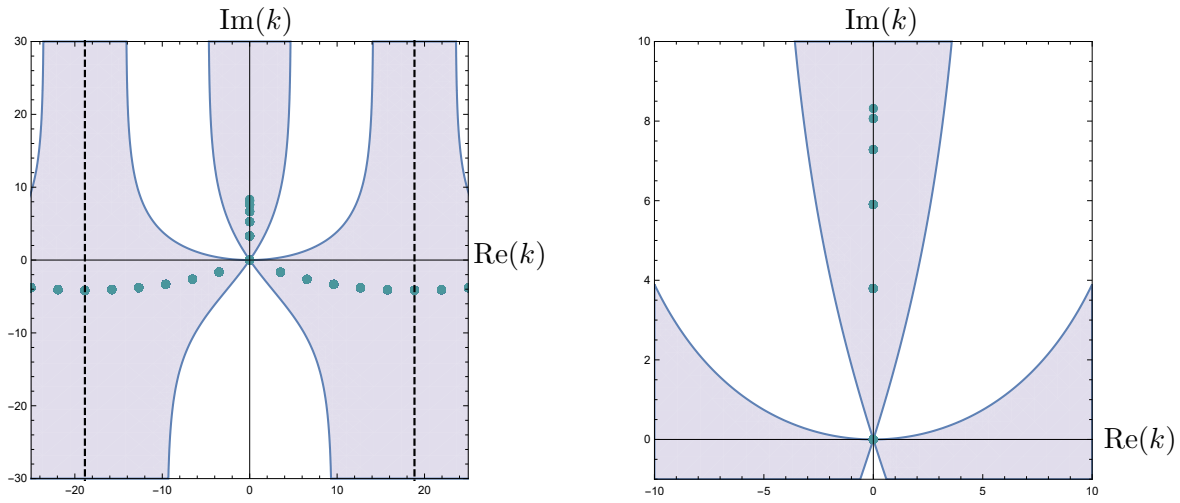

Figure 4.2.2: Numerically determined roots of $\lambda(k)$ with $h = 1/6$ (left) with zoomed in view of the poles on the positive imaginary axis (right).

and

$$\eta_1(k) = \frac{1}{h^2}\Big[e^{-2ik-i\nu_1 h-i\nu_2 h}\left(e^{ikh}-e^{i\nu_1 h}\right)\left(e^{ikh}-e^{i\nu_2 h}\right)\Big(e^{ikh+i\nu_2(h+L)+i\nu_1 h}-e^{ikh+i\nu_2 h+i\nu_1(h+L)} + e^{i\nu_2 h+i\nu_1 L}-e^{i\nu_1 h+i\nu_2 L}\Big)\Big],$$

$$\eta_2(k) = \frac{1}{h}\left[e^{-ikh}\left(e^{i\nu_1 L}-e^{i\nu_2 L}\right)\left(e^{ikh}-e^{i\nu_1 h}\right)\left(e^{ikh}-e^{i\nu_2 h}\right)\right],$$

$$\eta_3(k) = \frac{1}{h^2}\left\{2ie^{i(\nu_1+\nu_2)h}\left[\sin\left(h\left(k-\nu_1\right)\right)-\sin\left(h\left(k-\nu_2\right)\right)+\sin\left(h\left(\nu_1-\nu_2\right)\right)\right]\right\}.$$

The roots of $\lambda(k)$ must be determined numerically, but note that the origin is a root, since $\lambda(0) = e^{i\nu_1(0)h}-e^{i\nu_1(0)L}-e^{i\nu_2(0)h}+e^{i\nu_2(0)L}+e^{i\nu_2(0)h+i\nu_1(0)L}-e^{i\nu_1(0)h+i\nu_2(0)L} = 0$, where

$$\nu_1(0) = \frac{i}{h}\ln\left[\frac{1}{2}\left(3-1+\left[(1-3)^2-4\right]^{1/2}\right)\right] = 0,$$

$$\nu_2(0) = \frac{i}{h}\ln\left[\frac{1}{2}\left(3-1-\left[(1-3)^2-4\right]^{1/2}\right)\right] = 0.$$

Figure 4.2.2 depicts the numerical roots of $\lambda(k)$ for $L = 1$ and $N = 5$, *i.e.*, $h = 1/6$, with the shaded regions of exponential decay due to e^{-WT}. It turns out that with the choice of forward discretization for the Neumann boundary condition, we have a total of $3N + 1$ roots within the domain of interest $\big(\mathrm{Re}(k), \mathrm{Im}(k)\big) \in [-\pi/h, \pi/h] \times (-\infty, \infty)$. Figure 4.2.2 depicts three curves of roots: the two "wings" in the bottom half-plane and the vertical structure on the positive imaginary line. Excluding the root at the origin, each curve contains N roots – the wings appear to be evenly spaced away from the origin, while the roots on the imaginary line tend to clump near the uppermost

root. Varying L only has the effect of scaling the locations of the roots. It is important to note that all of the roots are placed in the shaded regions and do not interfere in any way with the integration paths $\partial\tilde{V}_{1,2}^{+}$ and $\partial\tilde{V}^{-}$. So, in view of this observation, we make the substitutions into (4.2.5):

$$\begin{aligned} q_n(T) = \frac{1}{2\pi}\int_{-\pi/h}^{\pi/h} e^{iknh}e^{-WT}\hat{q}(k,0)\,dk + \frac{1}{2\pi}\left(\int_{\partial\tilde{V}_1^+} + \int_{\partial\tilde{V}_2^+}\right) e^{iknh}e^{-WT}A(k,T)\,dk \\ - \frac{1}{2\pi}\int_{\partial\tilde{V}^-} e^{iknh}e^{-WT}B(k,T)\,dk \;+\; S(n), \end{aligned} \tag{4.2.6}$$

where

$$\begin{aligned} A(k,T) = \frac{1}{\lambda(k)}\Big\{ & e^{ikL}\left(e^{i\nu_2 h} - e^{i\nu_1 h}\right)\hat{q}(k,0) + e^{i\nu_1(h+L)-ikh}\left(e^{ikh} - e^{i\nu_2 h}\right)\hat{q}\,(\nu_1,0) \\ & + e^{i\nu_2(h+L)-ikh}\left(e^{i\nu_1 h} - e^{ikh}\right)\hat{q}\,(\nu_2,0) - \eta_1(k)f_0 + \eta_2(k)U^{(1)} + \eta_3(k)g_0\Big\}, \end{aligned}$$

$$\begin{aligned} B(k,T) = \frac{1}{\lambda(k)}\Big\{ & \left[e^{i\nu_2 L}\left(e^{i\nu_1 h} - e^{ikh}\right) + e^{i\nu_1 L}\left(e^{ikh} - e^{i\nu_2 h}\right)\right]\hat{q}(k,0) - e^{i\nu_1(h+L)-ikh}\left(e^{ikh} - e^{i\nu_2 h}\right)\hat{q}\,(\nu_1,0) \\ & - e^{i\nu_2(h+L)-ikh}\left(e^{i\nu_1 h} - e^{ikh}\right)\hat{q}\,(\nu_2,0) + \eta_1(k)f_0 - \eta_2(k)U^{(1)} - \eta_3(k)g_0\Big\}, \end{aligned}$$

and

$$\begin{aligned} S(n) = \frac{1}{2\pi}\left(\int_{\partial\tilde{V}_1^+} + \int_{\partial\tilde{V}_2^+}\right)\frac{e^{iknh}}{\lambda(k)}\Big\{ & e^{ikL}\left(e^{i\nu_1 h} - e^{i\nu_2 h}\right)\hat{q}(k,T) + e^{i\nu_1(h+L)-ikh}\left(e^{i\nu_2 h} - e^{ikh}\right)\hat{q}\,(\nu_1,T) \\ & + e^{i\nu_2(h+L)-ikh}\left(e^{ikh} - e^{i\nu_1 h}\right)\hat{q}\,(\nu_2,T)\Big\}\,dk \\ - \frac{1}{2\pi}\int_{\partial\tilde{V}^-}\frac{e^{iknh}}{\lambda(k)}\Big\{ & \left[e^{i\nu_2 L}\left(e^{ikh} - e^{i\nu_1 h}\right) + e^{i\nu_1 L}\left(e^{i\nu_2 h} - e^{ikh}\right)\right]\hat{q}(k,T) - e^{i\nu_1(h+L)-ikh}\left(e^{i\nu_2 h} - e^{ikh}\right)\hat{q}\,(\nu_1,T) \\ & - e^{i\nu_2(h+L)-ikh}\left(e^{ikh} - e^{i\nu_1 h}\right)\hat{q}\,(\nu_2,T)\Big\}\,dk. \end{aligned}$$

At this point, we apply the same tactics as before to remove $S(n)$ and all of its unwanted terms. Although the algebra involved may be messy, the process is clear and is easily completed with the help of symbolic software. From (4.2.6), the final solution to this off-centered discretization of the IBVP for $q_t = q_{xxx}$ is

$$\begin{aligned} q_n(T) = \frac{1}{2\pi}\int_{-\pi/h}^{\pi/h} e^{iknh}e^{-WT}\hat{q}(k,0)\,dk + \frac{1}{2\pi}\left(\int_{\partial\tilde{V}_1^+} + \int_{\partial\tilde{V}_2^+}\right) e^{iknh}e^{-WT}A(k,T)\,dk \\ - \frac{1}{2\pi}\int_{\partial\tilde{V}^-} e^{iknh}e^{-WT}B(k,T)\,dk. \end{aligned} \tag{4.2.7}$$

It is important to note that the standard backward stencil,

$$\frac{q_0(t) - q_{-1}(t)}{h} = u^{(1)}(t),$$

is better aligned with the main off-centered backward discretization (4.1.2) of the PDE. Furthermore, this discretization of the boundary condition will be feasible when comparing with finite-difference methods, assuming we want to apply the stencil (4.1.2) to all of the interior mesh points. Employing the same integration paths and following a similar approach as above, we find the alternative solution:

$$\begin{aligned} q_n(T) = \frac{1}{2\pi}\int_{-\pi/h}^{\pi/h} e^{iknh}e^{-WT}\hat{q}(k,0)\,dk + \frac{1}{2\pi}\left(\int_{\partial\tilde{V}_1^+} + \int_{\partial\tilde{V}_2^+}\right) e^{iknh}e^{-WT}\tilde{A}(k,T)\,dk \\ - \frac{1}{2\pi}\int_{\partial\tilde{V}^-} e^{iknh}e^{-WT}\tilde{B}(k,T)\,dk, \end{aligned} \tag{4.2.8}$$

where

$$\begin{aligned} \tilde{A}(k,T) = \frac{1}{\tilde{\lambda}(k)}\Big\{ & e^{ik(L+h)}\left(e^{i\nu_2 h} - e^{i\nu_1 h}\right)\hat{q}(k,0) + e^{i\nu_1(h+L)}\left(e^{ikh} - e^{i\nu_2 h}\right)\hat{q}\,(\nu_1,0) \\ & + e^{i\nu_2(h+L)}\left(e^{i\nu_1 h} - e^{ikh}\right)\hat{q}\,(\nu_2,0) + \tilde{\eta}_1(k)f_0 + \tilde{\eta}_2(k)U^{(1)} - \tilde{\eta}_3(k)g_0\Big\}, \end{aligned}$$

$$\begin{aligned} \tilde{B}(k,T) = \frac{1}{\tilde{\lambda}(k)}\Big\{ & \left[e^{ikh+i\nu_1(L+h)} - e^{ikh+i\nu_2(L+h)} - e^{i\nu_1(L+h)+i\nu_2 h} + e^{i\nu_2(L+h)+i\nu_1 h}\right]\hat{q}(k,0) \\ & - e^{i\nu_1(h+L)}\left(e^{ikh} - e^{i\nu_2 h}\right)\hat{q}\,(\nu_1,0) - e^{i\nu_2(h+L)}\left(e^{i\nu_1 h} - e^{ikh}\right)\hat{q}\,(\nu_2,0) \\ & - \tilde{\eta}_1(k)f_0 - \tilde{\eta}_2(k)U^{(1)} + \tilde{\eta}_3(k)g_0\Big\}, \end{aligned}$$

with

$$\tilde{\lambda}(k) = e^{ik(L+h)+i\nu_1 h} - e^{ikh+i\nu_1(L+h)} - e^{ik(L+h)+i\nu_2 h} + e^{ikh+i\nu_2(h+L)} + e^{i\nu_1(L+h)+i\nu_2 h} - e^{i\nu_2(L+h)+i\nu_1 h}$$

and

$$\begin{aligned} \tilde{\eta}_1(k) = \frac{1}{h^2}\Big[& e^{-2ik-i\nu_1 h-i\nu_2 h}\left(e^{ikh} - e^{i\nu_1 h}\right)\left(e^{ikh} - e^{i\nu_2 h}\right)\left(e^{ikh+i\nu_1 h+i\nu_2 L} - 2e^{ikh+i\nu_2(h+L)+i\nu_1 h} - e^{ikh+i\nu_2 h+i\nu_1 L}\right. \\ & \left. + 2e^{ikh+i\nu_2 h+i\nu_1(h+L)} - e^{i\nu_1(h+L)+i\nu_2 h} + e^{i\nu_2(h+L)+i\nu_1 h}\right)\Big], \end{aligned}$$

$$\tilde{\eta}_2(k) = \frac{1}{h}\left[e^{-ikh}\left(e^{i\nu_1 L} - e^{i\nu_2 L}\right)\left(e^{ikh} - e^{i\nu_1 h}\right)\left(e^{ikh} - e^{i\nu_2 h}\right)\right],$$

$$\tilde{\eta}_3(k) = \frac{1}{h^2}\left[\left(e^{i\nu_1 h} - e^{i\nu_2 h}\right)\left(e^{ikh} - e^{i\nu_1 h}\right)\left(e^{ikh} - e^{i\nu_2 h}\right)\right].$$

The roots of $\tilde{\lambda}(k)$ exhibit a comparable structure to those of $\lambda(k)$, as seen below in Figure 4.2.3, except now the three curves of roots each contain $N+1$ roots instead of N. Hence, with the root at the origin, $\tilde{\lambda}(k)$ contains $3N+4$ total roots within the domain of interest. As we will see, (4.2.8) tends to produce a smaller ∞-norm error than (4.2.7).

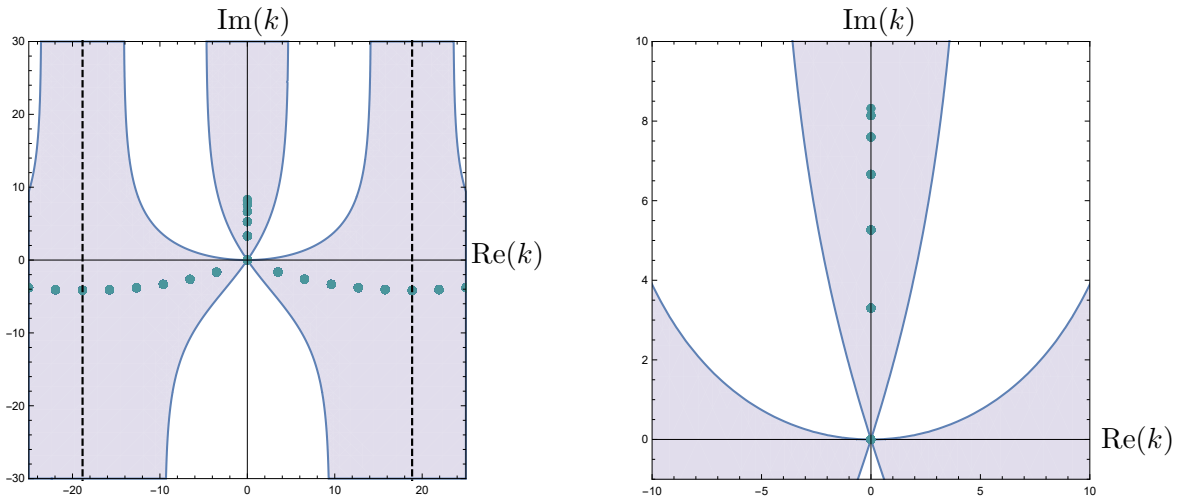

Figure 4.2.3: Numerically determined roots of $\tilde{\lambda}(k)$ with $h = 1/6$ (left) with zoomed in view of the poles on the positive imaginary axis (right).

For this third-order problem, there does not exist a purely series representation solution like for the previous first-order problems (advection equations) and second-order (heat and LS equations). We must directly evaluate the integral representation for arbitrary initial and boundary conditions. From our derivations, we saw that the main constraint of deformation originates from the growth of e^{-WT}, so we are permitted to deform anywhere in the shaded regions of Figure 4.1.1b, relative $\mathrm{Im}\,(k)$ from the e^{iknh} term. We chose the deformation paths $\partial\tilde{V}_{1,2}^{+}$ and $\partial\tilde{V}^{-}$ for analytic convenience, but note that we have decay on the real line due to e^{-WT}. For numerical purposes, it is beneficial to leave the real-line paths that were deformed to $\partial\tilde{V}_{1,2}^{+}$ on the real line, especially since the boundary between the unshaded and shaded region becomes vertical and extends to $+i\infty$, effectively trading a finite integration path for an infinite one. A similar argument can be made for $\partial\tilde{V}^{-}$, in the sense that in order to benefit from exponential decay due to e^{-WT}, we can stop the deformations before reaching the boundary of no decay, such that the new integration path sits between this boundary and the distribution of poles in the bottom half-plane.

We introduce Figure 4.2.4 with the computation integration paths $\partial C_{1,2}^{+}$ and ∂C^{-}, where the dots represent the waypoints implemented into MATLAB's `integral()` function. Relative to $\partial\tilde{V}_{1,2}^{+}$, the top wedges of $\partial C_{1,2}^{+}$ are truncated from stretching to $+i\infty$ and are shifted closer to the imaginary line, making use of exponential decay from e^{-WT}. The general structure persists as $h \to 0$, but for h very small, it is beneficial to additionally truncate the ends of ∂C^{-} and the paths on the real line of $\partial C_{1,2}^{+}$ in order to not only avoid `NaN` outputs due to underflow, but to also spare computation power on machine-error integration contributions. Other truncation analyses can be done for these integrands [25, 38].

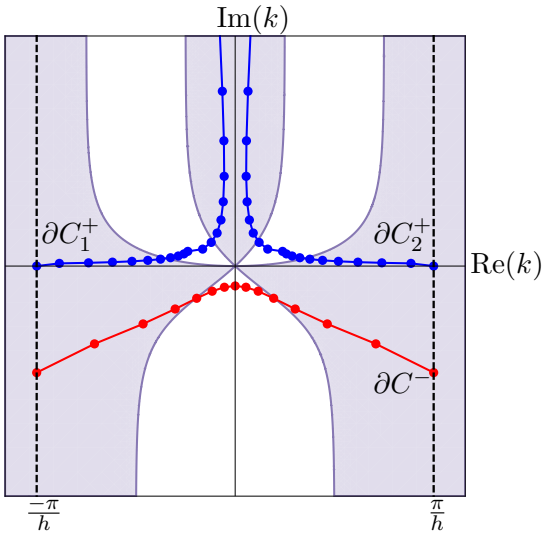

Figure 4.2.4: Computation paths $\partial C_{1,2}^+$ and ∂C^-.

Applying the continuous UTM to the IBVP (4.2.1) gives the dispersion relation $\tilde{W}(k) = ik^3$ and solution

$$\begin{aligned} q(x,T) = \frac{1}{2\pi}\int_{-\infty}^{\infty} e^{ikx}e^{-\tilde{W}T}\hat{q}(k,0)\,dk + \frac{1}{2\pi}\left(\int_{\partial\tilde{\Omega}_1^+} + \int_{\partial\tilde{\Omega}_2^+}\right) e^{ikx}e^{-\tilde{W}T}H^+\left(\tilde{W},T\right)\,dk \\ + \frac{1}{2\pi}\int_{\partial\tilde{\Omega}^-} e^{ikx}e^{-\tilde{W}T}H^-\left(\tilde{W},T\right)\,dk, \end{aligned} \tag{4.2.9}$$

where $\alpha = e^{2\pi i/3}$,

$$\begin{aligned} H^+\left(\tilde{W},T\right) = \frac{1}{\Lambda(k)}\Big\{ &-\alpha e^{ikL}\hat{q}(k,0) + (\alpha+1)e^{i\alpha kL}\hat{q}(\alpha k,0) - e^{i\alpha^2 kL}\hat{q}(\alpha^2 k,0) \\ &- k^2\left(\alpha^2-1\right)\left[\left(\alpha^2+1\right)e^{i\alpha^2 kL} - (\alpha+1)e^{i\alpha kL}\right]F_0 \\ &+ ik\left(\alpha^2-1\right)\left(e^{i\alpha^2 kL} - e^{i\alpha kL}\right)F_1 + \alpha k^2(\alpha-1)^2(\alpha+1)G_0\Big\}, \end{aligned}$$

$$\begin{aligned} H^-\left(\tilde{W},T\right) = \frac{1}{\Lambda(k)}\Big\{ &-\left[(\alpha+1)e^{i\alpha kL} - e^{i\alpha^2 kL}\right]\hat{q}(k,0) + (\alpha+1)e^{i\alpha kL}\hat{q}(\alpha k,0) - e^{i\alpha^2 kL}\hat{q}(\alpha^2 k,0) \\ &- k^2\left(\alpha^2-1\right)\left[\left(\alpha^2+1\right)e^{i\alpha^2 kL} - (\alpha+1)e^{i\alpha kL}\right]F_0 \\ &- ik\left(\alpha^2-1\right)\left(e^{i\alpha kL} - e^{i\alpha^2 kL}\right)F_1 + \alpha k^2(\alpha-1)^2(\alpha+1)G_0\Big\}, \end{aligned}$$

and

$$\Lambda(k) = e^{i\alpha^2 kL} + \alpha e^{ikL} - (\alpha+1)e^{i\alpha kL}.$$

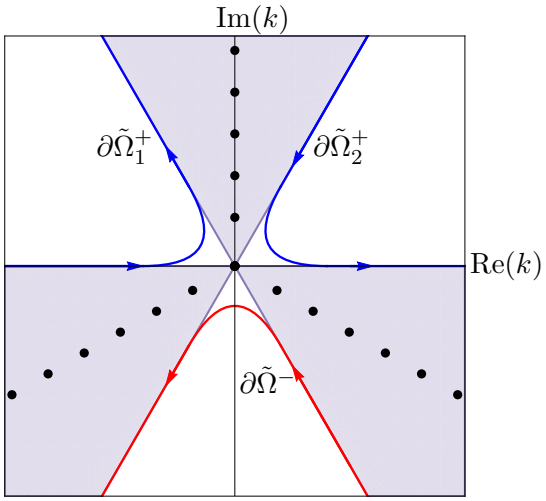

Figure 4.2.5: Modified integration paths $\partial\tilde{\Omega}_{1,2}^+$ and $\partial\tilde{\Omega}^-$.

Figure 4.2.5 depicts the integration paths $\partial\tilde{\Omega}_{1,2}^+$ and $\partial\tilde{\Omega}^-$, where the black dots denote the poles of $\Lambda(k)$ and

$$\Omega^{\pm} = \left\{ k \in \mathbb{C} \,\middle|\, \operatorname{Re}\left[-\tilde{W}(k)\right] > 0 \text{ and } \operatorname{Im}(k) \gtrless 0 \right\}.$$

Recall that we derived two solutions from the backward off-centered discretization to the linear KdV equation in IBVP (4.2.1): solution (4.2.7) by discretizing the Neumann data via the standard *forward* stencil and solution (4.2.8) by discretizing the Neumann data via the standard *backward* stencil. Since the latter better aligns with the PDE discretization, we show its continuum limit to solution (4.2.9), but the continuum limit of (4.2.7) is similarly obtained.

Because $\lim_{h\to 0} W(k) = ik^3$, $\lim_{h\to 0} \partial\tilde{V}_{1,2}^+ = \partial\tilde{\Omega}_{1,2}^+$, respectively, and $\lim_{h\to 0} \partial\tilde{V}^- = \partial\tilde{\Omega}^-$. We make use of symbolic mathematical software to calculate Taylor series expansions around $h = 0$ and to show symmetries and coefficients of solutions converge to their continuous counterpart. For example, we first find

$$\nu_1(k) = \frac{i}{2}\left[ik + \sqrt{3}\left(k^2\right)^{1/2}\right] - \frac{k\left(k^2\right)^{1/2}}{2\sqrt{3}}\,h + \mathcal{O}\left(h^2\right).$$

Since $k \in \mathbb{C}$, we must consider k in the upper-half plane $\mathbb{C}^+$ and k in the lower-half plane $\mathbb{C}^-$, implying we must consider the $\partial\tilde{V}_{1,2}^+$ and $\partial\tilde{V}^-$ integral terms separately, respectively.

Let us first look at $k \in \mathbb{C}^+$. Here, our choice of branch cut for the square-root function tells us $z^{1/2} = +\sqrt{z}$, such that

$$\lim_{h\to 0} \nu_1(k) = \lim_{h\to 0}\left[\frac{i}{2}\left(i + \sqrt{3}\right)k - \frac{k^2}{2\sqrt{3}}\,h + \mathcal{O}\left(h^2\right)\right] = \alpha k.$$

Similarly,

$$\nu_2(k) = \frac{i}{2}\left[ik - \sqrt{3}\left(k^2\right)^{1/2}\right] + \frac{k\left(k^2\right)^{1/2}}{2\sqrt{3}}\,h + \mathcal{O}\left(h^2\right),$$

so that

$$\lim_{h\to 0}\nu_2(k) = \lim_{h\to 0}\left[\frac{i}{2}\left(i-\sqrt{3}\right)k + \frac{k^2}{2\sqrt{3}}\,h + \mathcal{O}\left(h^2\right)\right] = \alpha^2 k.$$

Turning to the solutions (4.2.8) and (4.2.9), let us look at the coefficient of the $\hat{q}(k,0)$ term in the $\partial\tilde{V}^+_{1,2}$ and $\partial\tilde{\Omega}^+_{1,2}$ integrals. From the semi-discrete solution, denote this coefficient as

$$c_1 = \frac{e^{ik(L+h)}\left(e^{i\nu_2 h} - e^{i\nu_1 h}\right)}{e^{ik(L+h)+i\nu_1 h} - e^{ikh+i\nu_1(L+h)} - e^{ik(L+h)+i\nu_2 h} + e^{ikh+i\nu_2(h+L)} + e^{i\nu_1(L+h)+i\nu_2 h} - e^{i\nu_2(L+h)+i\nu_1 h}},$$

and from the continuous solution,

$$C_1 = \frac{-\alpha e^{ikL}}{e^{i\alpha^2 kL} + \alpha e^{ikL} - (\alpha+1)e^{i\alpha kL}}.$$

Taylor-series expanding c_1 about $h=0$, we find

$$c_1 = \frac{2\sqrt{3}\left(k^2\right)^{1/2} e^{\frac{1}{2}\left[\sqrt{3}\left(k^2\right)^{1/2}+3ik\right]L}}{3ik\left[e^{\sqrt{3}(k^2)^{1/2}L}-1\right] + \sqrt{3}\left(k^2\right)^{1/2}\left[e^{\sqrt{3}(k^2)^{1/2}L} - 2e^{\frac{1}{2}\left(\sqrt{3}(k^2)^{1/2}+3ik\right)L}+1\right]} + \mathcal{O}(h).$$

Since $\mathrm{Im}(k)\geq 0$, the leading-order term as $h\to 0$ becomes

$$\begin{aligned}
&\frac{2\sqrt{3}\left(k^2\right)^{1/2} e^{\frac{1}{2}\left[\sqrt{3}\left(k^2\right)^{1/2}+3ik\right]L}}{3ik\left[e^{\sqrt{3}(k^2)^{1/2}L}-1\right] + \sqrt{3}\left(k^2\right)^{1/2}\left[e^{\sqrt{3}(k^2)^{1/2}L} - 2e^{\frac{1}{2}\left(\sqrt{3}(k^2)^{1/2}+3ik\right)L}+1\right]} \\
&\qquad = \frac{2\sqrt{3}ke^{\frac{1}{2}\left(\sqrt{3}k+3ik\right)L}}{3ik\left(e^{\sqrt{3}kL}-1\right) + \sqrt{3}k\left(e^{\sqrt{3}kL} - 2e^{\frac{1}{2}\left(\sqrt{3}k+3ik\right)L}+1\right)} \\
&\qquad = \frac{2\sqrt{3}e^{\frac{1}{2}\left(\sqrt{3}+3i\right)kL}}{3i\left(e^{\sqrt{3}kL}-1\right) + \sqrt{3}\left(e^{\sqrt{3}kL} - 2e^{\frac{1}{2}\left(\sqrt{3}+3i\right)kL}+1\right)} \\
&\qquad = \frac{2\sqrt{3}e^{\frac{1}{2}\left(\sqrt{3}+3i\right)kL}}{3ie^{\sqrt{3}kL} - 3i + \sqrt{3}e^{\sqrt{3}kL} - 2\sqrt{3}e^{\frac{1}{2}\left(\sqrt{3}+3i\right)kL} + \sqrt{3}} \\
&\qquad = \frac{2\sqrt{3}e^{\frac{1}{2}\left(\sqrt{3}+3i\right)kL}}{\left(\sqrt{3}+3i\right)e^{\sqrt{3}kL} - 2\sqrt{3}e^{\frac{1}{2}\left(\sqrt{3}+3i\right)kL} - 3i + \sqrt{3}} \\
&\qquad = \frac{-\alpha e^{ikL}}{\frac{-\alpha e^{ikL}}{2\sqrt{3}}e^{\frac{-1}{2}\left(\sqrt{3}+3i\right)kL}\left[\left(\sqrt{3}+3i\right)e^{\sqrt{3}kL} - 2\sqrt{3}e^{\frac{1}{2}\left(\sqrt{3}+3i\right)kL} - 3i + \sqrt{3}\right]}.
\end{aligned} \tag{4.2.10}$$

Taking a closer look at the denominator and applying

$$\alpha = \frac{i}{2}\left(i+\sqrt{3}\right), \qquad \text{and} \qquad \alpha^2 = \frac{i}{2}\left(i-\sqrt{3}\right) = -(\alpha+1),$$

we have

$$\begin{aligned}
&\tfrac{-\alpha e^{ikL}}{2\sqrt{3}} e^{\frac{-1}{2}\left(\sqrt{3}+3i\right)kL}\left[\left(\sqrt{3}+3i\right)e^{\sqrt{3}kL} - 2\sqrt{3}e^{\frac{1}{2}\left(\sqrt{3}+3i\right)kL} - 3i+\sqrt{3}\right] \\
&\quad = \tfrac{-\alpha}{2}\left(1+\sqrt{3}i\right)e^{ikL}e^{\frac{-1}{2}\left(\sqrt{3}+3i\right)kL}e^{\sqrt{3}kL} + \alpha e^{ikL} + \tfrac{\alpha}{2}\left(\sqrt{3}i-1\right)e^{ikL}e^{\frac{-1}{2}\left(\sqrt{3}+3i\right)kL} \\
&\quad = -\alpha\left(-\alpha^2\right)e^{\frac{1}{2}\left(-i+\sqrt{3}\right)kL} + \alpha e^{ikL} + \alpha\left(\alpha\right)e^{\frac{1}{2}\left(-1-\sqrt{3}\right)kL} \\
&\quad = e^{\frac{-\alpha^2}{i}kL} + \alpha e^{ikL} + \alpha^2 e^{\frac{-\alpha}{i}kL} \\
&\quad = e^{i\alpha^2 kL} + \alpha e^{ikL} - (\alpha+1)e^{i\alpha kL}.
\end{aligned}$$

The leading order term of c_1 simplifies:

$$\begin{aligned}
&\frac{2\sqrt{3}\left(k^2\right)^{1/2}e^{\frac{1}{2}\left[\sqrt{3}\left(k^2\right)^{1/2}+3ik\right]L}}{3ik\left[e^{\sqrt{3}(k^2)^{1/2}L}-1\right]+\sqrt{3}\left(k^2\right)^{1/2}\left[e^{\sqrt{3}(k^2)^{1/2}L}-2e^{\frac{1}{2}\left(\sqrt{3}(k^2)^{1/2}+3ik\right)L}+1\right]} \\
&\qquad = \frac{-\alpha e^{ikL}}{e^{i\alpha^2 kL}+\alpha e^{ikL}-(\alpha+1)e^{i\alpha kL}} \\
&\qquad = C_1,
\end{aligned}$$

such that $\lim_{h\to 0} c_1 = C_1$.

Next, denote the coefficients of $\hat{q}\left(\nu_1, 0\right)$ and $\hat{q}\left(\alpha k, 0\right)$, respectively, as

$$c_2 = \frac{e^{i\nu_1(h+L)}\left(e^{ikh}-e^{i\nu_2 h}\right)}{e^{ik(L+h)+i\nu_1 h} - e^{ikh+i\nu_1(L+h)} - e^{ik(L+h)+i\nu_2 h} + e^{ikh+i\nu_2(h+L)} + e^{i\nu_1(L+h)+i\nu_2 h} - e^{i\nu_2(L+h)+i\nu_1 h}},$$

and

$$C_2 = \frac{(\alpha+1)e^{i\alpha kL}}{e^{i\alpha^2 kL}+\alpha e^{ikL}-(\alpha+1)e^{i\alpha kL}}.$$

In a similar fashion as before, we expand c_2 about $h=0$ to find

$$c_2 = \frac{3ik-\sqrt{3}\left(k^2\right)^{1/2}}{3ik\left[e^{\sqrt{3}(k^2)^{1/2}L}-1\right]+\sqrt{3}\left(k^2\right)^{1/2}\left[e^{\sqrt{3}(k^2)^{1/2}L}-2e^{\frac{1}{2}\left(\sqrt{3}(k^2)^{1/2}+3ik\right)L}+1\right]} + \mathcal{O}(h).$$

Since $k \in \mathbb{C}^+$, we know that $\lim_{h\to 0}\hat{q}\left(\nu_1,0\right) = \hat{q}\left(\alpha k, 0\right)$, so that we expect $\lim_{h\to 0} c_2 = C_2$. The leading order term of the expansion for c_2 simplifies to

$$\begin{aligned}
&\frac{3ik-\sqrt{3}\left(k^2\right)^{1/2}}{3ik\left[e^{\sqrt{3}(k^2)^{1/2}L}-1\right]+\sqrt{3}\left(k^2\right)^{1/2}\left[e^{\sqrt{3}(k^2)^{1/2}L}-2e^{\frac{1}{2}\left(\sqrt{3}(k^2)^{1/2}+3ik\right)L}+1\right]} \\
&\qquad = \frac{3ik-\sqrt{3}k}{3ik\left(e^{\sqrt{3}kL}-1\right)+\sqrt{3}k\left[e^{\sqrt{3}kL}-2e^{\frac{1}{2}\left(\sqrt{3}k+3ik\right)L}+1\right]} \\
&\qquad = \frac{3i-\sqrt{3}}{\left(\sqrt{3}+3i\right)e^{\sqrt{3}kL}-2\sqrt{3}e^{\frac{1}{2}\left(\sqrt{3}+3i\right)kL}-3i+\sqrt{3}}.
\end{aligned}$$

Since the denominator is equivalent to the denominator of the line above (4.2.10), showing that

$$\frac{(\alpha+1)e^{i\alpha kL}}{3i-\sqrt{3}} = \frac{-\alpha e^{ikL}}{2\sqrt{3}} e^{\frac{-1}{2}(\sqrt{3}+3i)kL}, \qquad \text{or} \qquad \frac{(\alpha+1)e^{i\alpha kL}}{3i-\sqrt{3}} + \frac{\alpha e^{ikL}}{2\sqrt{3}} e^{\frac{-1}{2}(\sqrt{3}+3i)kL} = 0,$$

is equivalent to proving $\lim_{h\to 0} c_2 = C_2$. Indeed, note that the exponentials from the second term simplify to

$$e^{ikL} e^{\frac{-1}{2}(\sqrt{3}+3i)kL} = \exp\left[\left(i - \frac{\sqrt{3}}{2} - \frac{3}{2}i\right)kL\right] = \exp\left[-\frac{\alpha}{i}kL\right] = e^{i\alpha kL}.$$

Then, we see that

$$\begin{aligned}
\left[\frac{(\alpha+1)}{3i-\sqrt{3}} + \frac{\alpha}{2\sqrt{3}}\right] e^{i\alpha kL} &= \left[\frac{2(\alpha+1)\sqrt{3} + \alpha\left(3i-\sqrt{3}\right)}{6i\sqrt{3}-6}\right] e^{i\alpha kL} \\
&= \left[\frac{-2\alpha^2\sqrt{3} + \alpha\left(3i-\sqrt{3}\right)}{6\left(i\sqrt{3}-1\right)}\right] e^{i\alpha kL} \\
&= \left[\frac{-2\left(\frac{i}{2}\right)\left(i-\sqrt{3}\right)\sqrt{3} + \left(\frac{i}{2}\right)\left(i+\sqrt{3}\right)\left(3i-\sqrt{3}\right)}{6\left(i\sqrt{3}-1\right)}\right] e^{i\alpha kL} \\
&= \left[\frac{\left(1+i\sqrt{3}\right)\sqrt{3} + \left(\frac{-1}{2} + \frac{i\sqrt{3}}{2}\right)\left(3i-\sqrt{3}\right)}{6\left(i\sqrt{3}-1\right)}\right] e^{i\alpha kL} \\
&= \left[\frac{\sqrt{3}+3i-\sqrt{3}-3i}{6\left(i\sqrt{3}-1\right)}\right] e^{i\alpha kL}, \\
&= 0.
\end{aligned}$$

Thus, $\lim_{h\to 0} c_2 = C_2$.

The coefficients of $\hat{q}\left(\nu_2, 0\right)$ and $\hat{q}\left(\alpha^2 k, 0\right)$ are, respectively,

$$c_3 = \frac{e^{i\nu_2(h+L)}\left(e^{i\nu_1 h} - e^{ikh}\right)}{e^{ik(L+h)+i\nu_1 h} - e^{ikh+i\nu_1(L+h)} - e^{ik(L+h)+i\nu_2 h} + e^{ikh+i\nu_2(h+L)} + e^{i\nu_1(L+h)+i\nu_2 h} - e^{i\nu_2(L+h)+i\nu_1 h}}$$

and

$$C_3 = \frac{-e^{i\alpha^2 kL}}{e^{i\alpha^2 kL} + \alpha e^{ikL} - (\alpha+1)e^{i\alpha kL}}.$$

For our chosen square-root function branch cut, we know that $\lim_{h\to 0} \hat{q}\left(\nu_2, 0\right) = \hat{q}\left(\alpha^2 k, 0\right)$ for $k \in \mathbb{C}^+$ and expect $\lim_{h\to 0} c_3 = C_3$. The leading order term of the series expansion for c_3 simplifies to

$$\begin{aligned}
&\frac{-\left[3ik + \sqrt{3}\left(k^2\right)^{1/2}\right] e^{\sqrt{3}\left(k^2\right)^{1/2}L}}{3ik\left[e^{\sqrt{3}\left(k^2\right)^{1/2}L} - 1\right] + \sqrt{3}\left(k^2\right)^{1/2}\left[e^{\sqrt{3}\left(k^2\right)^{1/2}L} - 2e^{\frac{1}{2}\left(\sqrt{3}\left(k^2\right)^{1/2}+3ik\right)L} + 1\right]} \\
&\qquad = \frac{-\left(3ik + \sqrt{3}k\right) e^{\sqrt{3}kL}}{3ik\left(e^{\sqrt{3}kL} - 1\right) + \sqrt{3}k\left[e^{\sqrt{3}kL} - 2e^{\frac{1}{2}\left(\sqrt{3}k+3ik\right)L} + 1\right]} \\
&\qquad = \frac{-\left(3i + \sqrt{3}\right) e^{\sqrt{3}kL}}{\left(\sqrt{3}+3i\right) e^{\sqrt{3}kL} - 2\sqrt{3}e^{\frac{1}{2}\left(\sqrt{3}+3i\right)kL} - 3i + \sqrt{3}}.
\end{aligned}$$

Like before, showing $\lim_{h\to 0} c_3 = C_3$ is equivalent to showing

$$\frac{e^{i\alpha^2 kL}}{\left(3i+\sqrt{3}\right)e^{\sqrt{3}kL}} + \frac{\alpha e^{ikL}}{2\sqrt{3}} e^{\frac{-1}{2}(\sqrt{3}+3i)kL} = 0.$$

We know that the exponentials from the second term can be rewritten as $e^{ikL}e^{\frac{-1}{2}(\sqrt{3}+3i)kL} = e^{i\alpha kL}$, so looking at the exponentials from the first term,

$$e^{i\alpha^2 kL}e^{-\sqrt{3}kL} = \exp\left[\left(i\alpha^2 - \sqrt{3}\right)kL\right] = \exp\left[\frac{-1}{2}\left(i+\sqrt{3}\right)kL\right] = e^{i\alpha kL}.$$

Then,

$$\begin{aligned}
\left[\frac{1}{3i+\sqrt{3}} + \frac{\alpha}{2\sqrt{3}}\right] e^{i\alpha kL} &= \left[\frac{2\sqrt{3}+\alpha\left(3i+\sqrt{3}\right)}{6+6i\sqrt{3}}\right] e^{i\alpha kL} \\
&= \left[\frac{2\sqrt{3}+\frac{i}{2}\left(i+\sqrt{3}\right)\left(3i+\sqrt{3}\right)}{6\left(1+i\sqrt{3}\right)}\right] e^{i\alpha kL} \\
&= \left[\frac{2\sqrt{3}+\left(\frac{-1}{2}+\frac{i\sqrt{3}}{2}\right)\left(3i+\sqrt{3}\right)}{6\left(1+i\sqrt{3}\right)}\right] e^{i\alpha kL} \\
&= \left[\frac{2\sqrt{3}-2\sqrt{3}-\frac{3i}{2}+\frac{3i}{2}}{6\left(1+i\sqrt{3}\right)}\right] e^{i\alpha kL}, \\
&= 0.
\end{aligned}$$

Thus, $\lim_{h\to 0} c_3 = C_3$. Sparing the details, we could show that the coefficients of $f_0(W,T)$, $U(W,T)$, and $g_0(W,T)$ from the $\partial\tilde{V}^+_{1,2}$ integrals likewise converge to their continuous counterparts from the $\partial\tilde{\Omega}^+_{1,2}$ integrals, where we always $\lim_{h\to 0} f_0 = F_0$, $\lim_{h\to 0} U = F_1$, and $\lim_{h\to 0} g_0 = G_0$ for all $k \in \mathbb{C}$.

Lastly, we consider the continuum limit of the $\partial\tilde{V}^-$ integral to the $\partial\tilde{\Omega}^-$ integral. Since the integration path $\partial\tilde{V}^-$ is in the lower-half plane, our choice of branch cut for $k \in \mathbb{C}^-$ implies

$$\begin{cases}
\lim\limits_{h\to 0} \nu_1(k) = \lim\limits_{h\to 0}\left[\dfrac{i}{2}\left(i-\sqrt{3}\right)k + \dfrac{k^2}{2\sqrt{3}}h + \mathcal{O}\left(h^2\right)\right] = \alpha^2 k, \\
\lim\limits_{h\to 0} \nu_2(k) = \lim\limits_{h\to 0}\left[\dfrac{i}{2}\left(i+\sqrt{3}\right)k - \dfrac{k^2}{2\sqrt{3}}h + \mathcal{O}\left(h^2\right)\right] = \alpha k.
\end{cases}$$

Let us look at the coefficient

$$c_4 = \frac{e^{ikh+i\nu_1(L+h)} - e^{ikh+i\nu_2(L+h)} - e^{i\nu_1(L+h)+i\nu_2 h} + e^{i\nu_2(L+h)+i\nu_1 h}}{e^{ik(L+h)+i\nu_1 h} - e^{ikh+i\nu_1(L+h)} - e^{ik(L+h)+i\nu_2 h} + e^{ikh+i\nu_2(h+L)} + e^{i\nu_1(L+h)+i\nu_2 h} - e^{i\nu_2(L+h)+i\nu_1 h}}$$

of $\hat{q}(k,0)$ from the semi-discrete solution and the coefficient

$$C_4 = \frac{(\alpha+1)e^{i\alpha kL} - e^{i\alpha^2 kL}}{e^{i\alpha^2 kL} + \alpha e^{ikL} - (\alpha+1)e^{i\alpha kL}},$$

of $\hat{q}(k,0)$ from the continuous solution. Following similar steps from above, we expand c_4 to find that the leading-order term becomes

$$\begin{aligned}
&\frac{-\sqrt{3}\left(k^2\right)^{1/2}\left[e^{\sqrt{3}\left(k^2\right)^{1/2}L}+1\right]-3ik\left[e^{\sqrt{3}\left(k^2\right)^{1/2}L}-1\right]}{3ik\left[e^{\sqrt{3}(k^2)^{1/2}L}-1\right]+\sqrt{3}\left(k^2\right)^{1/2}\left[e^{\sqrt{3}(k^2)^{1/2}L}-2e^{\frac{1}{2}\left(\sqrt{3}(k^2)^{1/2}+3ik\right)L}+1\right]} \\
&\qquad=\frac{\sqrt{3}k\left(e^{-\sqrt{3}kL}+1\right)-3ik\left(e^{-\sqrt{3}kL}-1\right)}{3ik\left(e^{-\sqrt{3}kL}-1\right)-\sqrt{3}k\left[e^{-\sqrt{3}kL}-2e^{\frac{1}{2}\left(-\sqrt{3}k+3ik\right)L}+1\right]} \\
&\qquad=\frac{\sqrt{3}\left(e^{-\sqrt{3}kL}+1\right)-3i\left(e^{-\sqrt{3}kL}-1\right)}{3i\left(e^{-\sqrt{3}kL}-1\right)-\sqrt{3}\left[e^{-\sqrt{3}kL}-2e^{\frac{1}{2}\left(-\sqrt{3}k+3ik\right)L}+1\right]} \\
&\qquad=\frac{\sqrt{3}+3i+\left(\sqrt{3}-3i\right)e^{-\sqrt{3}kL}}{\left(3i-\sqrt{3}\right)e^{-\sqrt{3}kL}+2\sqrt{3}e^{\frac{1}{2}\left(-\sqrt{3}+3i\right)kL}-3i-\sqrt{3}} \\
&\qquad=\frac{\sqrt{3}+3i+\left(\sqrt{3}-3i\right)e^{-\sqrt{3}kL}}{\left(3i-\sqrt{3}\right)e^{-\sqrt{3}kL}+2\sqrt{3}e^{\frac{1}{2}\left(-\sqrt{3}+3i\right)kL}-3i-\sqrt{3}}\cdot\frac{e^{\sqrt{3}kL}}{e^{\sqrt{3}kL}} \\
&\qquad=\frac{\left(\sqrt{3}+3i\right)e^{\sqrt{3}kL}+\sqrt{3}-3i}{3i-\sqrt{3}+2\sqrt{3}e^{\frac{1}{2}\left(\sqrt{3}+3i\right)kL}-\left(3i+\sqrt{3}\right)e^{\sqrt{3}kL}} \\
&\qquad=\frac{-\left(\sqrt{3}+3i\right)e^{\sqrt{3}kL}-\sqrt{3}+3i}{\left(3i+\sqrt{3}\right)e^{\sqrt{3}kL}-2\sqrt{3}e^{\frac{1}{2}\left(\sqrt{3}+3i\right)kL}-3i+\sqrt{3}}.
\end{aligned}$$

Showing $\lim_{h\to 0} c_4 = C_4$ is the same as showing

$$\frac{(\alpha+1)e^{i\alpha kL}-e^{i\alpha^2 kL}}{-\left(\sqrt{3}+3i\right)e^{\sqrt{3}kL}-\sqrt{3}+3i}+\frac{\alpha e^{ikL}}{2\sqrt{3}}e^{\frac{-1}{2}(\sqrt{3}+3i)kL}=0,$$

since we obtain the same denominator as before. After some manipulations like in previous steps, we indeed satisfy the equality above, such that $\lim_{h\to 0} c_4 = C_4$.

Next, denote the coefficient of $\hat{q}\left(\nu_1,0\right)$ as

$$c_5=\frac{-e^{i\nu_1(h+L)}\left(e^{ikh}-e^{i\nu_2 h}\right)}{e^{ik(L+h)+i\nu_1 h}-e^{ikh+i\nu_1(L+h)}-e^{ik(L+h)+i\nu_2 h}+e^{ikh+i\nu_2(h+L)}+e^{i\nu_1(L+h)+i\nu_2 h}-e^{i\nu_2(L+h)+i\nu_1 h}}.$$

Since $\partial\tilde{V}^-$ is in the lower-half plane where $\lim_{h\to 0}\nu_1(k)=\alpha^2 k$, we expect $\lim_{h\to 0} c_5 = C_5$, the coefficient of $\hat{q}\left(\alpha^2 k,0\right)$:

$$C_5=\frac{e^{i\alpha^2 kL}}{e^{i\alpha^2 kL}+\alpha e^{ikL}-(\alpha+1)e^{i\alpha kL}}.$$

Expanding c_5 in a Taylor series about $h=0$ and applying our choice of branch cut for $k\in\mathbb{C}^-$, we

find the $\mathcal{O}(1)$ term as

$$\begin{aligned}
&\frac{\sqrt{3}\left(k^2\right)^{1/2}-3ik}{3ik\left[e^{\sqrt{3}(k^2)^{1/2}L}-1\right]+\sqrt{3}\left(k^2\right)^{1/2}\left[e^{\sqrt{3}(k^2)^{1/2}L}-2e^{\frac{1}{2}\left(\sqrt{3}(k^2)^{1/2}+3ik\right)L}+1\right]} \\
&\qquad=\frac{-\sqrt{3}k-3ik}{3ik\left(e^{-\sqrt{3}kL}-1\right)-\sqrt{3}k\left[e^{-\sqrt{3}kL}-2e^{\frac{1}{2}\left(-\sqrt{3}k+3ik\right)L}+1\right]} \\
&\qquad=\frac{-\sqrt{3}-3i}{3i\left(e^{-\sqrt{3}kL}-1\right)-\sqrt{3}\left[e^{-\sqrt{3}kL}-2e^{\frac{1}{2}\left(-\sqrt{3}k+3ik\right)L}+1\right]} \\
&\qquad=\frac{-\sqrt{3}-3i}{\left(3i-\sqrt{3}\right)e^{-\sqrt{3}kL}+2\sqrt{3}e^{\frac{1}{2}\left(-\sqrt{3}+3i\right)kL}-3i-\sqrt{3}} \\
&\qquad=\frac{-\sqrt{3}-3i}{\left(3i-\sqrt{3}\right)e^{-\sqrt{3}kL}+2\sqrt{3}e^{\frac{1}{2}\left(-\sqrt{3}+3i\right)kL}-3i-\sqrt{3}}\cdot\frac{e^{\sqrt{3}kL}}{e^{\sqrt{3}kL}} \\
&\qquad=\frac{-\left(\sqrt{3}+3i\right)e^{\sqrt{3}kL}}{3i-\sqrt{3}+2\sqrt{3}e^{\frac{1}{2}\left(\sqrt{3}+3i\right)kL}-\left(3i+\sqrt{3}\right)e^{\sqrt{3}kL}} \\
&\qquad=\frac{\left(\sqrt{3}+3i\right)e^{\sqrt{3}kL}}{\left(3i+\sqrt{3}\right)e^{\sqrt{3}kL}-2\sqrt{3}e^{\frac{1}{2}\left(\sqrt{3}+3i\right)kL}-3i+\sqrt{3}}.
\end{aligned}$$

Without going through the algebraic steps, we find

$$\frac{e^{i\alpha^2kL}}{\left(\sqrt{3}+3i\right)e^{\sqrt{3}kL}}+\frac{\alpha e^{ikL}}{2\sqrt{3}}e^{\frac{-1}{2}\left(\sqrt{3}+3i\right)kL}=0,$$

so that $\lim_{h\to 0}c_5=C_5$ as expected.

The remaining coefficient of $\hat{q}\left(\nu_2,0\right)$ in the $\partial\tilde{V}^-$ integral must converge to the coefficient of $\hat{q}\left(\alpha,0\right)$ in the $\partial\tilde{\Omega}^-$ integral. In the same manner, we expand the semi-discrete coefficient about $h=0$, so that after simplifications from the branch cut and manipulations, we derive the condition

$$\frac{-(\alpha+1)e^{i\alpha kL}}{\sqrt{3}-3i}+\frac{\alpha e^{ikL}}{2\sqrt{3}}e^{\frac{-1}{2}\left(\sqrt{3}+3i\right)kL}=0,$$

which can be shown to be true, implying the continuum limit holds. The reader is encouraged to continue confirming that every coefficient in the semi-discrete solution converges to their corresponding coefficient in the continuous solution via the steps outlined above – although tedious, it can be done. Therefore, we conclude that the continuum limit is achieved. On a final note, Figure 4.2.6 depicts how the poles of the semi-discrete problem approach the poles of the continuous one as $h\to 0$.

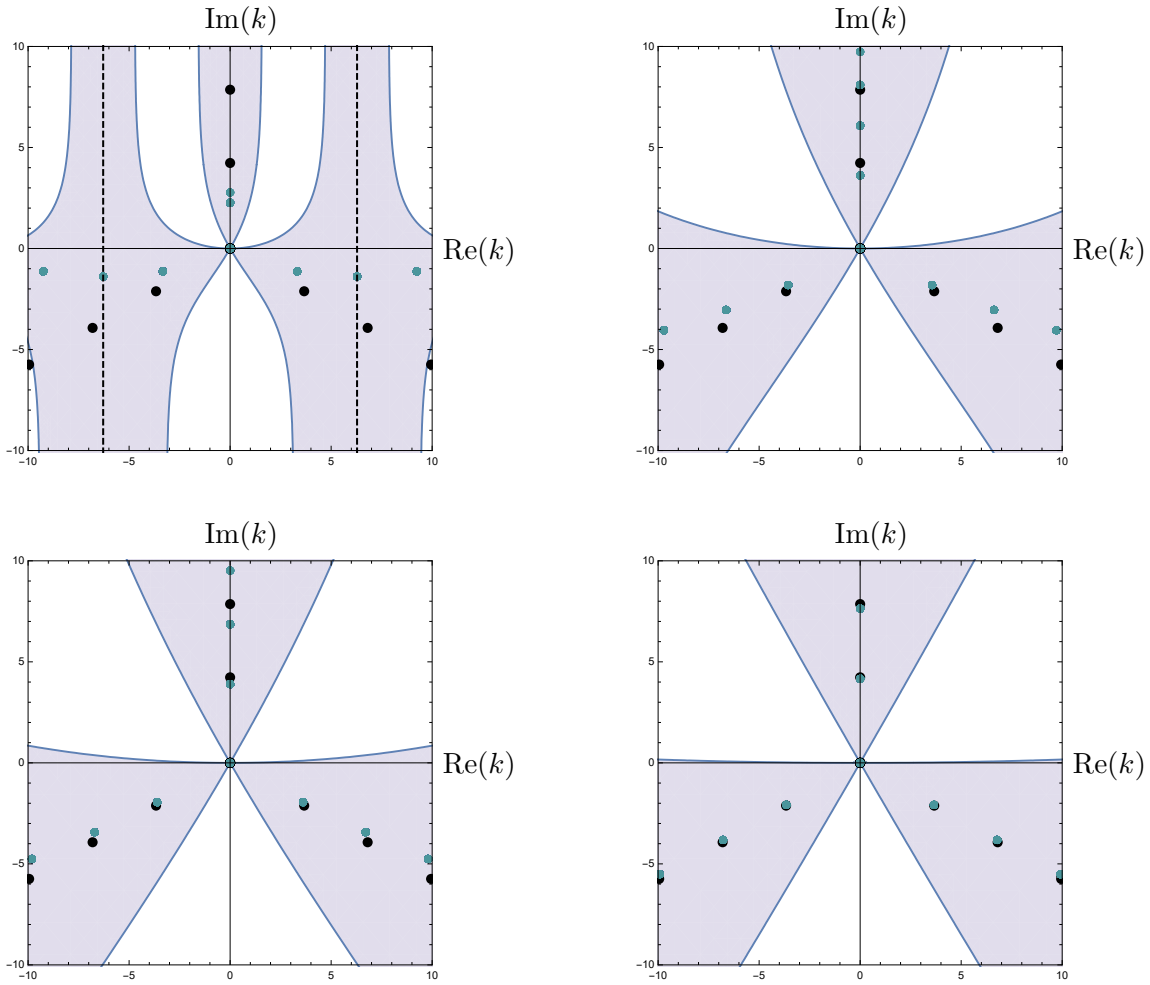

Figure 4.2.6: Roots of $\Lambda(k)$ (black) and $\tilde{\lambda}(k)$ (green) as $h \to 0$.

Chapter 5

ANALYTIC CONTINUATION

Together with Deconinck & Farkas, in [24] we produce solution formulas that are valid for x (and its discretized version x_n) outside of the original domain of definition for several linear IBVPs. As we have seen, the UTM and SD-UTM are applied systematically to linear PDEs, so we use these methods as a starting point to derive analytic continuation formulas. With them, we determine information at ghost points when solving linear problems with high-order finite-difference schemes or simply when Neumann data is given (see Chapter 6).

In the following sections, we present the derivations of those semi-discrete formulas for a handful of half-line problems. Although omitted, we could apply these steps to higher-order problems like those discussed in Chapter 4.

5.1 Advection Equations

5.1.1 Backward Discretization of $q_t = -c\,q_x$

We return to the advection problem (2.1.11) on the half-line with wave-speed $c > 0$ in Section 2.1.2. Discretizing the spacial derivative q_x using the standard backward stencil (2.1.12) gives solution (2.1.16):

$$q_n(T) = \frac{1}{2\pi}\int_{-\pi/h}^{\pi/h} e^{iknh}e^{-WT}\hat{q}(k,0)\,dk \;+\; \frac{c}{2\pi}\int_{-\pi/h}^{\pi/h} e^{ik(n-1)h}e^{-WT}f_0\,dk,$$

with dispersion relation (2.1.14). According to Figure 2.1.3, setting $n \to -n$ for $n \in \mathbb{Z}^+$ allows us to deform both integrals arbitrarily below the real line, such that $q_{-n}(T) = 0$. Note that in the continuum limit, (2.1.16) converges to (2.1.17), where one can also show $q(-x,T) = 0$ for $x > 0$.

Let us look at the first integral term of solution (2.1.16). Substituting the definition of $\hat{q}(k,0)$ gives us

$$\frac{1}{2\pi}\int_{-\pi/h}^{\pi/h} e^{iknh}e^{-WT}\hat{q}(k,0)\,dk = \sum_{m=1}^{\infty}\left[\frac{h}{2\pi}\int_{-\pi/h}^{\pi/h} e^{ik(n-m)h}e^{-WT}\,dk\right]q_m(0).$$

Making the substitution $z = e^{ikh}$ into the integral produces

$$\begin{aligned}\frac{h}{2\pi}\int_{-\pi/h}^{\pi/h} e^{ik(n-m)h}e^{-WT}\,dk &= \frac{1}{2\pi i}\oint_{|z|=1} z^{n-m-1}\exp\left[-c\left(\frac{1-z^{-1}}{h}\right)T\right]\,dz\\ &= e^{-cT/h}\operatorname*{Res}_{z=0}\left\{z^{n-m-1}\exp\left(\frac{cT}{h}\frac{1}{z}\right)\right\}.\end{aligned}$$

Expanding the exponential, we see that

$$z^{n-m-1}\exp\left(\frac{cT}{h}\,\frac{1}{z}\right)=z^{n-m-1}\sum_{\ell=0}^{\infty}\left(\frac{cT}{h}\right)^{\ell}\frac{z^{-\ell}}{\ell!}=\sum_{\ell=0}^{\infty}\left(\frac{cT}{h}\right)^{\ell}\frac{z^{-\ell+n-m-1}}{\ell!}.$$

The z^{-1} term occurs when $\ell=n-m$, so that the residue reads as

$$\frac{h}{2\pi}\int_{-\pi/h}^{\pi/h}e^{ik(n-m)h}e^{-WT}\,dk=e^{-cT/h}\left(\frac{cT}{h}\right)^{n-m}\frac{1}{(n-m)!}.$$

Hence,

$$\frac{1}{2\pi}\int_{-\pi/h}^{\pi/h}e^{iknh}e^{-WT}\hat{q}(k,0)\,dk=e^{-cT/h}\sum_{m=1}^{\infty}\left(\frac{cT}{h}\right)^{n-m}\frac{q_m(0)}{(n-m)!}.$$

We follow a similar procedure for the second integral term of solution (2.1.16), except here we substitute the definition of $f_0(W,T)$:

$$\frac{c}{2\pi}\int_{-\pi/h}^{\pi/h}e^{ik(n-1)h}e^{-WT}f_0\,dk=c\int_0^T\left[\frac{1}{2\pi}\int_{-\pi/h}^{\pi/h}e^{ik(n-1)h}e^{-W(T-t)}\,dk\right]u(t)\,dt.$$

With $z=e^{ikh}$, the inner integral becomes

$$\begin{aligned}\frac{1}{2\pi}\int_{-\pi/h}^{\pi/h}e^{ik(n-1)h}e^{-W(T-t)}\,dk&=\frac{1}{2\pi ih}\oint_{|z|=1}z^{n-2}e^{-W(T-t)}\,dz\\&=\frac{e^{-c(T-t)/h}}{h}\operatorname*{Res}_{z=0}\left\{z^{n-2}\exp\left(\frac{c(T-t)}{h}\,\frac{1}{z}\right)\right\}\\&=\frac{e^{-c(T-t)/h}}{h}\left(\frac{c(T-t)}{h}\right)^{n-1}\frac{1}{(n-1)!},\end{aligned}$$

and then,

$$\frac{c}{2\pi}\int_{-\pi/h}^{\pi/h}e^{ik(n-1)h}e^{-WT}f_0\,dk=\frac{c}{h(n-1)!}\int_0^T e^{-c(T-t)/h}\left(\frac{c(T-t)}{h}\right)^{n-1}u(t)\,dt.$$

Therefore, solution (2.1.16) is rewritten as

$$q_n(T)=e^{-cT/h}\sum_{m=1}^{\infty}\left(\frac{cT}{h}\right)^{n-m}\frac{q_m(0)}{(n-m)!}\;+\;I(n,T),\tag{5.1.1}$$

where

$$I(n,T)=\frac{c}{h(n-1)!}\int_0^T e^{-c(T-t)/h}\left(\frac{c(T-t)}{h}\right)^{n-1}u(t)\,dt.$$

Here, $q_{-n}(T)=0$ still, so a closer look at the formulation is required. The first term is rewritten using $1/(n-m)!=1/\Gamma(n-m+1)$, which may be evaluated for $n<0$. Since $1/\Gamma(\alpha)$ has simple

zeros at nonpositive integers α, the first term does not contribute for $n < 0$. We focus on the second term. With the substitution $s = c(T-t)/h$, we obtain

$$\begin{aligned} I(n,T) &= \frac{1}{(n-1)!}\int_0^{cT/h} e^{-s}s^{n-1}u\left(T-\frac{h}{c}s\right)\,ds \\ &= \frac{1}{(n-1)!}\int_0^{cT/h} e^{-s}s^{n-1}\sum_{\ell=0}^{\infty}\frac{u^{(\ell)}(T)(-1)^{\ell}}{\ell!}\left(\frac{h}{c}\right)^{\ell}s^{\ell}\,ds \\ &= \frac{1}{(n-1)!}\sum_{\ell=0}^{\infty}\frac{u^{(\ell)}(T)(-1)^{\ell}}{\ell!}\left(\frac{h}{c}\right)^{\ell}\int_0^{cT/h} e^{-s}s^{n+\ell-1}\,ds \\ I(n,T) &= \frac{1}{\Gamma(n)}\sum_{\ell=0}^{\infty}\frac{u^{(\ell)}(T)(-1)^{\ell}}{\ell!}\left(\frac{h}{c}\right)^{\ell}\gamma\left(n+\ell,\frac{cT}{h}\right), \end{aligned}$$

where $\gamma(\alpha, y)$ is the lower incomplete gamma function. Now, (5.1.1) is written as

$$q_n(T) = e^{-cT/h}\sum_{m=1}^{\infty}\left(\frac{cT}{h}\right)^{n-m}\frac{q_m(0)}{(n-m)!} + \sum_{\ell=0}^{\infty}\frac{u^{(\ell)}(T)(-1)^{\ell}}{\ell!}\left(\frac{h}{c}\right)^{\ell}\frac{\gamma\left(n+\ell,\frac{cT}{h}\right)}{\Gamma(n)}, \tag{5.1.2}$$

for $n \geq 1$. Note that the representation above is only valid for $\ell \geq 1-n$ and nonzero for $n \geq 1$ due to the ratio $\gamma(n+\ell, cT/h)/\Gamma(n)$. To evaluate the above expression at any $n \in \mathbb{Z}$, we must rewrite this ratio. Recursively applying $\Gamma(k+1) = k\,\Gamma(k)$, we find

$$\Gamma(a-b) = (a-b-1)(a-b-2)\cdot\ldots\cdot(-b)\,\Gamma(-b) = \frac{(-1)^a\,\Gamma(b+1)\,\Gamma(-b)}{\Gamma(b-a+1)}. \tag{5.1.3}$$

In addition, we derive a power series expression for $\gamma(a,y)$ by expanding the exponential in the definition:

$$\begin{aligned} \gamma(a,y) &= \int_0^y t^{a-1}e^{-t}\,dt = \sum_{k=0}^{\infty}\frac{(-1)^k}{k!}\int_0^y t^{a+k-1}\,dt = \sum_{k=0}^{\infty}\frac{(-1)^k}{k!}\cdot\frac{y^{a+k}}{a+k} \\ &= \sum_{k=0}^{\infty}\frac{(-1)^k\,y^{a+k}\,\Gamma(a+k)}{k!\,\Gamma(a+k+1)}. \end{aligned} \tag{5.1.4}$$

Combining (5.1.3) and (5.1.4) with $y = cT/h$, we have

$$\begin{aligned}
\frac{\gamma(n+\ell, y)}{\Gamma(n)} &= \frac{1}{\Gamma(n)} \sum_{k=0}^{\infty} \frac{(-1)^k\, y^{n+\ell+k}\, \Gamma(n+\ell+k)}{k!\, \Gamma(n+\ell+k+1)} \\
&= \sum_{k=0}^{\infty} \frac{(-1)^k\, y^{n+\ell+k}}{k!\, \Gamma(n+\ell+k+1)} \cdot \frac{\Gamma(\ell+k+n)}{\Gamma(n)} \\
&= \sum_{k=0}^{\infty} \frac{(-1)^k\, y^{n+\ell+k}}{k!\, \Gamma(n+\ell+k+1)} \cdot \frac{(-1)^{k+\ell}\, \Gamma(1-n)\, \Gamma(n)}{\Gamma(1-n-k-\ell)\, \Gamma(n)} \\
&= (-1)^{\ell} \sum_{k=0}^{\infty} \frac{y^{n+\ell+k}\, \Gamma(1-n)}{k!\, \Gamma(1+n+k+\ell)\, \Gamma(1-n-k-\ell)} \\
&= \frac{(-1)^{\ell}\, y^{n+\ell-n-\ell}\, \Gamma(1-n)}{(-n-\ell)!}, \\
\frac{\gamma(n+\ell, y)}{\Gamma(n)} &= \frac{(-1)^{\ell}\, \Gamma(1-n)}{\Gamma(1-n-\ell)!}.
\end{aligned}$$

This representation is now valid for $n \geq 0$ and nonzero for $\ell \leq -n$. Hence, treating the evaluation as a limiting process for any $n \in \mathbb{Z}$,

$$\lim_{\alpha \to n} q_{\alpha}(T) = \lim_{\alpha \to n} \left[e^{-cT/h} \sum_{m=1}^{\infty} \left(\frac{cT}{h}\right)^{\alpha-m} \frac{q_m(0)}{(\alpha-m)!} + \sum_{\ell=0}^{\infty} \frac{u^{(\ell)}(T)\,(-1)^{\ell}}{\ell!} \left(\frac{h}{c}\right)^{\ell} \frac{\gamma\left(\alpha+\ell, \frac{cT}{h}\right)}{\Gamma(\alpha)} \right]$$

$$\Rightarrow \quad q_n(T) = e^{-cT/h} \sum_{m=1}^{\infty} \left(\frac{cT}{h}\right)^{n-m} \frac{q_m(0)}{(n-m)!} + \sum_{\ell=0}^{\infty} \frac{u^{(\ell)}(T)\,(-1)^{\ell}}{\ell!} \left(\frac{h}{c}\right)^{\ell} \lim_{\alpha \to n} \frac{\gamma\left(\alpha+\ell, \frac{cT}{h}\right)}{\Gamma(\alpha)}, \quad (5.1.5)$$

where

$$\lim_{\alpha \to n} \frac{\gamma\left(\alpha+\ell, \frac{cT}{h}\right)}{\Gamma(\alpha)} = \begin{cases} \dfrac{\gamma\left(n+\ell, \frac{cT}{h}\right)}{\Gamma(n)}, & \ell \geq 1-n \quad \text{and} \quad n \geq 1, \\ \dfrac{(-1)^{\ell}\Gamma(1-n)}{\Gamma(1-n-\ell)}, & n \leq 0 \quad \text{and} \quad \ell \leq -n, \\ 0, & \text{otherwise.} \end{cases}$$

Then,

$$I(n,T) = \begin{cases} \displaystyle\sum_{\ell=0}^{-n} \frac{u^{(\ell)}(T)\,(-1)^{\ell}}{\ell!} \left(\frac{h}{c}\right)^{\ell} \cdot \frac{(-1)^{\ell}\Gamma(1-n)}{\Gamma(1-n-\ell)} = \sum_{\ell=0}^{-n} \frac{u^{(\ell)}(T)}{\ell!} \left(\frac{h}{c}\right)^{\ell} \frac{\Gamma(1-n)}{\Gamma(1-n-\ell)}, & n \leq 0 \\ \displaystyle\sum_{\ell=\max(1-n,0)}^{\infty} \frac{u^{(\ell)}(T)\,(-1)^{\ell}}{\ell!} \left(\frac{h}{c}\right)^{\ell} \cdot \frac{\gamma\left(n+\ell, \frac{cT}{h}\right)}{\Gamma(n)} = \sum_{\ell=0}^{\infty} \frac{u^{(\ell)}(T)\,(-1)^{\ell}}{\ell!} \left(\frac{h}{c}\right)^{\ell} \frac{\gamma\left(n+\ell, \frac{cT}{h}\right)}{\Gamma(n)}, & n \geq 1. \end{cases}$$

Now, we have the solution $q_n(T)$ for $n \geq 1$ as written in (5.1.2) and the solution $q_{-n}(T)$ for $n \geq 0$ as

$$q_{-n}(T) = I(-n,T) = \sum_{\ell=0}^{n} \frac{u^{(\ell)}(T)}{\ell!} \left(\frac{h}{c}\right)^{\ell} \frac{\Gamma(1+n)}{\Gamma(1+n-\ell)}. \quad (5.1.6)$$

Since (5.1.2) originates from (2.1.16), we combine both solutions (2.1.16) and (5.1.6) to create a formulation valid for all $n \in \mathbb{Z}$ as

$$\begin{aligned} q_n(T) = \frac{1}{2\pi}\int_{-\pi/h}^{\pi/h} e^{iknh}e^{-WT}\hat{q}(k,0)\,dk \;+\; \frac{c}{2\pi}\int_{-\pi/h}^{\pi/h} e^{ik(n-1)h}e^{-WT}f_0\,dk \\ + \sum_{\ell=0}^{-n}\frac{u^{(\ell)}(T)}{\ell!}\left(\frac{h}{c}\right)^{\ell}\frac{\Gamma(1-n)}{\Gamma(1-n-\ell)}, \end{aligned} \tag{5.1.7}$$

where the integral terms only contribute for $n \geq 1$ and the sum only contributes for $n \leq 0$.

Note that $q_0(T) = u(T)$, and, like the true continuous solution

$$q(-x,T) = u\left(T + \tfrac{x}{c}\right), \quad x > 0 \tag{5.1.8}$$

to this advection equation, the negative half-line solution (5.1.6) depends on only the boundary condition. Let us show that we recover (5.1.8) by taking $h \to 0$ of (5.1.6). By recursively applying $\Gamma(z+1) = z\Gamma(z)$, we have

$$f(n,\ell) = \frac{\Gamma(1+n)}{\Gamma(1+n-\ell)} = \prod_{p=0}^{\ell-1}(n-p) = \begin{cases} 1, & \ell = 0, \\ \displaystyle\sum_{p=0}^{\ell-1} a_p n^{p+1}, & \ell \geq 1, \end{cases}$$

such that $f(n,\ell)$ is a polynomial in n of degree ℓ with leading coefficient $a_{\ell-1} = 1$. Hence,

$$\begin{aligned} q_{-n}(T) &= \sum_{\ell=0}^{n}\frac{u^{(\ell)}(T)}{\ell!}\left(\frac{h}{c}\right)^{\ell} f(n,\ell) \\ &= \sum_{\ell=0}^{n}\frac{u^{(\ell)}(T)}{\ell!}\left(\frac{h}{c}\right)^{\ell}\left(n^{\ell} + a_{\ell-2}n^{\ell-1} + \ldots\right) \\ &= \sum_{\ell=0}^{n}\frac{u^{(\ell)}(T)}{\ell!}\left[\left(\frac{nh}{c}\right)^{\ell} + a_{\ell-2}\left(\frac{h}{c}\right)\left(\frac{nh}{c}\right)^{\ell-1} + \ldots\right], \end{aligned}$$

such that taking $h \to 0$ gives

$$\begin{aligned} \lim_{h\to 0} q_{-n}(T) &= \lim_{h\to 0}\sum_{\ell=0}^{n}\frac{u^{(\ell)}(T)}{\ell!}\left[\left(\frac{nh}{c}\right)^{\ell} + a_{\ell-2}\left(\frac{h}{c}\right)\left(\frac{nh}{c}\right)^{\ell-1} + \ldots\right] \\ \Rightarrow \quad q(-x,T) &= \sum_{\ell=0}^{\infty}\frac{u^{(\ell)}(T)}{\ell!}\left(\frac{x}{c}\right)^{\ell} = u\left(T + \tfrac{x}{c}\right). \end{aligned}$$

Figure 5.1.1 depicts the semi-discrete UTM solutions for $n \in \mathbb{Z}$ with formulas (2.1.16) and (5.1.6) on the left and formula (5.1.7) on the right with $h = 0.008$ for the IBVP

$$\begin{cases} q_t = -q_x, & x > 0,\ t > 0, \\ q(x,0) = \left(\dfrac{\sin(4\pi x)+1}{2}\right)e^{-2x}, & x > 0, \\ q(0,t) = \dfrac{1}{2} + (1-2\pi)te^{-t}, & t > 0. \end{cases} \tag{5.1.9}$$

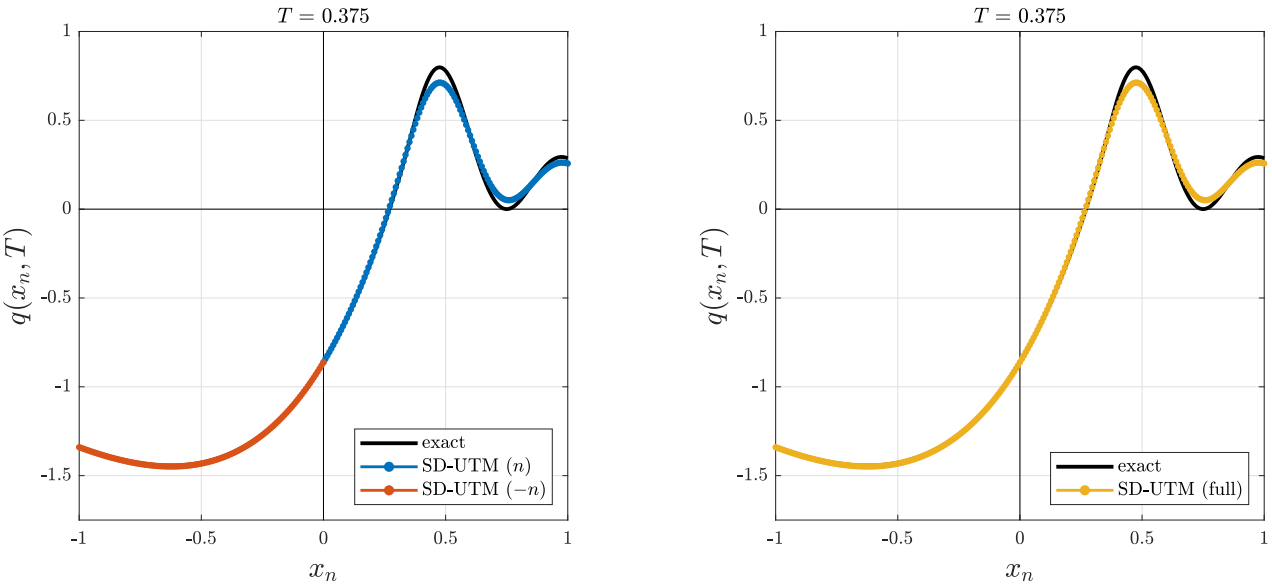

Figure 5.1.1: Extensions of half-line solution (2.1.16).

5.1.2 Centered Discretization of $q_t = -c\,q_x$

Next we study discretizing q_x using the standard centered stencil from Section 2.1.3 with dispersion relation (2.1.21) and nontrivial symmetry $\nu_1(k) = -k - \pi/h$. The SD-UTM solution (2.1.25) is

$$q_n(T) = \frac{1}{2\pi}\int_{-\pi/h}^{\pi/h} e^{iknh}e^{-WT}\left[\hat{q}(k,0) - \hat{q}\left(\nu_1,0\right)\right]\,dk + \frac{c}{2\pi}\int_{-\pi/h}^{\pi/h} e^{iknh}e^{-WT}\cos\left(kh\right)f_0\,dk.$$

With this representation, one can show that $q_{-n}(T) = (-1)^{n+1}q_n(T)$ for $n \in \mathbb{Z}^+$.

Like in the previous section, we substitute the definitions for $\hat{q}(k,0)$ and $\hat{q}\left(\nu_1,0\right)$ into the first integral term of (2.1.25) to obtain

$$\frac{1}{2\pi}\int_{-\pi/h}^{\pi/h} e^{iknh}e^{-WT}\left[\hat{q}(k,0) - \hat{q}\left(\nu_1,0\right)\right]\,dk = \sum_{m=1}^{\infty} I(n,T,m)q_m(0),$$

where

$$\begin{aligned}
I(n,T,m) &= \frac{h}{2\pi}\int_{-\pi/h}^{\pi/h} e^{iknh}e^{-WT}\left(e^{-ikmh}-e^{-i\nu_1 mh}\right)dk \\
&= \frac{h}{2\pi}\int_{-\pi/h}^{\pi/h} e^{ik(n-m)h}e^{-WT}\,dk - \frac{(-1)^m h}{2\pi}\int_{-\pi/h}^{\pi/h} e^{ik(n+m)h}e^{-WT}\,dk \\
&= \frac{1}{2\pi i}\oint_{|z|=1} z^{n-m-1}\exp\left[\frac{-cT}{2h}\left(z-\frac{1}{z}\right)\right]dz - \frac{(-1)^m}{2\pi i}\oint_{|z|=1} z^{n+m-1}\exp\left[\frac{-cT}{2h}\left(z-\frac{1}{z}\right)\right]dz \\
&= (-1)^{m-n}J\left(m-n,\frac{cT}{h}\right) - (-1)^m J\left(m+n,\frac{cT}{h}\right),
\end{aligned}$$

after making the substitution $z = e^{ikh}$ to use the Bessel function of the first kind:

$$J(n,a) = \frac{1}{2\pi i}\oint_{|z|=1}\exp\left[\frac{a}{2}\left(z-\frac{1}{z}\right)\right]\frac{1}{z^{n+1}}\,dz = \sum_{\ell=0}^{\infty}\frac{(-1)^\ell}{\ell!\,\Gamma(\ell+n+1)}\left(\frac{a}{2}\right)^{2\ell+n},$$

with the two vital properties $J(-n,a) = J(n,-a) = (-1)^n J(n,a)$ for $n \in \mathbb{Z}$ and $(2n/a)J(n,a) = J(n-1,a) + J(n+1,a)$. Hence,

$$\frac{1}{2\pi}\int_{-\pi/h}^{\pi/h} e^{iknh}e^{-WT}\left[\hat{q}(k,0) - \hat{q}\,(\nu_1,0)\right]dk = \sum_{m=1}^{\infty}(-1)^m\left[(-1)^n J\left(m-n,\frac{cT}{h}\right) - J\left(m+n,\frac{cT}{h}\right)\right]q_m(0).$$

The second integral term of (2.1.25) is similarly rewritten as

$$\begin{aligned}
\frac{c}{2\pi}\int_{-\pi/h}^{\pi/h} e^{iknh}e^{-WT}\cos(kh)\,f_0\,dk &= \frac{c}{h}\int_0^T\left[\frac{h}{2\pi}\int_{-\pi/h}^{\pi/h} e^{iknh}e^{-W(T-t)}\left(\frac{e^{ikh}+e^{-ikh}}{2}\right)dk\right]u(t)\,dt \\
&= \frac{c}{2h}\int_0^T\left[J\left(-n-1,\frac{-c(T-t)}{h}\right) + J\left(-n+1,\frac{-c(T-t)}{h}\right)\right]u(t)\,dt \\
&= n\int_0^T J\left(n,\frac{c(T-t)}{h}\right)\frac{u(t)}{T-t}\,dt.
\end{aligned}$$

Therefore, solution (2.1.25) is written as

$$q_n(T) = \sum_{m=1}^{\infty}(-1)^m\left[(-1)^n J\left(m-n,\frac{cT}{h}\right) - J\left(m+n,\frac{cT}{h}\right)\right]q_m(0) + M(n,T), \tag{5.1.10}$$

with

$$M(n,T) = n\int_0^T J\left(n,\frac{c(T-t)}{h}\right)\frac{u(t)}{T-t}\,dt.$$

Note that setting $n \to -n$ for $n \in \mathbb{Z}^+$ gives

$$\begin{aligned}
q_{-n}(T) &= \sum_{m=1}^{\infty}(-1)^m\left[(-1)^{-n}J\left(m+n,\frac{cT}{h}\right) - J\left(m-n,\frac{cT}{h}\right)\right]q_m(0) - n\int_0^T J\left(-n,\frac{c(T-t)}{h}\right)\frac{u(t)}{T-t}\,dt \\
&= -(-1)^n\sum_{m=1}^{\infty}(-1)^m\left[(-1)^n J\left(m-n,\frac{cT}{h}\right) - J\left(m+n,\frac{cT}{h}\right)\right]q_m(0) - (-1)^n n\int_0^T J\left(n,\frac{c(T-t)}{h}\right)\frac{u(t)}{T-t}\,d \\
&= (-1)^{n+1}q_n(T).
\end{aligned}$$

One can show that further breaking apart the first term of (5.1.10) via the expansions of $J\left(m-n, cT/h\right)$ and $J\left(m+n, cT/h\right)$ does not provide a helpful representation when $n \to -n$ for $n \in \mathbb{Z}^+$. Let us take a closer look at the second term of (5.1.10) instead. Making use of $s = c(T-t)/h$ and expanding, we have

$$\begin{aligned}
M(n,T) &= n\int_0^{cT/h} \frac{J\left(n,s\right)}{s} u\left(T-\frac{h}{c}s\right)\,ds \\
&= n\int_0^{cT/h} \frac{J\left(n,s\right)}{s} \sum_{p=0}^{\infty} \frac{u^{(p)}(T)(-1)^p}{p!}\left(\frac{h}{c}\right)^p s^p\,ds \\
&= n\sum_{p=0}^{\infty} \frac{u^{(p)}(T)(-1)^p}{p!}\left(\frac{h}{c}\right)^p \int_0^{cT/h} J\left(n,s\right) s^{p-1}\,ds \\
&= \frac{n}{2^n}\sum_{p=0}^{\infty} \frac{u^{(p)}(T)(-1)^p}{p!}\left(\frac{h}{c}\right)^p \sum_{\ell=0}^{\infty} \frac{(-1)^\ell}{\ell!\,\Gamma(\ell+n+1)2^{2\ell}} \int_0^{cT/h} s^{2\ell+n+p-1}\,ds \\
&= n\left(\frac{cT}{2h}\right)^n \sum_{p=0}^{\infty} \frac{u^{(p)}(T)(-T)^p}{p!}\, L(n,T,p),
\end{aligned}$$

where

$$L(n,T,p) = \sum_{\ell=0}^{\infty} \frac{(-1)^\ell}{\ell!}\left(\frac{cT}{2h}\right)^{2\ell} \frac{1}{\Gamma(\ell+n+1)(2\ell+n+p)}.$$

Suppose $n \in \mathbb{Z}$ and assume $\ell \neq 0 \neq p$ for now. Then, $L(n,T,p) = 0$ for $\ell \leq -n-1$ and $\ell \neq (-n-p)/2$. When $\ell = (-n-p)/2$, $1/\Gamma(\ell+n+1) = 2\ell+n+p = 0$, so a careful consideration is in order. Applying relation (5.1.3), we find

$$\begin{aligned}
\frac{1}{\Gamma(\ell+n+1)(2\ell+n+p)} &= \frac{1}{\Gamma(\ell+n+1)} \cdot \Gamma(2\ell+n+p) \cdot \frac{1}{\Gamma(1+2\ell+n+p)} \\
&= \frac{(-1)^{\ell+p+1}\,\Gamma(-n-\ell)}{\Gamma(1-2\ell-n-p)\,\Gamma(1+2\ell+n+p)},
\end{aligned}$$

which is only valid for $\ell \leq -n-1$. In fact, the left hand-side is nonzero only for $n = -2\ell - p$ or $p = -2\ell - n$. Therefore, we can split the sum as

$$\begin{aligned}
L(n,T,p) &= \sum_{\ell=0}^{-n-1} \frac{(-1)^\ell}{\ell!}\left(\frac{cT}{2h}\right)^{2\ell} \cdot \frac{(-1)^{\ell+p+1}\,\Gamma(-n-\ell)}{\Gamma(1-2\ell-n-p)\,\Gamma(1+2\ell+n+p)} \\
&\quad + \sum_{\ell=\max(-n,0)}^{\infty} \frac{(-1)^\ell}{\ell!}\left(\frac{cT}{2h}\right)^{2\ell} \cdot \frac{1}{\Gamma(\ell+n+1)(2\ell+n+p)} \\
&= (-1)^{p+1} \sum_{\ell=0}^{-n-1} \frac{\Gamma(-n-\ell)}{\ell!\,\Gamma(1-2\ell-n-p)\,\Gamma(1+2\ell+n+p)}\left(\frac{cT}{2h}\right)^{2\ell} \\
&\quad + \sum_{\ell=\max(-n,0)}^{\infty} \frac{(-1)^\ell}{\ell!\,\Gamma(\ell+n+1)(2\ell+n+p)}\left(\frac{cT}{2h}\right)^{2\ell}.
\end{aligned}$$

Now $L(n,T,p)$ is valid for all $n \in \mathbb{Z}$. Returning to $M(n,T)$, we have

$$M(n,T) = -n\left(\frac{cT}{2h}\right)^n \sum_{p=0}^{\infty} \frac{u^{(p)}(T)\,T^p}{p!} \sum_{\ell=0}^{-n-1} \frac{\Gamma(-n-\ell)}{\ell!\,\Gamma(1-2\ell-n-p)\,\Gamma(1+2\ell+n+p)} \left(\frac{cT}{2h}\right)^{2\ell} + n\left(\frac{cT}{2h}\right)^n \sum_{p=0}^{\infty} \frac{u^{(p)}(T)(-T)^p}{p!} \sum_{\ell=\max(-n,0)}^{\infty} \frac{(-1)^\ell}{\ell!\,\Gamma(\ell+n+1)(2\ell+n+p)} \left(\frac{cT}{2h}\right)^{2\ell}.$$

The first coupled sums reduce to

$$\begin{aligned} -n\left(\frac{cT}{2h}\right)^n \sum_{p=0}^{\infty} \frac{u^{(p)}(T)\,T^p}{p!} \sum_{\ell=0}^{-n-1} \frac{\Gamma(-n-\ell)}{\ell!\,\Gamma(1-2\ell-n-p)\,\Gamma(1+2\ell+n+p)} \left(\frac{cT}{2h}\right)^{2\ell} \\ = -n\left(\frac{cT}{2h}\right)^n \sum_{\ell=0}^{-n-1} \frac{\Gamma(-n-\ell)}{\ell!} \left(\frac{cT}{2h}\right)^{2\ell} \sum_{p=0}^{\infty} \frac{u^{(p)}(T)\,T^p}{p!\,\Gamma(1-2\ell-n-p)\,\Gamma(1+2\ell+n+p)} \\ = -n\left(\frac{cT}{2h}\right)^n \sum_{\ell=0}^{-n-1} \frac{\Gamma(-n-\ell)}{\ell!} \left(\frac{cT}{2h}\right)^{2\ell} \cdot \frac{u^{(-2\ell-n)}(T)\,T^{-2\ell-n}}{(-2\ell-n)!} \\ = -n\left(\frac{c}{2h}\right)^n \sum_{\ell=0}^{-n/2} u^{(-2\ell-n)}(T) \left(\frac{c}{2h}\right)^{2\ell} \frac{(-n-\ell-1)!}{\ell!\,(-2\ell-n)!}, \end{aligned}$$

so that

$$\begin{aligned} M(n,T) = -n\left(\frac{c}{2h}\right)^n \sum_{\ell=0}^{-n/2} u^{(-2\ell-n)}(T) \left(\frac{c}{2h}\right)^{2\ell} \frac{(-n-\ell-1)!}{\ell!\,(-2\ell-n)!} \\ + n\left(\frac{cT}{2h}\right)^n \sum_{p=0}^{\infty} \frac{u^{(p)}(T)(-T)^p}{p!} \sum_{\ell=\max(-n,0)}^{\infty} \frac{(-1)^\ell}{\ell!\,\Gamma(\ell+n+1)(2\ell+n+p)} \left(\frac{cT}{2h}\right)^{2\ell}. \end{aligned}$$

Therefore, solution (5.1.10) becomes

$$\begin{aligned} q_n(T) = \frac{1}{2\pi} \int_{-\pi/h}^{\pi/h} e^{iknh} e^{-WT} \left[\hat{q}(k,0) - \hat{q}\,(\nu_1,0)\right] dk \\ - n\left(\frac{c}{2h}\right)^n \sum_{\ell=0}^{-n/2} u^{(-2\ell-n)}(T) \left(\frac{c}{2h}\right)^{2\ell} \frac{(-n-\ell-1)!}{\ell!\,(-2\ell-n)!} \\ + n\left(\frac{cT}{2h}\right)^n \sum_{p=0}^{\infty} \frac{u^{(p)}(T)(-T)^p}{p!} \sum_{\ell=\max(-n,0)}^{\infty} \frac{(-1)^\ell}{\ell!\,\Gamma(\ell+n+1)(2\ell+n+p)} \left(\frac{cT}{2h}\right)^{2\ell}, \end{aligned} \tag{5.1.11}$$

where we replaced the initial condition sum from (5.1.10) by the integral in (2.1.25). If $n \in \mathbb{Z}^+$, then the representation (5.1.11) reduces to (5.1.10), and hence, the original solution (2.1.25), since the first sum of (5.1.11) vanishes and $\max(-n,0) = 0$. In addition, the representation (5.1.11) allows us to recover the boundary condition at $n = 0$. Here, the first two terms vanish. Let us expand the

third sum, where we choose to start the ℓ-indexed sum at $\ell = 0$, but we could similarly repeat the following with $\ell = -n$ as the starting index. We have

$$
\begin{aligned}
n\left(\frac{cT}{2h}\right)^n &\sum_{p=0}^{\infty}\frac{u^{(p)}(T)(-T)^p}{p!}\sum_{\ell=0}^{\infty}\frac{(-1)^\ell}{\ell!\,\Gamma(\ell+n+1)(2\ell+n+p)}\left(\frac{cT}{2h}\right)^{2\ell} \\
&= n\left(\frac{cT}{2h}\right)^n\left[\sum_{\ell=0}^{\infty}\frac{u(T)\,(-1)^\ell}{\ell!\,\Gamma(\ell+n+1)(2\ell+n)}\left(\frac{cT}{2h}\right)^{2\ell}\right. \\
&\qquad\left.+\sum_{p=1}^{\infty}\frac{u^{(p)}(T)(-T)^p}{p!}\sum_{\ell=0}^{\infty}\frac{(-1)^\ell}{\ell!\,\Gamma(\ell+n+1)(2\ell+n+p)}\left(\frac{cT}{2h}\right)^{2\ell}\right] \\
&= n\left(\frac{cT}{2h}\right)^n\left[\frac{u(T)}{\Gamma(n+1)n}+\sum_{\ell=1}^{\infty}\frac{u(T)\,(-1)^\ell}{\ell!\,\Gamma(\ell+n+1)(2\ell+n)}\left(\frac{cT}{2h}\right)^{2\ell}\right. \\
&\qquad\left.+\sum_{p=1}^{\infty}\frac{u^{(p)}(T)(-T)^p}{p!}\sum_{\ell=0}^{\infty}\frac{(-1)^\ell}{\ell!\,\Gamma(\ell+n+1)(2\ell+n+p)}\left(\frac{cT}{2h}\right)^{2\ell}\right] \\
&= \frac{u(T)}{\Gamma(n+1)}\left(\frac{cT}{2h}\right)^n + n\left(\frac{cT}{2h}\right)^n\sum_{\ell=1}^{\infty}\frac{u(T)\,(-1)^\ell}{\ell!\,\Gamma(\ell+n+1)(2\ell+n)}\left(\frac{cT}{2h}\right)^{2\ell} \\
&\quad + n\left(\frac{cT}{2h}\right)^n\sum_{p=1}^{\infty}\frac{u^{(p)}(T)(-T)^p}{p!}\sum_{\ell=0}^{\infty}\frac{(-1)^\ell}{\ell!\,\Gamma(\ell+n+1)(2\ell+n+p)}\left(\frac{cT}{2h}\right)^{2\ell}.
\end{aligned}
$$

Replacing the above into the representation (5.1.11) and setting $n = 0$ indeed gives $q_0(T) = u(T)$.

Let us treat the representation (5.1.11) with n and $-n$ separately for $n \in \mathbb{Z}^+$. With this restriction, we have

$$
\begin{aligned}
q_n(T) = \frac{1}{2\pi}&\int_{-\pi/h}^{\pi/h} e^{iknh}e^{-WT}\left[\hat{q}(k,0)-\hat{q}\,(\nu_1,0)\right]\,dk \\
&+ n\left(\frac{cT}{2h}\right)^n\sum_{p=0}^{\infty}\frac{u^{(p)}(T)(-T)^p}{p!}\sum_{\ell=0}^{\infty}\frac{(-1)^\ell}{\ell!\,\Gamma(\ell+n+1)(2\ell+n+p)}\left(\frac{cT}{2h}\right)^{2\ell},
\end{aligned}
\tag{5.1.12}
$$

and

$$
\begin{aligned}
q_{-n}(T) = \frac{1}{2\pi}&\int_{-\pi/h}^{\pi/h} e^{-iknh}e^{-WT}\left[\hat{q}(k,0)-\hat{q}\,(\nu_1,0)\right]\,dk \\
&+ n\left(\frac{c}{2h}\right)^{-n}\sum_{\ell=0}^{n/2}u^{(n-2\ell)}(T)\,\left(\frac{c}{2h}\right)^{2\ell}\frac{(n-\ell-1)!}{\ell!\,(n-2\ell)!} \\
&- n\left(\frac{cT}{2h}\right)^{-n}\sum_{p=0}^{\infty}\frac{u^{(p)}(T)(-T)^p}{p!}\sum_{\ell=n}^{\infty}\frac{(-1)^\ell}{\ell!\,\Gamma(\ell-n+1)(2\ell-n+p)}\left(\frac{cT}{2h}\right)^{2\ell}.
\end{aligned}
$$

Note that, with the re-indexing $\ell \to \ell - n$, the last term becomes

$$
\begin{aligned}
-n\left(\frac{cT}{2h}\right)^{-n}\sum_{p=0}^{\infty}\frac{u^{(p)}(T)(-T)^p}{p!}\sum_{\ell=n}^{\infty}\frac{(-1)^\ell}{\ell!\,\Gamma(\ell-n+1)(2\ell-n+p)}\left(\frac{cT}{2h}\right)^{2\ell}& \\
= -n\left(\frac{cT}{2h}\right)^{-n}\sum_{p=0}^{\infty}\frac{u^{(p)}(T)(-T)^p}{p!}\sum_{\ell=0}^{\infty}\frac{(-1)^{\ell+n}}{(\ell+n)!\,\Gamma(\ell+1)(2\ell+n+p)}\left(\frac{cT}{2h}\right)^{2\ell+2n}& \\
= (-1)^{n+1}n\left(\frac{cT}{2h}\right)^{n}\sum_{p=0}^{\infty}\frac{u^{(p)}(T)(-T)^p}{p!}\sum_{\ell=0}^{\infty}\frac{(-1)^{\ell}}{\Gamma(\ell+n+1)\,\ell!\,(2\ell+n+p)}\left(\frac{cT}{2h}\right)^{2\ell}&.
\end{aligned}
$$

Thus, using (5.1.12),

$$
\begin{aligned}
q_{-n}(T) = \frac{(-1)^{n+1}}{2\pi}\int_{-\pi/h}^{\pi/h} e^{iknh}e^{-WT}\left[\hat{q}(k,0)-\hat{q}\left(\nu_1,0\right)\right]\,dk& \\
+\,n\left(\frac{2h}{c}\right)^{n}\sum_{\ell=0}^{n/2}u^{(n-2\ell)}(T)\,\left(\frac{c}{2h}\right)^{2\ell}\frac{(n-\ell-1)!}{\ell!\,(n-2\ell)!}& \\
+\,(-1)^{n+1}n\left(\frac{cT}{2h}\right)^{n}\sum_{p=0}^{\infty}\frac{u^{(p)}(T)(-T)^p}{p!}\sum_{\ell=0}^{\infty}\frac{(-1)^{\ell}}{\Gamma(\ell+n+1)\,\ell!\,(2\ell+n+p)}\left(\frac{cT}{2h}\right)^{2\ell}&
\end{aligned}
$$

$$
\begin{aligned}
= (-1)^{n+1}\Bigg[\frac{1}{2\pi}\int_{-\pi/h}^{\pi/h} e^{iknh}e^{-WT}\left[\hat{q}(k,0)-\hat{q}\left(\nu_1,0\right)\right]\,dk& \\
+n\left(\frac{cT}{2h}\right)^{n}\sum_{p=0}^{\infty}\frac{u^{(p)}(T)(-T)^p}{p!}\sum_{\ell=0}^{\infty}\frac{(-1)^{\ell}}{\Gamma(\ell+n+1)\,\ell!\,(2\ell+n+p)}\left(\frac{cT}{2h}\right)^{2\ell}\Bigg]& \\
+\,n\left(\frac{2h}{c}\right)^{n}\sum_{\ell=0}^{n/2}u^{(n-2\ell)}(T)\,\left(\frac{c}{2h}\right)^{2\ell}\frac{(n-\ell-1)!}{\ell!\,(n-2\ell)!}&
\end{aligned}
$$

$$
q_{-n}(T) = (-1)^{n+1}q_n(T) \;+\; n\left(\frac{2h}{c}\right)^{n}\sum_{\ell=0}^{n/2}u^{(n-2\ell)}(T)\,\left(\frac{c}{2h}\right)^{2\ell}\frac{(n-\ell-1)!}{\ell!\,(n-2\ell)!}. \tag{5.1.13}
$$

Due to the entirely dispersive nature of the centered discretization (see Section 2.1.3), if the boundary function $u(t)$ and the initial condition $\phi(x)$ are not compatible (*i.e.* $u(t) \neq \phi(-ct)$), this solution exhibits "dispersive shock" behavior for $x_n < 0$. Because of the "dispersive" shock, the continuum limit for (5.1.13) will have a limit as $n \to \infty$ if and only if the initial and boundary conditions are compatible. The "dispersive shock" travels upwind at a speed of c. To illustrate this behavior, consider the IBVP (5.1.9) from the previous section. Figure 5.1.2 depicts the semi-discrete UTM solution with formulas (2.1.25) and (5.1.13) for $n > 0$ and $n < 0$, respectively, with $h = 0.04$ on the left and $h = 0.008$ on the right. Note that the oscillations do not diminish as $h \to 0$, implying

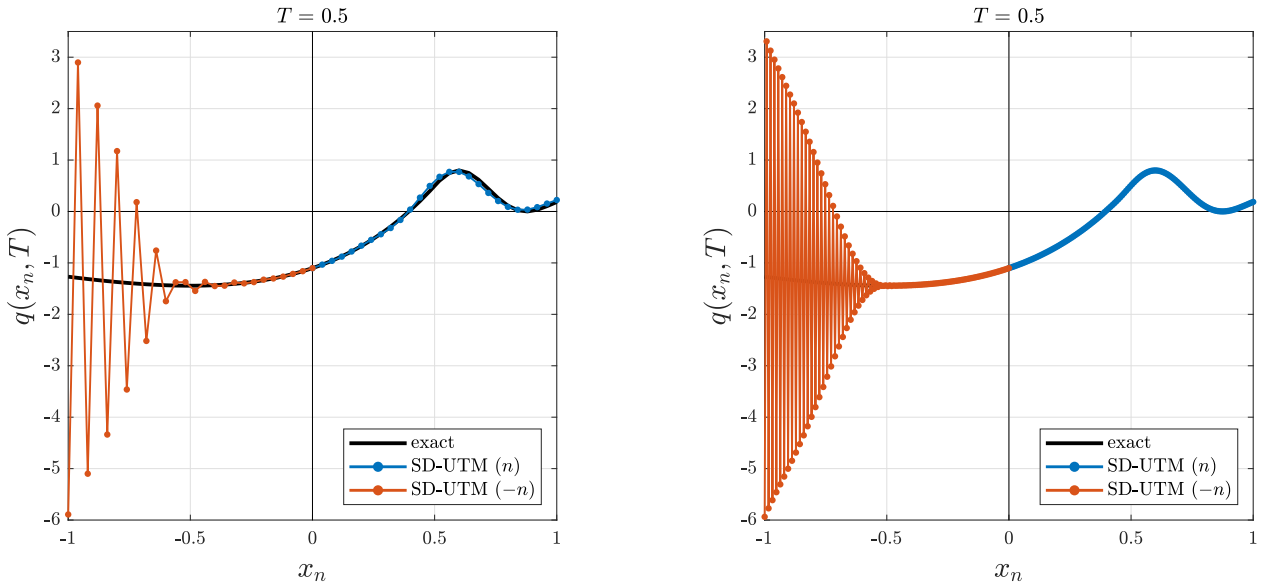

Figure 5.1.2: Extensions of half-line solution (2.1.25) for IBVP (5.1.9) with $h = 0.04$ (left) and $h = 0.008$ (right).

the growing error to the left of the $x = 0$ boundary is due to the choice in discretization – evidence this centered stencil is not the natural discretization for this PDE.

For $c < 0$, (2.1.11) does not specify a boundary condition, but the solution (2.1.25) still requires one, so we choose the compatible boundary condition $u(t) = \phi(-ct)$. Hence, for analytic $\phi(x)$, we will not see the "dispersive shock" behavior. However, if we start with a discontinuous (or non-analytic) $u_0(x)$ we see the "dispersive shock" for $x > 0$ ($n > 0$), demonstrating that this behavior is not a feature in the continuation formula (5.1.13), but a characterization of the inappropriate discretization (2.1.19) [43].

It is interesting to note that one can "average" out the "dispersive shock" wave to get the extension formula

$$q_{-n}(T) = \frac{n}{2} \sum_{k=0}^{n} u^{(k)}(T) \left(\frac{2h}{c}\right)^k \frac{\Gamma\left(\frac{n+k}{2}\right)}{k!\,\left(\frac{n-k}{2}\right)!}, \tag{5.1.14}$$

which is second-order accurate, but does not solve the discretized equation (2.1.19).

5.1.3 *Higher-Order One-Sided Discretization of* $q_t = -c\,q_x$

Applying the backward second-order discretization (2.1.26) to the IBVP (2.1.11) gives global relation (2.1.27), dispersion relation (2.1.28), and solution (2.1.33):

$$q_n(T) = \frac{1}{2\pi}\int_{-\pi/h}^{\pi/h} e^{iknh}e^{-WT}\hat{q}(k,0)\,dk + \frac{c}{2\pi}\int_{-\pi/h}^{\pi/h} e^{iknh}e^{-WT}\left[\left(\frac{3e^{-ikh}-e^{-2ikh}}{2}\right)f_0\right]dk$$
$$-\frac{1}{2\pi}\int_{-\pi/h}^{\pi/h} e^{ik(n-1)h}e^{-WT}\left(\frac{h}{2}\,V + \frac{h^2}{4}\,\tilde{V}\right)dk,$$

where $V(W,T)$ and $\tilde{V}(W,T)$ are the time transforms of $v(t) = u'(t)$ and $\tilde{v}(t) = u''(t)$, respectively. From Figure 2.1.7, one can show that (2.1.33) gives $q_{-n}(T) = 0$ for $n \in \mathbb{Z}^+$, similarly how (2.1.17) gives $q(-x,T) = 0$ for $x \in \mathbb{R}^+$. If we introduce

$$B_m(n,T,g) = \frac{1}{4\pi}\int_{-\pi/h}^{\pi/h} e^{ik(n-m)h-WT}G\,dk, \qquad G(W,T) = \int_0^T e^{Wt}g(t)\,dt, \tag{5.1.15}$$

for the boundary terms, then the semi-discrete solution is rewritten as

$$\begin{aligned} q_n(T) = {} & \frac{1}{2\pi}\int_{-\pi/h}^{\pi/h} e^{iknh}e^{-WT}\hat{u}(k,0)\,dk + 3cB_1(n,T,u) - cB_2(n,T,u) \\ & - hB_1(n,T,v) - \frac{h^2}{2c}B_1(n,T,\tilde{v}). \end{aligned} \tag{5.1.16}$$

Leaving the initial-condition as is, we focus on $B_m(n,T,g)$. We have

$$B_m(n,T,g) = \frac{1}{4\pi}\int_{-\pi/h}^{\pi/h} e^{ik(n-m)h-WT}\left[\int_0^T e^{Wt}g(t)\,dt\right]dk = \int_0^T I_m(n,T,t)g(t)\,dt,$$

with

$$\begin{aligned} I_m(n,T,t) &= \frac{1}{4\pi}\int_{-\pi/h}^{\pi/h} e^{ik(n-m)h-W(T-t)}\,dk = \frac{1}{4\pi}\oint_{|z|=1} z^{n-m}e^{-W(T-t)}\,\frac{dz}{ihz} \\ &= \frac{e^{\frac{-3c(T-t)}{2h}}}{2h}\operatorname*{Res}_{z=0}\left\{z^{n-m-1}\exp\left[\left(-z^{-2}+4z^{-1}\right)\frac{c(T-t)}{2h}\right]\right\} \\ &= \frac{e^{\frac{-3c(T-t)}{2h}}}{2h}\sum_{k=0}^{\frac{n-m}{2}}\frac{(-1)^k}{2^{2k}k!(n-m-2k)!}\left(\frac{2c(T-t)}{h}\right)^{n-m-k}. \end{aligned}$$

A tedious calculation shows that there is no contribution if $n-m$ is odd. Using the substitution

$s = 3c(T-t)/(2h)$ and expanding about $h = 0$, we have

$$\begin{aligned}
B_m(n,T,g) &= \int_0^T \left[\frac{e^{\frac{-3c(T-t)}{2h}}}{2h} \sum_{k=0}^{\frac{n-m}{2}} \frac{(-1)^k}{2^{2k}k!(n-m-2k)!} \left(\frac{2c(T-t)}{h}\right)^{n-m-k} \right] g(t)\,dt \\
&= \frac{1}{3c} \sum_{k=0}^{\frac{n-m}{2}} \frac{(-1)^k}{2^{2k}k!(n-m-2k)!} \left(\frac{4}{3}\right)^{n-m-k} \left[\int_0^{\frac{3cT}{2h}} e^{-s} s^{n-m-k} g\left(T - \frac{2h}{3c}s\right)\,ds \right] \\
&= \frac{1}{3c} \sum_{k=0}^{\frac{n-m}{2}} \frac{(-1)^k}{2^{2k}k!(n-m-2k)!} \left(\frac{4}{3}\right)^{n-m-k} \sum_{p=0}^{\infty} \frac{g^{(p)}(T)(-1)^p}{p!} \left(\frac{2h}{3c}\right)^p \int_0^{\frac{3cT}{2h}} e^{-s} s^{n-m-k+p}\,ds \\
&= \frac{1}{3c} \sum_{k=0}^{\frac{n-m}{2}} \frac{(-1)^k}{2^{2k}k!(n-m-2k)!} \left(\frac{4}{3}\right)^{n-m-k} \sum_{p=0}^{\infty} \frac{g^{(p)}(T)(-1)^p}{p!} \left(\frac{2h}{3c}\right)^p \gamma\left(n-m-k+p+1, \frac{3cT}{2h}\right).
\end{aligned}$$

Applying relations (5.1.3) and the power series of the lower incomplete gamma function (5.1.4), we have

$$\lim_{\alpha \to n} \frac{\gamma\left(\alpha - m - k + p + 1, \frac{3cT}{2h}\right)}{\Gamma(\alpha - m - 2k + 1)} = \begin{cases} \dfrac{\gamma\left(n-m-k+p+1, \frac{3cT}{2h}\right)}{\Gamma(n-m-2k+1)}, & p \geq k-n+m,\ k \leq \frac{n-m}{2}, \\ \dfrac{(-1)^{k+p}\Gamma(m+2k-n)}{\Gamma(m+k-p-n)}, & k \geq \frac{1+n-m}{2},\ p \leq m+k-n-1, \\ 0, & \text{otherwise.} \end{cases} \tag{5.1.17}$$

Collecting the summands in $S(n,T,k,p)$ and relaxing the upper bound on the summation over k (again by adding zero terms), we write

$$\begin{aligned}
B_m(n,T,g) &= \sum_{k=0}^{\infty} \sum_{p=0}^{\infty} S(n,T,k,p) \\
&= \left(\sum_{k=0}^{\frac{n-m}{2}} + \sum_{k=\max\left(\frac{1+n-m}{2},0\right)}^{\infty} \right) \left(\sum_{p=0}^{m+k-n-1} + \sum_{p=\max(k-n+m,0)}^{\infty} \right) S(n,T,k,p) \\
&= \sum_{k=0}^{\frac{n-m}{2}} \sum_{p=\max(k-n+m,0)}^{\infty} S(n,T,k,p) + \sum_{k=\max\left(\frac{1+n-m}{2},0\right)}^{\infty} \sum_{p=0}^{m+k-n-1} S(n,T,k,p),
\end{aligned}$$

where the other terms are shown to vanish. For $n > 0$, the second of the double sums above vanishes, and the first can be rewritten in the integral form from (2.1.33). For $n < 0$, the first pair vanishes.

We let $n \to -n$ for $n > 0$ from here on. Relaxing the bounds (re-introducing zero contributions),

$$\begin{aligned}
B_m(-n,T,g) &= \sum_{k=\max\left(\frac{1-n-m}{2},0\right)}^{\infty} \sum_{p=0}^{m+k+n-1} S(-n,T,k,p) \\
&= \frac{1}{3c}\sum_{k=0}^{\infty}\sum_{p=0}^{\infty} \frac{(-1)^k}{2^{2k}k!}\left(\frac{4}{3}\right)^{-n-m-k} \frac{g^{(p)}(T)(-1)^p}{p!}\left(\frac{2h}{3c}\right)^p \frac{(-1)^{k+p}\Gamma(m+2k+n)}{\Gamma(m+k-p+n)} \\
&= \frac{1}{3c}\left(\frac{3}{4}\right)^{n+m}\sum_{p=0}^{\infty}\frac{g^{(p)}(T)}{p!}\left(\frac{2h}{3c}\right)^p \sum_{k=0}^{\infty}\frac{1}{2^{2k}k!}\left(\frac{3}{4}\right)^k \frac{\Gamma(m+2k+n)}{\Gamma(m+k-p+n)} \\
&= \frac{1}{3c}\left(\frac{3}{4}\right)^{n+m}\sum_{p=0}^{\infty}\frac{g^{(p)}(T)}{p!}\left(\frac{2h}{3c}\right)^p \Gamma(m+n)\,{}_2\tilde{F}_1\left(\tfrac{m+n}{2},\tfrac{m+n+1}{2};m+n-p;\tfrac{3}{4}\right), \qquad (5.1.18)
\end{aligned}$$

where ${}_2\tilde{F}_1(a,b;c;z) = {}_2F_1(a,b;c;z)/\Gamma(c)$ is the regularized hypergeometric function [19]. In summary, the solution for $n > 0$ is given by (2.1.33), while the analytic continuation for negative values is

$$q_{-n}(T) = 3cB_1(-n,T,u) - cB_2(-n,T,u) - hB_1(-n,T,v) - \frac{h^2}{2c}B_1(-n,T,\tilde{v}), \qquad (5.1.19)$$

since the initial-condition integral vanishes.

Lastly, let us show that (5.1.19) converges to $q(-x,T) = u(T+\frac{x}{c})$ in the continuum limit. For the boundary terms with the given Dirichlet boundary condition $u(t)$, we have

$$\begin{aligned}
&3cB_1(-n,T,u) - cB_2(-n,T,u) \\
&= \left(\frac{3}{4}\right)^{n+1}\sum_{p=0}^{\infty}\frac{u^{(p)}(T)}{p!}\left(\frac{2h}{3c}\right)^p \Gamma(1+n)\,{}_2\tilde{F}_1\left(\tfrac{1+n}{2},\tfrac{n+2}{2};1+n-p;\tfrac{3}{4}\right) \\
&\quad - \frac{1}{3}\left(\frac{3}{4}\right)^{n+2}\sum_{p=0}^{\infty}\frac{u^{(p)}(T)}{p!}\left(\frac{2h}{3c}\right)^p \Gamma(2+n)\,{}_2\tilde{F}_1\left(\tfrac{2+n}{2},\tfrac{3+n}{2};2+n-p;\tfrac{3}{4}\right) \\
&= \sum_{p=0}^{\infty}\frac{u^{(p)}(T)}{p!}\left(\frac{h}{c}\right)^p \left\{\frac{3^{n+1-p}}{2^{2n+2-p}}\left[\Gamma(1+n)\,{}_2\tilde{F}_1\left(\tfrac{1+n}{2},\tfrac{n+2}{2};1+n-p;\tfrac{3}{4}\right) - \frac{\Gamma(2+n)}{4}\,{}_2\tilde{F}_1\left(\tfrac{2+n}{2},\tfrac{3+n}{2};2+n-p;\tfrac{3}{4}\right)\right]\right. \\
&= \sum_{p=0}^{\infty}\frac{u^{(p)}(T)}{p!}\left(\frac{h}{c}\right)^p f(n,p),
\end{aligned}$$

where

$$\begin{aligned}
f(n,p) &= \frac{3^{n+1-p}}{2^{2n+2-p}}\left[\Gamma(1+n)\,{}_2\tilde{F}_1\left(\tfrac{1+n}{2},\tfrac{n+2}{2};1+n-p;\tfrac{3}{4}\right) - \frac{\Gamma(2+n)}{4}\,{}_2\tilde{F}_1\left(\tfrac{2+n}{2},\tfrac{3+n}{2};2+n-p;\tfrac{3}{4}\right)\right] \\
&= \sum_{\ell=0}^{p} c_\ell\, n^{p-\ell},
\end{aligned}$$

with $c_0 = 1$. Hence,

$$\begin{aligned} 3cB_1(-n,T,u) - cB_2(-n,T,u) &= \sum_{p=0}^{\infty} \frac{u^{(p)}(T)}{p!} \left(\frac{h}{c}\right)^p \left(n^p + c_1 n^{p-1} + \ldots\right) \\ &= \sum_{p=0}^{\infty} \frac{u^{(p)}(T)}{p!} \left[\left(\frac{nh}{c}\right)^p + \frac{c_1 h}{c}\left(\frac{nh}{c}\right)^{p-1} + \ldots\right] \\ \Rightarrow \quad \lim_{h\to 0}\left[B_1^{3c}(-n,T,u) - B_2^{c}(-n,T,u)\right] &= \lim_{h\to 0} \sum_{p=0}^{\infty} \frac{u^{(p)}(T)}{p!} \left[\left(\frac{nh}{c}\right)^p + \frac{c_1 h}{c}\left(\frac{nh}{c}\right)^{p-1} + \ldots\right] \\ &= \sum_{p=0}^{\infty} \frac{u^{(p)}(T)}{p!} \left(\frac{x}{c}\right)^p \\ &= u\left(T + \frac{x}{c}\right). \end{aligned}$$

For the Neumann boundary term,

$$\begin{aligned} hB_1(-n,T,\dot{u}) &= \sum_{p=0}^{\infty} \frac{u^{(p+1)}(T)}{p!} \left(\frac{h}{c}\right)^{p+1} \left[\frac{3^{n-p}}{2^{2n+2-p}}\Gamma(1+n)\,{}_2\tilde{F}_1\left(\tfrac{1+n}{2}, \tfrac{2+n}{2}; 1+n-p; \tfrac{3}{4}\right)\right] \\ &= \sum_{p=0}^{\infty} \frac{u^{(p+1)}(T)}{p!} \left(\frac{h}{c}\right)^{p+1} \tilde{f}(n,p), \end{aligned}$$

where

$$\tilde{f}(n,p) = \frac{3^{n-p}}{2^{2n+2-p}}\Gamma(1+n)\,{}_2\tilde{F}_1\left(\tfrac{1+n}{2}, \tfrac{2+n}{2}; 1+n-p; \tfrac{3}{4}\right) = \frac{1}{2}\sum_{\ell=0}^{p} \tilde{c}_\ell\, n^{p-\ell},$$

with $\tilde{c}_0 = 1$. Thus,

$$\begin{aligned} hB_1(-n,T,\dot{u}) &= \sum_{p=0}^{\infty} \frac{u^{(p+1)}(T)}{2p!} \left(\frac{h}{c}\right)^{p+1} \left(n^p + \tilde{c}_1 n^{p-1} + \ldots\right) \\ &= \sum_{p=0}^{\infty} \frac{u^{(p+1)}(T)}{2p!} \left[\left(\frac{h}{c}\right)\left(\frac{nh}{c}\right)^p + \tilde{c}_1\left(\frac{h}{c}\right)^2\left(\frac{nh}{c}\right)^{p-1} + \ldots\right], \end{aligned}$$

and $\lim_{h\to 0} hB_1(-n,T,\dot{u}) = 0$. We reach a similar conclusion for the second-order derivative term: $\lim_{h\to 0} h^2/(2c)B_1(-n,T,\ddot{u}) = 0$. Therefore,

$$\begin{aligned} \lim_{h\to 0} q_{-n}(T) &= \lim_{h\to 0}\left[3cB_1(-n,T,u) - cB_2(-n,T,u) - hB_1(-n,T,\dot{u}) - \frac{h^2}{2c}B_1(-n,T,\ddot{u})\right] \\ &= u\left(T + \frac{x}{c}\right) = q(-x,T). \end{aligned}$$

5.2 The Heat Equation

5.2.1 Centered Discretization of $q_t = q_{xx}$ with Dirichlet condition

Next, we consider the heat equation on the half-line (3.2.1) with the standard centered stencil (2.2.2) that gives dispersion relation (2.2.4) and global relation (2.2.5). The SD-UTM gives solution

(2.2.9):

$$q_n(T) = \frac{1}{2\pi}\int_{-\pi/h}^{\pi/h} e^{iknh}e^{-WT}\left[\hat{q}(k,0) - \hat{q}(-k,0)\right]\,dk - \frac{i}{\pi h}\int_{-\pi/h}^{\pi/h} e^{iknh}e^{-WT}\sin(kh)f_0\,dk.$$

From this formulation, one could show that $q_{-n}(T) = -q_n(T)$ for $n \in \mathbb{Z}^+$ and $q_0(T) = 0$. In the continuum limit, solution (2.2.9) converges to (2.2.10), where one can also show $q(-x,T) = -q(x,T)$ for $x > 0$.

Let us look at the first term of (2.2.9) to introduce notation. Substituting the definitions of $\hat{q}(\pm k, 0)$, we have

$$\begin{aligned}\frac{1}{2\pi}\int_{-\pi/h}^{\pi/h} e^{iknh}e^{-WT}\left[\hat{q}(k,0) - \hat{q}(-k,0)\right]\,dk &= \frac{1}{2\pi}\int_{-\pi/h}^{\pi/h} e^{iknh}e^{-WT}\left[h\sum_{m=1}^{\infty}\left(e^{-ikmh} - e^{ikmh}\right)q_m(0)\right]\,dk \\ &= \sum_{m=1}^{\infty} I(n,T,m)q_m(0),\end{aligned}$$

where

$$I(n,T,m) = \frac{h}{2\pi}\int_{-\pi/h}^{\pi/h} e^{iknh}\left(e^{-ikmh} - e^{ikmh}\right)e^{-WT}\,dk = I_1(n,T,m) \;-\; I_1(n,T,-m),$$

with

$$I_1(n,T,m) = \frac{h}{2\pi}\int_{-\pi/h}^{\pi/h} e^{ik(n-m)h}e^{-WT}\,dk,$$

for brevity. The transformation $z = e^{ikh}$ allows

$$\begin{aligned}I_1(n,T,m) &= \frac{h}{2\pi}\oint_{|z|=1} z^{n-m}\exp\left[-\left(\frac{2-z-z^{-1}}{h^2}\right)T\right]\frac{dz}{ihz} \\ &= \frac{e^{-2T/h^2}}{2\pi i}\oint_{|z|=1} z^{n-m-1}\exp\left[\frac{1}{2}\left(\frac{2T}{h^2}\right)\left(z+\frac{1}{z}\right)\right]dz \\ &= e^{-2T/h^2}B\left(m-n,\frac{2T}{h^2}\right),\end{aligned} \tag{5.2.1}$$

where

$$B(n,a) = \frac{1}{2\pi i}\oint_{|z|=1}\exp\left[\frac{a}{2}\left(z+\frac{1}{z}\right)\right]\frac{1}{z^{n+1}}\,dz \equiv \sum_{\ell=0}^{\infty}\frac{1}{\ell!\,\Gamma(\ell+n+1)}\left(\frac{a}{2}\right)^{2\ell+n},$$

is the modified Bessel function of the first kind with the two vital properties: $B(-n,a) = B(n,a)$ for $n \in \mathbb{Z}$ and $B(n,a) = 2(n+1)B(n+1,a)/a + B(n+2,a)$. Returning to $I(n,T,m)$,

$$I(n,T,m) = e^{-2T/h^2}\left[B\left(m-n,\frac{2T}{h^2}\right) - B\left(m+n,\frac{2T}{h^2}\right)\right],$$

so that the first term of solution (2.2.9) is

$$\frac{1}{2\pi}\int_{-\pi/h}^{\pi/h} e^{iknh}e^{-WT}\left[\hat{q}(k,0)-\hat{q}(-k,0)\right]dk = e^{-2T/h^2}\sum_{m=1}^{\infty}\left[B\left(m-n,\frac{2T}{h^2}\right)-B\left(m+n,\frac{2T}{h^2}\right)\right]q_m(0).$$

Let us now look at the second term of solution (2.2.9) in a similar fashion:

$$\begin{aligned}\frac{i}{\pi h}\int_{-\pi/h}^{\pi/h} e^{iknh}e^{-WT}\sin(kh)f_0\,dk &= \frac{i}{\pi h}\int_{-\pi/h}^{\pi/h} e^{iknh}e^{-WT}\sin(kh)\left[\int_0^T e^{Wt}u(t)\,dt\right]dk\\ &= \frac{i}{\pi h}\int_0^T J(n,T-t)u(t)\,dt,\end{aligned}$$

with

$$\begin{aligned}J(n,T-t) &= \int_{-\pi/h}^{\pi/h} e^{iknh}e^{-W(T-t)}\sin(kh)\,dk\\ &= \int_{-\pi/h}^{\pi/h} e^{iknh}e^{-W(T-t)}\left(\frac{e^{ikh}-e^{-ikh}}{2i}\right)dk\\ &= \frac{1}{2i}\int_{-\pi/h}^{\pi/h} e^{ik(n+1)h}e^{-W(T-t)}\,dk - \frac{1}{2i}\int_{-\pi/h}^{\pi/h} e^{ik(n-1)h}e^{-W(T-t)}\,dk\\ &= \frac{\pi}{ih}I_1(n,T-t,-1)-\frac{\pi}{ih}I_1(n,T-t,1)\\ &= \frac{\pi e^{-2(T-t)/h^2}}{ih}\left[B\left(-1-n,\frac{2(T-t)}{h^2}\right)-B\left(1-n,\frac{2(T-t)}{h^2}\right)\right]\\ &= \frac{\pi e^{-2(T-t)/h^2}}{ih}\left[B\left(n+1,\frac{2(T-t)}{h^2}\right)-B\left(n-1,\frac{2(T-t)}{h^2}\right)\right]\\ J(n,T-t) &= \frac{-nh\pi e^{-2(T-t)/h^2}}{i(T-t)}B\left(n,\frac{2(T-t)}{h^2}\right).\end{aligned}$$

Hence, the second term simplifies to

$$\frac{i}{\pi h}\int_{-\pi/h}^{\pi/h} e^{iknh}e^{-WT}\sin(kh)f_0\,dk = -n\int_0^T \frac{e^{-2(T-t)/h^2}}{T-t}B\left(n,\frac{2(T-t)}{h^2}\right)u(t)\,dt.$$

Solution (2.2.9) is now rewritten as

$$q_n(T) = e^{-2T/h^2}\sum_{m=1}^{\infty}\left[B\left(m-n,\frac{2T}{h^2}\right)-B\left(m+n,\frac{2T}{h^2}\right)\right]q_m(0) \;+\; K(n,T), \tag{5.2.2}$$

where

$$K(n,T) = n\int_0^T \frac{e^{-2(T-t)/h^2}}{T-t}B\left(n,\frac{2(T-t)}{h^2}\right)u(t)\,dt.$$

Like solution (2.2.9), it is clear that this formulation continues to give $q_{-n}(T) = -q_n(T)$ and $q_0(T) = 0$.

Following a similar technique from the advection equation, we take a closer look at the second integral term of (5.2.2). With the transformation $s = 2(T-t)/h^2$, we have

$$\begin{aligned}
K(n,T) &= n\int_0^{2T/h^2} \frac{e^{-s}}{s} B(n,s)\, u\left(T - \frac{h^2}{2}s\right)\, ds \\
&= n\int_0^{2T/h^2} \frac{e^{-s}}{s} B(n,s) \sum_{p=0}^{\infty} \frac{u^{(p)}(T)(-1)^p}{p!}\left(\frac{h^2}{2}\right)^p s^p\, ds \\
&= n\sum_{p=0}^{\infty} \frac{u^{(p)}(T)(-1)^p}{p!}\left(\frac{h^2}{2}\right)^p \int_0^{2T/h^2} e^{-s} B(n,s)\, s^{p-1}\, ds \\
&= n\sum_{p=0}^{\infty} \frac{u^{(p)}(T)(-1)^p}{p!}\left(\frac{h^2}{2}\right)^p \int_0^{2T/h^2} e^{-s} \left[\sum_{\ell=0}^{\infty} \frac{1}{\ell!\,\Gamma(\ell+n+1)}\left(\frac{s}{2}\right)^{2\ell+n}\right] s^{p-1}\, ds \\
&= n\sum_{p=0}^{\infty} \frac{u^{(p)}(T)(-1)^p}{p!}\left(\frac{h^2}{2}\right)^p \sum_{\ell=0}^{\infty} \frac{1}{\ell!\,\Gamma(\ell+n+1)\,2^{2\ell+n}} \int_0^{2T/h^2} e^{-s} s^{2\ell+n+p-1}\, ds, \\
K(n,T) &= \frac{n}{2^n}\sum_{p=0}^{\infty} \frac{u^{(p)}(T)(-1)^p}{p!}\left(\frac{h^2}{2}\right)^p \sum_{\ell=0}^{\infty} \frac{1}{\ell!\,\Gamma(\ell+n+1)\,2^{2\ell}}\, \gamma\left(2\ell+n+p, \frac{2T}{h^2}\right).
\end{aligned}$$

Now, to apply any $n \in \mathbb{Z}$, we take the limit:

$$\begin{aligned}
\lim_{\alpha\to n} K(\alpha,T) &= \lim_{\alpha\to n} \frac{\alpha}{2^\alpha} \sum_{p=0}^{\infty} \frac{u^{(p)}(T)(-1)^p}{p!}\left(\frac{h^2}{2}\right)^p \sum_{\ell=0}^{\infty} \frac{1}{\ell!\,2^{2\ell}} \frac{\gamma\left(2\ell+\alpha+p, \frac{2T}{h^2}\right)}{\Gamma(\ell+\alpha+1)} \\
K(n,T) &= \frac{n}{2^n}\sum_{p=0}^{\infty} \frac{u^{(p)}(T)(-1)^p}{p!}\left(\frac{h^2}{2}\right)^p \sum_{\ell=0}^{\infty} \frac{1}{\ell!\,2^{2\ell}} \lim_{\alpha\to n} \frac{\gamma\left(2\ell+\alpha+p, \frac{2T}{h^2}\right)}{\Gamma(\ell+\alpha+1)},
\end{aligned}$$

where the relations (5.1.3) and (5.1.4) with $y = 2T/h^2$ tell us

$$\begin{aligned}
\frac{\gamma(2\ell+n+p,y)}{\Gamma(\ell+n+1)} &= \frac{1}{\Gamma(\ell+n+1)} \sum_{k=0}^{\infty} \frac{(-1)^k\, y^{2\ell+n+p+k}}{k!\,\Gamma(1+2\ell+n+p+k)} \cdot \Gamma(2\ell+n+p+k) \\
&= \frac{\Gamma(1-n-\ell-1)}{(-1)^{\ell+1}\,\Gamma(1-n)\,\Gamma(n)} \sum_{k=0}^{\infty} \frac{(-1)^k\, y^{2\ell+n+p+k}}{k!\,\Gamma(1+2\ell+n+p+k)} \cdot \frac{(-1)^{2\ell+p+k}\,\Gamma(1-n)\,\Gamma(n)}{\Gamma(1-2\ell-n-p-k)} \\
&= (-1)^{\ell+p+1}\,\Gamma(-n-\ell) \sum_{k=0}^{\infty} \frac{y^{2\ell+n+p+k}}{k!\,\Gamma(1+2\ell+n+p+k)\,\Gamma(1-2\ell-n-p-k)} \\
&= (-1)^{\ell+p+1}\,\Gamma(-n-\ell) \cdot \frac{y^{2\ell+n+p-2\ell-n-p}}{(-2\ell-n-p)!}, \\
\frac{\gamma(2\ell+n+p,y)}{\Gamma(\ell+n+1)} &= \frac{(-1)^{\ell+p+1}\,\Gamma(-n-\ell)}{\Gamma(1-2\ell-n-p)},
\end{aligned}$$

so that

$$\lim_{\alpha\to n}\frac{\gamma\left(2\ell+\alpha+p,\frac{2T}{h^2}\right)}{\Gamma(\ell+\alpha+1)}=\begin{cases}\dfrac{\gamma\left(2\ell+n+p,\frac{2T}{h^2}\right)}{\Gamma(\ell+n+1)}, & 2\ell+p\geq 1-n \quad\text{and}\quad \ell\geq -n,\\ \dfrac{(-1)^{\ell+p+1}\Gamma(-n-\ell)}{\Gamma(1-n-2\ell-p)}, & \ell\leq -n-1 \quad\text{and}\quad 2\ell+p\leq -n,\\ 0, & \text{otherwise.}\end{cases}$$

Hence, let us split the ℓ and p-indexed sums. For brevity, define

$$S(n,T,\ell,p)=\frac{u^{(p)}(T)(-1)^p}{p!}\left(\frac{h^2}{2}\right)^p\frac{1}{\ell!\,2^{2\ell}}\lim_{\alpha\to n}\frac{\gamma\left(2\ell+\alpha+p,\frac{2T}{h^2}\right)}{\Gamma(\ell+\alpha+1)},$$

so that

$$K(n,T)=\frac{n}{2^n}\sum_{p=0}^{\infty}\sum_{\ell=0}^{\infty}S(n,T,\ell,p)=\frac{n}{2^n}\sum_{\ell=0}^{\infty}\sum_{p=0}^{\infty}S(n,T,\ell,p)$$

$$=\frac{n}{2^n}\left(\sum_{\ell=0}^{-n-1}+\sum_{\ell=\max(-n,0)}^{\infty}\right)\left(\sum_{p=0}^{-n-2\ell}+\sum_{p=\max(-n-2\ell+1,0)}^{\infty}\right)S(n,T,\ell,p),$$

$$K(n,T)=\frac{n}{2^n}\sum_{\ell=0}^{-n-1}\sum_{p=0}^{-n-2\ell}S(n,T,\ell,p)+\frac{n}{2^n}\sum_{\ell=\max(-n,0)}^{\infty}\sum_{p=0}^{-n-2\ell}S(n,T,\ell,p)$$
$$+\frac{n}{2^n}\sum_{\ell=0}^{-n-1}\sum_{p=\max(-n-2\ell+1,0)}^{\infty}S(n,T,\ell,p)+\frac{n}{2^n}\sum_{\ell=\max(-n,0)}^{\infty}\sum_{p=\max(-n-2\ell+1,0)}^{\infty}S(n,T,\ell,p).$$

Consider $n<0$, so that the ℓ-indexed sum from the second pair of sums begins at $\ell=-n$, which then gives the upper bound of the p-indexed sum as $-n-2\ell=n<0$. Since the starting index is $p=0$, this pair of sums does not contribute for $n<0$. Now consider $n\geq 0$, so that $\ell=0$ is the starting index for the first sum, which gives $-n-2\ell=-n\leq 0$ for the upper bound of the p-indexed sum. Thus, this pair of sums does not contribute for any $n\in\mathbb{Z}$. The third pair of sums likewise vanishes for all $n\in\mathbb{Z}$, since $S(n,T,\ell,p)=0$ for these ranges of ℓ and p, regardless of $\lim_{\alpha\to n}\gamma\left(2\ell+\alpha+p,\frac{2T}{h^2}\right)/\Gamma(\ell+\alpha+1)$. We then have

$$K(n,T)=\frac{-n}{2^n}\sum_{\ell=0}^{-n-1}\frac{(-1)^\ell}{\ell!\,2^{2\ell}}\sum_{p=0}^{-n-2\ell}\frac{u^{(p)}(T)}{p!}\left(\frac{h^2}{2}\right)^p\frac{\Gamma(-n-\ell)}{\Gamma(1-n-2\ell-p)}$$
$$+\frac{n}{2^n}\sum_{\ell=\max(-n,0)}^{\infty}\frac{1}{\ell!\,2^{2\ell}}\sum_{p=\max(-n-2\ell+1,0)}^{\infty}\frac{u^{(p)}(T)(-1)^p}{p!}\left(\frac{h^2}{2}\right)^p\frac{\gamma\left(2\ell+n+p,\frac{2T}{h^2}\right)}{\Gamma(\ell+n+1)}.$$

In the first coupled sum, we relax the upper bound of the p-indexed sum allowing us to interchange the sums themselves:

$$\begin{aligned}\frac{-n}{2^n}\sum_{\ell=0}^{-n-1}\frac{(-1)^\ell}{\ell!\,2^{2\ell}}\sum_{p=0}^{-n-2\ell}\frac{u^{(p)}(T)}{p!}\left(\frac{h^2}{2}\right)^p\frac{\Gamma(-n-\ell)}{\Gamma(1-n-2\ell-p)} &= \frac{-n}{2^n}\sum_{\ell=0}^{-n-1}\frac{(-1)^\ell}{\ell!\,2^{2\ell}}\sum_{p=0}^{\infty}\frac{u^{(p)}(T)}{p!}\left(\frac{h^2}{2}\right)^p\frac{\Gamma(-n-\ell)}{\Gamma(1-n-2\ell-p)}\\ &= \frac{-n}{2^n}\sum_{p=0}^{\infty}\frac{u^{(p)}(T)}{p!}\left(\frac{h^2}{2}\right)^p\sum_{\ell=0}^{-n-1}\frac{(-1)^\ell}{\ell!\,2^{2\ell}}\frac{\Gamma(-n-\ell)}{\Gamma(1-n-2\ell-p)}\\ &= \frac{-n}{2^n}\sum_{p=0}^{\infty}u^{(p)}(T)\left(\frac{h^2}{2}\right)^p L(n,p)\end{aligned}$$

where

$$L(n,p)=\frac{1}{p!}\sum_{\ell=0}^{\frac{-n-p}{2}}\frac{(-1)^\ell}{\ell!\,2^{2\ell}}\frac{\Gamma(-n-\ell)}{\Gamma(1-n-2\ell-p)}=\frac{2^{n+p}(-1)^{n+p}\pi\,C_{-n-p}^{(p)}(1)}{p!\,\sin(\pi n)\,\Gamma(1-p)},$$

with the Gegenbauer polynomial

$$C_n^{(m)}(1)=\frac{\Gamma(2m+n)}{\Gamma(2m)\,\Gamma(n+1)}.$$

By grouping terms, we can employ relation (5.1.3) to give

$$\begin{aligned}\Gamma(1+n+p)&=\frac{(-1)^{1+n}\,\Gamma(1-p)\,\Gamma(p)}{\Gamma(-p-n)}=\frac{(-1)^{1+p}\,\Gamma(1-n)\,\Gamma(n)}{\Gamma(-p-n)}\\ \Rightarrow\quad \Gamma(1-p)&=\frac{(-1)^{p+n}\,\Gamma(1-n)\,\Gamma(n)}{\Gamma(p)}.\end{aligned}$$

Thus,

$$\begin{aligned}L(n,p)&=\frac{2^{n+p}(-1)^{n+p}\pi}{\Gamma(p+1)\,\sin(\pi n)}\cdot C_{-n-p}^{(p)}(1)\cdot\frac{1}{\Gamma(1-p)}\\ &=\frac{2^{n+p}(-1)^{n+p}\,\Gamma(1-n)\,\Gamma(n)}{\Gamma(p+1)}\cdot\frac{\Gamma(2p-n-p)}{\Gamma(2p)\,\Gamma(1-n-p)}\cdot\frac{\Gamma(p)}{(-1)^{p+n}\,\Gamma(1-n)\,\Gamma(n)}\\ &=\frac{2^{n+p}\,\Gamma(p-n)}{\Gamma(1-n-p)}\cdot\frac{\Gamma(p)}{\Gamma(p+1)\,\Gamma(2p)}\\ &=\frac{2^{n+p}\,\Gamma(p-n)}{\Gamma(1-n-p)}\cdot\frac{2}{\Gamma(2p+1)}\\ &=\frac{2^{n+p+1}\,\Gamma(p-n)}{\Gamma(1-n-p)\,\Gamma(2p+1)}.\end{aligned}$$

Returning to the first pair of sums in $K(n,t)$, we find

$$\begin{aligned}\frac{-n}{2^n}\sum_{\ell=0}^{\frac{-n-p}{2}}\frac{(-1)^\ell}{\ell!\,2^{2\ell}}\sum_{p=0}^{\infty}\frac{u^{(p)}(T)}{p!}\left(\frac{h^2}{2}\right)^p\frac{\Gamma(-n-\ell)}{\Gamma(1-n-2\ell-p)} &= \frac{-n}{2^n}\sum_{p=0}^{\infty}u^{(p)}(T)\left(\frac{h^2}{2}\right)^p\cdot\frac{2^{n+p+1}\,\Gamma(p-n)}{\Gamma(1-n-p)\,\Gamma(2p+1)}\\ &= -2n\sum_{p=0}^{-n}\frac{u^{(p)}(T)\,h^{2p}\,\Gamma(p-n)}{\Gamma(1-n-p)\,\Gamma(2p+1)},\end{aligned}$$

where the infinite sum can be truncated to start from $p = 0$ and end at $p = -n$. Hence, $K(n,T)$ becomes

$$K(n,T) = -2n \sum_{p=0}^{-n} \frac{u^{(p)}(T)\, h^{2p}\, \Gamma(p-n)}{\Gamma(1-n-p)\,\Gamma(2p+1)} + \frac{n}{2^n} \sum_{\ell=\max(-n,0)}^{\infty} \frac{1}{\ell!\, 2^{2\ell}} \sum_{p=\max(-n-2\ell+1,0)}^{\infty} \frac{u^{(p)}(T)(-1)^p}{p!} \left(\frac{h^2}{2}\right)^p \frac{\gamma\left(2\ell+n+p, \frac{2T}{h^2}\right)}{\Gamma(\ell+n+1)},$$

so that the solution representation (5.2.2) is now

$$\begin{aligned} q_n(T) = \frac{1}{2\pi} \int_{-\pi/h}^{\pi/h} e^{iknh} e^{-WT} \left[\hat{q}(k,0) - \hat{q}(-k,0)\right] dk \; - \; 2n \sum_{p=0}^{-n} \frac{u^{(p)}(T)\, h^{2p}\, \Gamma(p-n)}{\Gamma(1-n-p)\,\Gamma(2p+1)} \\ + \; \frac{n}{2^n} \sum_{\ell=\max(-n,0)}^{\infty} \frac{1}{\ell!\, 2^{2\ell}} \sum_{p=\max(-n-2\ell+1,0)}^{\infty} \frac{u^{(p)}(T)(-1)^p}{p!} \left(\frac{h^2}{2}\right)^p \frac{\gamma\left(2\ell+n+p, \frac{2T}{h^2}\right)}{\Gamma(\ell+n+1)}, \end{aligned} \tag{5.2.3}$$

where we have replaced the initial conditions terms from (5.2.2) by those from the original representation (2.2.9).

If we now consider $n > 0$ only, the second term above vanishes and we have

$$\begin{aligned} q_n(T) = \frac{1}{2\pi} \int_{-\pi/h}^{\pi/h} e^{iknh} e^{-WT} \left[\hat{q}(k,0) - \hat{q}(-k,0)\right] dk \\ + \; \frac{n}{2^n} \sum_{\ell=0}^{\infty} \frac{1}{\ell!\, 2^{2\ell}} \sum_{p=0}^{\infty} \frac{u^{(p)}(T)(-1)^p}{p!} \left(\frac{h^2}{2}\right)^p \frac{\gamma\left(2\ell+n+p, \frac{2T}{h^2}\right)}{\Gamma(\ell+n+1)}, \end{aligned} \tag{5.2.4}$$

which can, of course, reduce back to the original representation (2.2.9). If we consider $n \leq 0$ or

$n \to -n$ for $n \geq 0$, then, with a re-index $\ell \to \ell - n$, we have

$$
\begin{aligned}
q_{-n}(T) = \frac{1}{2\pi}\int_{-\pi/h}^{\pi/h} e^{-iknh} e^{-WT}\left[\hat{q}(k,0) - \hat{q}(-k,0)\right]\, dk \;+\; 2n\sum_{p=0}^{n} \frac{u^{(p)}(T)\, h^{2p}\, \Gamma(p+n)}{\Gamma(1+n-p)\,\Gamma(2p+1)} \\
-\; \frac{n}{2^{-n}} \sum_{\ell=n}^{\infty} \frac{1}{\ell!\, 2^{2\ell}} \sum_{p=\max(n-2\ell+1,0)}^{\infty} \frac{u^{(p)}(T)(-1)^p}{p!} \left(\frac{h^2}{2}\right)^p \frac{\gamma\left(2\ell - n + p, \frac{2T}{h^2}\right)}{\Gamma(\ell - n + 1)} \\
= \frac{-1}{2\pi}\int_{-\pi/h}^{\pi/h} e^{iknh} e^{-WT}\left[\hat{q}(k,0) - \hat{q}(-k,0)\right]\, dk \;+\; 2n\sum_{p=0}^{n} \frac{u^{(p)}(T)\, h^{2p}\, \Gamma(p+n)}{\Gamma(1+n-p)\,\Gamma(2p+1)} \\
-\; \frac{n}{2^{-n}} \sum_{\ell=0}^{\infty} \frac{1}{(\ell+n)!\, 2^{2\ell+2n}} \sum_{p=\max(-n-2\ell+1,0)}^{\infty} \frac{u^{(p)}(T)(-1)^p}{p!} \left(\frac{h^2}{2}\right)^p \frac{\gamma\left(2\ell + n + p, \frac{2T}{h^2}\right)}{\Gamma(\ell + 1)} \\
= \frac{-1}{2\pi}\int_{-\pi/h}^{\pi/h} e^{iknh} e^{-WT}\left[\hat{q}(k,0) - \hat{q}(-k,0)\right]\, dk \;+\; 2n\sum_{p=0}^{n} \frac{u^{(p)}(T)\, h^{2p}\, \Gamma(p+n)}{\Gamma(1+n-p)\,\Gamma(2p+1)} \\
-\; \frac{n}{2^n} \sum_{\ell=0}^{\infty} \frac{1}{\ell!\, 2^{2\ell}} \sum_{p=0}^{\infty} \frac{u^{(p)}(T)(-1)^p}{p!} \left(\frac{h^2}{2}\right)^p \frac{\gamma\left(2\ell + n + p, \frac{2T}{h^2}\right)}{\Gamma(\ell + n + 1)} \\
= 2n\sum_{p=0}^{n} \frac{u^{(p)}(T)\, h^{2p}\, \Gamma(p+n)}{\Gamma(1+n-p)\,\Gamma(2p+1)} \;-\; \left[\frac{1}{2\pi}\int_{-\pi/h}^{\pi/h} e^{iknh} e^{-WT}\left[\hat{q}(k,0) - \hat{q}(-k,0)\right]\, dk \right. \\
\left. +\; \frac{n}{2^n} \sum_{\ell=0}^{\infty} \frac{1}{\ell!\, 2^{2\ell}} \sum_{p=0}^{\infty} \frac{u^{(p)}(T)(-1)^p}{p!} \left(\frac{h^2}{2}\right)^p \frac{\gamma\left(2\ell + n + p, \frac{2T}{h^2}\right)}{\Gamma(\ell + n + 1)} \right],
\end{aligned}
$$

$$
q_{-n}(T) = 2n\sum_{p=0}^{n} \frac{u^{(p)}(T)\, h^{2p}\, \Gamma(p+n)}{\Gamma(1+n-p)\,\Gamma(2p+1)} \;-\; q_n(T). \tag{5.2.5}
$$

To recover the boundary condition at $n = 0$, first extract the first term of the sum:

$$
\begin{aligned}
q_{-n}(T) &= 2n\left[\frac{u(T)}{n} + \sum_{p=1}^{n} \frac{u^{(p)}(T)\, h^{2p}\, \Gamma(p+n)}{\Gamma(1+n-p)\,\Gamma(2p+1)}\right] - q_n(T) \\
&= 2u(T) \;-\; 2n\sum_{p=1}^{n} \frac{u^{(p)}(T)\, h^{2p}\, \Gamma(p+n)}{\Gamma(1+n-p)\,\Gamma(2p+1)} - q_n(T),
\end{aligned}
$$

so that $q_0(T) = 2u(T) - q_0(T) = u(T)$.

The analytic continuation of the continuous solution [24] is

$$
q(-x,T) = 2\sum_{p=0}^{\infty} \frac{u^{(p)}(T)}{(2p)!} x^{2p} - q(x,T). \tag{5.2.6}
$$

We can recover (5.2.6) from the continuum limit of (5.2.5) by noting that

$$f(n,p)=\frac{n\Gamma(p+n)}{\Gamma(1+n-p)}=\prod_{\ell=0}^{p-1}(n-\ell)(n+\ell)=\begin{cases}1, & p=0,\\ \displaystyle\sum_{\ell=1}^{p}a_\ell\, n^{2\ell}, & p\geq 1,\end{cases}$$

such that $f(n,p)$ is a polynomial in n of degree $2p$ with leading coefficient $a_p=1$. Hence,

$$\begin{aligned}
q_{-n}(T)&=2\sum_{p=0}^{n}\frac{u^{(p)}(T)\,h^{2p}}{(2p)!}\,f(n,p)-q_n(T)\\
&=2\sum_{p=0}^{n}\frac{u^{(p)}(T)\,h^{2p}}{(2p)!}\left(n^{2p}+a_{p-1}n^{2p-2}+\ldots\right)-q_n(T),\\
q_{-n}(T)&=2\sum_{p=0}^{n}\frac{u^{(p)}(T)}{(2p)!}\left[(nh)^{2p}+a_{p-1}h^2(nh)^{2p-2}+\ldots\right]-q_n(T)\\
\Rightarrow\quad \lim_{h\to 0}q_{-n}(T)&=\lim_{h\to 0}\left[2\sum_{p=0}^{n}\frac{u^{(p)}(T)}{(2p)!}\left[(nh)^{2p}+a_{p-1}h^2(nh)^{2p-2}+\ldots\right]-q_n(T)\right]\\
&=2\sum_{p=0}^{\infty}\frac{u^{(p)}(T)}{(2p)!}\,x^{2p}-q(x,T).
\end{aligned}$$

As an example, solving the IBVP

$$\begin{cases}q_t=q_{xx}, & x>0,\ t>0,\\ q(x,0)=3xe^{-x}, & x>0,\\ q(0,t)=\sin(4\pi t), & t>0,\end{cases}\tag{5.2.7}$$

gives Figure 5.2.1 on two different spatial grids.

5.2.2 Centered Discretization of $q_t=q_{xx}$ with Neumann Condition

For the Neumann half-line problem (3.2.16), the same centered stencil from the previous section gives the SD-UTM solution (2.2.18):

$$q_n(T)=\frac{1}{2\pi}\int_{-\pi/h}^{\pi/h}e^{iknh}e^{-WT}\left[\hat{q}(k,0)+e^{ikh}\hat{q}(-k,0)\right]\,dk-\frac{1}{2\pi}\int_{-\pi/h}^{\pi/h}e^{iknh}e^{-WT}\left(1+e^{ikh}\right)U\,dk.$$

From here, one could show that $q_{-n}(T)=q_{n-1}(T)$ for $n\in\mathbb{Z}^+$, while the continuous UTM solution (2.2.19) gives $q(-x,T)=q(x,T)$ for $x>0$.

Following the usual tactics from this chapter, the first term of (2.2.18) is rewritten as

$$\frac{1}{2\pi}\int_{-\pi/h}^{\pi/h}e^{iknh}e^{-WT}\left[\hat{q}(k,0)+e^{ikh}\hat{q}(-k,0)\right]\,dk=e^{-2T/h^2}\sum_{m=1}^{\infty}\left[B\left(m-n,\frac{2T}{h^2}\right)+B\left(m+n+1,\frac{2T}{h^2}\right)\right]q_m(0).$$

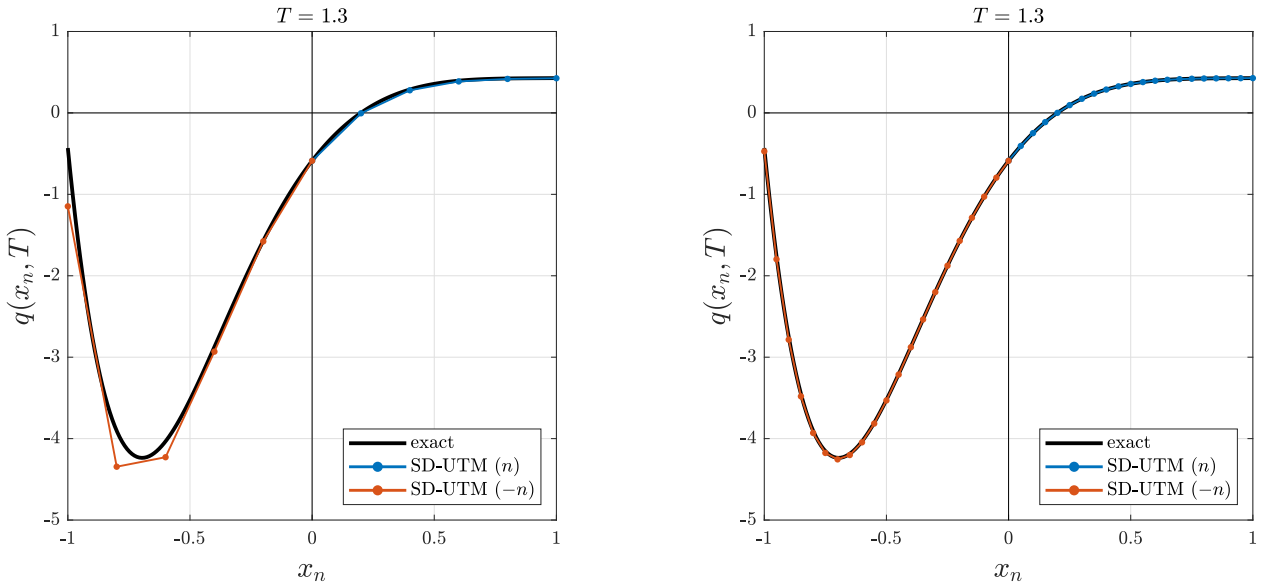

Figure 5.2.1: Extensions of half-line solution (2.2.9) for IBVP (5.2.7) with $h = 0.2$ (left) and $h = 0.05$ (right).

Next, we substitute the definition of $U(W,T)$ into the second term of (2.2.18) to obtain

$$\frac{1}{2\pi}\int_{-\pi/h}^{\pi/h} e^{iknh}e^{-WT}\left(1+e^{ikh}\right)U\,dk = \frac{1}{h}\int_0^T \tilde{I}(n,T,t)u(t)\,dt,$$

with

$$\begin{aligned}
\tilde{I}(n,T,t) &= \frac{h}{2\pi}\int_{-\pi/h}^{\pi/h} e^{iknh}e^{-W(T-t)}\left(1+e^{ikh}\right)\,dk \\
&= \frac{h}{2\pi}\int_{-\pi/h}^{\pi/h} e^{iknh}e^{-W(T-t)}\,dk + \frac{h}{2\pi}\int_{-\pi/h}^{\pi/h} e^{ik(n+1)h}e^{-W(T-t)}\,dk \\
&= I_1(n,T-t,0) + I_1(n,T-t,-1) \\
&= e^{-2(T-t)/h^2}\left[B\left(n,\frac{2(T-t)}{h^2}\right) + B\left(n+1,\frac{2(T-t)}{h^2}\right)\right],
\end{aligned}$$

where $I_1(n,T-t,m)$ is defined in (5.2.1) when solving the heat equation with a Dirichlet boundary condition. Then,

$$\frac{1}{2\pi}\int_{-\pi/h}^{\pi/h} e^{iknh}e^{-WT}\left(1+e^{ikh}\right)U\,dk = \frac{1}{h}\int_0^T e^{-2(T-t)/h^2}\left[B\left(n,\frac{2(T-t)}{h^2}\right) + B\left(n+1,\frac{2(T-t)}{h^2}\right)\right]u(t)\,dt.$$

Hence, solution (2.2.18) is rewritten as

$$q_n(T) = e^{-2T/h^2}\sum_{m=1}^{\infty}\left[B\left(m-n,\frac{2T}{h^2}\right) + B\left(m+n+1,\frac{2T}{h^2}\right)\right]q_m(0) - P(n,T), \tag{5.2.8}$$

where

$$P(n,T)=\frac{1}{h}\int_0^T e^{-2(T-t)/h^2}\left[B\left(n,\frac{2(T-t)}{h^2}\right)+B\left(n+1,\frac{2(T-t)}{h^2}\right)\right]u(t)\,dt.$$

Even with this representation, setting $n\to -n$ for $n\in\mathbb{Z}^+$ gives $q_{-n}(T)=q_{n-1}(T)$.

Let us take a closer look at the second term of (5.2.8). With the substitution $s=2(T-t)/h^2$, we have

$$\begin{aligned}
P(n,T)&=\frac{1}{h}\int_{2T/h^2}^0 e^{-s}\left[B\left(n,s\right)+B\left(n+1,s\right)\right]u\left(T-\frac{h^2}{2}\right)\left(\frac{-h^2}{2}\right)\,ds\\
&=\frac{h}{2}\int_0^{2T/h^2} e^{-s}\left[B\left(n,s\right)+B\left(n+1,s\right)\right]u\left(T-\frac{h^2}{2}\right)\,ds\\
&=\frac{h}{2}\int_0^{2T/h^2} e^{-s}\left[B\left(n,s\right)+B\left(n+1,s\right)\right]\sum_{p=0}^{\infty}\frac{u^{(p)}(T)(-1)^p}{p!}\left(\frac{h^2}{2}\right)^p s^p\,ds,\\
P(n,T)&=\frac{h}{2}\sum_{p=0}^{\infty}\frac{u^{(p)}(T)(-1)^p}{p!}\left(\frac{h^2}{2}\right)^p\int_0^{2T/h^2} e^{-s}\left[B\left(n,s\right)+B\left(n+1,s\right)\right]s^p\,ds.
\end{aligned}$$

Note that

$$\begin{aligned}
B\left(n,s\right)+B\left(n+1,s\right)&=\sum_{\ell=0}^{\infty}\frac{1}{\ell!\,\Gamma(\ell+n+1)}\left(\frac{s}{2}\right)^{2\ell+n}+\sum_{\ell=0}^{\infty}\frac{1}{\ell!\,\Gamma(\ell+n+2)}\left(\frac{s}{2}\right)^{2\ell+n+1}\\
&=\sum_{\ell=0}^{\infty}\frac{1}{\ell!\,2^{2\ell+n}}\left[\frac{s^{2\ell+n}}{\Gamma(\ell+n+1)}+\frac{s^{2\ell+n+1}}{2\,\Gamma(\ell+n+2)}\right],
\end{aligned}$$

so that

$$\begin{aligned}
P(n,T)&=\frac{h}{2}\sum_{p=0}^{\infty}\frac{u^{(p)}(T)(-1)^p}{p!}\left(\frac{h^2}{2}\right)^p\int_0^{2T/h^2} e^{-s}\sum_{\ell=0}^{\infty}\frac{1}{\ell!\,2^{2\ell+n}}\left[\frac{s^{2\ell+n}}{\Gamma(\ell+n+1)}+\frac{s^{2\ell+n+1}}{2\,\Gamma(\ell+n+2)}\right]s^p\,ds\\
&=\frac{h}{2^{n+1}}\sum_{p=0}^{\infty}\frac{u^{(p)}(T)(-1)^p}{p!}\left(\frac{h^2}{2}\right)^p\sum_{\ell=0}^{\infty}\frac{1}{\ell!\,2^{2\ell}}\int_0^{2T/h^2}\left[\frac{e^{-s}s^{2\ell+n+p}}{\Gamma(\ell+n+1)}+\frac{e^{-s}s^{2\ell+n+p+1}}{2\,\Gamma(\ell+n+2)}\right]ds\\
&=\frac{h}{2^{n+1}}\sum_{p=0}^{\infty}\frac{u^{(p)}(T)(-1)^p}{p!}\left(\frac{h^2}{2}\right)^p\sum_{\ell=0}^{\infty}\frac{1}{\ell!\,2^{2\ell}}\left[\frac{\gamma\left(2\ell+n+p+1,\frac{2T}{h^2}\right)}{\Gamma(\ell+n+1)}+\frac{\gamma\left(2\ell+n+p+2,\frac{2T}{h^2}\right)}{2\,\Gamma(\ell+n+2)}\right]\\
&=\frac{h}{2^{n+1}}\sum_{p=0}^{\infty}\frac{u^{(p)}(T)(-1)^p}{p!}\left(\frac{h^2}{2}\right)^p\sum_{\ell=0}^{\infty}\frac{1}{\ell!\,2^{2\ell}}\cdot\frac{\gamma\left(2\ell+n+p+1,\frac{2T}{h^2}\right)}{\Gamma(\ell+n+1)}\\
&\quad+\frac{h}{2^{n+2}}\sum_{p=0}^{\infty}\frac{u^{(p)}(T)(-1)^p}{p!}\left(\frac{h^2}{2}\right)^p\sum_{\ell=0}^{\infty}\frac{1}{\ell!\,2^{2\ell}}\cdot\frac{\gamma\left(2\ell+n+p+2,\frac{2T}{h^2}\right)}{\Gamma(\ell+n+2)}\\
&=\tilde{P}(n,T)+\tilde{P}(n+1,T),
\end{aligned}$$

where we have introduced

$$\tilde{P}(n,T) = \frac{h}{2^{n+1}} \sum_{p=0}^{\infty} \frac{u^{(p)}(T)(-1)^p}{p!} \left(\frac{h^2}{2}\right)^p \sum_{\ell=0}^{\infty} \frac{1}{\ell!\, 2^{2\ell}} \cdot \frac{\gamma\left(2\ell+n+p+1, \frac{2T}{h^2}\right)}{\Gamma(\ell+n+1)},$$

for brevity. Applying relations (5.1.3) and (5.1.4) with $y = 2T/h^2$, we find

$$\begin{aligned}
\frac{\gamma\left(2\ell+n+p+1, y\right)}{\Gamma(\ell+n+1)} &= \frac{1}{\Gamma(\ell+n+1)} \sum_{k=0}^{\infty} \frac{(-1)^k\, y^{2\ell+n+p+k+1}}{k!\,\Gamma(2\ell+n+p+k+2)} \cdot \Gamma(2\ell+n+p+k+1) \\
&= \frac{\Gamma(1-n-\ell-1)}{(-1)^{\ell+1}\,\Gamma(1-n)\,\Gamma(n)} \sum_{k=0}^{\infty} \frac{(-1)^k\, y^{2\ell+n+p+k+1}}{k!\,\Gamma(2\ell+n+p+k+2)} \cdot \frac{(-1)^{2\ell+p+k+1}\,\Gamma(1-n)\,\Gamma(n)}{\Gamma(-2\ell-n-p-k)} \\
&= (-1)^{\ell+p}\,\Gamma(-n-\ell) \sum_{k=0}^{\infty} \frac{y^{2\ell+n+p+k+1}}{k!\,\Gamma(2\ell+n+p+k+2)\,\Gamma(-2\ell-n-p-k)} \\
&= \frac{(-1)^{\ell+p}\,\Gamma(-n-\ell)}{\Gamma(-2\ell-n-p)},
\end{aligned}$$

so that

$$\lim_{\alpha\to n} \frac{\gamma\left(2\ell+\alpha+p+1, \frac{2T}{h^2}\right)}{\Gamma(\ell+\alpha+1)} = \begin{cases} \dfrac{\gamma\left(2\ell+n+p+1, \frac{2T}{h^2}\right)}{\Gamma(\ell+n+1)}, & 2\ell+p \geq -n \quad \text{and} \quad \ell \geq -n, \\ \dfrac{(-1)^{\ell+p}\,\Gamma(-n-\ell)}{\Gamma(-2\ell-n-p)}, & \ell \leq -n-1 \quad \text{and} \quad 2\ell+p \leq -1-n, \\ 0, & \text{otherwise.} \end{cases}$$

To be concise, denote

$$S(n,T,\ell,p) = \frac{u^{(p)}(T)(-1)^p}{p!} \left(\frac{h^2}{2}\right)^p \cdot \frac{1}{\ell!\, 2^{2\ell}} \lim_{\alpha\to n} \frac{\gamma\left(2\ell+\alpha+p+1, \frac{2T}{h^2}\right)}{\Gamma(\ell+\alpha+1)},$$

so that splitting the sum similar to those in Section 5.2.1, we obtain

$$\begin{aligned}
\tilde{P}(n,T) &= \frac{h}{2^{n+1}}\sum_{p=0}^{\infty}\sum_{\ell=0}^{\infty} S(n,T,\ell,p) = \frac{h}{2^{n+1}}\sum_{\ell=0}^{\infty}\sum_{p=0}^{\infty} S(n,T,\ell,p) \\
&= \frac{h}{2^{n+1}}\left(\sum_{\ell=0}^{-n-1} + \sum_{\ell=\max(-n,0)}^{\infty}\right)\left(\sum_{p=0}^{-n-2\ell-1} + \sum_{p=\max(-n-2\ell,0)}^{\infty}\right) S(n,T,\ell,p) \\
&= \frac{h}{2^{n+1}}\sum_{\ell=0}^{-n-1}\sum_{p=0}^{-n-2\ell-1} S(n,T,\ell,p) \;+\; \frac{h}{2^{n+1}}\sum_{\ell=\max(-n,0)}^{\infty}\sum_{p=0}^{-n-2\ell-1} S(n,T,\ell,p) \\
&\quad + \frac{h}{2^{n+1}}\sum_{\ell=0}^{-n-1}\sum_{p=\max(-n-2\ell,0)}^{\infty} S(n,T,\ell,p) \;+\; \frac{h}{2^{n+1}}\sum_{\ell=\max(-n,0)}^{\infty}\sum_{p=\max(-n-2\ell,0)}^{\infty} S(n,T,\ell,p) \\
&= \frac{h}{2^{n+1}}\sum_{\ell=0}^{-n-1}\sum_{p=0}^{-n-2\ell-1} \frac{u^{(p)}(T)(-1)^p}{p!}\left(\frac{h^2}{2}\right)^p \cdot \frac{1}{\ell!\,2^{2\ell}} \cdot \frac{(-1)^{\ell+p}\,\Gamma(-n-\ell)}{\Gamma(-2\ell-n-p)} \\
&\quad + \frac{h}{2^{n+1}}\sum_{\ell=\max(-n,0)}^{\infty}\sum_{p=\max(-n-2\ell,0)}^{\infty} \frac{u^{(p)}(T)(-1)^p}{p!}\left(\frac{h^2}{2}\right)^p \cdot \frac{1}{\ell!\,2^{2\ell}} \cdot \frac{\gamma\left(2\ell+n+p+1,\frac{2T}{h^2}\right)}{\Gamma(\ell+n+1)} \\
&= \frac{h}{2^{n+1}}\sum_{\ell=0}^{-n-1}\frac{(-1)^\ell}{\ell!\,2^{2\ell}}\sum_{p=0}^{-n-2\ell-1} \frac{u^{(p)}(T)}{p!}\left(\frac{h^2}{2}\right)^p \frac{\Gamma(-n-\ell)}{\Gamma(-2\ell-n-p)} \\
&\quad + \frac{h}{2^{n+1}}\sum_{\ell=\max(-n,0)}^{\infty}\frac{1}{\ell!\,2^{2\ell}}\sum_{p=\max(-n-2\ell,0)}^{\infty} \frac{u^{(p)}(T)(-1)^p}{p!}\left(\frac{h^2}{2}\right)^p \frac{\gamma\left(2\ell+n+p+1,\frac{2T}{h^2}\right)}{\Gamma(\ell+n+1)}.
\end{aligned}$$

For the first pair of sums, we relax the upper bound on the p-indexed sum, so that we can now interchange the sums and tighten the upper bound on the ℓ-indexed sum:

$$\begin{aligned}
\frac{h}{2^{n+1}}\sum_{\ell=0}^{-n-1}\frac{(-1)^\ell}{\ell!\,2^{2\ell}}\sum_{p=0}^{-n-2\ell-1} \frac{u^{(p)}(T)}{p!}\left(\frac{h^2}{2}\right)^p \frac{\Gamma(-n-\ell)}{\Gamma(-2\ell-n-p)} &= \frac{h}{2^{n+1}}\sum_{\ell=0}^{-n-1}\frac{(-1)^\ell}{\ell!\,2^{2\ell}}\sum_{p=0}^{\infty} \frac{u^{(p)}(T)}{p!}\left(\frac{h^2}{2}\right)^p \frac{\Gamma(-n-\ell)}{\Gamma(-2\ell-n-p)} \\
&= \frac{h}{2^{n+1}}\sum_{p=0}^{\infty} u^{(p)}(T)\left(\frac{h^2}{2}\right)^p L(n,p),
\end{aligned}$$

where

$$L(n,p) = \frac{1}{p!}\sum_{\ell=0}^{\frac{-n-p-1}{2}} \frac{(-1)^\ell}{\ell!\,2^{2\ell}}\frac{\Gamma(-n-\ell)}{\Gamma(-2\ell-n-p)} = \frac{2^{n+p+1}\,\Gamma(1+p-n)}{\Gamma(-n-p)\,\Gamma(2p+2)},$$

after similar procedures from the previous section. Hence,

$$\frac{h}{2^{n+1}}\sum_{\ell=0}^{-n-1}\frac{(-1)^\ell}{\ell!\,2^{2\ell}}\sum_{p=0}^{-n-2\ell-1} \frac{u^{(p)}(T)}{p!}\left(\frac{h^2}{2}\right)^p \frac{\Gamma(-n-\ell)}{\Gamma(-2\ell-n-p)} = h\sum_{p=0}^{\infty}\frac{u^{(p)}(T)h^{2p}}{(2p+1)!}\,\frac{\Gamma(1+p-n)}{\Gamma(-n-p)},$$

so that

$$\tilde{P}(n,T) = \frac{h}{2^{n+1}} \sum_{\ell=\max(-n,0)}^{\infty} \frac{1}{\ell!\, 2^{2\ell}} \sum_{p=\max(-n-2\ell,0)}^{\infty} \frac{u^{(p)}(T)(-1)^p}{p!} \left(\frac{h^2}{2}\right)^p \frac{\gamma\left(2\ell+n+p+1, \frac{2T}{h^2}\right)}{\Gamma(\ell+n+1)} + h\sum_{p=0}^{\infty} \frac{u^{(p)}(T)h^{2p}}{(2p+1)!} \frac{\Gamma(1+p-n)}{\Gamma(-n-p)},$$

and

$$\tilde{P}(n+1,T) = \frac{h}{2^{n+2}} \sum_{\ell=\max(-n-1,0)}^{\infty} \frac{1}{\ell!\, 2^{2\ell}} \sum_{p=\max(-n-2\ell-1,0)}^{\infty} \frac{u^{(p)}(T)(-1)^p}{p!} \left(\frac{h^2}{2}\right)^p \frac{\gamma\left(2\ell+n+p+2, \frac{2T}{h^2}\right)}{\Gamma(\ell+n+2)} + h\sum_{p=0}^{\infty} \frac{u^{(p)}(T)h^{2p}}{(2p+1)!} \frac{\Gamma(p-n)}{\Gamma(-n-p-1)}.$$

Returning to $P(n,T)$, we find

$$\begin{aligned} P(n,T) = {} & \frac{h}{2^{n+1}} \sum_{\ell=\max(-n,0)}^{\infty} \frac{1}{\ell!\, 2^{2\ell}} \sum_{p=\max(-n-2\ell,0)}^{\infty} \frac{u^{(p)}(T)(-1)^p}{p!} \left(\frac{h^2}{2}\right)^p \frac{\gamma\left(2\ell+n+p+1, \frac{2T}{h^2}\right)}{\Gamma(\ell+n+1)} \\ & + \frac{h}{2^{n+2}} \sum_{\ell=\max(-n-1,0)}^{\infty} \frac{1}{\ell!\, 2^{2\ell}} \sum_{p=\max(-n-2\ell-1,0)}^{\infty} \frac{u^{(p)}(T)(-1)^p}{p!} \left(\frac{h^2}{2}\right)^p \frac{\gamma\left(2\ell+n+p+2, \frac{2T}{h^2}\right)}{\Gamma(\ell+n+2)} \\ & + h\sum_{p=0}^{\infty} \frac{u^{(p)}(T)h^{2p}}{(2p+1)!} \frac{\Gamma(1+p-n)}{\Gamma(-n-p)} + h\sum_{p=0}^{\infty} \frac{u^{(p)}(T)h^{2p}}{(2p+1)!} \frac{\Gamma(p-n)}{\Gamma(-n-p-1)}. \end{aligned}$$

The last two finite sums simplify:

$$\begin{aligned} & h\sum_{p=0}^{\infty} \frac{u^{(p)}(T)h^{2p}}{(2p+1)!} \frac{\Gamma(1+p-n)}{\Gamma(-n-p)} + h\sum_{p=0}^{\infty} \frac{u^{(p)}(T)h^{2p}}{(2p+1)!} \frac{\Gamma(p-n)}{\Gamma(-n-p-1)} \\ & \qquad = h\sum_{p=0}^{\infty} \frac{u^{(p)}(T)h^{2p}}{(2p+1)!} \left[\frac{\Gamma(1+p-n)}{\Gamma(-n-p)} + \frac{\Gamma(p-n)}{\Gamma(-n-p-1)}\right] \\ & \qquad = h\sum_{p=0}^{\infty} \frac{u^{(p)}(T)h^{2p}}{(2p+1)!} \left[\frac{(p-n)\,\Gamma(p-n)}{\Gamma(-n-p)} + \frac{(-n-p-1)\,\Gamma(p-n)}{\Gamma(-n-p)}\right] \\ & \qquad = h\sum_{p=0}^{\infty} \frac{u^{(p)}(T)h^{2p}}{(2p+1)!} \left[\frac{\Gamma(p-n)}{\Gamma(-p-n)}(p-n-n-p-1)\right] \\ & \qquad = -(2n+1)h \sum_{p=0}^{-n-1} \frac{u^{(p)}(T)h^{2p}}{(2p+1)!} \frac{\Gamma(p-n)}{\Gamma(-p-n)}, \end{aligned}$$

so that

$$P(n,T) = \frac{h}{2^{n+1}} \sum_{\ell=\max(-n,0)}^{\infty} \frac{1}{\ell!\, 2^{2\ell}} \sum_{p=\max(-n-2\ell,0)}^{\infty} \frac{u^{(p)}(T)(-1)^p}{p!} \left(\frac{h^2}{2}\right)^p \frac{\gamma\left(2\ell+n+p+1, \frac{2T}{h^2}\right)}{\Gamma(\ell+n+1)}$$
$$+ \frac{h}{2^{n+2}} \sum_{\ell=\max(-n-1,0)}^{\infty} \frac{1}{\ell!\, 2^{2\ell}} \sum_{p=\max(-n-2\ell-1,0)}^{\infty} \frac{u^{(p)}(T)(-1)^p}{p!} \left(\frac{h^2}{2}\right)^p \frac{\gamma\left(2\ell+n+p+2, \frac{2T}{h^2}\right)}{\Gamma(\ell+n+2)}$$
$$- (2n+1)h \sum_{p=0}^{-n-1} \frac{u^{(p)}(T) h^{2p}}{(2p+1)!} \frac{\Gamma(p-n)}{\Gamma(-p-n)}.$$

Therefore, combining the solution representations (2.2.18) and (5.2.8), we obtain a lengthy representation valid for all $n \in \mathbb{Z}$:

$$\begin{aligned} q_n(T) = {} & \frac{1}{2\pi} \int_{-\pi/h}^{\pi/h} e^{iknh} e^{-WT} \left[\hat{q}(k,0) + e^{ikh} \hat{q}(-k,0)\right] dk \\ & - \frac{h}{2^{n+1}} \sum_{\ell=\max(-n,0)}^{\infty} \frac{1}{\ell!\, 2^{2\ell}} \sum_{p=\max(-n-2\ell,0)}^{\infty} \frac{u^{(p)}(T)(-1)^p}{p!} \left(\frac{h^2}{2}\right)^p \frac{\gamma\left(2\ell+n+p+1, \frac{2T}{h^2}\right)}{\Gamma(\ell+n+1)} \\ & - \frac{h}{2^{n+2}} \sum_{\ell=\max(-n-1,0)}^{\infty} \frac{1}{\ell!\, 2^{2\ell}} \sum_{p=\max(-n-2\ell-1,0)}^{\infty} \frac{u^{(p)}(T)(-1)^p}{p!} \left(\frac{h^2}{2}\right)^p \frac{\gamma\left(2\ell+n+p+2, \frac{2T}{h^2}\right)}{\Gamma(\ell+n+2)} \\ & + (2n+1)h \sum_{p=0}^{-n-1} \frac{u^{(p)}(T) h^{2p}}{(2p+1)!} \frac{\Gamma(p-n)}{\Gamma(-p-n)}. \end{aligned} \tag{5.2.9}$$

If we are interested in the negative half-line only, letting $n \to -n$ for $n \geq 1$, we have

$$q_{-n}(T) = (1-2n)h \sum_{p=0}^{n-1} \frac{u^{(p)}(T) h^{2p}}{(2p+1)!} \frac{\Gamma(p+n)}{\Gamma(n-p)} + q_{n-1}(T). \tag{5.2.10}$$

We can also recover the Neumann boundary condition $u(T)$ from (5.2.10). Note that

$$\sum_{p=0}^{n-1} \frac{u^{(p)}(T) h^{2p}}{(2p+1)!} \frac{\Gamma(p+n)}{\Gamma(n-p)} = u(T) + \sum_{p=1}^{n-1} \frac{u^{(p)}(T) h^{2p}}{(2p+1)!} \frac{\Gamma(p+n)}{\Gamma(n-p)},$$

so that

$$q_{-n}(T) = (1-2n)h\, u(T) + (1-2n)h \sum_{p=1}^{n-1} \frac{u^{(p)}(T) h^{2p}}{(2p+1)!} \frac{\Gamma(p+n)}{\Gamma(n-p)} + q_{n-1}(T).$$

Since $q_x(0,t)$ was discretized via the standard backward stencil, we have

$$\frac{q_0(T) - q_{-1}(T)}{h} = \frac{q_0(T) + h\, u(T) - q_0(T)}{h} = u(T).$$

From [24], the analytic continuation to the continuous problem is

$$q(-x,T) = q(x,T) - 2 \sum_{p=0}^{\infty} \frac{u^{(p)}(T)\, x^{2p+1}}{(2p+1)!}. \tag{5.2.11}$$

We now show the semi-discrete continuation (5.2.10) converges to (5.2.11) in the continuum limit. Let

$$f(n,p) = \frac{\Gamma(p+n)}{\Gamma(n-p)} = \begin{cases} 1, & p = 0, \\ \displaystyle\sum_{\ell=0}^{2p-1} a_\ell \, n^{2p-\ell}, & p \geq 1, \end{cases}$$

with $a_0 = 1$. Then, we have

$$\begin{aligned} q_{-n}(T) &= q_{n-1}(T) + (h-2nh) \sum_{p=0}^{n-1} \frac{u^{(p)}(T) h^{2p}}{(2p+1)!} \, f(n,p) \\ &= q_{n-1}(T) + (h-2nh) \sum_{p=0}^{n-1} \frac{u^{(p)}(T) h^{2p}}{(2p+1)!} \left(n^{2p} + a_1 \, n^{2p-1} + \ldots \right) \\ q_{-n}(T) &= q_{n-1}(T) + (h-2nh) \sum_{p=0}^{n-1} \frac{u^{(p)}(T)}{(2p+1)!} \left[(nh)^{2p} + a_1 \, h (nh)^{2p-1} + \ldots \right] \\ \Rightarrow \quad \lim_{h \to 0} q_{-n}(T) &= \lim_{h \to 0} \left[q_{n-1}(T) + (h-2nh) \sum_{p=0}^{n-1} \frac{u^{(p)}(T)}{(2p+1)!} \left[(nh)^{2p} + a_1 \, h (nh)^{2p-1} + \ldots \right] \right] \\ q(-x,T) &= q(x,T) - 2x \sum_{p=0}^{n-1} \frac{u^{(p)}(T)}{(2p+1)!} \, x^{2p}. \end{aligned}$$

Solving the IBVP

$$\begin{cases} q_t = q_{xx}, & x > 0, \, t > 0, \\ q(x,0) = e^{-x} \cos(3\pi x), & x > 0, \\ q_x(0,t) = \frac{-\sin(4\pi t)}{4\pi}, & t > 0, \end{cases} \tag{5.2.12}$$

gives Figure 5.2.2 for two different h values.

5.2.3 Higher-Order Discretization of $q_t = q_{xx}$ with Dirichlet Condition

For our last example, we return to Section 2.2.3 with the fourth-order centered discretization (2.2.26) to the heat equation with a Dirichlet boundary condition. After several steps, the dispersion relation (2.2.28) and global relation (2.2.27) give solution (2.2.32):

$$q_n(T) = \frac{1}{2\pi} \int_{-\pi/h}^{\pi/h} e^{iknh} e^{-WT} \left[\hat{q}(k,0) - \hat{q}(-k,0) \right] dk + \frac{1}{2\pi} \int_{-\pi/h}^{\pi/h} e^{iknh} e^{-WT} \tilde{F}(k,T) \, dk,$$

with

$$\tilde{F}(k,T) = \frac{e^{-2ikh} \left(14 e^{ikh} - 14 e^{3ikh} + e^{4ikh} - 1 \right)}{12h} f_0 + \frac{h e^{-ikh} \left(e^{2ikh} - 1 \right)}{12} V + \frac{h^3 e^{-ikh} \left(e^{2ikh} - 1 \right)}{144} \tilde{V},$$

where $V(W,T)$ is the time transform of $v(t) = u'(t)$ and $\tilde{V}(W,T)$ of $\tilde{v}(t) = u''(t)$.

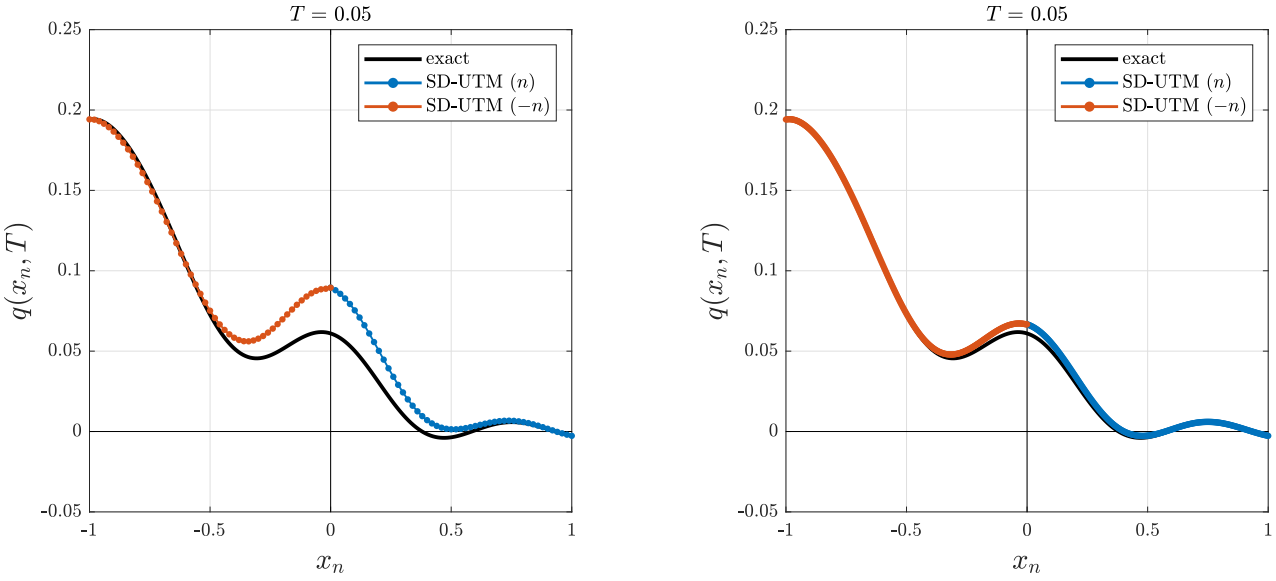

Figure 5.2.2: Extensions of half-line solution (2.2.18) for IBVP (5.2.12) with $h = 0.02$ (left) and $h = 0.004$ (right).

Like (2.2.9), one can show that (2.2.32) gives $q_{-n}(T) = -q_n(T)$ for $n \in \mathbb{Z}^+$. Following similar steps from the previous sections, albeit more laborious, we can obtain the valid analytic extension for the negative half-line solution. We introduce

$$B_m(n,T,g) = \frac{1}{24\pi h}\int_{-\pi/h}^{\pi/h} e^{ik(n+m)h - WT} G\, dk, \qquad G(W,T) = \int_0^T e^{Wt} g(t)\, dt,$$

for the boundary terms, so that (2.2.32) is rewritten as

$$\begin{aligned} q_n(T) = {} & \frac{1}{2\pi}\int_{-\pi/h}^{\pi/h} e^{iknh} e^{-WT}\left[\hat{q}(k,0) - \hat{q}(-k,0)\right] dk + 14B_{-1}(n,T,u) - 14B_1(n,T,u) + B_2(n,T,u) \\ & - B_{-2}(n,T,u) + h^2 B_1(n,T,v) - h^2 B_{-1}(n,T,v) + \frac{h^4}{12} B_1(n,T,\tilde{v}) - \frac{h^4}{12} B_{-1}(n,T,\tilde{v}). \end{aligned} \tag{5.2.13}$$

Breaking down $B_m(n,T,g)$ by replacing the definition for $G(W,T)$, we have

$$B_m(n,T,g) = \int_0^T \left[\frac{1}{24\pi h}\int_{-\pi/h}^{\pi/h} e^{ik(n+m)h - W(T-t)}\, dk\right] g(t)\, dt = \int_0^T J_m(n,T,t) g(t)\, dt,$$

where

$$J_m(n,T,t) = \frac{1}{24\pi h}\int_{-\pi/h}^{\pi/h} e^{ik(n+m)h - W(T-t)}\,dk$$
$$= \frac{e^{\frac{-5(T-t)}{2h^2}}}{12h^2}\operatorname*{Res}_{z=0}\left\{z^{n+m-1}\exp\left[\left(-z^{-2}+16z^{-1}+16z-z^2\right)\frac{T-t}{12h^2}\right]\right\}.$$

After determining the residues, we find

$$B_m(n,T,g) = \frac{1}{30}\sum_{j=-\infty}^{\infty}(-1)^j\int_0^{\frac{5T}{2h^2}} e^{-s} I_j(s/15) I_{-n-m-2j}(16s/15)\, g\left(T-\frac{2h^2}{5}s\right)\,ds.$$

At this stage, we take Taylor series expansions about $h = 0$, rewrite ratios of Gamma functions, and determine which summation terms contribute for negative n. These tedious steps are left to the reader.

Chapter 6

SPLIT-STEP FINITE-DIFFERENCE METHOD

6.1 Background

Our goal is to solve nonlinear IBVPs with finite difference schemes, while addressing ghost points and the complications they present. We propose a split-step method that separately solves the linear subproblem (1.1.3) and the nonlinear subproblem (1.1.4).

A split-step method owes part of its success to the fact that it avoids solving a nonlinear algebraic system at each time step. Instead, it decomposes the original problem (1.1.2) into simpler subproblems, building an approximate solution of the original problem by using exact or approximate solutions of subproblems in a given sequential order [54]. How that sequential order takes place determines the order of accuracy of the split-step method [34, 49].

Many approaches have been developed over the years to efficiently solve the linear subproblem (1.1.3) with numerical methods, but two main ones stand out. The first approach relies on *Fourier methods*, using the (discrete) Fourier transform and computing approximate solutions with fast Fourier techniques [33, 48, 65]. However, this requires periodic boundary conditions on the interval, often in contrast to actual physical problems with outflow and inflow boundary data. The second approach uses *finite-difference methods* that provide an approximate solution by discretizing the spatial derivative and applying a time-stepping method (see Section 1.1 and Chapter 3) [32, 36, 70]. This approach is more general and is better equipped to handle non-periodic boundary conditions than the Fourier methods, but wide discretization stencils lead to ghost points, which in turn lead to numerical instabilities [68]. Other popular approaches, like Chebyshev spectral methods, do not introduce ghost points, but often introduce stability conditions that are restrictive and challenging to analyze when applied to boundary problems [66]. Most numerical studies center on full-line problems with sufficiently decaying boundary conditions to treat them as homogeneous or finite interval problems with periodic boundary conditions [20, 58, 72]. Others develop unique tactics to address the difficulties with non-periodic IBVPs, but struggle to be generalizable to higher-order problems [2, 39, 40, 69, 73, 74]. Additionally, when full-line or half-line problems are truncated to a finite domain, the common argument is that these artificial boundaries are merely placed "far enough" apart in order to not interfere with dispersive effects within the window of interest (see the introduction to Chapter 2). In general, non-periodic finite-interval IBVPs for nonlinear evolution equations, most notably dispersive PDEs, have received little attention [56, 57].

In order to tackle the vast class of PDEs (1.1.1) and their given boundary conditions, we treat the

linear subproblem (1.1.3) in split-step methods with finite-difference schemes. Hence, we refer to this as a split-step finite-difference (SSFD) method. Since the PDEs are quasi-linear, the spatial stencil of accuracy $\mathcal{O}(h^r)$ applied to (1.1.3) is *at least as nonlocal* as stencils of $\mathcal{O}(h^r)$ applied to the nonlinear subproblem (1.1.4), when no exact solution can be provided for the latter. In practice, (1.1.3) is most affected by boundary conditions and ghost points. As discussed in Section 1.2, the UTM can be applied to solve (1.1.3) with general boundary conditions, but the evaluation of the resulting integral representations are numerically costly, especially when computing the solution several hundreds or thousands of times within a split-step implementation, and series representations cannot be obtained for all orders M of (1.1.1). Unfortunately, similar arguments can be made against the SD-UTM solutions and their representations.

Thus, we apply the UTM or SD-UTM at only the ghost points of a spatial discretization of (1.1.3). Although Chapters 2 – 4 lay out the framework for SD-UTM, with Chapter 5 presenting the semi-discrete analytic-continuation formulas, we first tackle our goal with UTM and the analytic continuation formulas produced by Farkas *et al.* [24].

6.2 The Nonlinear Schrödinger Equation

We consider the nonlinear Schrödinger (NLS) equation on the finite interval with, say, Dirichlet boundary conditions:

$$\begin{cases} q_t = i\sigma q_{xx} + i\lambda |q|^2 q, & 0 < x < L,\ t > 0, \\ q(x,0) = \phi(x), & 0 < x < L, \\ q(0,t) = u^{(0)}(t), & t > 0, \\ q(L,t) = v^{(0)}(t), & t > 0, \end{cases} \tag{6.2.1}$$

where $\sigma, \lambda \in \mathbb{R}$. The NLS equation is one of the most widely applicable equations in the physical sciences used to characterize nonlinear dispersive phenomena, like waves in plasmas, nonlinear optics, water, and molecular dynamics [52]. In many real-world applications, like propagation of a laser beam in an optical fiber, the domain is finite, so physical boundaries and the numerical implementations of the boundary conditions are vital [1, 9, 33].

A split-step method applied to the NLS equation consists of iteratively combining the separate solutions to the linear, dispersive subproblem

$$\begin{cases} q_t = i\sigma q_{xx}, & 0 < x < L,\ t > 0, \\ q(x,0) = \phi(x), & 0 < x < L, \\ q(0,t) = u(t), & t > 0, \\ q(L,t) = v(t), & t > 0, \end{cases} \tag{6.2.2}$$

and the nonlinear subproblem,

$$\begin{cases} q_t = i\lambda|q|^2 q, & 0 < x < L,\ t > 0, \\ q(x,0) = \phi(x), & 0 < x < L. \end{cases} \tag{6.2.3}$$

Note that (6.2.3) is an ODE in time that has an exact solution and has no dependence on the given boundary conditions, while (6.2.2) incorporates the boundary data appropriately derived from the full problem (6.2.1) [42, 44]. Many works have studied various orders of accuracy for split-step methods that solve the NLS equation [3, 4, 7, 23, 37, 45, 46, 50, 54, 61]. For simplicity, we implement second-order Strang splitting to solve (6.2.1), where (6.2.2) is solved once and (6.2.3) is solved twice per time-step [36]. We denote the split-step time step between iterations as $\tau = T/N_{t,SS}$ for $N_{t,SS}$ total time steps. Details of the split-step implementation itself are discussed where necessary.

To solve (6.2.2) with a finite-difference scheme, suppose we apply a fourth-order spatial discretization, so that the linear Schrödinger equation from (6.2.2) becomes

$$\dot{q}_n = i\sigma \left(\frac{-q_{n-2} + 16q_{n-1} - 30q_n + 16q_{n+1} - q_{n+2}}{12h^2} \right). \tag{6.2.4}$$

Since we have Dirichlet data at $n = 0$ and $n = N_x + 1$, (6.2.4) is used at $n = 1, \ldots, N_x$ with $h = L/(N_x + 1)$. Precisely, at $n = 1$, (6.2.4) introduced the dependence on a ghost point at $n = -1$, while at $n = N_x$, we have a ghost point at $n = N_x + 2$:

$$\begin{cases} \dot{q}_1 = i\sigma \left(\dfrac{-q_{-1} + 16u(t) - 30q_1 + 16q_2 - q_3}{12h^2} \right), \\ \dot{q}_{N_x} = i\sigma \left(\dfrac{-q_{N_x-2} + 16q_{N_x-1} - 30q_{N_x} + 16v(t) - q_{N_x+2}}{12h^2} \right). \end{cases} \tag{6.2.5}$$

The sections that follow address the standard and alternative approaches when dealing with ghost points when solving (6.2.2). They are also applicable to not only other discretizations of the NLS equation, but to other PDEs as well.

6.2.1 Standard Approach

The standard approach is to altogether avoid these ghost points by applying certain spatial stencils near the boundaries, *i.e.,* at $n = 1$ and $n = N_x$. The method of undetermined coefficients derives approximations to derivatives up to a desired order of accuracy and is perhaps the most straightforward approach that generalizes to other cases, like higher-order accurate methods, nonuniform grids, and higher-order derivative boundary conditions [43, 73]. Instead of applying the centered stencil (6.2.4), we solve systems of equations to obtain one-sided stencils of accuracy $\mathcal{O}(h^4)$. When

respectively applied at $n = 1$ and $n = N_x$, they do not introduce ghost points:

$$\begin{cases} \dot{q}_1 = i\sigma \left(\dfrac{10u(t) - 15q_1 - 4q_2 + 14q_3 - 6q_4 + q_5}{12h^2} \right), \\ \dot{q}_{N_x} = i\sigma \left(\dfrac{q_{N_x-4} - 6q_{N_x-3} + 14q_{N_x-2} - 4q_{N_x-1} - 15q_{N_x} + 10v(t)}{12h^2} \right). \end{cases} \tag{6.2.6}$$

Writing the main stencil (6.2.4) for $n = 2, \ldots, N_x - 1$ and the boundary stencils (6.2.6) into a method-of-lines formulation gives

$$\dot{Q}(t) = AQ(t) + Lu(t) + Rv(t), \tag{6.2.7}$$

where $Q(t), L, R \in \mathbb{R}^{N_x \times 1}$ and $A \in \mathbb{R}^{N_x \times N_x}$. Note that A, L, and R are sparse and contain stencil coefficients. Here, we apply our choice of ODE solver to obtain an approximate solution in space and time to (6.2.2). Usually, this formulation allows for von Neumann stability analysis of finite-difference schemes via eigenvalues of A if A is normal $\left(A^T A = AA^T\right)$ (at least in the full-line or periodic problem, but if either of these is unstable, then it is likely that the finite interval problem will also be unstable [43]). However, many times with this standard approach of deriving new stencils near the boundaries, A can be highly nonnormal, such that the familiar eigenvalue stability analysis for the linear problem is misleading and unhelpful, having to resort to studying the ϵ-pseudospectrum [31, 43, 67]. This is the case for the coefficient matrix A in the system (6.2.7).

6.2.2 Analytic Continuation

Alternative to the standard approach above, we propose to keep whatever ghost points develop and determine their data according to the analytic continuation formulas for that linear IBVP. The UTM solution to the second-order IBVP (6.2.2) is

$$\begin{aligned} q(x,T) = {} & \frac{1}{2\pi} \int_{-\infty}^{\infty} e^{ikx - i\sigma k^2 T} \hat{q}(k,0)\, dk \\ & + \frac{1}{2\pi} \int_{\partial\tilde{\Omega}^+} e^{ikx - i\sigma k^2 T} \left[\frac{\hat{q}(-k,0) - e^{2ikL}\hat{q}(k,0) - 2k\sigma \left(F_0 - e^{ikL} G_0\right)}{e^{2ikL} - 1} \right] dk \\ & - \frac{1}{2\pi} \int_{\partial\tilde{\Omega}^-} e^{ikx - i\sigma k^2 T} \left[\frac{\hat{q}(k,0) - e^{2ikL}\hat{q}(-k,0) + 2k\sigma \left(F_0 - e^{ikL} G_0\right)}{e^{2ikL} - 1} \right] dk, \end{aligned} \tag{6.2.8}$$

where $\Omega^{\pm} = \{k \in \mathbb{C}^{\pm} \,\big|\, \mathrm{Re}\left(-i\sigma k^2\right) > 0\}$ and $\partial\tilde{\Omega}^{\pm}$ is along the boundary of $\Omega^{\pm}$ while avoiding the singularities along the real line in the complex k-plane [17]. After substituting definitions into (6.2.8) and applying Taylor series expansions [24], the following relations are valid outside of the original interval $[0, L]$, but near it:

$$q(-x,T) = 2 \sum_{\ell=0}^{\infty} \frac{x^{2\ell}}{(2\ell)!(i\sigma)^{\ell}}\, u^{(\ell)}(T) - q(x,T), \tag{6.2.9a}$$

$$q(L+x,T) = 2\sum_{\ell=0}^{\infty} \frac{x^{2\ell}}{(2\ell)!(i\sigma)^{\ell}}\, v^{(\ell)}(T) - q(L-x,T), \tag{6.2.9b}$$

where $u^{(\ell)}(T)$ and $v^{(\ell)}(T)$ denote the ℓ^{th} derivatives of the respective boundary conditions at $T = t$. The information for ghost points that develop in (6.2.5) are given as

$$\begin{cases} q_{-1}(T) = 2\displaystyle\sum_{\ell=0}^{\infty} \frac{h^{2\ell}}{(2\ell)!(i\sigma)^{\ell}}\, u^{(\ell)}(T) - q_1(T), \\ q_{N_x+2}(T) = 2\displaystyle\sum_{\ell=0}^{\infty} \frac{h^{2\ell}}{(2\ell)!(i\sigma)^{\ell}}\, v^{(\ell)}(T) - q_{N_x}(T), \end{cases} \tag{6.2.10}$$

so that (6.2.5) is written as

$$\begin{cases} \dot{q}_1 = i\sigma\left(\dfrac{16u(T) - 29q_1 + 16q_2 - q_3}{12h^2}\right) - \dfrac{2i\sigma}{12h^2}\displaystyle\sum_{\ell=0}^{\infty} \frac{h^{2\ell}}{(2\ell)!(i\sigma)^{\ell}}\, u^{(\ell)}(T), \\ \dot{q}_{N_x} = i\sigma\left(\dfrac{-q_{N_x-2} + 16q_{N_x-1} - 29q_{N_x} + 16v(T)}{12h^2}\right) - \dfrac{2i\sigma}{12h^2}\displaystyle\sum_{\ell=0}^{\infty} \frac{h^{2\ell}}{(2\ell)!(i\sigma)^{\ell}}\, v^{(\ell)}(T). \end{cases} \tag{6.2.11}$$

With these relations, the method-of-lines formulation becomes

$$\dot{Q}(t) = AQ(t) + Lu(t) + Rv(t) + L_{AC}(t) + R_{AC}(t). \tag{6.2.12}$$

which differs from (6.2.7) with the addition of time-dependent terms $L_{AC}(t), R_{AC}(t) \in \mathbb{R}^{N_x \times 1}$. Because the main fourth-order stencil (6.2.4) was applied at all points and no special stencils were introduced near the boundaries, it can be shown that the coefficient matrix A exhibits a normal structure. However, the main complication with this alternative approach is that the analytic continuation terms $L_{AC}(t), R_{AC}(t)$ are time-dependent and consist of infinite sums. However, we can choose how many terms to include in the sums based on how quickly the sum converges. In (6.2.11), note that specifically the ratio $h^{2\ell}/(2\ell)! \to 0$ as $\ell \to \infty$ and as $h \to 0$. In fact, the numerical examples that follow show that these sums rarely require more than 2 terms.

6.2.3 Numerical Examples

Let us clarify the notation used to solve the overall original problem (6.2.1) with the SSFD method. We denote the number of time steps in the split-step method as $N_{t,SS}$ with time step $\tau = T/N_{t,SS}$, where $T > 0$ is the time over which we are solving the original problem. For the finite-difference method to solve the linear subproblem (6.2.2), we denote the number of interior spatial grid points as N_x with uniform spacing $h = L/(N_x + 1)$, and the number of time steps as $N_{t,FD}$ with time step $k = \tau_i/N_{t,FD}$,where τ_i is the i^{th} time interval we are solving (6.2.2) across in a given split-step iteration.

For the following examples, the linear subproblem (6.2.2) is always solved with the fourth-order spatial stencil (6.2.4) and time-stepped with the trapezoidal method (TR). The Strang splitting for the overall problem implies the numerical solutions are fourth-order accurate in space and second-order accurate in time. What varies is the approach we use to address ghost points: either the standard approach (SA) of introducing new stencils near the boundaries to avoid ghost points or the analytic continuation (AC) formulas to determine information at the ghost points.

Soliton Solution

The easiest readily available solution to the NLS equation is the soliton solution, based on the full-line problem. For a given explicit solution, we can impose an initial condition and boundary conditions to generate a well-posed finite interval IBVP. The first numerical example we consider is a truncated soliton solution from [64] with $\sigma = -1$ and $\lambda = -2$:

$$\tilde{q}(x,t) = \frac{2\eta e^{-i\left[2x\xi - 4(\xi^2-\eta^2)t + \psi_0 + \pi/2\right]}}{\cosh\left(2\eta x - 8\eta\xi t - x_0\right)}, \tag{6.2.13}$$

where η, ξ, ψ_0, and x_0 are parameters. From here, we want to now solve

$$\begin{cases} q_t = -iq_{xx} - 2i|q|^2 q, & 0 < x < 1,\ t > 0, \\ q(x,0) = \phi(x) = \tilde{q}(x,0), & 0 < x < 1, \\ q(0,t) = u(t) = \tilde{q}(0,t), & t > 0, \\ q(1,t) = v(t) = \tilde{q}(1,t), & t > 0. \end{cases} \tag{6.2.14}$$

The exact solution (6.2.13) allows us to easily compare numerical solutions.

With $N_x = 2^7 - 1$, $N_{t,FD} = 2^4$, and $N_{t,SS} = 2^5$, we solve (6.2.14) up to $T = 0.1$ with the SA and AC formulations. The real part of the solutions is depicted as green curves in Figure 6.2.1. At least graphically on the same grid and time-stepping parameters, we see that the AC formulation leads to a better approximation with less numerical oscillations than the SA formulation. The blue dashed lines in Figure 6.2.1 show the differences between the exact and SSFD solutions. The TR method is dispersive itself, so if the finite-difference solution to the linear subproblem is not well resolved, numerical dispersion is introduced into the solution. Although not shown, the imaginary component and the modulus squared of the SSFD solutions show similar behavior as in Figure 6.2.1. For Figure 6.2.1b, the AC formulation used $\ell = 4$ summation terms at each of the ghost points (6.2.11). In fact, Figure 6.2.2 shows that 2 terms would have sufficed, reaching an ∞-norm error between $q_n(0.1) - q(x_n, 0.1)$ of order 10^{-5}. Note that $\ell = 0$ reduces (6.2.10) to a reflection principle with error around 0.4, while simply including one term drastically reduces the error by a factor of 100, down to nearly 0.003 in the ∞-norm. After just 2 terms, the error plateaus and other errors from the numerical method dominate, such as from the finite-difference time stepping.

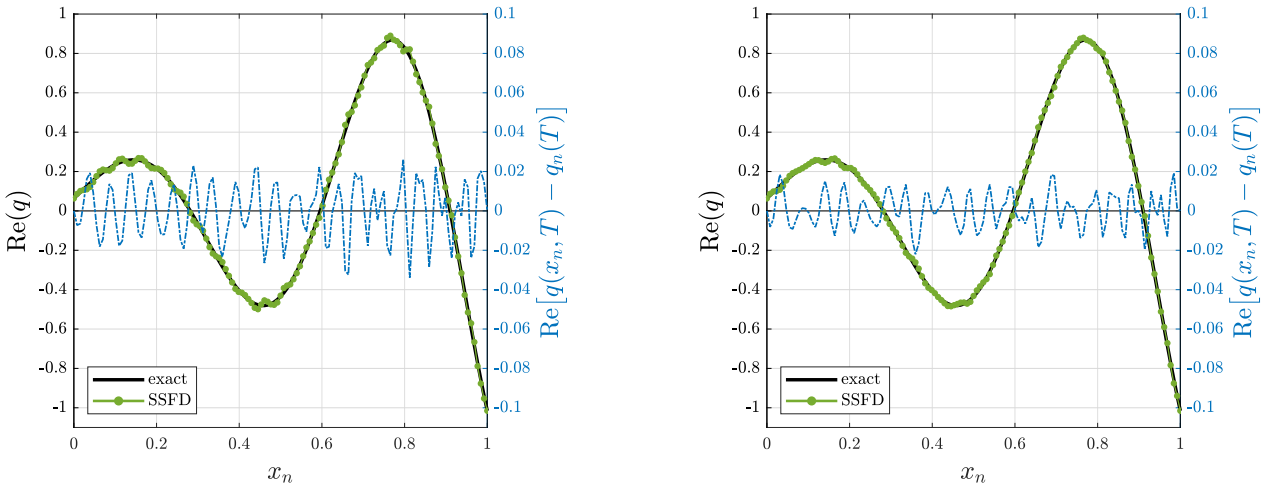

Figure 6.2.1: The real part of the SSFD solutions to IBVP (6.2.14) with (a) the SA formulation and (b) the AC formulation for the linear subproblem.

Figure 6.2.3 shows the convergence of the split-step method as we refine the spatial grid with small split-step time-steps τ and vary the finite-difference time-step k in the TR method. Both plots in Figure 6.2.3 exhibit the expected $\mathcal{O}(h^4)$ convergence rate, but the AC formulation appears to be more consistent and produces slightly more accurate results on a coarse grid compared to the SA formulation. As $h \to 0$, the temporal truncation errors begin to dominate, causing the curves to plateau for smaller h. Of course, the smaller the time-steps in the Strang splitting and TR methods, the more accurate the SSFD solution on a fixed spatial grid. To confirm this, we include Figure 6.2.3 for this example, depicting the $\mathcal{O}(\tau^2)$ convergence rate from the second-order splitting as $\tau \to 0$ for both SA and AC formulations. Once again, both formulations perform similarly, with the AC approach slightly outperforming SA in generating smaller errors.

Incompatible Corner

Our final example attempts to capture the dispersive nature of the NLS equation by tackling an IBVP that has a discontinuity at $(x, t) = (1, 0)$, *i.e.,* the initial condition is incompatible with the right boundary condition at $t = 0$. For $t > 0$, a dispersive wave train develops at the right boundary, quickly spreading toward the left boundary. Hence, we focus on small T for this IBVP where we

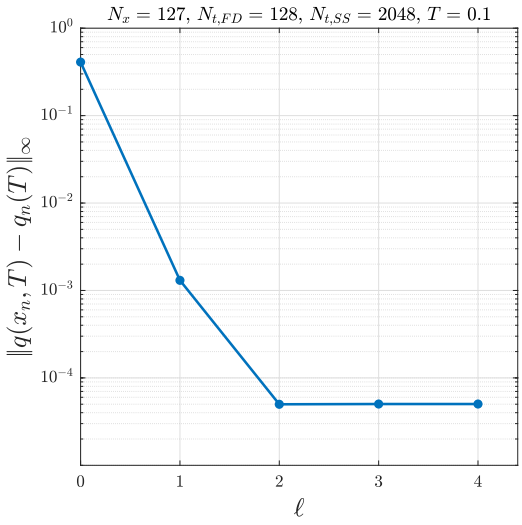

Figure 6.2.2: The ∞-norm error of the AC-formulated SSFD solution to IBVP (6.2.14) with ℓ terms.

aim to capture these oscillations specifically near $x = 1$. Consider the IBVP

$$\begin{cases} q_t = iq_{xx} + i|q|^2 q, & 0 < x < 1,\ t > 0, \\ q(x,0) = \phi(x) = 1, & 0 < x < 1, \\ q(0,t) = u(t) = e^{-t}, & t > 0, \\ q(1,t) = v(t) = \cos(2\pi t)/2, & t > 0. \end{cases} \tag{6.2.15}$$

Of course, there is no exact solution to (6.2.15). Instead, we must solve the IBVP on a very fine grid with small split-step and finite-difference time-steps in order to guarantee an accurate solution to this highly dispersive problem. We take the SSFD solution with an SA formulation and $N_x = 2^{15}$, $N_{t,FD} = 2^7$, and $N_{t,SS} = 2^8$ to be the "exact" solution to (6.2.15). We solve the problem across the entire unit interval, but the following figures depict results for the narrowed window $x \in [0.9, 1]$.

Figure 6.2.5 shows the real part of the solutions to (6.2.15) with SA and AC formulations at $T = 10^{-5}$ when $N_x = 2^{12}$, $N_{t,FD} = 2^5$, and $N_{t,SS} = 2^4$. Again, the AC formulation used $\ell = 4$ summation terms at each of the ghost points (6.2.11). Although both formulations are treated with the same finite-difference and splitting methods, it is clear that the AC formulation outperforms the SA formulation (see the blue dashed lines in Figure 6.2.5). Both approaches capture the large oscillations near the boundary and both eventually fail as $x_n \to 0^+$, but when the SA formulation is implemented, the numerical dispersion introduced by the TR method significantly overpowers the true dispersive nature of the NLS equation. For larger $T \sim 10^{-1}$, the wave train reaches the left boundary and induces further oscillations where even the most tailored methods struggle to solve

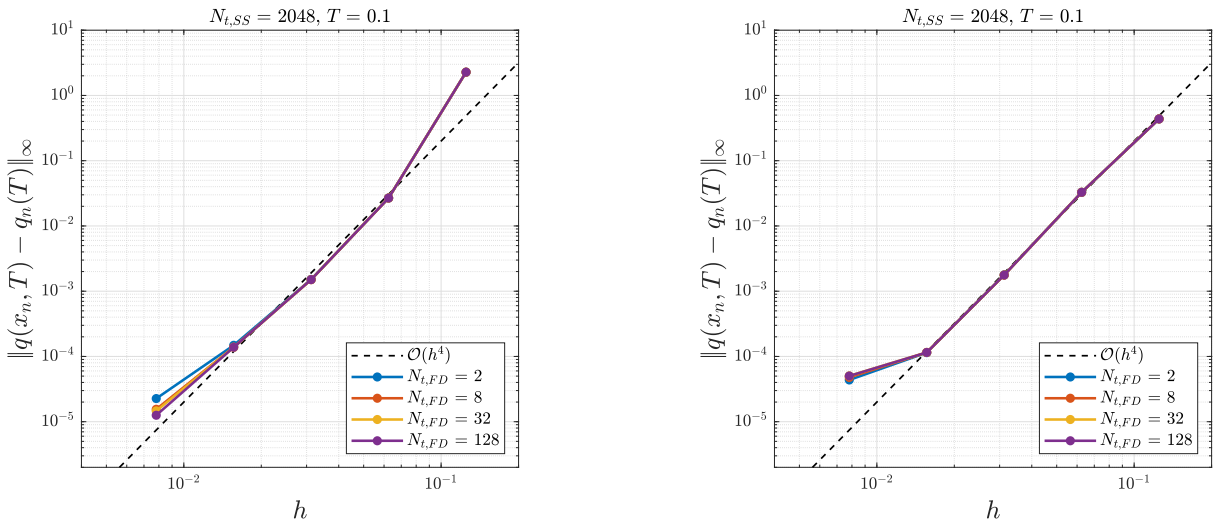

Figure 6.2.3: Error plot as $h \to 0$ of the SSFD solutions to IBVP (6.2.14) with (a) the SA formulation and (b) the AC formulation for the linear subproblem. We vary the number of finite-difference time steps $N_{t,FD}$ in each plot.

the NLS equation.

Figure 6.2.6 shows a faster convergence than Figure 6.2.2 from the previous section, with the error plateauing after $\ell = 1$. Since the error is less than 10^{-2}, we could save computational power in computing the SSFD-AC solutions by solely considering $u(t)$ and its first derivative. In this case, the ℓ^{th} derivative of the right boundary condition has a closed form, but this is not the case in more complicated examples, like with IBVP (6.2.14). In general for sufficiently smooth derivatives, one could symbolically determine the ℓ^{th} derivative, but this adds to the overall computational costs.

Lastly, Figure 6.2.7 shows the $\mathcal{O}(h^4)$ convergence rate, but only for sufficiently small h where the SSFD solutions are refined enough to capture both the magnitude and phase of the oscillations within the narrow window $x \in [0.9, 1]$. Once the solutions satisfy this "threshold," the SA formulations lead to an uptick in the ∞-norm errors for relatively large finite-difference time-steps. The SSFD-AC formulations follow a more expected plateauing behavior as $h \to 0$, where the temporal truncation errors begin to dominate for small enough h.

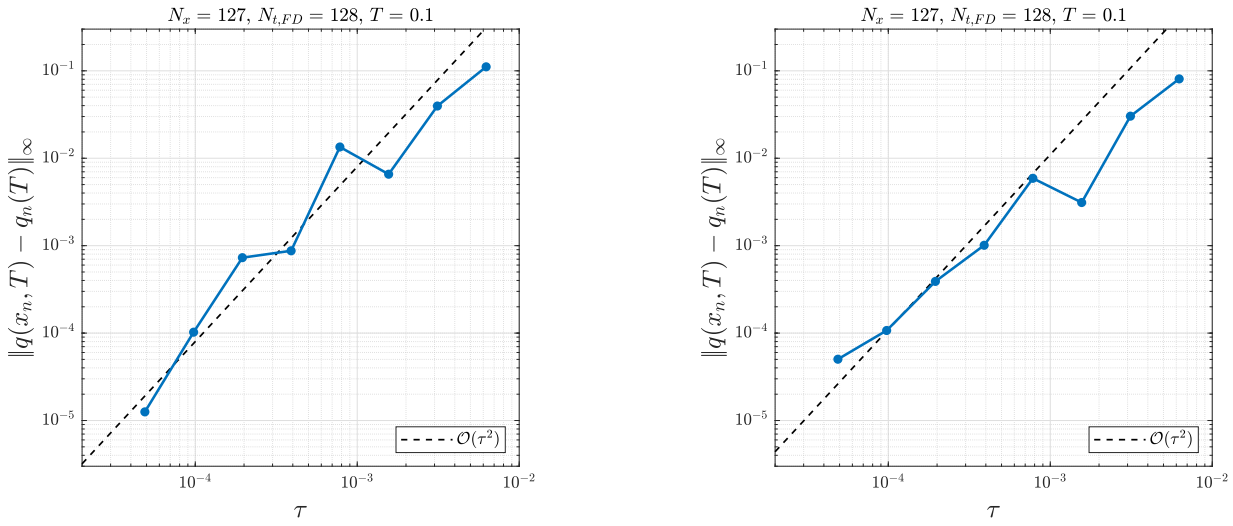

(a) (b)

Figure 6.2.4: Error plot as $\tau \to 0$ of the SSFD solutions to IBVP (6.2.14) with (a) the SA formulation and (b) the AC formulation for the linear subproblem.

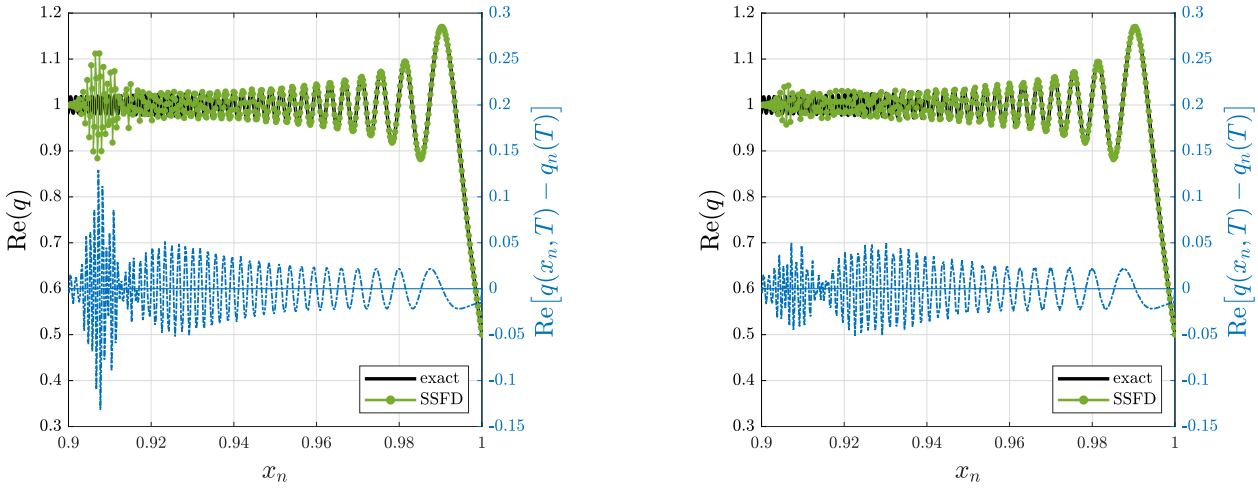

(a) (b)

Figure 6.2.5: The real part of the SSFD solutions to IBVP (6.2.15) with (a) the SA formulation and (b) the AC formulation for the linear subproblem.

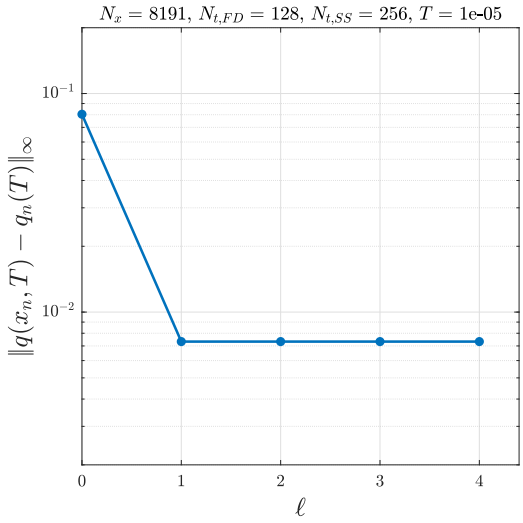

Figure 6.2.6: The ∞-norm error of the AC-formulated SSFD solution to IBVP (6.2.15) with ℓ terms.

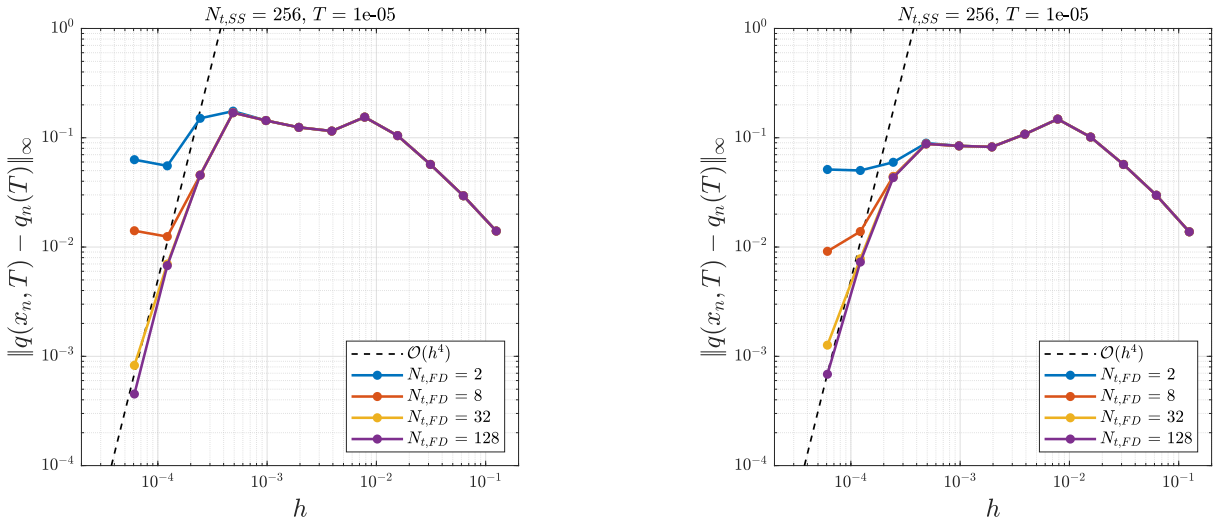

(a) (b)

Figure 6.2.7: Error plot as $h \to 0$ of the SSFD solutions to IBVP (6.2.15) with (a) the SA formulation and (b) the AC formulation for the linear subproblem. We vary the number of finite-difference time steps $N_{t,FD}$ in each plot.

Chapter 7

CONCLUSION AND FUTURE WORK

Finite difference methods continue to be one of the most intuitive and direct ways to solve IBVPs. Setting out to solve quasi-linear IBVPs, the application of wide spatial stencils leads to troublesome ghost points that are commonly tackled in limited approaches that do not easily generalize to higher-order problems.

Chapters 2 – 4 discuss the semi-discrete UTM and its continuum limit when applied to half-line and finite interval IBVPs of various orders and discretizations. With minor differences in the calculations, the procedure for the semi-discrete UTM is almost identical to that from the continuous UTM, with Steps (7) and (8) added. The steps themselves become more tedious for higher-order problems, but like the continuous UTM, the SD-UTM reduces the burden of solving a semi-discrete IBVP to solving for the roots of polynomials and dealing with a set of algebraic equations.

For a given discretization of a PDE, the global relation and its regions of validity under the symmetries $\nu_j(k)$ impose which stencils can be selected for derivative boundary conditions, as we saw with the higher-order discretizations and the Neumann problems. Similar to how the continuous UTM determines which types of boundary conditions result in a well-posed problem [28], "natural" discretizations reduce the variety of stencils to those that are compatible with the IBVP. We reiterate that a natural discretization for a PDE is (i) of the same order as the spatial order of the PDE, (ii) not purely one sided (except for first-order problems), and (iii) the one that optimally aligns with the available boundary conditions.

Lastly, the extended semi-discrete solutions presented in Chapter 5 and in [24] provide information at ghost points, *i.e.*, outside of the original domain of definition. Chapter 6 capitalizes on these analytic continuation formulas to develop split-step finite-difference methods for quasi-linear IBVPs, like the NLS equation. These methods are comparable to existing approaches that solve this class of problems, but most notably preserve the normal structure of the coefficient matrix in a method-of-lines formulation where the usual eigenvalue analysis can be done. The systematic derivation for these methods will open doors to novel numerical techniques that efficiently solve dispersive IBVPs. Specifically, some of the directions for future research include:

(i) **Derive and implement small-time approximations to the UTM formulas.** Like we did in Sections 2.5 and 3.5 for SD-UTM integral representations, one could repeat the steps for the continuous UTM. Choosing the same order of temporal accuracy as the splitting and finite-difference method to solve the linear subproblem, these small-time approximations could

lead to more efficient SSFD-AC methods with analytic continuation formulas that are easier to implement.

(ii) **Apply the SD-UTM extension formulas within SSFD methods.** Chapter 6 exhibits SSFD methods with AC formulations that derive from the continuous UTM that could be replaced with the SD-UTM extension formulas following the ideas from Chapter 5. Throughout the bulk of this dissertation, we have seen that the SD-UTM representations tend to be simpler to work with than the continuous UTM representations, so perhaps the SSFD-AC formulas could increase efficiency while retaining the same level of spatial accuracy. The small-time approximations from Section 3.5 could similarly be tested.

(iii) **Explore alternative approaches when solving the full quasi-linear IBVP.** There exist quasi-linear PDEs where the nonlinear subproblem does not have an exact solution. Now, both linear and nonlinear subproblems require finite-difference schemes, potentially introducing ghost points at each subproblem if all spatial derivatives have stencils applied to them of the same order of accuracy. For these types of IBVPs, it might be beneficial to solve the original problem entirely without any splitting [65, 68]. Two approaches are worth exploring in this context. The first is to apply the linear analytic continuation formulas at the ghost points directly, such that information there is known. However, this requires the evaluation of the linear solution at ghost points for general, high-order IBVPs, perhaps creating too much of a discrepancy between ghost and the (nonlinearly-related) interior points. Solving this nonlinear system with additional time-dependencies might be time consuming and problematic near boundaries. The second approach is to apply the linear analytic continuation formulas to relate the ghost points back into the domain and solve them with the rest of the interior points (closely related to Section 6.2.2). We expect this approach to be more efficient than the first, without the need to compute the linear solution itself. Although the relations are linear at the ghost points, the grid points for the full nonlinear problem are all solved together simultaneously. Note that both approaches are equivalent for linear, monomial PDEs.

(iv) **Set up a black-box solver.** Ideally, we want to culminate all of these findings into a black-box solver that could potentially be applied to a variety of IBVPs. There is an emphasis to focus on dispersive problems, like NLS-type and KdV-type equations. With an expansive numerical solver, we could additionally treat dissipative problems, like nonlinear heat equations.

Appendix A

STARTING INDEX ON SEMI-DISCRETE TRANSFORM PAIR

Let us define the discrete transform pair for the half-line problems as:

$$\hat{q}(k,t) = h\sum_{n=a}^{\infty} e^{-iknh} q_n(t), \quad a \in \mathbb{Z} \tag{A.1a}$$

$$q_n(t) = \frac{1}{2\pi}\int_{-\pi/h}^{\pi/h} e^{iknh}\hat{q}(k,t)\,dk, \quad n = a, a+1, a+2, \ldots, \tag{A.1b}$$

where we will call (A.1a) the forward transform and (A.1b) the inverse transform. Of course, we usually set $a = 0$, but let us proceed in a general manner. For comparison, recall the continuous Fourier transform pair for half-line problems:

$$\hat{q}(k,t) = \int_0^{\infty} e^{-ikx} q(x,t)\,dx,$$
$$q(x,t) = \frac{1}{2\pi}\int_{-\infty}^{\infty} e^{ikx}\hat{q}(k,t)\,dk.$$

In the continuous pair, we assume that $q(x,t) = 0$ for $x < 0$. This is not necessary in the discrete pair: we do not have to assume that $q_n(t) = 0$ for all $n \leq a-1$. If we do so, then there will be contradictions when ghost points develop in the global relation. Instead, we ignore $q_n(t)$ for all $n \leq a-1$ and treat them as unknowns; they may be zero or nonzero, but will not matter until they come into play.

The transform pair (A.1a) and (A.1b) still hold for any a, regardless of $q_n(t)$ for $n \leq a-1$. In a way, we are defining (A.1a) and (A.1b) as the half-line transform pair ourselves, instead of originating from the full-line (bi-lateral) transform pair

$$\hat{q}(k,t) = h\sum_{n=-\infty}^{\infty} e^{-iknh} q_n(t)$$
$$q_n(t) = \frac{1}{2\pi}\int_{-\pi/h}^{\pi/h} e^{iknh}\hat{q}(k,t)\,dk, \quad n = \ldots, -1, 0, 1, \ldots$$

and assuming $q_n(t) = 0$ for all $n \leq a-1$ to obtain (A.1a) and (A.1b).

So, using the definitions (A.1a) and (A.1b), let us show these are still inverses of each other,

regardless of a and $q_n(t)$ for $n \le a-1$. Plugging the inverse transform into the forward transform:

$$\begin{aligned}
q_n(t) &= \frac{1}{2\pi}\int_{-\pi/h}^{\pi/h} e^{iknh}\hat{q}(k,t)\,dk \\
&= \frac{1}{2\pi}\int_{-\pi/h}^{\pi/h} e^{iknh}\left[h\sum_{m=a}^{\infty} e^{-ikmh}q_m(t)\right]dk \\
&= \frac{h}{2\pi}\sum_{m=a}^{\infty} q_m(t)\left[\int_{-\pi/h}^{\pi/h} e^{ik(n-m)h}\,dk\right] \\
&= \frac{h}{2\pi}\sum_{m=a}^{\infty} q_m(t)\left[\frac{1}{ih}\oint_{|z|=1} z^{n-m-1}\,dz\right], \quad z = e^{ikh} \\
&= \frac{h}{2\pi}\sum_{m=a}^{\infty} q_m(t)\left[\frac{2\pi}{h}\delta_{nm}\right] \\
&= q_n(t).
\end{aligned}$$

Note that the range of n nor m was not important. All we cared about was whenever $n = m$.

Instead of plugging the forward transform into the inverse transform, let us write out what the forward transform is:

$$\begin{aligned}
\hat{q}(k,t) &= h\sum_{n=a}^{\infty} e^{-iknh}q_n(t) \\
\hat{q}(z,t) &= h\sum_{n=a}^{\infty} z^{-n}q_n(t), \quad z = e^{ikh} \\
\frac{1}{h}\,\hat{q}(z,t) &= \frac{q_a(t)}{z^a} + \frac{q_{a+1}(t)}{z^{a+1}} + \frac{q_{a+2}(t)}{z^{a+2}} + \ldots + \frac{q_n(t)}{z^n} + \ldots \\
\frac{z^{n-1}}{h}\,\hat{q}(z,t) &= \frac{q_a(t)}{z^{a+1-n}} + \frac{q_{a+1}(t)}{z^{a+2-n}} + \frac{q_{a+2}(t)}{z^{a+3-n}} + \ldots + \frac{q_n(t)}{z} + \ldots.
\end{aligned}$$

It follows that

$$\begin{aligned}
q_n(t) &= \operatorname*{Res}_{z=0}\left[\frac{z^{n-1}}{h}\,\hat{q}(z,t)\right] \\
&= \frac{1}{2\pi i}\cdot 2\pi i \operatorname*{Res}_{z=0}\left[\frac{z^{n-1}}{h}\,\hat{q}(z,t)\right] \\
&= \frac{1}{2\pi i h}\oint_{|z|=1} z^{n-1}\hat{q}(z,t)\,dz \\
&= \frac{1}{2\pi i h}\int_{-\pi/h}^{\pi/h} e^{ik(n-1)h}\hat{q}(k,t)\,ihe^{ikh}\,dk \\
q_n(t) &= \frac{1}{2\pi}\int_{-\pi/h}^{\pi/h} e^{iknh}\hat{q}(k,t)\,dk.
\end{aligned}$$

Again, the starting index of n was not important, as long as it was finite. Only the $q_n(t)$ for $n = a, a+1, a+2, \ldots$ showed up.

So, if we treat $q_n(t)$ for $n \leq a-1$ as unknowns instead of setting them to zero, the transform pair (A.1a) and (A.1b) still hold for any a. That way, when the Unified Transform Method introduces ghost points, they are treated as legit unknowns and there is no clashing of previously setting them to zero.

A similar approach can be shown for the finite-interval transform pair:

$$\hat{q}(k,t) = h\sum_{n=a}^{A} e^{-iknh} q_n(t), \quad a, A \in \mathbb{Z} \text{ with } a < A \tag{A.2a}$$

$$q_n(t) = \frac{1}{2\pi}\int_{-\pi/h}^{\pi/h} e^{iknh}\hat{q}(k,t)\,dk, \quad n = a, a+1\ldots, A. \tag{A.2b}$$

Appendix B

THE "TIME-REVERSED" HEAT EQUATION

It is well known that the "time-reversed" (TR) heat equation

$$q_t = -q_{xx} \tag{B.1}$$

leads an ill-posed problem, but not to be confused with the "backward" discretization for the heat equation $q_t = q_{xx}$. For this continuous problem, UTM fails when taking the inverse transform of the global relation, since $\tilde{W}(k) = -k^2$ does not allow the integral representation to be valid for any nonzero $x \in \mathbb{R}$. We show next that the SD-UTM integral representation is well-posed for a finite h, but becomes ill-posed in the continuum limit.

Suppose we study the standard centered discretization. The TR equation is written as

$$\dot{q}_n = \frac{-q_{n+1} + 2q_n - q_{n-1}}{h^2}, \tag{B.2}$$

such that the local relation is the same as (2.2.3), except the right-hand side has a minus:

$$\partial_t \left(e^{-iknh} e^{Wt} q_n \right) = -\frac{1}{h^2} \Delta \left(e^{-ik(n-1)h} e^{Wt} q_n - e^{-iknh} e^{Wt} q_{n-1} \right) \tag{B.3}$$

with

$$W(k) = \frac{e^{ikh} + e^{-ikh} - 2}{h^2}. \tag{B.4}$$

The global relation

$$e^{WT} \hat{q}(k,T) - \hat{q}(k,0) + \left[\frac{e^{-ikh} f_0 - f_1}{h} \right] = 0.$$

gives rise to the "solution"

$$q_n(T) = \frac{1}{2\pi} \int_{-\pi/h}^{\pi/h} e^{iknh} e^{-WT} \hat{q}(k,0)\, dk - \frac{1}{2\pi} \int_{-\pi/h}^{\pi/h} e^{iknh} e^{-WT} \left[\frac{e^{-ikh} f_0 - f_1}{h} \right] dk, \tag{B.5}$$

such that (B.5) is composed of proper integrals, so it is valid for all $k \in \mathbb{C}$, unlike in the continuous case, where we have to verify that the "solution" is valid at least on the real line. With the same nontrivial symmetry $\nu_1(k) = -k$, suppose we have a Dirichlet boundary condition, so that we solve for $f_1(W,T)$ and substitute into (B.5):

$$\begin{aligned} q_n(T) = &\frac{1}{2\pi} \int_{-\pi/h}^{\pi/h} e^{iknh} e^{-WT} \hat{q}(k,0)\, dk \\ &- \frac{1}{2\pi} \int_{-\pi/h}^{\pi/h} e^{iknh} e^{-WT} \left[\hat{q}(-k,0) - \frac{2i \sin(kh) f_0}{h} \right] dk \end{aligned} \tag{B.6}$$

after removing the integral term with $\hat{q}(-k,T)$. Taking the continuum limit, is clear that (B.6) converges to

$$q(x,T) = \frac{1}{2\pi}\int_{-\infty}^{\infty} e^{ikx}e^{-WT}\hat{q}(k,0)\,dk - \frac{1}{2\pi}\int_{-\infty}^{\infty} e^{ikx}e^{-WT}\left[\hat{q}(-k,0) - 2ikF_0\right]\,dk,$$

where the integrals are not defined with $\lim_{h\to 0} W(k) = -k^2$. Therefore, we see that the semi-discrete problem is well-posed for a relatively large h, but ill-posed as $h \to 0$. In fact, the integrals in (B.6) exponentially grow, such that any attempt at numerically evaluating it for a practical h is futile.

BIBLIOGRAPHY

[1] Shalva Amiranashvili, Raimondas Čiegis, and Mindaugas Radziunas. Numerical methods for a class of generalized nonlinear schrödinger equations. *Kinetic & Related Models*, 8(2):215–234, 2015.

[2] Xavier Antoine, Christophe Besse, and Stéphane Descombes. Artificial boundary conditions for one-dimensional cubic nonlinear schrödinger equations. *SIAM Journal on Numerical Analysis*, 43(6):2272–2293, 2006.

[3] Weizhu Bao. Numerical methods for the nonlinear schrödinger equation with nonzero far-field conditions. *Methods Appl. Anal.*, 11(3):367–387, 2006.

[4] Christophe Besse, Brigitte Bidégaray, and Stéphane Descombes. Order estimates in time of splitting methods for the nonlinear schrödinger equation. *SIAM Journal on Numerical Analysis*, 40(1):26–40, 2002.

[5] Gino Biondini and Guenbo Hwang. Initial-boundary-value problems for discrete evolution equations: discrete linear Schrödinger and integrable discrete nonlinear Schrödinger equations. *Inverse Problems*, 24(6):065011, 44, 2008.

[6] Gino Biondini and Danhua Wang. Initial-boundary-value problems for discrete linear evolution equations. *IMA J. Appl. Math.*, 75(6):968–997, 2010.

[7] Ya. L. Bogomolov and A.D. Yunakovsky. Split-step fourier method for nonlinear schrodinger equation. In *DAYS on DIFFRACTION 2006*, pages 34–42, 2006.

[8] D. Britz, R. Baronas, E. Gaidamauskaitė, and F. Ivanauskas. Further comparisons of finite difference schemes for computational modelling of biosensors. *Nonlinear Analysis: Modelling and Control*, 14(4):419–433, 2009.

[9] J. G. Caputo, N. K. Efremidis, and Chao Hang. Fourier-mode dynamics for the nonlinear schrödinger equation in one-dimensional bounded domains. *Phys. Rev. E*, 84:036601, Sep 2011.

[10] T. A. Cheema. Higher-order finite-difference methods for partial differential equations. *PhD Thesis, Brunel University, Middlesex, England*, 1997.

[11] Jorge Cisneros and Bernard Deconinck. The numerical solutions of linear semidiscrete evolution problems on the half-line using the unified transform method. *Studies in Applied Mathematics*, 147(4):1240–1276, 2021.

[12] Jorge Cisneros and Bernard Deconinck. The numerical solutions of third-order linear semi-discrete evolution problems using the unified transform method. *In preparation*, 2021.

[13] Jorge Cisneros and Bernard Deconinck. The numerical solution of semidiscrete linear evolution problems on the finite interval using the unified transform method. *Quarterly of Applied Mathematics*, 2022.

[14] Armando Coco and Giovanni Russo. Finite-difference ghost-point multigrid methods on cartesian grids for elliptic problems in arbitrary domains. *J. Comput. Phys.*, 241:464–501, 2013.

[15] Matthew J. Colbrook, Zdravko I. Botev, Karsten Kuritz, and Shev MacNamara. Kernel density estimation with linked boundary conditions. *Studies in Applied Mathematics*, 145(3):357–396, 2020.

[16] F.P.J. de Barros, M.J. Colbrook, and A.S. Fokas. A hybrid analytical-numerical method for solving advection-dispersion problems on a half-line. *International Journal of Heat and Mass Transfer*, 139:482–491, 2019.

[17] Bernard Deconinck, Thomas Trogdon, and Vishal Vasan. The method of Fokas for solving linear partial differential equations. *SIAM Rev.*, 56(1):159–186, 2014.

[18] Bernard Deconinck, Thomas Trogdon, and Xin Yang. The numerical unified transform method for initial-boundary value problems on the half-line. *IMA Journal of Numerical Analysis*, 2021.

[19] *NIST Digital Library of Mathematical Functions*. http://dlmf.nist.gov/, Release 1.1.4 of 2022-01-15. F. W. J. Olver, A. B. Olde Daalhuis, D. W. Lozier, B. I. Schneider, R. F. Boisvert, C. W. Clark, B. R. Miller, B. V. Saunders, H. S. Cohl, and M. A. McClain, eds.

[20] B. Ducomet and A. Zlotnik. On stability of the crank-nicolson scheme with approximate transparent boundary conditions for the schrödinger equation. i. *Communications in Mathematical Sciences*, 4(4):741 – 766, 2006.

[21] Daniel J. Duffy. *Finite difference methods in financial engineering: a partial differential equation approach*. John Wiley & Sons Ltd, 2006.

[22] Dale R. Durran. *Numerical methods for fluid dynamics*, volume 32 of *Texts in Applied Mathematics*. Springer, New York, second edition, 2010. With applications to geophysics.

[23] Neveen G. A. Farag, Ahmed H. Eltanboly, M. S. EL-Azab, and S. S. A. Obayya. On the analytical and numerical solutions of the one-dimensional nonlinear schrodinger equation. *Mathematical Problems in Engineering*, 2021:1–15, 2021.

[24] Matthew Farkas, Jorge Cisneros, and Bernard Deconinck. The analytic extension of solutions to initial-boundary value problems outside their domain of definition. *In preparation*, 2022.

[25] N. Flyer and A. S. Fokas. A hybrid analytical-numerical method for solving evolution partial differential equations. I. The half-line. *Proc. R. Soc. Lond. Ser. A Math. Phys. Eng. Sci.*, 464(2095):1823–1849, 2008.

[26] A. S. Fokas. A unified transform method for solving linear and certain nonlinear PDEs. *Proc. Roy. Soc. London Ser. A*, 453(1962):1411–1443, 1997.

[27] A. S. Fokas and B. Pelloni, editors. *Unified transform for boundary value problems*. Society for Industrial and Applied Mathematics, Philadelphia, PA, 2015. Applications and advances.

[28] Athanassios S. Fokas. *A unified approach to boundary value problems*, volume 78 of *CBMS-NSF Regional Conference Series in Applied Mathematics*. Society for Industrial and Applied Mathematics (SIAM), Philadelphia, PA, 2008.

[29] E. Gaidamauskaitė and R. Baronas. A comparison of finite difference schemes for computational modelling of biosensors. *Nonlinear Analysis: Modelling and Control*, 12(3):359–369, 2007.

[30] K. George and E.H. Twizell. Stable second-order finite-difference methods for linear initial-boundary-value problems. *Applied Mathematics Letters*, 19(2):146–154, 2006.

[31] Bertil Gustafsson, Heinz-Otto Kreiss, and Arne Sundström. Stability theory of difference approximations for mixed initial boundary value problems. ii. *Math. Comp.*, 26:649–686, 1972.

[32] Clemens Heitzinger, Christian Ringhofer, and Siegfried Selberherr. Finite difference solutions of the nonlinear schrödinger equation and their conservation of physical quantities. *Communications in Mathematical Sciences*, 5(4):779–788, 2007.

[33] F. If, P. Berg, P. L. Christiansen, and O. Skovgaard. Split-step spectral method for nonlinear schrödinger equation with absorbing boundaries. *Journal of Computational Physics*, 72(2):501–503, 1987.

[34] Liviu I. Ignat and Enrique Zuazua. Numerical dispersive schemes for the nonlinear schrödinger equation. *SIAM Journal on Numerical Analysis*, 47(2):1366–1390, 2009.

[35] Arieh Iserles. *A first course in the numerical analysis of differential equations*. Cambridge Texts in Applied Mathematics. Cambridge University Press, Cambridge, second edition, 2009.

[36] M. Izadi. Split-step finite difference schemes for solving the nonlinear fisher equation. *Journal of Mahani Mathematical Research Center*, 7(1):37–55, 2018.

[37] Tobias Jahnke, Marcel Mikl, and Roland Schnaubelt. Strang splitting for a semilinear schrödinger equation with damping and forcing. *Journal of Mathematical Analysis and Applications*, 455(2):1051–1071, 2017.

[38] Emine Kesici, Beatrice Pelloni, Tristan Pryer, and David Smith. A numerical implementation of the unified Fokas transform for evolution problems on a finite interval. *European J. Appl. Math.*, 29(3):543–567, 2018.

[39] Taras I. Lakoba. Instability of the finite-difference split-step method applied to the nonlinear schrödinger equation. i. standing soliton. *Numerical Methods for Partial Differential Equations*, 32(3):1002–1023, 2015.

[40] Taras I. Lakoba. Instability of the finite-difference split-step method applied to the generalized nonlinear schrödinger equation. iii. external potential and oscillating pulse solutions. *Numerical Methods for Partial Differential Equations*, 33(3):633–650, 2017.

[41] Hans Petter Langtangen and Svein Linge. *Finite Difference Computing with PDEs*. Springer, 2017.

[42] Randall J. LeVeque. Intermediate boundary conditions for time-split methods applied to hyperbolic partial differential equations. *Math. Comp.*, 47(175):37–54, 1986.

[43] Randall J. LeVeque. *Finite difference methods for ordinary and partial differential equations*. Society for Industrial and Applied Mathematics (SIAM), Philadelphia, PA, 2007. Steady-state and time-dependent problems.

[44] Randall J. LeVeque and Joseph Oliger. Numerical methods based on additive splittings for hyperbolic partial differential equations. *Math. Comp.*, 40(162):469–497, 1983.

[45] Jianfeng Lu and Jeremy L. Marzuola. Strang splitting methods for a quasilinear schrödinger equation: convergence, instability, and dynamics. *Commun. Math. Sci.*, 13(5):1051–1074, 2015.

[46] Christian Lubich. On splitting methods for schrödinger-poisson and cubic nonlinear schrödinger equations. *Math. Comp.*, 77:2141–2153, 2008.

[47] Shev MacNamara and Gilbert Strang. Operator splitting. In *Splitting methods in communication, imaging, science, and engineering*, Sci. Comput., pages 95–114. Springer, Cham, 2016.

[48] Malachy McConnell. *On the numerical solution of selected nonlinear wave equations*. PhD thesis, University of Reading, 2002.

[49] Robert I. McLachlan and G. Reinout W. Quispel. Splitting methods. *Acta Numerica*, 11:341–434, 2002.

[50] Akbar Mohebbi. On the split-step method for the solution of nonlinear schrödinger equation with the riesz space fractional derivative. volume 4, pages 54–69, 2016.

[51] Byungsoo Moon and Guenbo Hwang. Discrete linear evolution equations in a finite lattice. *J. Difference Equ. Appl.*, 25(5):630–646, 2019.

[52] Frederick Ira Moxley III, David T. Chuss, and Weizhong Dai. An implicit generalized finite-difference time-domain scheme for solving nonlinear schrödinger equations. *Contemporary Mathematics*, 618:181–193, 2014.

[53] Gerrit Mur. Absorbing boundary conditions for the finite-difference approximation of the time-domain electromagnetic-field equations. *IEEE Transactions on Electromagnetic Compatibility,*, 23(4):377–382, 1981.

[54] G.M. Muslu and H.A. Erbay. Higher-order split-step fourier schemes for the generalized nonlinear schrödinger equation. *Mathematics and Computers in Simulation*, 67(6):581–595, 2005.

[55] Theodore S. Papatheodorou and Anastasia N. Kandili. Novel numerical techniques based on Fokas transforms, for the solution of initial boundary value problems. *J. Comput. Appl. Math.*, 227(1):75–82, 2009.

[56] J.I. Ramos and F.R. Villatoro. The nonlinear schrödinger equation in the finite line. *Mathematical and Computer Modelling*, 20(3):31–59, 1994.

[57] Norikazu Saito and Takiko Sasaki. Finite difference approximation for nonlinear schrödinger equations with application to blow-up computation. *Japan Journal of Industrial and Applied Mathematics*, 33(2):427–470, 2016.

[58] Anastassiya Semenova, Sergey A. Dyachenko, Alexander O. Korotkevich, and Pavel M. Lushnikov. Comparison of split-step and hamiltonian integration methods for simulation of the nonlinear schrödinger type equations. *Journal of Computational Physics*, 427:110061, 2021.

[59] Chaopeng Shen, Jing-Mei Qiu, and Andrew Christlieb. Adaptive mesh refinement based on high order finite difference WENO scheme for multi-scale simulations. *J. Comput. Phys.*, 230(10):3780–3802, 2011.

[60] John C. Strikwerda. *Finite difference schemes and partial differential equations*. Society for Industrial and Applied Mathematics (SIAM), Philadelphia, PA, second edition, 2004.

[61] Chunmei Su and Xiaofei Zhao. On time-splitting methods for nonlinear schrödinger equation with highly oscillatory potential. *ESAIM: M2AN*, 54(5):1491–1508, 2020.

[62] Surattana Sungnul, Bubpha Jitsom, and Mahosut Punpocha. Numerical solutions of the modified Burger's equation using FTCS implicit scheme. *IAENG Int. J. Appl. Math.*, 48(1):53–61, 2018.

[63] Béla Szilágyi, Denis Pollney, Luciano Rezzolla, Jonathan Thornburg, and Jeffrey Winicour. An explicit harmonic code for black-hole evolution using excision. *Classical Quantum Gravity*, 24(12):S275–S293, 2007.

[64] Thiab R Taha and Mark I Ablowitz. Analytical and numerical aspects of certain nonlinear evolution equations. ii. numerical, nonlinear schrödinger equation. *Journal of Computational Physics*, 55(2):203–230, 1984.

[65] Luke Taylor. A comparison between the split step fourier and finite-difference method in analysing the soliton collision of a type of nonlinear schrödinger equation found in the context of optical pulses, 2017.

[66] Lloyd N. Trefethen. *Finite Difference and Spectral Methods for Ordinary and Partial Differential Equations*. unpublished, available at https://people.maths.ox.ac.uk/trefethen/pdetext.html, 1996.

[67] Lloyd N. Trefethen and Mark Embree. *Spectra and pseudospectra*. Princeton University Press, Princeton, NJ, 2005. The behavior of nonnormal matrices and operators.

[68] V. A. Trofimov and N. V. Peskov. Comparison of finite-difference schemes for the gross-pitaevskii equation. *Mathematical Modeling and Analysis*, 14(1):109–126, 2009.

[69] Bo Wang and Dong Liang. The finite difference scheme for nonlinear schrödinger equations on unbounded domain by artificial boundary conditions. *Applied Numerical Mathematics*, 128:183–204, 2018.

[70] Hanquan Wang. Numerical studies on the split-step finite difference method for nonlinear schrödinger equations. *Applied Mathematics and Computation*, 170(1):17–35, 2005.

[71] R. F. Warming and B. J. Hyett. The modified equation approach to the stability and accuracy analysis of finite-difference methods. *J. Comput. Phys.*, 14:159–179, 1974.

[72] J. A. C. Weideman and B. M. Herbst. Split-step methods for the solution of the nonlinear schrodinger equation. *SIAM Journal on Numerical Analysis*, 23(3):485–507, 1986.

[73] Jennifer Zhao, Weizhong Dai, and Tianchan Niu. Fourth-order compact schemes of a heat conduction problem with neumann boundary conditions. *Numerical Methods for Partial Differential Equations*, 23(5):949–959, 2007.

[74] Andrea Zisowsky and Matthias Ehrhardt. Discrete artificial boundary conditions for nonlinear schrödinger equations. *Mathematical and Computer Modelling*, 47(11):1264–1283, 2008.

[75] Daniel Zwillinger. *CRC standard mathematical tables and formulae.* CRC Press, Boca Raton, FL, second edition, 2012.